AD-A156 616 NUMERICAL MODEL INVESTIGATION OF MISSISSIPPI SOUND AND ADJACENT AREAS(U) COASTAL ENGINEERING RESEARCH CENTER VICKSBURG MS R A SCHMALZ FEB 85 CERC-MP-85-2 1/3

UNCLASSIFIED F/G 8/8 NL

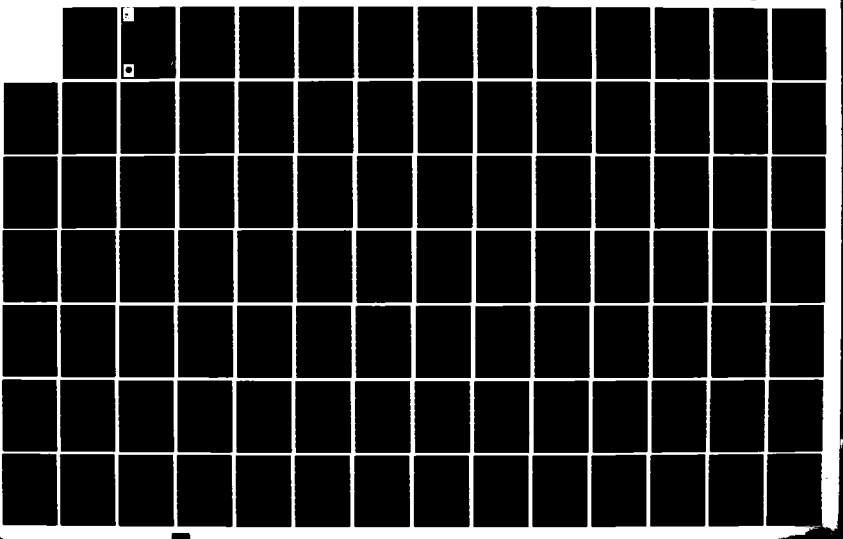

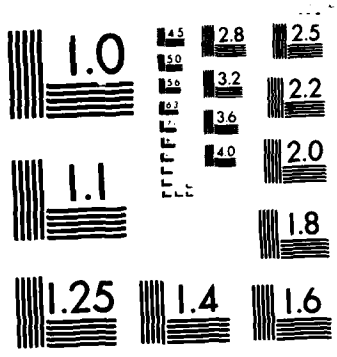

MICROCOPY RESOLUTION TEST CHART
NATIONAL BUREAU OF STANDARDS 1963-A

US Army Corps of Engineers

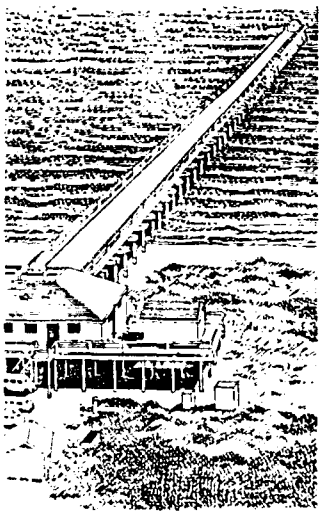

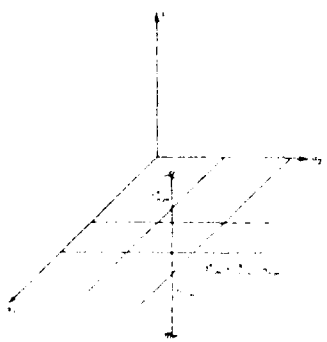

AD-A156 616

MISCELLANEOUS PAPER CERC-85-2

NUMERICAL MODEL INVESTIGATION OF MISSISSIPPI SOUND AND ADJACENT AREAS

by

Richard A. Schmalz, Jr.

Coastal Engineering Research Center

DEPARTMENT OF THE ARMY
Waterways Experiment Station, Corps of Engineers
PO Box 631
Vicksburg, Mississippi 39180-0631

February 1985
Final Report

Approved For Public Release; Distribution Unlimited

DTIC FILE COPY

DTIC ELECTE JUL 05 1985 S D G

Prepared for
US Army Engineer District, Mobile
Mobile, Alabama 36628

85 06 10 [illegible]

Destroy this report when no longer needed. Do not return it to the originator.

The findings in this report are not to be construed as an official Department of the Army position unless so designated by other authorized documents.

The contents of this report are not to be used for advertising, publication, or promotional purposes. Citation of trade names does not constitute an official endorsement or approval of the use of such commercial products.

Unclassified
SECURITY CLASSIFICATION OF THIS PAGE *(When Data Entered)*

REPORT DOCUMENTATION PAGE

READ INSTRUCTIONS BEFORE COMPLETING FORM

1. REPORT NUMBER: Miscellaneous Paper CERC-85-2	2. GOVT ACCESSION NO.
3. RECIPIENT'S CATALOG NUMBER	
4. TITLE *(and Subtitle)*: NUMERICAL MODEL INVESTIGATION OF MISSISSIPPI SOUND AND ADJACENT AREAS	5. TYPE OF REPORT & PERIOD COVERED: Final report
	6. PERFORMING ORG. REPORT NUMBER
7. AUTHOR(s): Richard A. Schmalz, Jr.	8. CONTRACT OR GRANT NUMBER(s)
9. PERFORMING ORGANIZATION NAME AND ADDRESS: US Army Engineer Waterways Experiment Station, Coastal Engineering Research Center, PO Box 631, Vicksburg, Mississippi 39180-0631	10. PROGRAM ELEMENT, PROJECT, TASK AREA & WORK UNIT NUMBERS
11. CONTROLLING OFFICE NAME AND ADDRESS: US Army Engineer District, Mobile, PO Box 2208, Mobile, Alabama 36628	12. REPORT DATE: February 1985
	13. NUMBER OF PAGES: 262
14. MONITORING AGENCY NAME & ADDRESS *(If different from Controlling Office)*	15. SECURITY CLASS. *(of this report)*: Unclassified
	15a. DECLASSIFICATION DOWNGRADING SCHEDULE

16. DISTRIBUTION STATEMENT *(of this Report)*

Approved for public release; distribution unlimited

17. DISTRIBUTION STATEMENT *(of the abstract entered in Block 20, if different from Report)*

18. SUPPLEMENTARY NOTES

Available from National Technical Information Service, 5285 Port Royal Road, Springfield, Virginia 22161.

19. KEY WORDS *(Continue on reverse side if necessary and identify by block number)*

Dredge disposal	Hydrodynamics	Salinity transport
Finite difference	Mississippi Sound	Tidal constituents
Gulf of Mexico	Navigation channels	
Harmonic analysis	Numerical modeling	

20. ABSTRACT *(Continue on reverse side if necessary and identify by block number)*

This report documents a numerical investigation of Mississippi Sound and adjacent areas. A model of the complete Gulf of Mexico, (GTM) developed by Reid and Whitaker (1981) is employed to develop tidal constituent (O_1, K_1, P_1, M_2, and S_2) boundary conditions for the two-dimensional vertically integrated Waterways Implicit Flooding Model (WIFM) (Butler 1980), which was extended to include salinity by Schmalz (1983). In order to calibrate and verify the extended model (WIFM-SAL), an intensive data collection program
(Continued)

DD FORM 1 JAN 73 1473 EDITION OF 1 NOV 65 IS OBSOLETE

Unclassified
SECURITY CLASSIFICATION OF THIS PAGE *(When Data Entered)*

20. ABSTRACT (Continued).

was conducted by Raytheon Ocean Systems and the National Oceanic and Atmospheric Administration. Data were analyzed for tidal constituents by Outlaw (1983). A global grid representing Mississippi Sound and adjacent areas was constructed to interface with the GTM grid. Bottom friction mechanics were calibrated on this global grid for 20-24 September 1980 and subsequently verified for 12-16 June 1980. A hypothetical regional dredge disposal plan was considered on the global grid by increasing the size of Sand Island. A refined grid was constructed around the Pascagoula Channel in order to study alternative channel configuration effects on Mississippi Sound. Previously calibrated and verified bottom friction mechanics were further substantiated by simulating hydrodynamic conditions for the 20-24 September period over the refined grid using global grid results to supply water surface elevation boundary conditions. (The effects of doubling the width of the main Pascagoula Channel were then studied by simulating this same period with the modified channel.) Study conclusions are drawn and recommendations for additional simulation work are presented.

In addition, horizontal salinity conditions were also investigated for the 20-24 September period. Wind speed and direction were specified as meteorological inputs. A constant drag coefficient of 0.001 was employed to develop the surface wind stress, and the friction mechanism previously developed was used to implement bottom stress. Simulation results for both the Flux-Corrected Transport and the Three Time Level Explicit schemes are presented for the global grid. Effective dispersion coefficients in each coordinate direction were calibrated. The Flux-Corrected Transport global grid salinity levels and water surface elevation saved at the boundary of the refined grid were used to supply the boundary conditions for a Flux-Corrected Transport simulation on the refined grid. Previously calibrated global grid effective dispersion coefficients were used in the refined grid simulation.

Supplied Keywords

Accession For
NTIS GRA&I ☒
DTIC TAB ☐
Unannounced ☐
Justification
By
Distribution/
Availability Codes
Dist | Avail and/or Special
A/1

PREFACE

The Mississippi Sound and Adjacent Areas Study was authorized by congressional resolutions of 1 February 1977 and 10 May 1977. The main purpose of the study as stated in the resolutions is to determine whether the present and proposed dredged material disposal methods for maintenance and construction of the various projects in Mississippi Sound should be modified in any way in the interest of economic efficiency and environmental quality. The resolutions request an investigation by the US Army Corps of Engineers of various dredging techniques and the possibility of developing a coordinated program for the region, with appropriate consideration of ecological factors. The region under study is defined to include the body of water and adjacent land and estuarine areas extending from Chandeleur Sound and Lake Borgne, on the west, along the Mississippi and Alabama coasts to the eastern shore of Mobile Bay, on the east. It is bounded on the north by Interstate Highway 10 and on the south by the 120-ft bottom contour of the Gulf of Mexico.

The numerical model investigation described herein was authorized by the US Army Engineer District, Mobile (SAM). This study was conducted at the US Army Engineer Waterways Experiment Station (WES) in the Wave Dynamics Division (WDD), Hydraulics Laboratory, under the direction of Mr. H. B. Simmons, Chief of the Hydraulics Laboratory, Dr. R. W. Whalin, former Chief of the Wave Dynamics Division, and Mr. C. E. Chatham, Jr., present Chief of the Wave Dynamics Division.

The investigation was performed and this report prepared by Dr. R. A. Schmalz, WDD. Ms. Mary Ann Leggett retuned the Gulf Tide Model in order to provide revised tidal constituent information. Ms. J. I. Jones prepared the geophysical data and developed Appendix A.

The cooperation of and coordination with SAM personnel, including Messrs. Dennis McCann, Maurice James, Dru Barrineau, and Timothy Phillips, enabled the work to remain focused on district needs and provided for an effective transfer of the technology developed. The numerical computations associated with this work were performed on CYBER 175 and CRAY 1 computers located at the Air Force Weapons Laboratory, Kirtland Air Force Base, New Mexico. The numerical model and all datasets were transferred to SAM. WES provided assistance in installing the model on the Boeing Computer System for use by SAM.

Directors of WES during the course of the investigation and the preparation and publication of this report were COL John L. Cannon, CE, COL Nelson P. Conover, CE, COL Tilford C. Creel, CE, and COL Robert C. Lee, CE. Technical Director was Mr. F. R. Brown.

CONTENTS

	Page
PREFACE	1
LIST OF TABLES	5
LIST OF FIGURES	8
CONVERSION FACTORS, NON-SI TO SI (METRIC) UNITS OF MEASUREMENT	12
PART I: INTRODUCTION	13
PART II: DATA COLLECTION PROGRAM ESTABLISHMENT	18
Raytheon Ocean Systems Program	18
NOAA Data Collection Program	18
PART III: PROTOTYPE DATA ANALYSIS	25
Water Surface Elevations	25
Currents	26
PART IV: GULF TIDE MODEL DEVELOPMENT AND RESULTS	37
PART V: SALINITY ALGORITHM DEVELOPMENT	43
Constituent Transport Equation in Cartesian Coordinates	43
Constituent Transport Equation in Transformed Coordinates	44
Numerical Approximations	45
Dispersion Coefficient Formulation	66
PART VI: DEVELOPMENT OF A GLOBAL GRID FOR MISSISSIPPI SOUND	71
Initial Depth Assignment	77
Incorporation of Hydrographic Survey Information	77
Comparison of Previously Assigned Depths to Surveyed Depth	86
Barrier Island Configuration	90
Flow Inputs	90
Calibration/Verification Stations	90
PART VII: SELECTION OF THE CALIBRATION AND VERIFICATION PERIODS	97
River Inflows	97
Meteorological Station Wind Data	103
Salinity Transect Data	103
Calibration and Verification Periods	107
PART VIII: CALIBRATION PERIOD 20-25 SEPTEMBER 1980	110
Wind Information	110
Instantaneous Salinity Information	110
Salinity Transect Information	110
Water Surface Elevation Information	119
Current Component Information	124
PART IX: VERIFICATION PERIOD 12-16 JUNE 1980	129
Wind Information	129
Instantaneous Salinity Information	129
Salinity Transect Information	129
Water Surface Elevation and Current Component Information	135

Page

PART X: GLOBAL GRID HYDRODYNAMIC CALIBRATION AND VERIFICATION AND SYSTEM MODIFICATION 138

PART XI: REFINED GRID METHODOLOGY AND APPLICATION 179

PART XII: REFINED GRID HYDRODYNAMIC CALIBRATION AND CHANNEL MODIFICATION 190

PART XIII: SALINITY CALIBRATION ON THE GLOBAL AND REFINED GRID SYSTEMS 205

Global Grid Salinity Simulations 206
Refined Grid Salinity Simulation 211

PART XIV: STUDY RESULTS, CONCLUSIONS, AND RECOMMENDATIONS 224

REFERENCES 229

APPENDIX A: GUIDE TO WIFM MODEL INPUT REQUIREMENTS A1

Mapping the Global Subgrid of Pascagoula Region A1
Mapping of Pascagoula Channel A2
Depth Field Specification A4
Barrier Specification A4
Flow Specification A5
Tidal Signal Input Specification A6
Salinity Initial Condition Specification A8
Specification of Wind Information A8
Development of Simulation Control Variables A8

APPENDIX B: PROGRAM TIDE B1

APPENDIX C: CUBIC POLYNOMIAL FEATHERING C1

APPENDIX D: SUBROUTINE ADVBAR D1

LIST OF TABLES

Table		Page
II-1	NOAA Tide Station Locations	24
III-1	Mean Elevation of Observed NOAA Data Record Relative to Mean Lower Low Water	27
III-2	Surface Elevation Mean Amplitude	28
III-3	Surface Elevation Local Epoch	29
III-4	Surface Elevation Record Length and Root Mean Square Error	30
III-5	Station Mean Velocity Components	32
III-6	North/South Velocity Component Mean Amplitude	33
III-7	North/South Velocity Component Local Epoch	34
III-8	East/West Velocity Component Mean Amplitude	35
III-9	East/West Velocity Component Local Epoch	36
IV-1	Least Squares Analysis Constituent O1	38
IV-2	Least Squares Analysis Constituent K1	39
IV-3	Least Squares Analysis Constituent P1	40
IV-4	Least Squares Analysis Constituent M2	41
IV-5	Least Squares Analysis Constituent S2	42
V-1	X-Sweep Modification FTUS	54
V-2	Y-Sweep Modification FTUS	55
V-3	Computer Program for Determination of the Eigenvalues for the General Three Time Level Explicit Scheme	67
V-4	Eigenvalue Analysis Results for the General Three Time Level Explicit Scheme	68
VI-1	Horizontal Mapping Results	74
VI-2	Vertical Mapping Results	75
VI-3	Global Grid Charts	76
VI-4	Program TGRID Subgrid Plots	78
VI-5	Global Grid Depth Field	79
VI-6	Hydrographic Survey Journal	85
VI-7	Comparison of Initial Cell to Survey Range Depths	87
VI-8	Barrier Configuration	91
VI-9	Flow Inputs in the Global Grid	94
VI-10	Water Surface Elevation Stations	95
VI-11	Meteorological Stations	96
VI-12	Velocity/Salinity Continuous Stations	96

Table		Page
VII-1	Daily Discharges into Mississippi Sound, in Cfs April-September 1980	98
VII-2	Wind Characteristics for Meteorological Station 4, Horn Island	104
VII-3	Wind Characteristics for Meteorological Station 2, Ship Island	106
VII-4	Representative Spatial Salinity Transect Data, 1980	108
VIII-1	Hourly Meteorological Data (Wind Speed and Direction), 20-25 September 1980, Stations M1-M5	111
VIII-2	Range of Hourly Salinity Data for CT Stations, 20-25 September 1980	117
VIII-3	Comparison of 20-21 September Salinity Transect Data with Instantaneous Salinity Data	120
VIII-4	Verification Period Astronomic Tide Conditions, 20 September 1980, Hour 0000	121
VIII-5	Tidal Constituents at Pascagoula (874-1196)	122
VIII-6	Pascagoula 874-1196 Water Surface Elevation, 20 September 1980, Hour 00	123
VIII-7	Station V10-S Tidal Constituents	125
VIII-8	Station V10-S Velocity Comparisons	126
IX-1	Hourly Meteorological Data (Wind Speed and Direction), 12-16 June 1980, Stations M1-M5	130
IX-2	12-16 June 1980 Continuous Station Salinity Levels	133
IX-3	Verification Period Astronomical Tide Conditions, 6 June 1980, Hour 0000	136
IX-4	Pascagoula 874-1196 Water Surface Elevation	137
X-1	Gulf Tide Model Boundary Inputs	139
X-2	Comparison of Outlaw Analysis and Reid and Whitaker GTM Results	143
X-3	Calibrated Depth Versus Manning's n Relationship	144
X-4	Global Grid Alternative (Sand Island Complex)	173
X-5	Simulated Global Grid Velocity Components for the Original Sand Island Configuration at Hr 72	175
X-6	Simulated Global Grid Velocity Components for the Original Sand Island Configuration at Hr 120	176
X-7	Simulated Global Grid Velocity Components for the Sand Island Alternative at Hr 72	177
X-8	Simulated Global Grid Velocity Components for the Sand Island Alternative at Hr 120	178
XI-1	East-West Orientation	182

Table		Page
XI-2	North-South Orientation	182
XI-3	Refined Grid Depth Field	184
XI-4	Barrier Configuration	187
XI-5	Calibration Station Locations on the Refined Grid	188
XI-6	Global Grid Cell-Refined Grid Cell Boundary Assignment	189
XII-1	Pascagoula Channel Widening	200
XII-2	Simulated Velocity Components for the 330-Ft Channel Width at Hr 72	203
XII-3	Simulated Velocity Compcnents for the 660-Ft Channel Width at Hr 72	204
XIII-1	Initial Salinity Conditions on the Global Grid	208
XIII-2	Global Grid Boundary Salinity Conditions	209
XIII-3	Wind Data for 20-24 September 1980	210
XIII-4	Calibrated Dispersion Coefficient Parameters	212
XIII-5	Global Grid Salinity Calibration	213
XIII-6	Upper Mobile Bay Simulation Results on the Global Grid After 120 Hours, Scheme 1	214
XIII-7	Salinity Conditions on the Refined Grid	221
XIII-8	Behavior of Refined Grid Salinity Simulation in the Vicinity of the Pascagoula River Inflow	222
A1	WIFM Input Requirements for a Refined Grid	A1
A2	Y Direction Mapping	A3
A3	X Direction Mapping	A3
A4	Global Grid Cell-Refined Grid Cell Boundary Assignment	A7
A5	Data Station Location Summary	A11
C1	Subroutine POLY	C4
D1	Subroutine ADVBAR	D2

LIST OF FIGURES

Figure		Page
I-1	Mississippi Sound and adjacent waters	14
II-1	Mississippi Sound instantaneous data stations	19
II-2	Mississippi Sound meteorological stations	20
II-3	Mississippi water surface elevation stations	21
II-4	Mississippi Sound salinity transect stations	22
II-5	Mississippi Sound hydrographic survey transects	23
V-1	Space staggered finite difference grid in transformed coordinates	46
V-2	Datum convention employed within the space staggered grid system	47
VI-1	Global grid, GTM boundary orientation	72
VI-2	Mississippi Sound global grid	73
VIII-1	September 20-21 salinity transect data	118
IX-1	12-13 June salinity transect data	134
X-1	Water surface elevations, simulated and predicted, at station 874-7437, 20-24 September 1980	145
X-2	Water surface elevations, simulated and predicted, at station 876-0742, 20-24 September 1980	145
X-3	Water surface elevations, simulated and predicted, at station 874-6819, 20-24 September 1980	146
X-4	Water surface elevations, simulated and predicted, at station 874-4586, 20-24 September 1980	146
X-5	Water surface elevations, simulated and predicted, at station 874-3735, 20-24 September 1980	147
X-6	Water surface elevations, simulated and predicted, at station 874-3081, 20-24 September 1980	147
X-7	Water surface elevations, simulated and predicted, at station 874-2221, 20-24 September 1980	148
X-8	Water surface elevations, simulated and predicted, at station 874-1196, 20-24 September 1980	148
X-9	Water surface elevations, simulated and predicted, at station 874-0405, 20-24 September 1980	149
X-10	Water surface elevations, simulated and predicted, at station 874-0199, 20-24 September 1980	149
X-11	Water surface elevations, simulated and predicted, at station 873-5587, 20-24 September 1980	150
X-12	Velocity components, simulated and predicted, at station V2-M, 20-24 September 1980	151

Figure		Page
X-13	Velocity components, simulated and predicted, at station V4-S, 20-24 September 1980	152
X-14	Velocity components, simulated and predicted, at station V7-S, 20-24 September 1980	153
X-15	Velocity components, simulated and predicted, at station V11-M, 20-24 September 1980	154
X-16	Velocity components, simulated and predicted, at station V13-S, 20-24 September 1980	155
X-17	Velocity components, simulated and predicted, at station V19-S, 20-24 September 1980	156
X-18	Velocity components, simulated and predicted, at station V20-M, 20-24 September 1980	157
X-19	Water surface elevations, simulated and predicted, at station 874-7437, 12-14 June 1980	159
X-20	Water surface elevations, simulated and predicted, at station 876-0742, 12-14 June 1980	159
X-21	Water surface elevations, simulated and predicted, at station 874-6819, 12-14 June 1980	160
X-22	Water surface elevations, simulated and predicted, at station 874-4586, 12-14 June 1980	160
X-23	Water surface elevations, simulated and predicted, at station 874-3735, 12-14 June 1980	161
X-24	Water surface elevations, simulated and predicted, at station 874-3081, 12-14 June 1980	161
X-25	Water surface elevations, simulated and predicted, at station 874-2221, 12-14 June 1980	162
X-26	Water surface elevations, simulated and predicted, at station 874-1196, 12-14 June 1980	162
X-27	Water surface elevations, simulated and predicted, at station 874-0405, 12-14 June 1980	163
X-28	Water surface elevations, simulated and predicted, at station 874-0199, 12-14 June 1980	163
X-29	Water surface elevations, simulated and predicted, at station 873-5587, 12-14 June 1980	164
X-30	Velocity components, simulated and predicted, at station V2-M, 20-24 September 1980	165
X-31	Velocity components, simulated and predicted, at station V4-S, 20-24 September 1980	166
X-32	Velocity components, simulated and predicted, at station V7-S, 20-24 September 1980	167
X-33	Velocity components, simulated and predicted, at station V11-M, 20-24 September 1980	168

Figure		Page
X-34	Velocity components, simulated and predicted, at station V13-S, 20-24 September 1980	169
X-35	Velocity components, simulated and predicted, at station V19-S, 20-24 September 1980	170
X-36	Velocity components, simulated and predicted, at station V20-M, 20-24 September 1980	171
XI-1	General orientation of major navigation channels in Mississippi Sound	180
XI-2	Pascagoula Channel configuration	181
XI-3	Pascagoula Channel refined grid	183
XII-1	Simulated versus reconstructed water surface elevations at station 874-0199, 20-24 September 1980	191
XII-2	Simulated versus reconstructed water surface elevations at station 874-0405, 20-24 September 1980	191
XII-3	Simulated versus reconstructed water surface elevations at station 874-1196, 20-24 September 1980	192
XII-4	Simulated versus reconstructed water surface elevations at station 874-2221, 20-24 September 1980	192
XII-5	Simulated current velocities at station 48 22, 20-24 September 1980	193
XII-6	Simulated current velocities at station 48 23, 20-24 September 1980	194
XII-7	Simulated current velocities at station 30 27, 20-24 September 1980	195
XII-8	Simulated current velocities at station 33 26, 20-24 September 1980	196
XII-9	Simulated current velocities at station 24 25, 20-24 September 1980	197
XII-10	Simulated current velocities at station 35 20, 20-24 September 1980	198
XII-11	Simulated current velocities at station 3 20, 20-24 September 1980	199
XII-12	Computed and reconstructed water surface elevations at station 874-2221, 20-24 September 1980	201
XII-13	Computed and reconstructed water surface elevations at station 874-1196, 20-24 September 1980	201
XII-14	Computed and reconstructed water surface elevations at station 874-0405, 20-24 September 1980	202
XII-15	Computed and reconstructed water surface elevations at station 874-0199, 20-24 September 1980	202
XIII-1	Refined grid, 24-ppt salinity contour, 48 hr	216

Figure		Page
XIII-2	Refined grid, 24-ppt salinity contour, 72 hr	217
XIII-3	Refined grid, 24-ppt salinity contour, 96 hr	218
XIII-4	Refined grid, 24-ppt salinity contour, 120 hr	219
XIII-5	Simulated global grid water surface elevation at Pascagoula including wind effect	220
A1	Barrier cell face orientation	A4
C1	Periodic boundary signal	C2
C2	Cubic polynomial feathering conditions	C3

CONVERSION FACTORS, NON-SI TO SI (METRIC) UNITS OF MEASUREMENT

Non-SI units of measurement used in this report can be converted to metric (SI) units as follows:

Multiply	By	To Obtain
cubic feet per second	0.02831685	cubic metres per second
feet	0.3048	metres
feet per second	0.3048	metres per second
miles (US statute)	1.852	kilometres
square feet	0.09290304	square metres
square feet per second	0.09290304	square metres per second
square miles (US statute)	0.4470400	square metres

NUMERICAL MODEL INVESTIGATION OF MISSISSIPPI SOUND AND ADJACENT AREAS

PART I: INTRODUCTION

1. Mississippi Sound and its adjacent waters as shown in Figure I-1 comprise an extremely productive aquatic ecosystem. Major navigation channels maintained by dredge operations within Mississippi Sound are located at Gulfport, Biloxi, and Pascagoula. In order to protect the ecosystem as well as provide for efficient navigation a study was authorized by congressional resolutions of the Senate Committee on Environment and Public Works and the House Committee on Public Works and Transportation. The US Army Engineer District, Mobile, has specific authority and jurisdiction to conduct the study.

2. A numerical modeling approach is required to develop in an efficient manner a quantitative knowledge of tidal circulation and salinity distribution. The US Army Engineer Waterways Experiment Station (WES) was requested to apply WIFM, a two-dimensional vertically integrated model (Butler 1980). In addition, model capability was to be extended to include the prediction of salinity. In order to calibrate and verify the model, Raytheon Ocean Systems was contracted by the Mobile District to collect prototype velocity, temperature, conductivity, and meteorological data. The National Oceanic and Atmospheric Administration (NOAA) was responsible for obtaining tidal elevation data. Texas A&M was contracted to develop a numerical Gulf Tide Model (GTM) to provide accurate tidal elevation information at the boundary of the WIFM model global grid.

3. This report is structured in the following manner.

   a. In Part II, both the Raytheon Ocean System and NOAA Data Collection Programs features are presented. Harmonic analysis results are presented in Part III for both water surface elevations and currents. The GTM is outlined and the results for the O_1, K_1, P_1, M_2, and S_2 tidal constituents are presented in Part IV. Major features of the salinity algorithm incorporated within WIFM are discussed in Part V in terms of the equations considered, the numerical approximations, and the effective dispersion coefficient formulation.

   b. The remaining parts of this report comprise the numerical modeling effort and are presented in the order in which this work was performed.

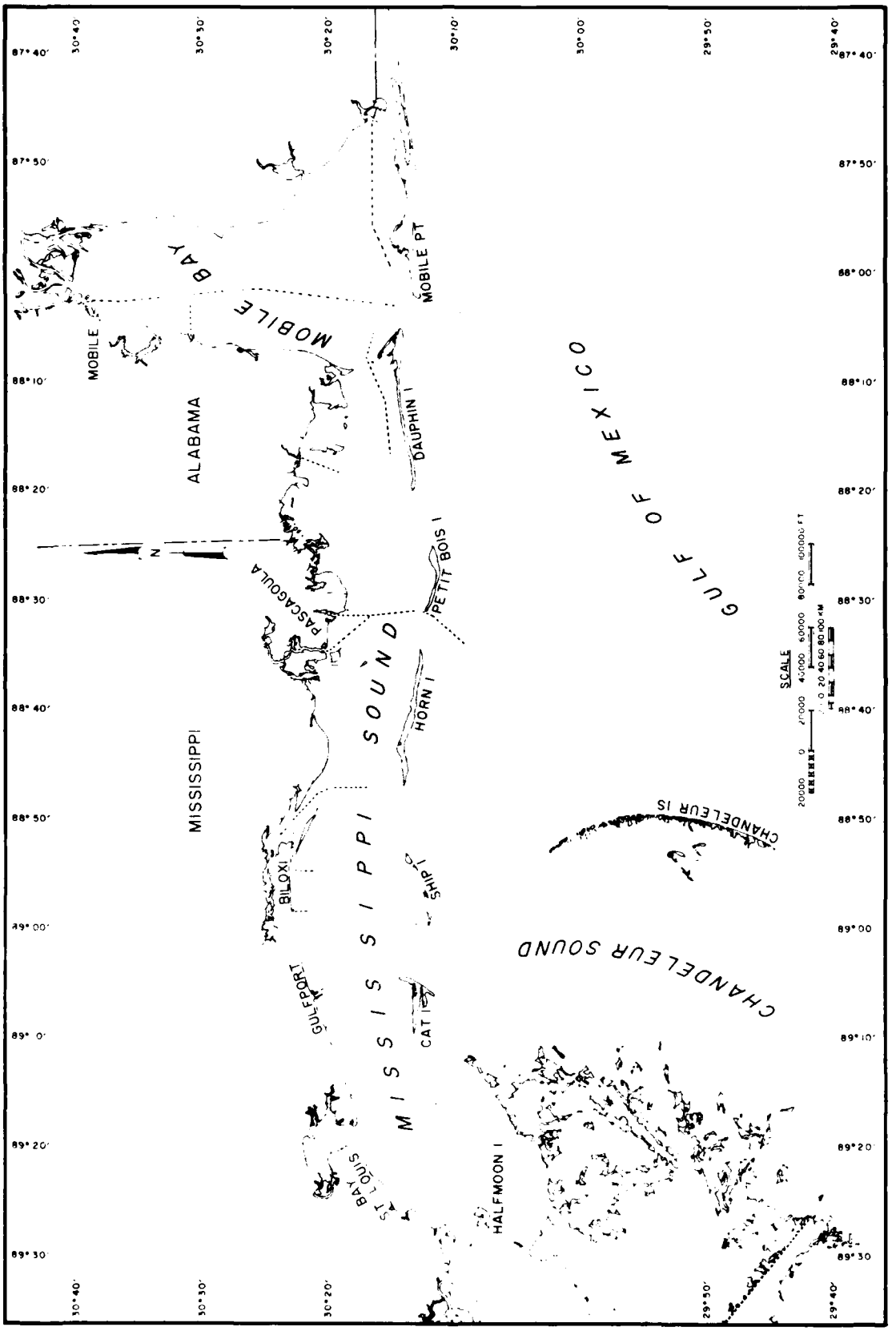

Figure I-1. Mississippi Sound and adjacent waters

c. Initially, a global grid representing Mississippi Sound and adjacent areas was constructed to interface with the GTM grid encompassing the entire Gulf of Mexico. The development of the global grid depth field, barrier island configuration, freshwater inputs, and location of the gaging stations is presented in Part VI.

d. In order to determine periods for study on the global grid, data over the entire 180-day survey period were reviewed. Part VII outlines the data review in terms of both hydrodynamic and salinity simulation requirements. Water surface elevation and current tidal constituent constants developed in the harmonic analysis represent astronomic influences only; i.e., all meteorological effects are assumed to be removed in the filtering process employed in the analysis. In contrast, no harmonic analysis was conducted for measured salinity values and, as a result, the meteorological effects have not been removed. The meteorological effects are assumed to consist of wind only; pressure anomalies were not considered. Therefore, in the simulation of salinity, the wind distribution over the grid must also be specified. Since this represents an additional input, salinity simulations were considered after all hydrodynamic simulation work had been completed. The hydrodynamics were considered first on the global and subsequently on a refined grid encompassing the Pascagoula Channel.

e. In Part VIII the 20-25 September 1980 period is studied in detail in order to identify a suitable time for calibration. The first five days (20-24 September) were selected as the calibration period. In Part IX detailed data for the period 12-16 June 1980 are presented as a separate verification period.

f. Global grid hydrodynamics are presented in Part X. Bottom friction mechanics are calibrated for the 20-24 September period and subsequently verified for the 12-16 June 1980 period. A hypothetical regional dredge plan involving increasing the size of Sand Island was considered by modifying the depth field in the vicinity of this feature in the global grid. Hydrodynamics for the 20-24 September 1980 period were simulated. By comparing the flow structure with the Sand Island complex in place with the original flow structure it was possible to directly determine the extent of influence of this type of change within the global grid.

g. The methodology to be employed in constructing refined grids around alternative navigation channel projects is developed in Part XI along with the development of a refined grid around the Pascagoula Ship Channel.

h. Refined grid hydrodynamics are presented in Part XII. Bottom friction mechanics calibrated and verified on the global grid were employed in a simulation of the 20-24 September 1980 period. Water surface elevations developed in the global grid were used to drive the refined grid boundary.

i. All salinity simulation work is presented in Part XIII. The 20-24 September 1980 period was considered. Wind speed and direction were specified as meteorological inputs. A constant drag coefficient of 0.001 was employed to develop the surface wind stress, and the friction mechanism previously developed was used to implement bottom stress. Simulation results for both the Flux-Corrected Transport and the Three Time Level Explicit schemes are presented for the global grid. Effective dispersion coefficients in each coordinate direction were calibrated. The Flux-Corrected Transport global grid salinity levels and water surface elevation saved at the boundary of the refined grid were used to supply the boundary conditions for a Flux-Corrected Transport simulation on the refined grid. Previously calibrated global grid effective dispersion coefficients were used in the refined grid simulation.

j. Study conclusions and recommendations for additional simulation work are presented in Part XIV. The procedures for constructing the input dataset for the Pascagoula Channel refined grid are outlined in Appendix A. This appendix is intended to provide a guide for District use in developing refined grids encompassing the Biloxi and Gulfport Ship Channels. A general tide generation program is documented in Appendix B. This program was used to generate the predicted tide based on the five major constituents and compare the predicted tide levels with the unfiltered and filtered water levels and currents at each gaging station. In addition, the tide generation portion of the program was incorporated within WIFM in order to generate water surface elevations at the boundary of the global grid. A cubic polynominal feathering technique is presented in Appendix C in order to smoothly transition from the zero elevation and velocity state to the predicted tide levels on the boundary. In order to efficiently specify linearized advection conditions around barrier islands, subroutine ADVBAR was developed as documented in Appendix D and incorporated within WIFM.

4. In the numerical work presented in this report a nested grid modelling philosophy is utilized. Simulation results over the outer nest are used to provide the boundary conditions for the next inner nest. The nesting is taken to level two (GTM drives WIFM global grid, which drives WIFM refined grid). Inherent in this approach is the premise that changes made on the inner grid nest do not cause hydrodynamic and/or salinity fluctuations which propagate to the boundary of the inner grid nest, thereby destroying the integrity of boundary values. As part of this study, in order to demonstrate the validity of this nested grid approach, the region of extent of fluctuations in hydrodynamics and salinity generated by changes in the global grid and refined grids was investigated. Prior to this study, the region of extent of navigation channel induced changes on flow structure was not known. Thus

it was not known whether contemplated deepening and widening alterations for the Biloxi Ship Channel might influence Pascagoula Channel conditions and vice versa. A major concern was that to study any one single channel alteration an extremely large refined grid encompassing all navigation channels would need to be employed. The numerical work presented was focused to address these issues.

PART II: DATA COLLECTION PROGRAM ESTABLISHMENT

5. WES Wave Dynamics Division personnel participated in a series of meetings held at WES with the Mobile District and their consultants to develop prototype data collection requirements for calibration and verification of the numerical model. Preliminary meetings were conducted in March and April 1979 prior to formal study authorization. In March 1980, station locations and data collection procedures were finalized.

Raytheon Ocean Systems Program

6. Raytheon Ocean Systems collected oceanographic and meteorological data over the period 23 April through 20 October 1980. Approximately 40 current meters and 18 conductivity-temperature instruments were deployed among the 21 stations shown in Figure II-1. Wind speed and direction, air temperature, and air pressure were measured at the five meteorological stations shown in Figure II-2. Bottom pressure measurements were recorded at the three deep-sea sites shown in Figure II-3. Salinity and temperature depth profiles were acquired at three-week intervals for the stations shown in Figure II-4. Hydrographic surveys of the barrier island passes, major navigation channels, and bay passes as shown in Figure II-5 were conducted during the period 23 June through 11 July 1980.

7. Deployment procedures, quality control, data reduction, instrument specifications, and data return are as reported by Raytheon Ocean Systems (1981).

NOAA Data Collection Program

8. NOAA and their contractors obtained tidal elevation data over the April-November 1980 period at the stations shown in Figure II-3. Six-minute and hourly data were edited and furnished to WES on magnetic tape. Tide gage reference levels were connected to NGVD (1929) to provide for a consistent geodetic reference. The relations between mean lower low water (MLLW) and NGVD (1929) as well as the exact station locations are shown in Table II-1.

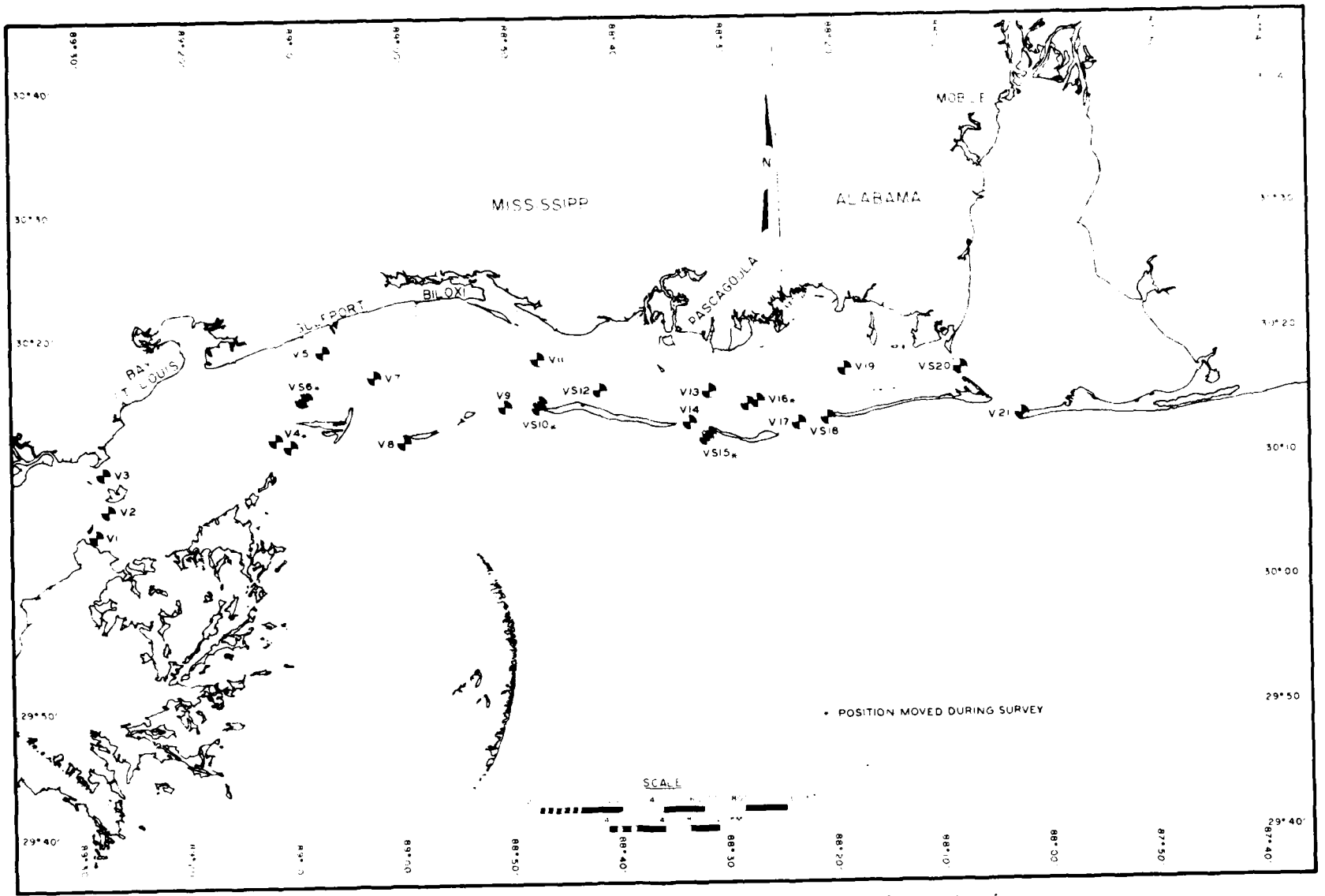

Figure II-1. Mississippi Sound instantaneous data stations
VS = current velocity and conductivity/temperature
V = current velocity

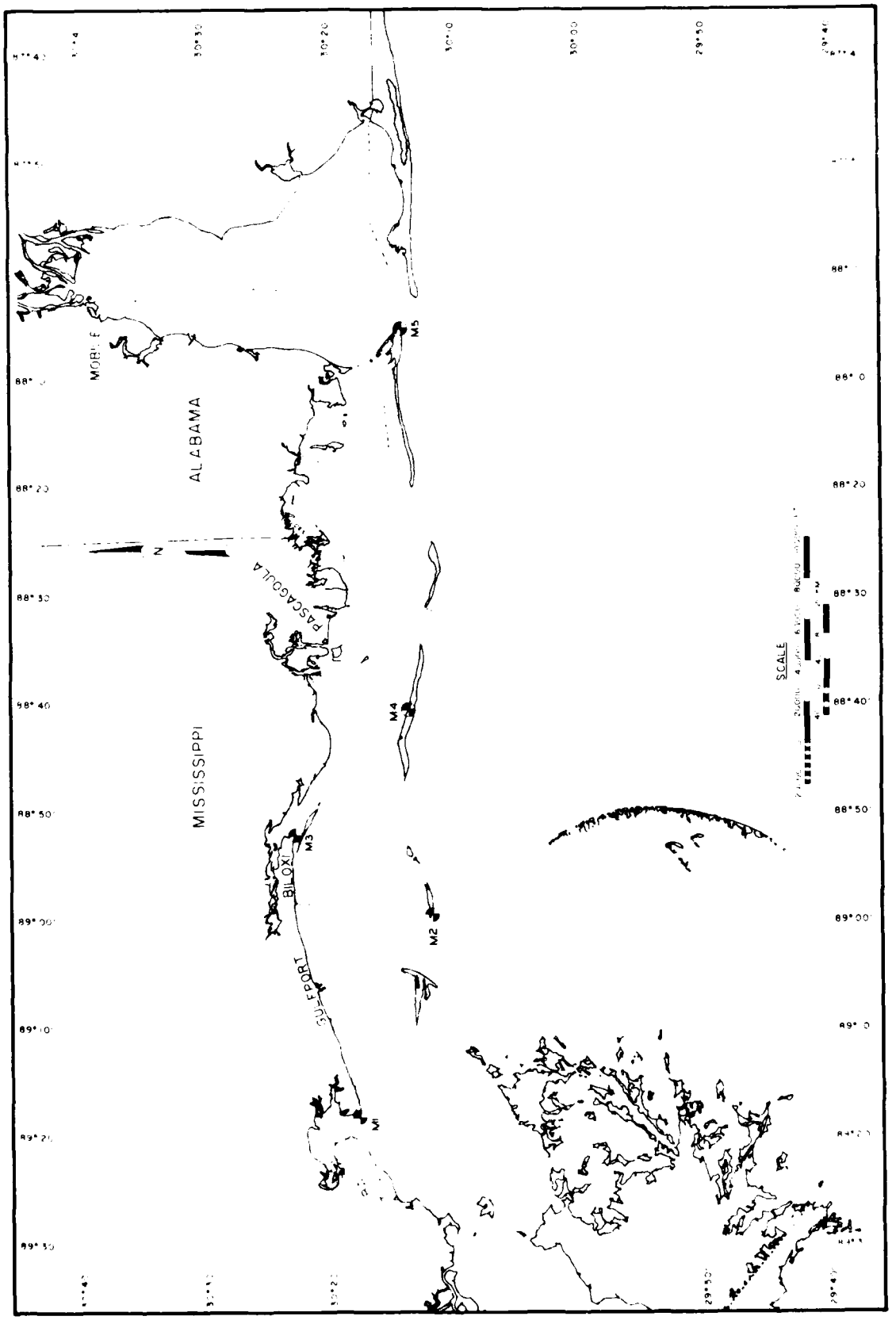

Figure II-2. Mississipi Sound meteorological stations

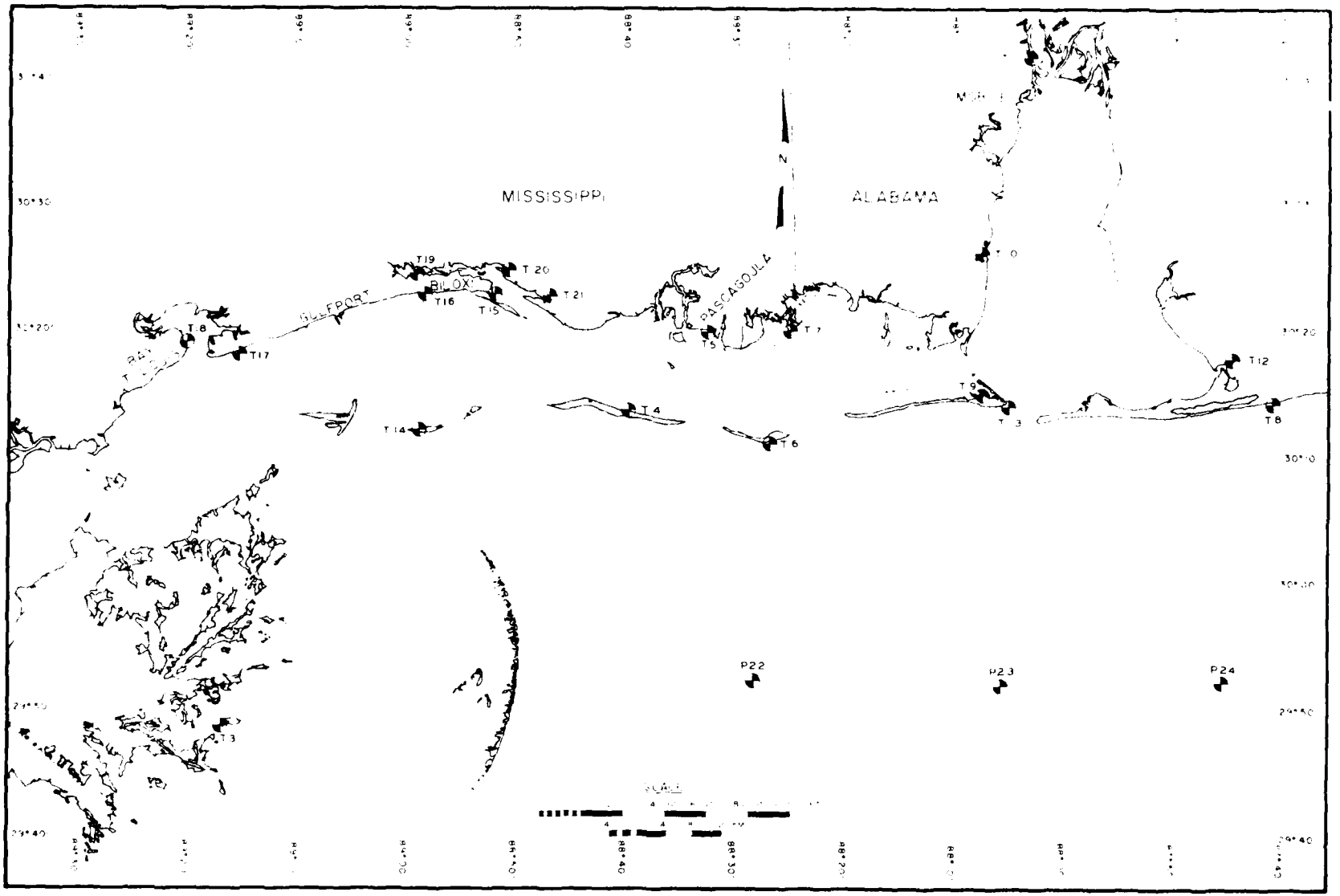

Figure II-3. Mississippi water surface elevation stations
T = NOAA tide gage (gages T1 and T2 are not shown)
P = deep sea pressure gage

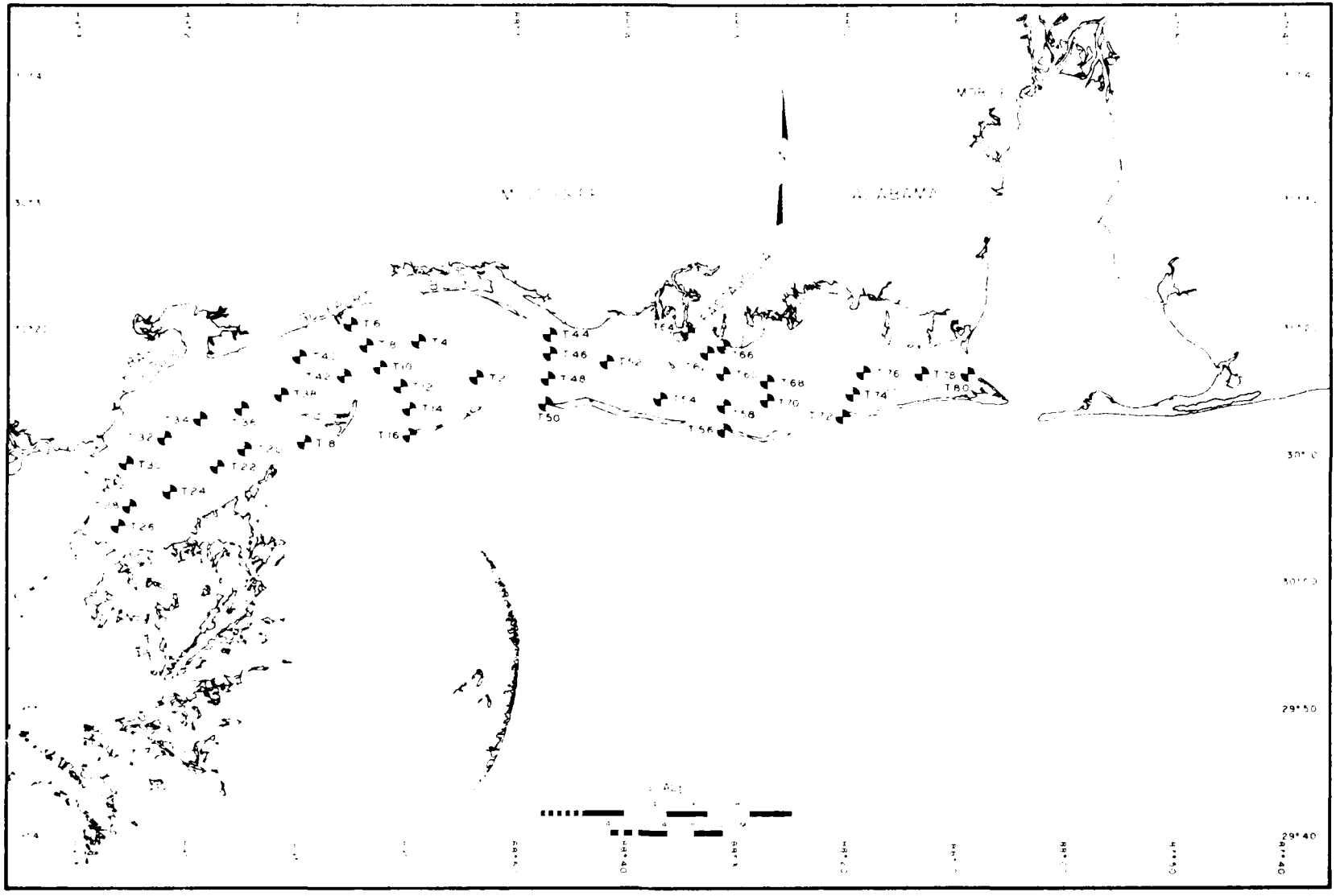

Figure II-4. Mississippi Sound salinity transect stations

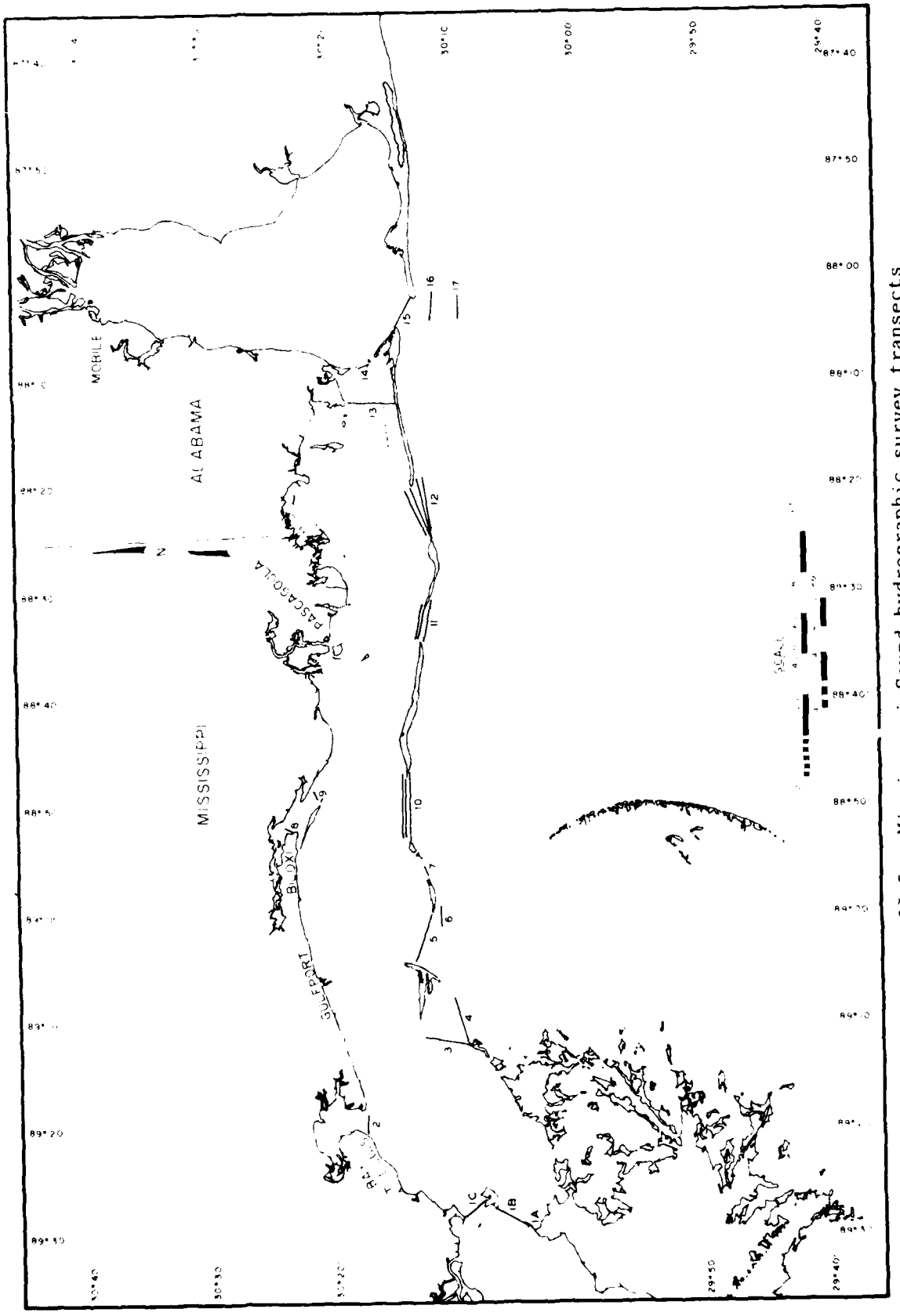

Figure II-5. Mississippi Sound hydrographic survey transects

Table II-1

NOAA Tide Station Locations

Gage No.	Station No.	Mean Lower Low Water ft*	Latitude (N)	Longitude (W)	Location
T8	873-1269	-0.29	30°14.9	87°40.1	Gulf Shores, AL
T12	873-1952	-0.21	30°18.2	87°44.1	Bon Secour, AL
T13	873-5184	(-0.29)**	30°15.0	88°04.5	Dauphin Island, AL
T10	873-5523	-0.24	30°26.6	88°06.8	Fowl River, AL
T9	873-5587	-0.40	30°15.5	88°06.8	North Point, AL
T11	873-7048	(-0.32)**	30°42.3	88°02.4	Mobile, AL
T7	874-0199	-0.24	30°20.5	88°24.4	Grand Batture Island, MS
T6	874-0405	-0.26	30°12.2	88°26.5	Petit Bois Island, MS
T5	874-1196	-0.30	30°20.4	88°32.0	Pascagoula, MS
T4	874-2221	-0.29	30°14.1	88°39.2	Horn Island, MS
T21	874-3081	-0.44	30°23.2	88°46.4	Davis Bayou, MS
T20	874-3495	(-0.40)**	30°25.2	88°49.7	Old Fort Bayou, MS
T15	874-3735	-0.36	30°23.4	88°51.4	Cadet Point, MS
T16	874-4586	-0.42	30°23.3	88°57.8	Broadwater Marina, MS
T19	874-4671	(-0.40)**	30°24.8	88°58.5	Popps Ferry Bridge, MS
T14	874-4756	-0.28	30°12.7	88°58.3	Ship Island, MS
T17	874-6819	-0.39	30°18.6	88°14.7	Pass Christian, MS
T18	874-7437	-0.27	30°19.5	89°19.5	Bay Waveland, MS
T22	874-9704	(-0.27)**	30°14.7	89°36.8	Pearl River at Burlington, MS
T1	876-0412	(-0.28)**	29°12.3	89°02.2	North Pass, LA†
T2	876-0596	(-0.28)**	29°29.6	89°10.4	Breton Island, LA†
T3	876-0742	(-0.28)**	29°49.4	89°16.2	Comfort Island, LA

* MLLW referenced to NGVD.
** Approximated from nearby stations.
† Not shown in Figure II-3.

PART III: PROTOTYPE DATA ANALYSIS

9. A harmonic analysis was performed on both water surface elevation and current data. The analysis techniques are presented in detail by Outlaw (1983). We outline briefly the techniques and results of the analysis for water surface elevations and currents in turn below.

Water Surface Elevations

10. The harmonic analysis for surface elevation tidal constituents was conducted for 22 NOAA tidal elevation stations and three Raytheon pressure cells employing hourly data. Station numbers and locations are as shown in Table II-1. The NOAA stations are representative of tidal elevations in the nearshore region and along the Mississippi Sound barrier islands. The pressure cell data are representative of the tide in the Gulf approximately 27 miles* south of the barrier islands.

11. The harmonic analysis included:

a. Editing to remove data spikes, insertion of missing data, and subtraction of the mean from the data record.

b. Filtering to remove high and low frequency trends from the data.

c. Harmonic analysis for tidal constituents.

The NOAA surface elevation data had been edited by NOAA and was continuous over the record length. During the analysis, pressure cell data were converted to surface elevation and corrected for barometric pressure changes prior to removing the mean.

12. A digital band-pass filter was applied to eliminate frequencies in the data outside the semidiurnal to diurnal tidal frequency range.

13. In the harmonic analysis, the tidal elevation at a given station is represented as follows:

$$h(t) = H_o + \sum_{i=1}^{n} f_i H_i \cos\left(\frac{2\pi t}{T_i} + (V_o + u)_i - \kappa_i\right)$$

---

* A table of factors for converting non-SI units of measurement to SI (metric) units is presented on page 12.

where

$h(t)$ = tidal elevation as a function of time

t = time

H_o = mean of the filtered data record

f_i = node factor for constituent i

$(V_o + u)_i$ = equilibrium argument for constituent i

T_i = period for constituent i

n = number of constituents considered

H_i = mean amplitude for constituent i

κ_i = local epoch for constituent i

The constituents included in the analysis and their periods are:

Harmonic Constituent	Symbol	Period, hr
Principal lunar diurnal	O1	25.82
Lunisolar diurnal	K1	23.94
Principal solar diurnal	P1	24.07
Smaller lunar elliptic	M1	24.84
Small lunar elliptic	J1	23.10
Larger lunar elliptic	Q1	26.87
Principal lunar	M2	12.42
Principal solar	S2	12.00
Larger lunar elliptic	N2	12.66

14. The mean amplitude, H_i, and local epoch, κ_i are determined by minimizing the variance between the filtered record and the predicted record given in the equation above.

15. Mean elevations of the NOAA Data Record relative to mean lower low water are given in Table III-1. The constituent amplitude and phases are presented in Tables III-2 and III-3, respectively. The length of the data record and the root mean square (RMS) error are given in Table III-4. The principal tidal constituents are the diurnal constituents O1, K1, P1, and the semi-diurnal constituents M2 and S2.

Currents

16. The harmonic analysis for currents was conducted for all observed data separately for the east-west and north-south components. In this manner analyzed current components correspond in orientation to the numerical model current components thereby facilitating comparisons.

Table III-1

Mean Elevation of Observed NOAA Data Record

Relative to Mean Lower Low Water

Station*	Elevation, ft
873-1269	0.71
873-1952	0.69
873-5184	--
873-5523	0.73
873-5587	0.96
873-7048	0.85
874-0199	0.85
874-0405	0.88
874-1196	0.88
874-2221	0.90
874-3081	1.07
874-3495	--
874-3735	1.01
874-4586	1.04
874-4671	--
874-4756	0.90
874-6819	0.99
874-7437	0.87
874-9704	--
876-0412	0.56
876-0595	0.71
876-0742	0.92

* Refer to Table II-1 for T designations used in Figure II-3.

Table III-2

Surface Elevation Mean Amplitude (ft)

Station	Constituent								
	O1	K1	P1	M1	J1	Q1	M2	S2	N2
P22	0.46	0.47	0.15	0.01	0.02	0.11	0.09	0.05	0.02
P23	0.46	0.48	0.15	0.01	0.02	0.10	0.09	0.05	0.02
P24	0.47	0.47	0.14	0.02	0.02	0.12	0.09	0.06	0.02
873-1269*	0.45	0.46	0.16	0.01	0.02	0.12	0.10	0.05	0.02
873-1952	0.48	0.48	0.13	0.01	0.02	0.11	0.07	0.01	0.01
873-5184	0.40	0.41	0.13	0.01	0.03	0.11	0.04	0.02	0.01
873-5523	0.48	0.48	0.16	0.03	0.01	0.11	0.08	0.02	0.02
873-5587	0.51	0.51	0.15	0.02	0.03	0.12	0.10	0.04	0.03
873-7048	0.49	0.47	0.16	0.01	0.02	0.12	0.08	0.05	0.02
874-0199	0.48	0.48	0.13	0.02	0.02	0.10	0.09	0.05	0.02
874-0405	0.49	0.49	0.14	0.01	0.03	0.11	0.09	0.04	0.02
874-1196	0.49	0.47	0.14	0.02	0.03	0.12	0.09	0.05	0.02
874-2221	0.51	0.51	0.15	0.02	0.02	0.12	0.09	0.05	0.02
874-2981	0.54	0.52	0.14	0.03	0.03	0.13	0.11	0.08	0.03
874-3495	0.55	0.53	0.14	0.03	0.03	0.14	0.12	0.09	0.04
874-3735	0.54	0.54	0.13	0.02	0.02	0.13	0.11	0.08	0.03
874-4586	0.55	0.53	0.14	0.03	0.03	0.14	0.11	0.08	0.03
874-4671	0.56	0.57	0.13	0.02	0.03	0.13	0.13	0.10	0.04
874-4756	0.53	0.51	0.15	0.03	0.02	0.14	0.11	0.05	0.03
874-6819	0.54	0.55	0.15	0.02	0.02	0.13	0.11	0.08	0.03
874-7437	0.53	0.57	0.13	0.02	0.01	0.12	0.10	0.08	0.03
874-9704	0.34	0.38	0.13	0.02	0.03	0.10	0.06	0.04	0.02
876-0412	0.36	0.36	0.14	0.00	0.02	0.07	0.04	0.03	0.01
876-0595	0.42	0.44	0.13	0.01	0.01	0.09	0.05	0.02	0.01
876-0742	0.49	0.52	0.15	0.02	0.01	0.12	0.09	0.06	0.02

* Refer to Table II-1 for T designations used in Figure II-3.

Table III-3

Surface Elevation Local Epoch (deg)

Station	Constituent								
	O1	K1	P1	M1	J1	Q1	M2	S2	N2
P22	299.1	309.2	305.8	351.5	303.7	286.8	320.6	328.6	345.8
P23	297.5	308.1	304.3	349.7	289.7	283.7	312.0	321.9	330.3
P24	296.4	309.9	300.5	338.0	320.5	281.1	311.0	321.5	329.4
873-1269*	283.8	293.6	292.6	348.9	268.8	266.0	278.5	285.4	297.8
873-1952	317.1	326.9	331.3	54.4	332.3	306.6	356.9	9.6	8.0
873-5184	313.3	325.7	326.2	332.8	281.3	293.3	321.0	309.6	339.1
873-5523	323.8	334.9	347.8	22.2	250.6	320.8	24.7	55.1	55.6
873-5587	300.1	307.9	308.4	356.2	299.5	290.6	332.8	332.0	347.4
873-7048	330.9	348.5	350.8	27.7	327.3	319.8	45.6	75.2	76.2
874-0199	297.7	307.9	313.7	9.4	294.1	285.0	323.2	341.0	354.3
874-0405	295.4	305.2	304.2	356.5	287.3	280.8	320.8	327.4	346.0
874-1196	295.9	306.6	309.4	359.8	284.3	283.7	323.6	339.5	350.4
874-2221	299.1	309.0	310.5	356.0	288.1	288.1	334.0	349.3	359.4
874-3081	307.6	322.4	328.9	353.4	290.0	297.3	3.7	30.5	37.0
874-3495	306.8	322.3	329.0	350.3	267.7	293.5	4.7	30.3	39.2
874-3735	303.6	317.3	324.3	351.4	266.0	288.1	355.3	24.5	21.1
874-4586	300.0	314.9	319.9	340.5	255.0	286.6	349.2	11.0	16.6
874-4671	315.1	329.8	336.0	7.4	278.4	295.2	26.1	60.3	59.7
874-4756	299.4	311.1	309.8	4.5	266.3	297.6	344.7	2.3	354.5
874-6819	310.1	327.0	334.5	355.5	245.7	299.7	15.0	29.4	43.8
874-7437	320.6	336.4	354.4	8.2	195.7	305.0	35.1	49.8	67.4
874-9704	358.8	16.9	353.9	62.8	318.4	344.0	119.8	133.8	129.8
876-0412	286.1	297.6	289.3	356.9	310.1	270.1	295.5	299.5	320.2
876-0595	302.5	312.4	316.7	21.2	282.9	295.7	1.3	14.2	30.3
876-0742	310.3	323.8	335.4	6.6	245.8	301.0	22.2	32.4	38.3

* Refer to Table II-1 for T designations used in Figure II-3.

Table III-4

Surface Elevation Record Length and Root Mean Square (RMS) Error

Station	Analysis Record Length, days	RMS Error, ft
873-1269*	182	0.06
873-1952	182	0.13
873-5184	182	0.09
873-5523	141	0.12
873-5587	182	0.10
873-7048	182	0.15
874-0199	182	0.10
874-0405	182	0.08
874-1196	182	0.10
874-2221	182	0.09
874-3081	182	0.16
874-3495	182	0.17
874-3735	182	0.16
874-4586	182	0.16
874-4671	182	0.18
874-4756	122	0.10
874-6819	182	0.16
874-7437	182	0.17
874-9704	182	0.17
876-0412	182	0.07
876-0595	146	0.06
876-0742	182	0.11
P22	182	0.05
P23	182	0.05
P24	159	0.09

* Refer to Table II-1 for T designations used in Figure II-3.

17. The harmonic analysis included:

a. Editing of the current data and selecting periods which contained the longest continuous data return.

b. Filtering to remove high and low frequency trends.

c. Determination of the tidal constituents for both current components.

18. The same harmonic analysis procedures as outlined previously for water surface elevations were employed in the current component analysis. Velocity component means are given in Table III-5. Amplitude and phases for each component are given in Tables III-6 through III-9. In these tables, S, M, and B denote surface, middepth, and bottom meter locations, respectively. At stations where only one meter is located it is denoted by M.

Table III-5

Station Mean Velocity Components

Station	1980 Analysis Period Start	End	Mean, fps North/South	East/West
V1-M*	9 Apr	17 Jun	0.01 N	0.16 E
V2-M*	9 Apr	17 Jun	0.01 S	0.11 E
V3-S*	20 Apr	17 Jun	0.00	0.02 E
V3-B	20 Apr	17 Jun	0.05 N	0.03 E
V4-S*	9 Apr	17 Jun	0.02 N	0.02 W
V4-B	9 Apr	17 Jun	0.08 N	0.00
V5-M	20 Apr	12 Jun	0.04 N	0.05 E
V6-S*,**	10 Apr	17 Jun	0.01 N	0.12 E
V6-B**	10 Apr	14 Jun	0.04 N	0.05 E
V7-S	10 Apr	17 Jun	0.02 N	0.12 E
V7-M*	20 Sep	21 Oct	0.01 S	0.02 E
V7-B	2 May	17 Jun	0.04 N	0.01 E
V8-S	10 Apr	17 Jun	0.08 N	0.13 W
V8-M*	10 Apr	17 Jun	0.08 N	0.18 W
V8-B	2 May	30 May	0.05 N	0.03 W
V9-S*	11 Apr	19 Jun	0.14 S	0.06 E
V9-B	2 May	19 Jun	0.00	0.00
V10-S*,**	10 Jul	21 Oct	0.02 S	0.01 E
V10-B**	10 Jul	21 Oct	0.14 N	0.04 E
V11-M*	3 May	15 Jun	0.03 S	0.02 E
V12-S*,**	5 May	19 Jun	0.01 S	0.10 E
V12-B**	16 Apr	19 Jun	0.01 N	0.10 E
V13-S*	11 Apr	20 Jun	0.01 S	0.05 E
V13-B	11 Apr	20 Jun	0.05 N	0.03 E
V14-M*	11 Apr	20 Jun	0.07 S	0.11 E
V15-S**	3 May	20 Jun	0.05 N	0.03 W
V15-M*,**	5 May	20 Jun	0.12 N	0.07 W
V15-B**	16 Apr	20 Jun	0.13 N	0.11 W
V16-S	16 Apr	7 May	--	--
V16-B	16 Apr	1 May	--	--
V17-M*	12 Aug	22 Oct	0.02 N	0.00
V18-M*,**	12 Aug	22 Oct	0.02 N	0.07 W
V19-S*	16 Apr	20 Jun	0.06 S	0.06 E
V19-B	16 Apr	20 Jun	0.03 S	0.05 E
V20-M*,**	17 Apr	20 Jun	0.08 N	0.05 W
V21-S	22 Apr	20 Jun	0.51 S	0.33 W
V21-M*	22 Apr	20 Jun	0.34 S	0.19 W
V21-B	22 Apr	15 Jun	0.29 S	0.10 W

* Stations considered in the two-dimensional numerical modeling effort as shown in Figure II-1.

** These stations are designated VS in Figure II-1.

Table III-6

North/South Velocity Component Mean Amplitude (fps)

Station	Constituent							
	O1	K1	M1	J1	Q1	M2	S2	N2
V1-M	0.01	0.04	0.02	0.04	0.06	0.01	0.01	0.02
V2-M	0.04	0.05	0.01	0.01	0.02	0.01	0.01	0.00
V3-S	0.20	0.26	0.02	0.03	0.05	0.06	0.03	0.01
V3-B	0.25	0.31	0.02	0.02	0.06	0.04	0.05	0.01
V4-S	0.33	0.44	0.03	0.05	0.08	0.05	0.05	0.01
V4-B	0.19	0.27	0.01	0.01	0.05	0.06	0.03	0.01
V5-M	0.08	0.06	0.01	0.03	0.02	0.02	0.04	0.01
V6-S	0.04	0.03	0.01	0.02	0.00	0.01	0.02	0.01
V6-B	0.06	0.04	0.02	0.02	0.01	0.03	0.03	0.00
V7-S	0.08	0.10	0.01	0.01	0.02	0.02	0.02	0.01
V7-M	0.08	0.06	0.01	0.03	0.01	0.02	0.01	0.01
V7-B	0.07	0.11	0.03	0.05	0.04	0.02	0.02	0.01
V8-S	0.29	0.36	0.02	0.05	0.09	0.12	0.08	0.03
V8-M	0.17	0.23	0.02	0.01	0.04	0.08	0.05	0.03
V8-B	0.08	0.12	0.03	0.03	0.05	0.02	0.03	0.02
V9-S	0.55	0.69	0.03	0.05	0.13	0.21	0.15	0.07
V9-B	0.38	0.51	0.01	0.03	0.13	0.15	0.06	0.06
V10-S	0.23	0.20	0.02	0.01	0.05	0.08	0.04	0.02
V10-B	0.22	0.18	0.02	0.03	0.04	0.07	0.05	0.01
V11-M	0.09	0.13	0.03	0.02	0.02	0.04	0.03	0.03
V12-S	0.02	0.06	0.01	0.03	0.01	0.02	0.02	0.03
V12-B	0.07	0.07	0.00	0.03	0.01	0.02	0.03	0.02
V13-S	0.11	0.20	0.03	0.02	0.08	0.02	0.05	0.01
V13-B	0.13	0.23	0.03	0.03	0.07	0.03	0.06	0.02
V14-M	0.51	0.61	0.04	0.04	0.14	0.16	0.10	0.04
V15-S	0.34	0.35	0.06	0.05	0.15	0.12	0.07	0.06
V15-M	0.26	0.34	0.03	0.03	0.11	0.07	0.06	0.05
V15-B	0.22	0.28	0.02	0.02	0.06	0.06	0.04	0.01
V17-M	0.22	0.16	0.02	0.03	0.04	0.09	0.05	0.03
V18-M	0.56	0.43	0.07	0.10	0.17	0.31	0.14	0.10
V19-S	0.08	0.10	0.00	0.02	0.04	0.04	0.03	0.01
V19-B	0.06	0.09	0.00	0.01	0.03	0.02	0.02	0.01
V20-M	0.07	0.07	0.01	0.03	0.06	0.03	0.02	0.01
V21-S	0.55	0.72	0.02	0.03	0.07	0.19	0.07	0.05
V21-M	0.34	0.47	0.02	0.04	0.05	0.22	0.06	0.04
V21-B	0.26	0.30	0.04	0.03	0.04	0.21	0.08	0.03

Table III-7

North/South Velocity Component Local Epoch (deg)

Station	Constituent							
	O1	K1	M1	J1	Q1	M2	S2	N2
V1-M	342.3	281.2	58.3	326.4	300.9	160.7	160.2	87.7
V2-M	110.8	112.2	224.2	60.1	55.0	341.5	218.0	301.3
V3-S	126.2	127.1	213.3	282.8	75.1	342.3	275.8	276.0
V3-B	135.1	131.7	210.3	46.6	97.5	328.0	244.7	274.3
V4-S	283.9	284.5	42.7	171.0	253.0	138.4	339.7	75.4
V4-B	279.6	271.3	18.9	359.5	241.2	106.9	10.6	12.6
V5-M	112.0	131.8	242.1	66.1	83.9	255.0	260.2	250.7
V6-S	152.6	150.3	352.8	2.4	139.9	225.8	281.5	157.6
V6-B	140.5	143.6	25.3	17.7	53.3	250.7	239.5	210.9
V7-S	258.4	277.2	24.3	64.1	136.5	324.3	343.5	252.4
V7-M	250.1	229.9	43.9	347.1	255.1	341.6	282.0	255.3
V7-B	216.0	262.4	327.1	312.2	245.8	65.5	291.9	354.6
V8-S	238.7	253.3	9.2	177.4	246.4	56.6	353.4	2.1
V8-M	246.3	241.8	315.4	178.6	225.8	39.3	329.1	336.7
V8-B	274.4	244.7	229.2	302.8	198.5	30.0	356.5	280.5
V9-S	236.0	245.3	350.3	113.9	224.2	52.2	330.2	329.9
V9-B	238.3	249.8	338.0	43.3	219.2	48.3	339.0	341.5
V10-S	239.0	266.8	256.5	162.3	222.0	38.9	350.3	327.7
V10-B	237.4	269.7	284.1	83.9	215.5	43.2	327.3	318.1
V11-M	272.4	231.7	337.6	251.9	324.4	91.0	322.3	90.0
V12-S	156.0	233.4	123.6	19.3	126.9	281.9	314.9	345.4
V12-B	138.6	199.1	143.8	21.7	241.9	233.0	281.3	284.1
V13-S	247.9	250.0	326.5	300.6	214.1	8.6	306.7	348.4
V13-B	262.0	250.2	327.5	4.7	222.5	58.0	315.6	337.9
V14-M	228.8	227.2	322.4	223.0	208.8	27.5	301.1	327.4
V15-S	214.5	221.2	194.7	286.8	191.8	17.7	302.0	290.1
V15-M	232.4	231.5	193.4	230.0	191.7	18.4	291.4	298.7
V15-B	237.4	232.1	147.5	227.7	191.5	29.9	291.9	334.1
V17-M	219.5	228.2	308.6	137.1	214.5	6.0	288.7	264.9
V18-M	210.5	213.8	304.9	176.6	208.2	354.2	262.4	278.1
V19-S	194.2	220.2	7.4	298.4	199.2	332.2	292.1	251.1
V19-B	205.9	238.3	333.1	331.1	211.0	323.0	287.3	290.4
V20-M	248.9	249.4	184.4	301.6	227.3	13.7	313.7	309.5
V21-S	250.9	250.4	147.0	228.3	193.6	51.2	330.9	297.9
V21-M	234.8	231.2	346.0	92.4	159.3	40.8	5.2	254.8
V21-B	236.8	219.8	315.7	136.0	171.9	20.5	15.9	293.3

Table III-8

East/West Velocity Component Mean Amplitude (fps)

Station	Constituent							
	O1	K1	M1	J1	Q1	M2	S2	N2
V1-M	0.35	0.44	0.02	0.03	0.10	0.08	0.07	0.04
V2-M	0.36	0.44	0.03	0.05	0.08	0.07	0.07	0.03
V3-S	0.48	0.63	0.04	0.01	0.13	0.08	0.11	0.03
V3-B	0.41	0.54	0.03	0.02	0.11	0.08	0.09	0.03
V4-S	0.47	0.62	0.02	0.02	0.14	0.11	0.07	0.02
V4-B	0.35	0.45	0.01	0.04	0.09	0.11	0.04	0.02
V5-M	0.24	0.30	0.10	0.03	0.08	0.08	0.04	0.03
V6-S	0.27	0.36	0.02	0.04	0.03	0.08	0.03	0.01
V6-B	0.19	0.26	0.02	0.02	0.03	0.05	0.01	0.01
V7-S	0.28	0.34	0.03	0.02	0.06	0.07	0.05	0.00
V7-M	0.21	0.15	0.04	0.03	0.08	0.05	0.03	0.01
V7-B	0.20	0.24	0.02	0.04	0.05	0.07	0.02	0.03
V8-S	0.42	0.43	0.00	0.08	0.06	0.19	0.13	0.03
V8-M	0.40	0.40	0.02	0.04	0.13	0.16	0.10	0.03
V8-B	0.20	0.26	0.03	0.06	0.07	0.13	0.07	0.02
V9-S	0.07	0.09	0.02	0.03	0.02	0.04	0.04	0.02
V9-B	0.06	0.09	0.01	0.02	0.04	0.03	0.	0.02
V10-S	0.23	0.19	0.02	0.01	0.05	0.07	0.03	0.02
V10-B	0.25	0.20	0.03	0.01	0.05	0.08	0.05	0.01
V11-M	0.08	0.06	0.03	0.00	0.04	0.01	0.01	0.02
V12-S	0.12	0.12	0.01	0.03	0.02	0.03	0.03	0.02
V12-B	0.08	0.12	0.02	0.02	0.03	0.02	0.02	0.01
V13-S	0.08	0.11	0.02	0.01	0.03	0.01	0.01	0.01
V13-B	0.03	0.07	0.01	0.01	0.02	0.01	0.02	0.01
V14-M	0.11	0.16	0.01	0.01	0.04	0.01	0.02	0.02
V15-S	0.06	0.06	0.01	0.01	0.02	0.01	0.01	0.01
V15-M	0.05	0.01	0.01	0.00	0.02	0.01	0.01	0.01
V15-B	0.04	0.06	0.01	0.02	0.02	0.02	0.02	0.02
V17-M	0.04	0.02	0.01	0.00	0.01	0.02	0.02	0.00
V18-M	0.28	0.20	0.03	0.04	0.07	0.14	0.08	0.04
V19-S	0.16	0.19	0.01	0.04	0.04	0.03	0.03	0.01
V19-B	0.13	0.14	0.01	0.03	0.04	0.02	0.02	0.00
V20-M	0.29	0.33	0.01	0.04	0.10	0.09	0.02	0.02
V21-S	0.30	0.39	0.06	0.06	0.01	0.10	0.05	0.03
V21-M	0.22	0.28	0.02	0.01	0.04	0.14	0.04	0.02
V21-B	0.12	0.13	0.01	0.01	0.02	0.09	0.04	0.01

Table III-9

East/West Velocity Component Local Epoch (deg)

Station	Constituent							
	O1	K1	M1	J1	O1	M2	S2	N2
V1-M	136.1	124.4	263.8	350.8	101.3	344.9	240.4	281.5
V2-M	126.7	126.7	230.6	16.0	108.8	340.5	238.6	275.4
V3-S	129.4	126.0	189.0	84.2	105.8	316.9	225.9	289.5
V3-B	126.1	126.0	196.7	54.3	99.4	322.2	231.5	279.7
V4-S	100.1	100.7	212.5	301.6	65.4	286.2	186.3	237.7
V4-B	106.0	91.7	119.4	220.5	50.3	284.8	198.5	178.8
V5-M	97.3	95.1	350.7	274.2	56.4	282.6	178.2	198.5
V6-S	109.1	104.1	229.2	19.8	63.0	291.0	216.5	278.9
V6-B	105.1	103.4	240.9	302.7	1.0	289.6	228.9	286.2
V7-S	96.1	104.8	218.5	14.3	89.1	284.1	199.3	53.0
V7-M	93.8	107.2	154.9	249.7	53.1	271.7	177.4	141.6
V7-B	95.6	95.9	155.7	120.2	93.9	272.1	199.1	209.8
V8-S	38.9	50.2	342.4	251.3	28.6	217.9	153.4	161.7
V8-M	43.1	51.4	181.8	322.1	50.5	212.2	152.0	125.9
V8-B	28.4	41.4	296.5	1.1	349.6	195.7	142.6	79.2
V9-S	56.8	45.8	15.0	172.3	344.7	224.2	141.5	80.4
V9-B	53.0	68.1	25.3	113.0	36.0	235.6	144.6	155.6
V10-S	240.2	256.6	260.0	348.0	194.6	33.6	292.3	331.1
V10-B	235.5	263.4	279.6	115.8	221.5	42.5	331.4	316.3
V11-M	4.8	326.2	91.1	357.7	65.0	295.9	39.0	255.8
V12-S	330.3	347.1	58.1	192.1	347.7	204.7	94.0	136.1
V12-B	340.8	332.1	44.2	118.7	243.6	145.4	90.0	30.8
V13-S	331.3	312.2	49.6	174.4	253.9	219.7	65.9	141.1
V13-B	328.9	331.7	264.0	171.4	314.8	170.7	91.8	106.2
V14-M	246.8	245.3	27.5	231.4	241.3	78.2	324.8	318.7
V15-S	319.8	297.5	8.0	81.1	354.3	275.2	245.6	263.0
V15-M	285.2	292.0	292.9	53.3	309.2	113.4	313.6	279.1
V15-B	331.3	38.6	115.2	203.7	320.2	132.2	23.5	291.2
V17-M	4.4	306.0	67.5	328.4	76.4	151.0	95.4	64.1
V18-M	28.7	30.3	120.4	356.0	29.2	169.5	81.1	91.8
V19-S	277.7	266.2	297.0	343.5	262.1	20.0	340.7	341.2
V19-B	266.1	258.7	253.6	340.2	243.9	10.3	351.3	3.6
V20-M	286.8	285.7	260.4	307.0	243.4	94.0	41.9	23.0
V21-S	241.1	247.6	23.7	162.0	185.4	36.0	323.6	305.2
V21-M	241.7	228.5	330.0	6.5	157.0	45.7	47.0	317.3
V21-B	240.5	221.3	269.5	41.2	182.0	31.5	45.4	8.7

PART IV: GULF TIDE MODEL DEVELOPMENT AND RESULTS

19. Consider the depth integrated linearized equations of motion and continuity for a homogeneous and incompressible fluid in spherical coordinates. Reid and Whitaker (1981) have employed alternating direction implicit finite difference approximations to these equations. In an application to the Gulf of Mexico a 15- by 15-minute latitude and longitude grid employing 2228 computational cells has been employed. Wind forcing and stratification effects have not been considered. The tides are forced by direct tide potential and by volume transport (flux) at the Florida Strait and Yucatan Channel.

20. Tidal forcing (flux potential at the two ports and the effective amplitude and phase of the direct tide potential) is determined separately for each of the five major tidal constituents in the Gulf (O_1 , K_1 , P_1 , M_2 , and S_2) by minimizing the sum of the squared errors between the measured constituent amplitude and phase and the model constituent amplitude and phase for all gaging stations. In the original application, Reid and Whitaker considered 20 stations located around the entire Gulf of Mexico. In the least squares analysis, each of the 20 stations was given equal weight. In order to improve results along the northern Gulf coast stretching from Atchafalaya Bay to Pensacola Bay, stations along this coastal segment were weighted more heavily than those occurring outside this segment. The least squares analysis was repeated for all five constituents with the final results for the amplitudes (centimetres) and phases (Greenwich epoch) presented in Tables IV-1 through IV-5 for the O_1 , K_1 , P_1 , M_2 , and S_2 tidal constituents, respectively.

Table IV-1

Least Squares Analysis

Constituent 01

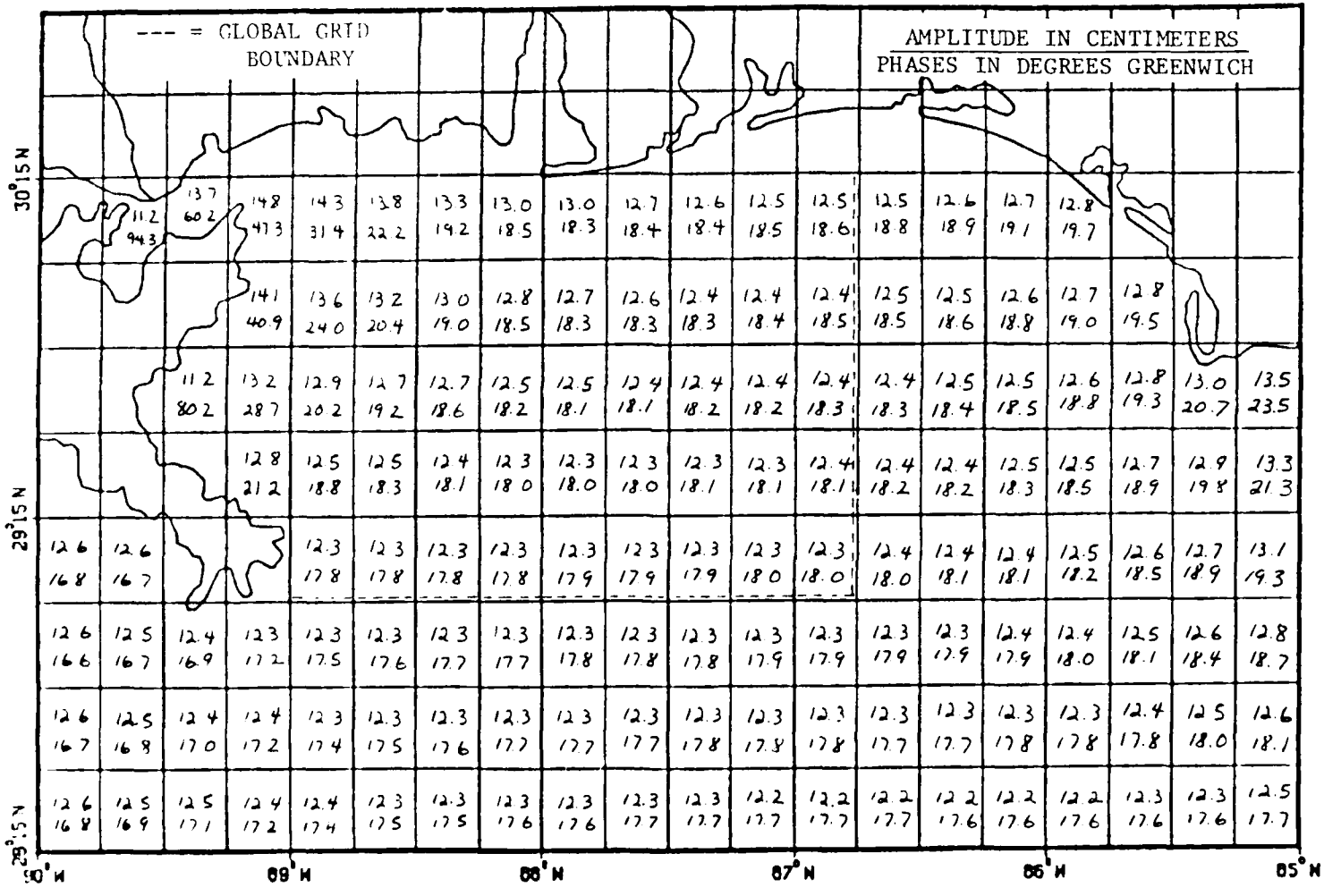

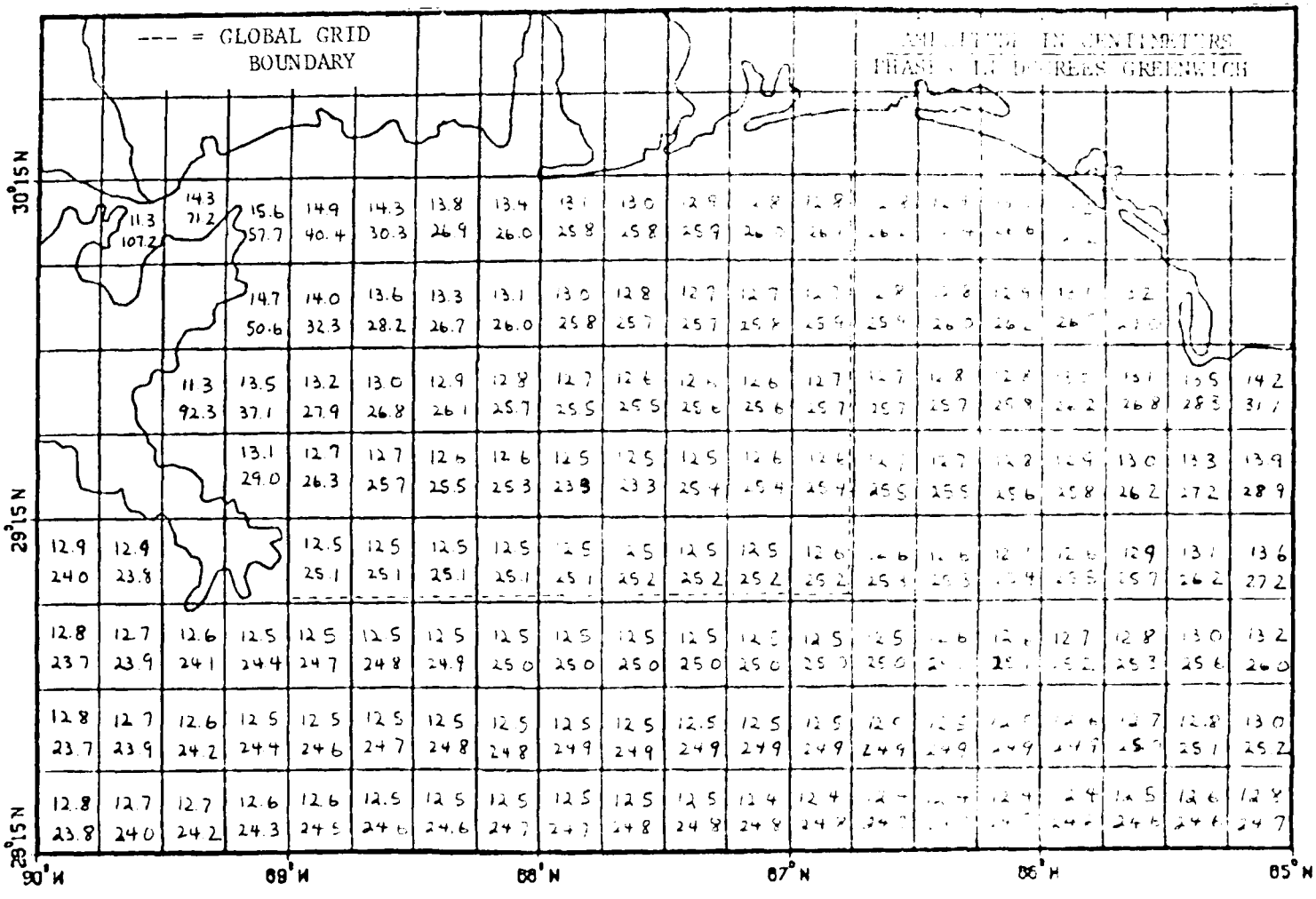
--- = GLOBAL GRID BOUNDARY
AMPLITUDE IN CENTIMETERS
PHASE LAG IN DEGREES GREENWICH
30°15 N
29°15 N
28°15 N
90° W
89° W
88° W
87° W
86° W
85° W

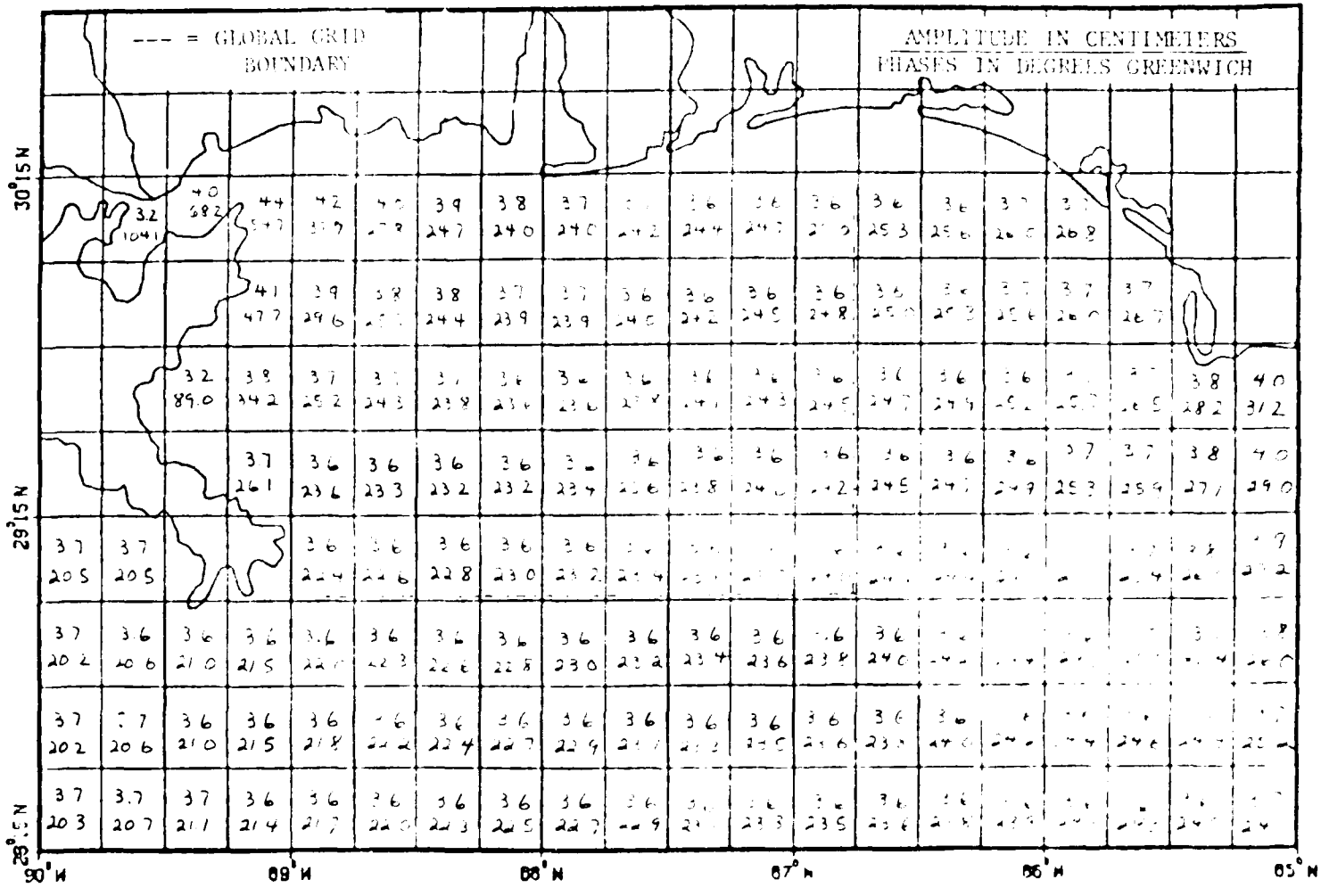
--- = GLOBAL GRID BOUNDARY
AMPLITUDE IN CENTIMETERS
PHASES IN DEGREES GREENWICH
30°15 N
29°15 N
28°15 N
90° W
89° W
88° W
87° W
86° W
85° W

Table IV-4

Least Squares Analysis

Constituent M2

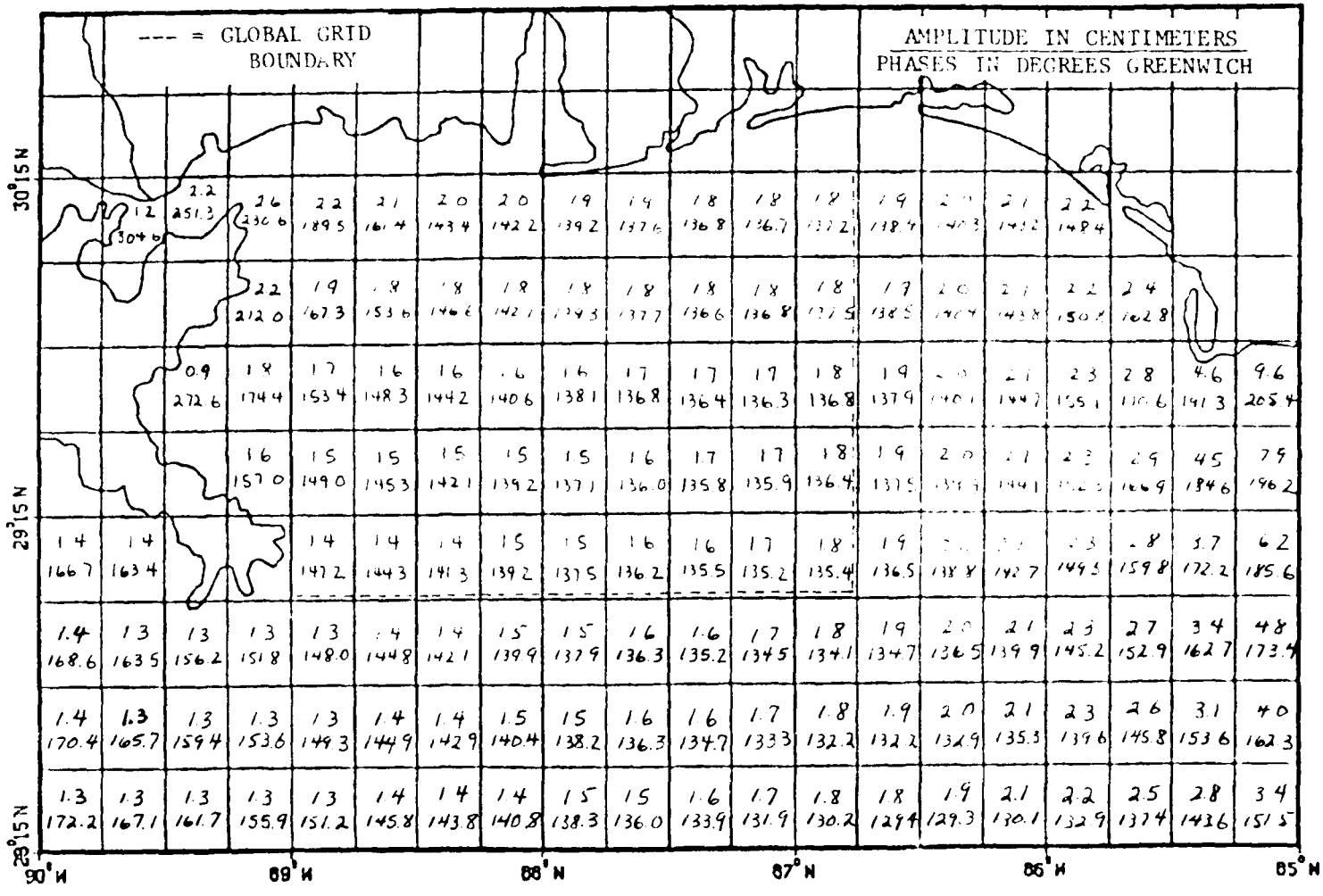

Table IV-5

Least Squares Analysis

Constituent S2

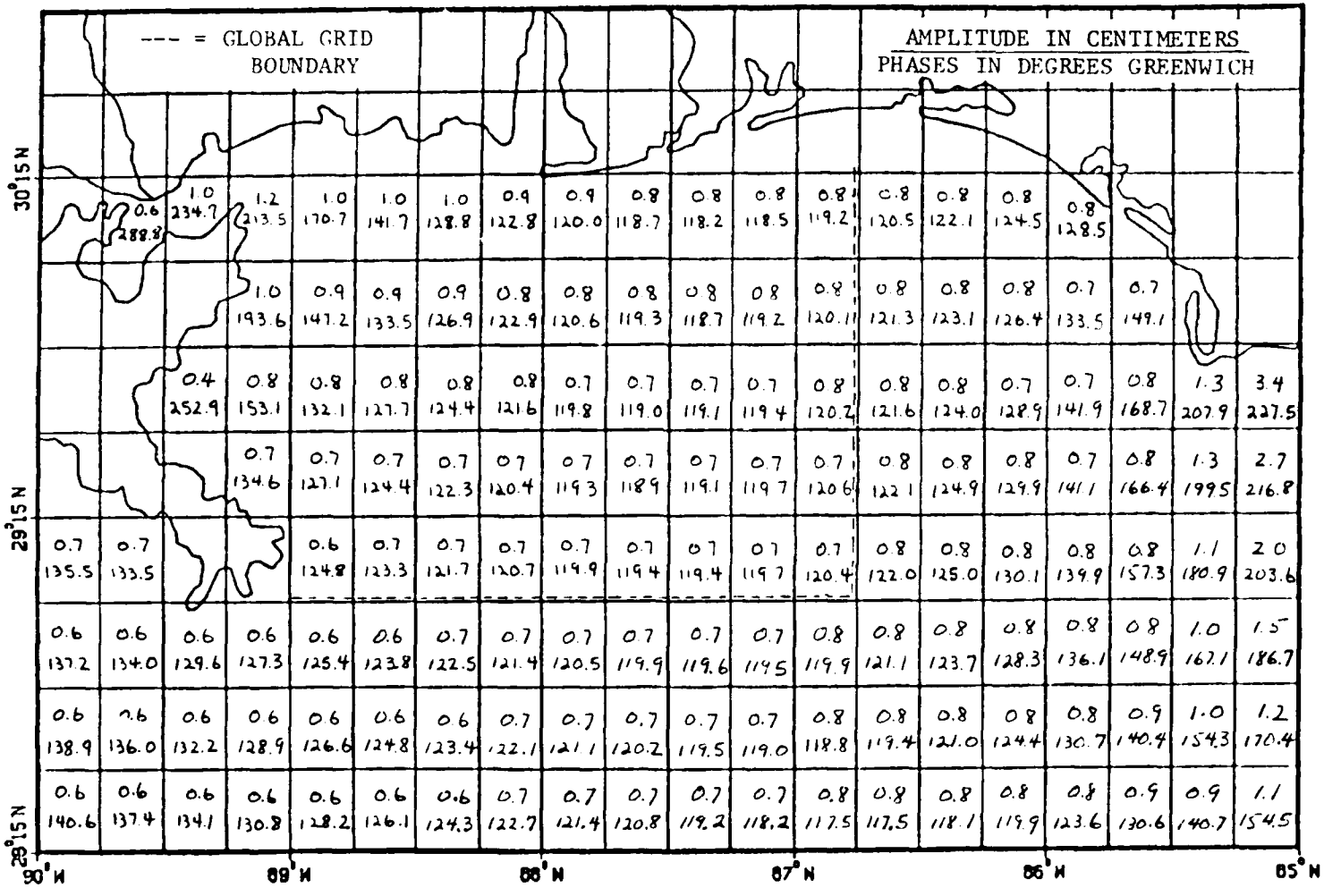

PART V: SALINITY ALGORITHM DEVELOPMENT

21. Salinity is considered as a conservative (passive) constituent. The three-dimensional passive constituent transport equation for laminar flow is presented followed by the modifications necessary for turbulent flow. The turbulent flow equation is depth integrated. The transport equation obtained is then transformed using an exponential stretch. Numerical approximations to the transformed equation are presented followed by the development of relations for the effective dispersion coefficients.

Constituent Transport Equation in Cartesian Coordinates

22. The constituent transport equation is given for laminar flow as

$$\frac{\partial s}{\partial t} + u \frac{\partial s}{\partial x} + v \frac{\partial s}{\partial y} + w \frac{\partial s}{\partial z} = \frac{\partial}{\partial x}\left(D_x \frac{\partial s}{\partial x}\right) + \frac{\partial}{\partial y}\left(D_y \frac{\partial s}{\partial y}\right) + \frac{\partial}{\partial z}\left(D_z \frac{\partial s}{\partial z}\right) \qquad (V.1)$$

where

s ≡ concentration of the material of concern

D_x ≡ molecular diffusion coefficient in the x direction

D_y ≡ molecular diffusion coefficient in the y direction

D_z ≡ molecular diffusion coefficient in the z direction

x,y,z ≡ Cartesian coordinates

u,v,w ≡ velocity components in the x, y, and z directions, respectively

t ≡ time

For a turbulent flow, the eddy dispersion is significantly larger than the molecular diffusion. The following analogous formula holds where time averaging over the time scale of the turbulence has been performed.

$$\frac{\partial s}{\partial t} + u \frac{\partial s}{\partial x} + v \frac{\partial s}{\partial y} + w \frac{\partial s}{\partial z} = \frac{\partial}{\partial x}\left(K_x \frac{\partial s}{\partial x}\right) + \frac{\partial}{\partial y}\left(K_y \frac{\partial s}{\partial y}\right) + \frac{\partial}{\partial z}\left(K_z \frac{\partial s}{\partial z}\right) \qquad (V.2)$$

where K_x, K_y, and K_z are turbulent eddy dispersion coefficients. Equation V.2 may be written in conservation form by adding s times the continuity

equation (namely, zero) to the left-hand side to obtain

$$\frac{\partial s}{\partial t} + \frac{\partial (us)}{\partial x} + \frac{\partial (vs)}{\partial y} + \frac{\partial (ws)}{\partial z} = \frac{\partial}{\partial x}\left(K_x \frac{\partial s}{\partial x}\right) + \frac{\partial}{\partial y}\left(K_y \frac{\partial s}{\partial y}\right) + \frac{\partial}{\partial z}\left(K_z \frac{\partial s}{\partial z}\right) \quad (V.3)$$

This form of the equation is then depth integrated as described in Schmalz (1983a) to obtain:

$$\frac{\partial}{\partial t}(hs) + \frac{\partial}{\partial x}(hus) + \frac{\partial}{\partial y}(hvs) = \frac{\partial}{\partial x}\left(hK_x^* \frac{\partial s}{\partial x}\right) + \frac{\partial}{\partial y}\left(hK_y^* \frac{\partial s}{\partial y}\right) \quad (V.4)$$

where h is the water depth and K_x^* and K_y^* are effective dispersion coefficients.

Constituent Transport Equation in Transformed Coordinates

23. The transport equation is transformed from x-y space to α_1-α_2 space by means of the following coordinate transformation as considered by Butler (1980).

$$x = a_1 + b_1 \alpha_1^{c_1} \rightleftharpoons \alpha_1 = \left(\frac{x - a_1}{b_1}\right)^{1/c_1} \quad (V.5)$$

$$y = a_2 + b_2 \alpha_2^{c_2} \rightleftharpoons \alpha_2 = \left(\frac{y - a_2}{b_2}\right)^{1/c_2} \quad (V.6)$$

Then for an arbitrary hydrodynamic variable $\rho(x,y,t)$

$$\frac{\partial \rho}{\partial x} = \frac{\partial \rho}{\partial \alpha_1}\frac{d\alpha_1}{dx} \qquad \frac{\partial \rho}{\partial y} = \frac{\partial \rho}{\partial \alpha_2}\frac{d\alpha_2}{dy} \quad (V.7)$$

If we introduce $\mu_1 = dx/d\alpha_1$ and $\mu_2 = dy/d\alpha_2$ then

$$\frac{\partial \rho}{\partial x} = \frac{1}{\mu_1}\frac{\partial \rho}{\partial \alpha_1} \qquad \frac{\partial \rho}{\partial y} = \frac{1}{\mu_2}\frac{\partial \rho}{\partial \alpha_2} \quad (V.8)$$

24. Transforming Equation V.4 in x-y space to α_1-α_2 space we obtain the following result.

$$(ds)_t + \frac{(dus)_{\alpha_1}}{\mu_1} + \frac{(dvs)_{\alpha_2}}{\mu_2} = \frac{1}{\mu_1}\left[dK_{\alpha_1}\ \frac{(s)_{\alpha_1}}{\mu_1}\right]_{\alpha_1} + \frac{1}{\mu_2}\left[dK_{\alpha_2}\ \frac{(s)_{\alpha_2}}{\mu_2}\right]_{\alpha_2} \qquad (V.9)$$

where d is used to indicate water depth in place of h and

$$(\ )_t = \partial/\partial t$$

$$(\ )_{\alpha_1} = \partial/\partial\alpha_1$$

$$(\ )_{\alpha_2} = \partial/\partial\alpha_2$$

Equation V.9 is the relation that is the subject of numerical approximation.

Numerical Approximations

25. Schmalz (1983a, 1983b, 1983c) considered several alternate techniques for approximating the linear form of Equation V.9. The Flux-Corrected Transport (FCT) scheme was selected as the most accurate scheme and has been incorporated in the Waterways Experiment Station Implicit Flooding Model (WIFM). In addition a Three Time Level Explicit Transport scheme was also incorporated in the model. A space staggered grid as shown in Figure V.1 was employed in all of the formulations. The datum convention is presented in Figure V.2.

26. Let us introduce the following notation as a prelude to the approximations. Define for an arbitrary variable $F^k_{n,m}$, where $t = k\Delta t$, $y = n\Delta y$, $x = m\Delta x$:

$$\delta_t^k\left(F^k_{n,m}\right) = F^{k+1/2}_{n,m} - F^k_{n,m} \qquad (V.10a)$$

$$\delta_t'^k\left(F^k_{n,m}\right) = F^{k+1}_{n,m} - F^k_{n,m} \qquad (V.10b)$$

$$\delta_{\alpha_1}\left(F^k_{n,m}\right) = F^k_{n,m+1/2} - F^k_{n,m-1/2} \qquad (V.10c)$$

$$\delta_{\alpha_2}\left(F^k_{n,m}\right) = F^k_{n+1/2,m} - F^k_{n-1/2,m} \qquad (V.10d)$$

$$\frac{\alpha_1}{F_{n,m}} = \frac{\left(F^k_{n,m+1/2} + F^k_{n,m-1/2}\right)}{2} \qquad (V.10e)$$

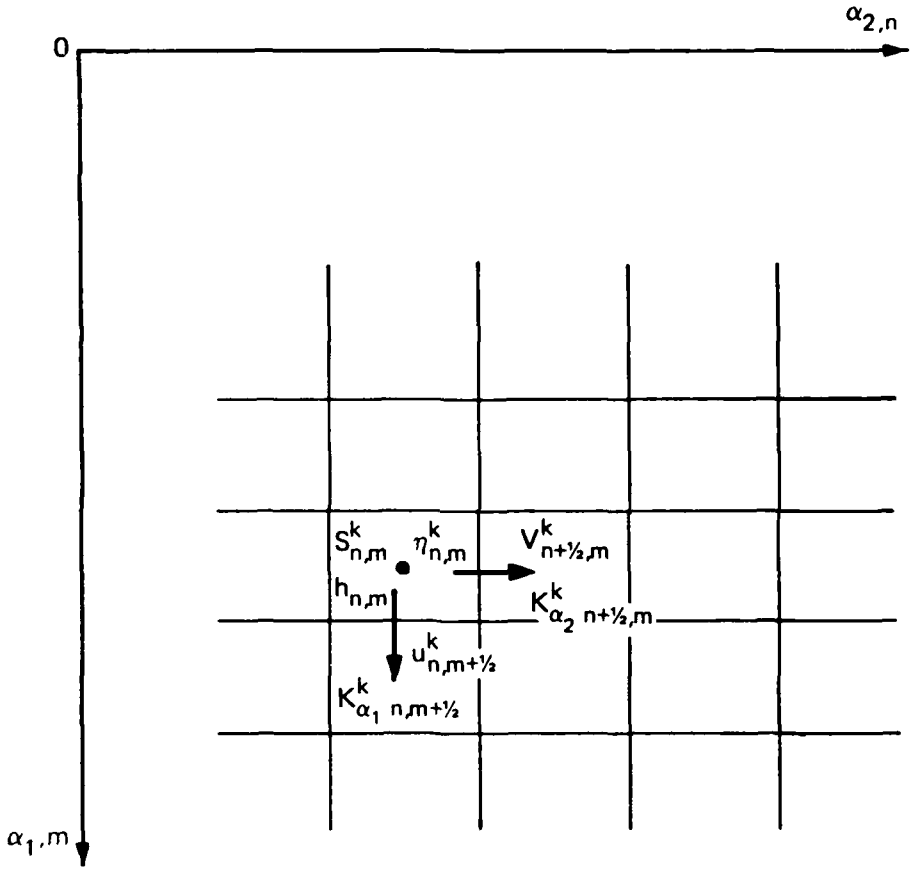

Figure V-1. Space staggered finite difference grid in transformed coordinates

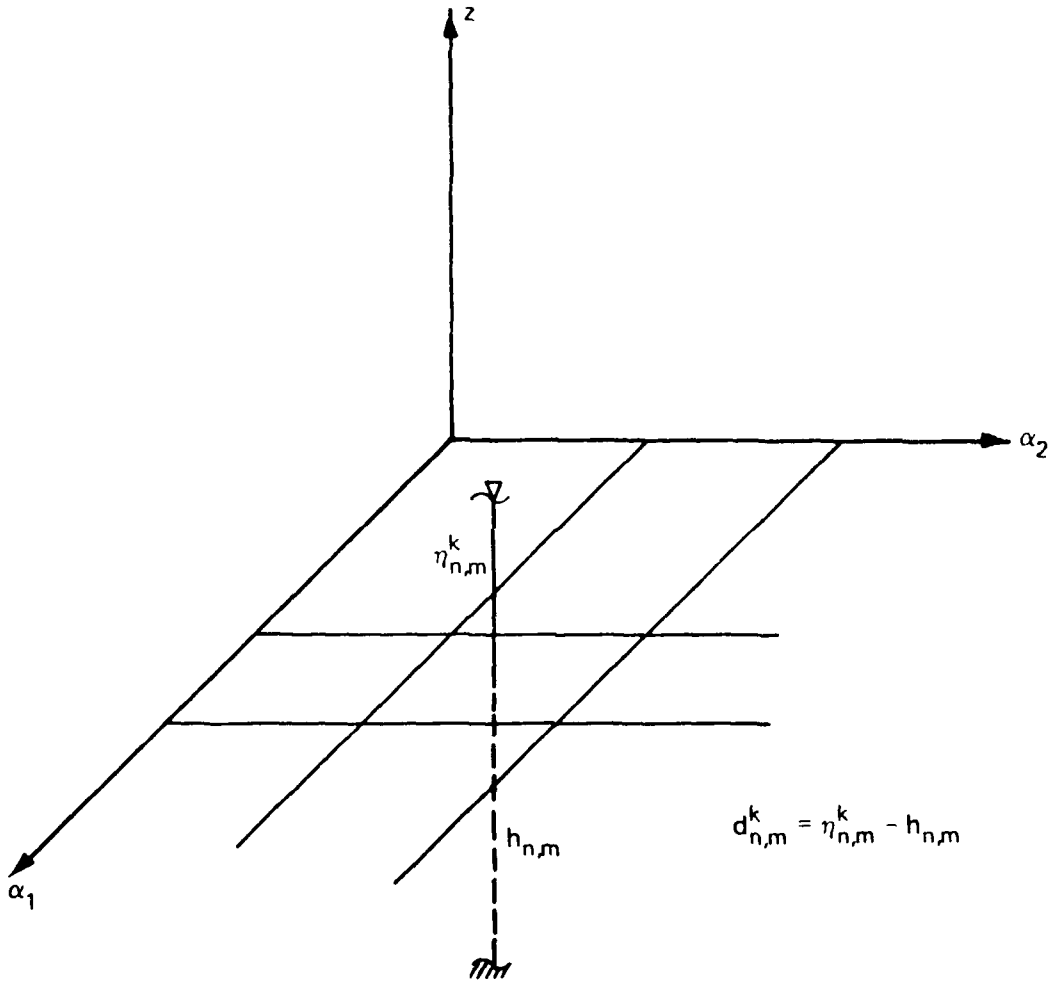

Figure V-2. Datum convention employed within the space staggered grid system

$$\overset{\alpha_2}{F}_{n,m} = \frac{\left(F^k_{n+1/2,m} + F^k_{n-1/2,m}\right)}{2} \qquad \text{(V.10f)}$$

Flux-corrected transport

27. Two schemes are used in implementing this approach: a lower order in space nonoscillatory scheme and a higher order in space scheme subject to oscillation. In the method implemented, two time level implicit multioperational ADI schemes were employed. The forward time upwind space (FTUS) and forward time centered space (FTCS) schemes were used as the lower and higher order in space schemes, respectively, and are discussed in turn below. Finally, the necessary flux correction procedures are developed.

Leendertse FTCS multioperational scheme

28. The following finite difference equation is considered as an approximation to the nonlinear transport Equation V.9.

$$\begin{aligned}
&{}^{\alpha}{}^{k}_{t}(ds) + \frac{\Delta t}{2\Delta\alpha_1(\mu_1)_m}\,{}^{\alpha}{}_1\left({}^{\alpha_1}_{d}{}^{k+1}_{k+1}\,{}^{\alpha_1}_{s}{}^{k+1}_{k+1}\,{}^{k+1}_{u}{}^{k+1}_{k+1} + {}^{\alpha_1}_{d}{}^{k}_{k}\,{}^{\alpha_1}_{s}{}^{k}_{k}\,{}^{k}_{u}{}^{k}_{k}\right) \\
&+ \frac{\Delta t}{2\Delta\alpha_2(\mu_2)_n}\,{}^{\alpha}{}_2\left({}^{\alpha_2}_{d}{}^{k+1}_{k+1}\,{}^{\alpha_2}_{s}{}^{k+1}_{k+1}\,{}^{k+1}_{v}{}^{k+1}_{k+1} + {}^{\alpha_2}_{d}{}^{k}_{k}\,{}^{\alpha_2}_{s}{}^{k}_{k}\,{}^{k}_{v}{}^{k}_{k}\right) \\
&- \frac{\Delta t}{2(\Delta\alpha_1)^2(\mu_1)_m}\,{}^{\alpha}{}_1\left[{}^{\alpha_1}_{d}{}^{k+1}_{k+1}\,K^{k+1}_{\alpha_1}\,\frac{\delta_{\alpha_1}(s^{k+1})}{(\mu_1)_m} + {}^{\alpha_1}_{d}{}^{k}_{k}\,K^{k}_{\alpha_1}\,\frac{\delta_{\alpha_1}(s^{k})}{(\mu_1)_m}\right] \\
&- \frac{\Delta t}{2(\Delta\alpha_2)^2(\mu_2)_n}\,{}^{\alpha}{}_2\left[{}^{\alpha_2}_{d}{}^{k+1}_{k+1}\,K^{k+1}_{\alpha_2}\,\frac{\delta_{\alpha_2}(s^{k+1})}{(\mu_2)_n} + {}^{\alpha_2}_{d}{}^{k}_{k}\,K^{k}_{\alpha_2}\,\frac{\delta_{\alpha_2}(s^{k})}{(\mu_2)_n}\right] = 0 \quad \text{at } (n,m)
\end{aligned} \qquad \text{(V.11)}$$

29. The above equation is assumed to be contained within the alternating direction difference equations presented in paragraphs 30 and 31 below. For the linear case obtained for $(\mu_2)_n = (\mu_1)_m = 1$, K_{α_2}, K_{α_1} constants in space and time, and u, v, d constant in space and time, the constituent intermediate time level (k+1/2* in paragraphs 30 and 31) may be eliminated in the alternating direction approach and the total difference equation obtained equals the above difference equation plus some higher order in time

factorization terms. The total difference equation is consistent with the linear transport equation. For the nonlinear case considered, it is not possible to eliminate the constituent intermediate time level. Thus the exact form of the factorization terms can not be determined. However, their numerical effect can be tested.

30. The approximations for the X-Sweep may now be written as follows:

$$
\begin{aligned}
&\delta_t^k(ds) + \frac{\Delta t}{2\Delta\alpha_1(\mu_1)_m}\left(\frac{\alpha_1}{d^{k+1/2*}}\,\frac{\alpha_1}{s^{k+1/2*}}\,u^{k+1/2*}\right) \\
&- \frac{\Delta t}{2\Delta\alpha_1^2(\mu_1)_m}\left[\frac{\alpha_1}{d^{k+1/2*}}\,K_{\alpha_1}^{k+1/2*}\,\frac{\alpha_1\left(s^{k+1/2*}\right)}{(\mu_1)_m}\right] \\
&+ \frac{\Delta t}{2(\mu_2)_n\Delta\alpha_2}\,\delta_{\alpha_2}\left(\frac{\alpha_2}{d^k}\,\frac{\alpha_2}{s^k v^k}\right) \\
&- \frac{\Delta t}{2\Delta\alpha_2^2(\mu_2)_n}\left[\frac{\alpha_2}{d^k}\,K_{\alpha_2}^k\,\frac{\alpha_2(s^k)}{(\mu_2)_n}\right] = 0 \quad \text{at } (n,m)
\end{aligned}
\tag{V.12}
$$

If we place all terms at time level $K+1/2^*$ on the left-hand side of the equation and expand K_x [illegible], the left-hand side of V.12 is

$$
\begin{aligned}
&[illegible]\Big[\Big(\ldots\Big)_{K_{n,m+1/2}}\Big(\ldots\Big) \\
&\Big(\ldots\Big)_{K_{n,m-1/2}}\Big(\ldots\Big)\Big] \\
&[illegible]\Big[\Big(\ldots\Big)\Big(\ldots\Big)_{K_{n,m+1/2}}^{k+1/2*} \\
&\Big(\ldots\Big)\Big(\ldots\Big)_{K_{n,m-1/2}}^{k+1/2*}\Big]
\end{aligned}
\tag{V.13}
$$

Collecting all terms in Equation V.12 at time level k, denoting the result as B_m, we obtain with $K_y = K_{\alpha_2}$

$$
\begin{aligned}
&[illegible] \Bigg[\left([illegible] \right) [illegible] \left(\frac{[illegible] + s^k_{n,m}}{2.} \right) \\
&\quad - \left([illegible] \right) [illegible] \left(\frac{[illegible] + s^k_{n,m}}{2.} \right) \Bigg] \\
&+ [illegible] \Bigg[\left([illegible] \right) \left([illegible] \right) [illegible] \\
&\quad - \left([illegible] \right) \left([illegible] \right) [illegible] \Bigg]
\end{aligned}
\tag{V.14}
$$

In Equation V.13 we define $-a_{n,m-1}$, $a_{n,m+1}$, and $a_{n,m}$ as follows

$$
-a_{n,m-1} = \frac{\Delta t \left(\frac{\alpha_1}{d}\right)^{k+1/2*}_{n,m-1/2}}{2\Delta\alpha_1 (\mu_1)_m} \left[\frac{u^{k+1/2*}_{n,m-1/2}}{2.} + \frac{(K_x)^{k+1/2*}_{n,m-1/2}}{\Delta\alpha_1 (\mu_1)_{m-1/2}} \right] \tag{V.15}
$$

$$
a_{n,m+1} = \frac{\Delta t \left(\frac{\alpha_1}{d}\right)^{k+1/2*}_{n,m+1/2}}{2\Delta\alpha_1 (\mu_1)_m} \left[\frac{u^{k+1/2*}_{n,m+1/2}}{2} - \frac{(K_x)^{k+1/2*}_{n,m+1/2}}{\Delta\alpha_1 (\mu_1)_{m+1/2}} \right] \tag{V.16}
$$

$$
\begin{aligned}
a_{n,m} = d^{k+1/2*}_{n,m} &+ \frac{\Delta t}{2\Delta\alpha_1 (\mu_1)_m} \left[\frac{\left(\frac{\alpha_1}{du}\right)^{k+1/2*}_{n,m+1/2}}{2} - \frac{\left(\frac{\alpha_1}{du}\right)^{k+1/2*}_{n,m-1/2}}{2} \right] \\
&+ \frac{\Delta t}{2\Delta\alpha_1^2 (\mu_1)_m} \left[\frac{\left(\frac{\alpha_1}{dK_x}\right)^{k+1/2*}_{n,m+1/2}}{(\mu_1)_{m+1/2}} + \frac{\left(\frac{\alpha_1}{dK_x}\right)^{k+1/2*}_{n,m-1/2}}{(\mu_1)_{m-1/2}} \right]
\end{aligned}
\tag{V.17}
$$

31. Collecting all results we obtain the following interior equation for the X-Sweep

$$
a_{n,m-1}\, s^{k+1/2*}_{n,m-1} + a_{n,m}\, s^{k+1/2*}_{n,m} + a_{n,m+1}\, s^{k+1/2*}_{n,m+1} = B_m \tag{V.18}
$$

32. The approximations for the Y-Sweep may now be written as follows:

$$\epsilon_t^{k+1/2*}(ds) + \frac{\Delta t\ \delta_{a_2}}{2\Delta a_2(\mu_2)_n}\left(\frac{\alpha_2}{d^{k+1}}\ s^{k+1}v^{k+1}\right) - \frac{\Delta t\ \delta_{a_2}}{2\Delta a_2^2(\mu_2)_n}\left[\frac{\alpha_2}{d^{k+1}}\ K_{a_2}^{k+1}\ \frac{\delta_{a_2}(s^{k+1})}{(\mu_2)_n}\right]$$

$$+ \frac{\Delta t\ \delta_{a_1}}{2\Delta a_1(\mu_1)_m}\left(\frac{\alpha_1}{d^{k+1/2*}}\ s^{k+1/2*}u^{k+1/2*}\right) - \frac{\Delta t\ \delta_{a_1}}{2\Delta a_1^2(\mu_1)_m}\left[\frac{\alpha_1}{d^{k+1/2*}}\ K_{a_1}^{k+1/2*}\ \frac{\delta_{a_1}(s^{k+1/2*})}{(\mu_1)_m}\right] = 0 \quad \text{at } (n,m) \tag{V.19}$$

Expanding Equation V.19 by employing V.10 and collecting terms at time level k+1 on the left side and leaving terms at time level K+1/2* on the right side the following interior equation for the Y-Sweep is obtained.

$$a_{n-1,m}\ s_{n-1,m}^{k+1} + a_{n,m}\ s_{n,m}^{k+1} + a_{n+1,m}\ s_{n+1,m}^{k+1} = B_n \tag{V.20}$$

where $K_x = K_{\alpha_1}$ and $K_y = K_{\alpha_1}$

$$-a_{n-1,m} = \frac{\Delta t\left(\frac{\alpha_2}{d}\right)_{n-1/2,m}^{k+1}}{2\Delta a_2(\mu_2)_n}\left[\frac{v_{n-1/2,m}^{k+1}}{2} + \frac{(K_y)_{n-1/2,m}^{k+1}}{\Delta a_2(\mu_2)_{n-1/2}}\right] \tag{V.21}$$

$$a_{n+1,m} = \frac{\Delta t\left(\frac{\alpha_2}{d}\right)_{n+1/2,m}^{k+1}}{2\Delta a_2(\mu_2)_n}\left[\frac{v_{n+1/2,m}^{k+1}}{2} - \frac{(K_y)_{n+1/2,m}^{k+1}}{\Delta a_2(\mu_2)_{n+1/2}}\right] \tag{V.22}$$

$$a_{n,m} = d_{n,m}^{k+1} + \frac{\Delta t}{2\Delta a_2(\mu_2)_n}\left[\frac{\left(\frac{\alpha_2}{dv}\right)_{n+1/2,m}^{k+1}}{2} - \frac{\left(\frac{\alpha_2}{dv}\right)_{n-1/2,m}^{k+1}}{2}\right]$$

$$+ \frac{\Delta t}{2\Delta a_2^2(\mu_2)_n}\left[\frac{\left(\frac{\alpha_2}{dK_y}\right)_{n+1/2,m}^{k+1}}{(\mu_2)_{n+1/2}} + \frac{\left(\frac{\alpha_2}{dK_y}\right)_{n-1/2,m}^{k+1}}{(\mu_2)_{n-1/2}}\right] \tag{V.23}$$

$$B_n = (ds)^{k+1/2*}_{n,m} - \frac{\Delta t}{2(\mu_1)_m \Delta\alpha_1}\left[\left(\frac{\alpha_1}{ds}\frac{\alpha_1}{}\right)^{k+1/2*}_{n,m+1/2} u^{k+1/2*}_{n,m+1/2} - \left(\frac{\alpha_1}{ds}\frac{\alpha_1}{}\right)^{K+1/2*}_{n,m-1/2} u^{k+1/2*}_{n,m-1/2}\right]$$

$$+ \frac{\Delta t}{2(\mu_1)_m(\Delta\alpha_1)^2}\left[\left(\frac{\alpha_1}{dK_x}\right)^{k+1/2*}_{n,m+1/2} \frac{\left(s^{k+1/2*}_{n,m+1} - s^{k+1/2*}_{n,m}\right)}{(\mu_1)_{m+1/2}} - \left(\frac{\alpha_1}{dK_x}\right)^{k+1/2*}_{n,m-1/2} \frac{\left(s^{k+1/2*}_{n,m} - s^{k+1/2*}_{n,m-1}\right)}{(\mu_1)_{m-1/2}}\right] \qquad (V.24)$$

Leendertse FTUS multioperational scheme

33. The following finite difference equation is considered as an approximation to the nonlinear transport Equation V.9:

$$c'^k_t(ds) + \frac{\Delta t}{2\Delta\alpha_1(\mu_1)_m}\delta_{\alpha_1}\left(\frac{\alpha_1}{d}^{k+1}\frac{u}{s_1}^{k+1} u^{k+1} + \frac{\alpha_1}{d}^{k}\frac{u}{s_1}^{k} u^{k}\right)$$

$$+ \frac{\Delta t}{2\Delta\alpha_2(\mu_2)_n}\delta_{\alpha_2}\left(\frac{\alpha_2}{d}^{k+1}\frac{v}{s_2}^{k+1} v^{k+1} + \frac{\alpha_2}{d}^{k}\frac{v}{s_2}^{k} v^{k}\right)$$

$$- \frac{\Delta t}{2(\Delta\alpha_1)^2(\mu_1)_m}\delta_{\alpha_1}\left[\frac{\alpha_1}{d}^{k+1} K^{k+1}_{\alpha_1}\frac{\delta_{\alpha_1}(s^{k+1})}{(\mu_1)_m} + \frac{\alpha_1}{d}^{k} K^{k}_{\alpha_1}\frac{\delta_{\alpha_1}(s^{k})}{(\mu_1)_m}\right] \qquad (V.25)$$

$$- \frac{\Delta t}{2(\Delta\alpha_2)^2(\mu_2)_n}\delta_{\alpha_2}\left[\frac{\alpha_2}{d}^{k+1} K^{k+1}_{\alpha_2}\frac{\delta_{\alpha_2}(s^{k+1})}{(\mu_2)_n} + \frac{\alpha_2}{d}^{k} K^{k}_{\alpha_2}\frac{\delta_{\alpha_2}(s^{k})}{(\mu_2)_n}\right] = 0 \quad \text{at } (n,m)$$

34. The following upwind difference operators used in the above equation are defined at (n,m) as follows:

$$\frac{f}{s_1}^k = \begin{cases} s^k_{n,m-1/2} & f^k_{n,m} \geq 0 \\ s^k_{n,m+1/2} & f^k_{n,m} < 0 \end{cases} \qquad (V.26)$$

$$\frac{f}{s_2}^k = \begin{cases} s^k_{n-1/2,m} & f^k_{n,m} \geq 0 \\ s^k_{n+1/2,m} & f^k_{n,m} < 0 \end{cases}$$

35. For the linear case $\left[(\mu_1)_m = (\mu_2)_n = 1.0 \ , \ K_{\alpha_1} \ , \ K_{\alpha_2} \ , \ u \ , \ v \ , \right.$ and d constant$\left.\right]$, the constituent intermediate time level in the alternating direction approach may be eliminated. The difference equation obtained is consistent with the linear transport equation and equals the above difference equations plus some higher order in time factorization terms. For the non-linear case considered here, it is not possible to eliminate the constituent intermediate time level. Therefore the exact form of the factorization terms can not be determined. However, their numerical effect can be assessed.

36. This scheme is similar to the standard ADI technique except that upwind differencing is employed for the advective terms. The necessary modifications for the X-Sweep are shown in Table V-1 and those employed for the Y-Sweep are given in Table V-2.

Table V-1

X-Sweep Modification FTUS

Equation	FTCS	FTUS
V.14	$\frac{\left(s^k_{n+1,m} + s^k_{n,m}\right)}{2.}$	$s^k_{n,m}$ $v^k_{n+1/2,m} \geq 0$
		$s^k_{n+1,m}$ $v^k_{n+1/2,m} < 0$
V.14	$\frac{\left(s^k_{n-1,m} + s^k_{n,m}\right)}{2.}$	$s^k_{n-1,m}$ $v^k_{n-1/2,m} \geq 0$
		$s^k_{n,m}$ $v^k_{n-1/2,m} < 0$
V.15	$\frac{u^{k+1/2*}_{n,m-1/2}}{2}$	$\max\left(0., u^{k+1/2*}_{n,m-1/2}\right)$
V.16	$\frac{u^{k+1/2*}_{n,m+1/2}}{2}$	$\min\left(0., u^{k+1/2*}_{n,m+1/2}\right)$
V.17	$\frac{\left(\frac{\alpha_1}{du}\right)^{k+1/2*}_{n,m+1/2}}{2}$	$\max\left[0., \left(\frac{\alpha_1}{du}\right)^{k+1/2*}_{n,m+1/2}\right]$
V.17	$\frac{\left(\frac{\alpha_1}{du}\right)^{k+1/2*}_{n,m-1/2}}{2}$	$\min\left[0., \left(\frac{\alpha_1}{du}\right)^{k+1/2*}_{n,m-1/2}\right]$

Table V-2

Y-Sweep Modifications FTUS

Equation	FTCS	FTUS
V.21	$\frac{v^{k+1}_{n-1/2,m}}{2}$	$\max\left(0., v^{k+1}_{n-1/2,m}\right)$
V.22	$\frac{v^{k+1}_{n+1/2,m}}{2}$	$\min\left(0., v^{k+1}_{n+1/2,m}\right)$
V.23	$\frac{\left(\frac{\alpha_2}{dv}\right)^{k+1}_{n+1/2,m}}{2}$	$\max\left[0., \left(\frac{\alpha_2}{dv}\right)^{k+1}_{n+1/2,m}\right]$
V.23	$\frac{\left(\frac{\alpha_2}{dv}\right)^{k+1}_{n-1/2,m}}{2}$	$\min\left[0., \left(\frac{\alpha_2}{dv}\right)^{k+1}_{n-1/2,m}\right]$
V.24	$\left(\frac{\alpha_1}{ds}\frac{\alpha_1}{}\right)^{k+1/2*}_{n,m-1/2}$	$\frac{\alpha_1}{d}^{k+1/2*}_{n,m+1/2} s^{k+1/2*}_{n,m} \quad u^{k+1/2*}_{n,m+1/2} \geq 0$
		$\frac{\alpha_1}{d}^{k+1/2*}_{n,m+1/2} s^{k+1/2*}_{n,m+1} \quad u^{k+1/2*}_{n,m+1/2} < 0$
V.24	$\left(\frac{\alpha_1}{ds}\frac{\alpha_1}{}\right)^{k+1/2*}_{n,m-1/2}$	$\frac{\alpha_1}{d}^{k+1/2*}_{n,m-1/2} s^{k+1/2*}_{n,m-1} \quad u^{k+1/2*}_{n,m-1/2} \geq 0$
		$\frac{\alpha_1}{d}^{k+1/2*}_{n,m-1/2} s^{k+1/2*}_{n,m} \quad u^{k+1/2*}_{n,m-1/2} < 0$

Flux correction procedures

37. If the factorization terms are ignored, the schemes above may be written in the following flux format.

$$d^{k+1}_{n,m}\, s^{I}_{n,m} = d^{k}_{n,m}\, S^{k}_{n,m} - \left[\Delta\alpha_1(\mu_1)_m \Delta\alpha_2(\mu_2)_n\right]^{-1} \times \left(F^{I}_{n+1/2,m} - F^{I}_{n-1/2,m} + F^{I}_{n,m+1/2} - F^{I}_{n,m-1/2}\right) \quad (V.27)$$

where $t = k\Delta t$, $x = \sum_i (\mu_1)_i \Delta\alpha_1$, $y = \sum_i (\mu_2)_i \Delta\alpha_2$

$S^{k}_{n,m} \equiv$ concentration at location (n,m) at time level k

$\Delta\alpha_1(\mu_1)_m \equiv$ x space step at m

$\Delta\alpha_2(\mu_2)_m \equiv$ y space step at n

$I \equiv$ general index at time level k+1 , which we set to H or L for the higher or lower scheme, respectively

$F^{I}_{n\pm1/2,m\pm1/2} \equiv$ fluxes through the appropriate cell faces of cell (n,m). Form is dependent upon the finite difference formulation

We observe from Equation V.27 that the difference between the higher and lower order scheme at (n,m) may be written as follows:

$$\left(S^{H}_{n,m} - S^{L}_{n,m}\right) = -\left[\Delta\alpha_1(\mu_1)_m \Delta\alpha_2(\mu_2)_n d^{k+1}_{n,m}\right]^{-1} \left[\left(F^{H}_{n+1/2,m} - F^{L}_{n+1/2,m}\right) - \left(F^{H}_{n-1/2,m} - F^{L}_{n-1/2,m}\right) + \left(F^{H}_{n,m+1/2} - F^{L}_{n,m+1/2}\right) - \left(F^{H}_{n,m-1/2} - F^{L}_{n,m-1/2}\right)\right] \quad (V.28)$$

Note that this difference can be expressed as an array of fluxes between adjacent grid points and is the condition required for flux correction. We next develop the flux expressions for the higher (F^H) and lower (F^L) order schemes. In order to aid in notation, we make the following definition for an arbitrary variable, F .

$$F_{n,m}^{k+1/2} = \left(F_{n,m}^{k+1} + F_{n,m}^{k}\right)\Big/2. \qquad (V.29)$$

38. For the higher order scheme we employ the FTCS scheme written in Equation V.11 in which the factorization terms developed in the multioperational method are not shown. Equation V.11 may be written in the form of V.27, where the total fluxes are presented as the sum of advective and diffusive fluxes.

39. From Equation V.11 one then obtains for the advective fluxes:

$$F^{H_A}_{n\pm1/2,m} = v^{k+1/2}_{n\pm1/2,m}\Delta t(\mu_1)_m\Delta\alpha_1\left[\left(\frac{S^H + S^k}{2}\right)_{n\pm1,m} d^{k+1/2}_{n\pm1,m} + \left(\frac{S^H + S^k}{2}\right)_{n,m} d^{k+1/2}_{n,m}\right]\Big/2. \qquad (V.30)$$

$$F^{H_A}_{n,m\pm1/2} = u^{k+1/2}_{n,m\pm1/2}\Delta t(\mu_2)_n\Delta\alpha_2\left[\left(\frac{S^H + S^k}{2}\right)_{n,m\pm1} d^{k+1/2}_{n,m\pm1} + \left(\frac{S^H + S^k}{2}\right)_{n,m} d^{k+1/2}_{n,m}\right]\Big/2. \qquad (V.31)$$

Note the subscript A denotes advection. The diffusive fluxes are then given by the following relations.

$$F^{H_O}_{n\pm1/2,m} = \pm K_{y\,n\pm1/2,m}^{k+1/2}\,\frac{\Delta t(\mu_1)_m\Delta\alpha_1}{2} \times \frac{\left[(S^H + S^k)_{n,m} - (S^H + S^k)_{n\pm1,m}\right]}{\Delta\alpha_2(\mu_2)_{n\pm1/2}}\,\frac{\left(d^{k+1/2}_{n\pm1,m} + d^{k+1/2}_{n,m}\right)}{2} \qquad (V.32)$$

$$F^{H_O}_{n,m\pm1/2} = \pm K_{x\,n,m\pm1/2}^{k+1/2}\,\frac{\Delta t(\mu_2)_n\Delta\alpha_2}{2} \times \frac{\left[(S^H + S^k)_{n,m} - (S^H + S^k)_{n,m\pm1}\right]}{\Delta\alpha_1(\mu_1)_{m\pm1/2}}\,\frac{\left(d^{k+1/2}_{n,m\pm1} + d^{k+1/2}_{n,m}\right)}{2} \qquad (V.33)$$

Note the subscript 0 denotes diffusion.

40. For the lower order scheme, the FTUS scheme written in Equation V.25 is employed. Factorization terms generated by the multioperational method are not considered. Equation V.25 is written in the form of V.27. The total fluxes are presented as the sum of advective and diffusive fluxes.

41. From Equation V.25 one obtains the following set of advective fluxes.

$$F^{L_A}_{n+1/2,m} = \begin{cases} v^{k+1/2}_{n+1/2,m} \geq 0 & v^{k+1/2}_{n+1/2,m}\Delta t(\mu_1)_m \Delta\alpha_1 \left(\frac{S^L + S^k}{2}\right)_{n,m} d^{k+1/2}_{n,m} \\ v^{k+1/2}_{n+1/2,m} < 0 & v^{k+1/2}_{n+1/2,m}\Delta t(\mu_1)_m \Delta\alpha_1 \left(\frac{S^L + S^k}{2}\right)_{n+1,m} d^{k+1/2}_{n+1,m} \end{cases} \quad (V.34)$$

$$F^{L_A}_{n-1/2,m} = \begin{cases} v^{k+1/2}_{n-1/2,m} \geq 0 & v^{k+1/2}_{n-1/2,m}\Delta t(\mu_1)_m \Delta\alpha_1 \left(\frac{S^L + S^k}{2}\right)_{n-1,m} d^{k+1/2}_{n-1,m} \\ v^{k+1/2}_{n-1/2,m} < 0 & v^{k+1/2}_{n-1/2,m}\Delta t(\mu_1)_m \Delta\alpha_1 \left(\frac{S^L + S^k}{2}\right)_{n,m} d^{k+1/2}_{n,m} \end{cases} \quad (V.35)$$

$$F^{L_A}_{n,m+1/2} = \begin{cases} u^{k+1/2}_{n,m+1/2} \geq 0 & u^{k+1/2}_{n,m+1/2}\Delta t(\mu_2)_n \Delta\alpha_2 \left(\frac{S^L + S^k}{2}\right)_{n,m} d^{k+1/2}_{n,m} \\ u^{k+1/2}_{n,m+1/2} < 0 & u^{k+1/2}_{n,m+1/2}\Delta t(\mu_2)_n \Delta\alpha_2 \left(\frac{S^L + S^k}{2}\right)_{n,m+1} d^{k+1/2}_{n,m+1} \end{cases} \quad (V.36)$$

$$F^{L_A}_{n,m-1/2} = \begin{cases} u^{k+1/2}_{n,m-1/2} \geq 0 & u^{k+1/2}_{n,m-1/2}\Delta t(\mu_2)_n \Delta\alpha_2 \left(\frac{S^L + S^k}{2}\right)_{n,m-1} d^{k+1/2}_{n,m-1} \\ u^{k+1/2}_{n,m-1/2} < 0 & u^{k+1/2}_{n,m-1/2}\Delta t(\mu_2)_n \Delta\alpha_2 \left(\frac{S^L + S^k}{2}\right)_{n,m} d^{k+1/2}_{n,m} \end{cases} \quad (V.37)$$

The diffusive fluxes are obtained from Equations V.32 and V.33 with H replaced by L .

42. The antidiffusive fluxes are then computed as follows.

$$A_{n\pm1/2,m} = F^{H_A}_{n\pm1/2,m} - F^{L_A}_{n\pm1/2,m} + F^{H_O}_{n\pm1/2,m} - F^{L_O}_{n\pm1/2,m} \qquad (V.38)$$

$$A_{n,m\pm1/2} = F^{H_A}_{n,m\pm1/2} - F^{L_A}_{n,m\pm1/2} + F^{H_O}_{n,m\pm1/2} - F^{L_O}_{n,m\pm1/2} \qquad (V.39)$$

In computing the difference between the diffusive fluxes (third and fourth terms in the above expressions), note that the terms with $S^k_{n,m}$ are of opposite signs and drop out of the equations.

43. Next the maximum and minimum cell values are determined.

$$S^n_{n,m} = \max\left(S^k_{n,m}, S^L_{n,m}\right) \qquad S^b_{n,m} = \min\left(S^k_{n,m}, S^L_{n,m}\right) \qquad (V.40)$$

$$S^{max}_{n,m} = \max\left(S^a_{n-1,m}, S^a_{n,m}, S^a_{n+1,m}, S^a_{n,m-1}, S^a_{n,m+1}\right) \qquad (V.41)$$

$$S^{min}_{n,m} = \min\left(S^b_{n-1,m}, S^b_{n,m}, S^b_{n+1,m}, S^b_{n,m-1}, S^b_{n,m+1}\right) \qquad (V.42)$$

44. Next the sum of all antidiffusive fluxes into cell (n,m), $P^+_{n,m}$, is determined.

$$P^+_{n,m} = \max\left(0, A_{n-1/2,m}\right) - \min\left(0, A_{n+1/2,m}\right) + \max\left(0, A_{n,m-1/2}\right) - \min\left(0, A_{n,m+1/2}\right) \qquad (V.43)$$

The maximum allowable mass into the cell, $Q^+_{n,m}$, is then computed as follows:

$$Q^+_{n,m} = \left(S^{max}_{n,m} - S^L_{n,m}\right)\left[(\mu_1)_m \Delta\alpha_1 (\mu_2)_n \Delta\alpha_2 d^{k+1}_{n,m}\right] \qquad (V.44)$$

45. Similarly, the sum of all antidiffusive fluxes into cell (n,m), $P^-_{n,m}$, is determined.

$$P^-_{n,m} = \max\left(0, A_{n+1/2,m}\right) - \min\left(0, A_{n-1/2,m}\right) + \max\left(0, A_{n,m+1/2}\right) - \min\left(0, A_{n,m-1/2}\right) \qquad (V.45)$$

The maximum allowable mass to leave the cell, $Q^-_{n,m}$, is then computed.

$$Q^{-}_{n,m} = S^{L}_{n,m} - S^{max}_{n,m} \quad (\mu_1)_m \Delta\alpha_1 (\mu_2)_n \Delta\alpha_2 d^{k+1}_{n,m} \tag{V.46}$$

46. The following ratios are next computed for use in determining the limiting coefficients.

$$R^{+}_{n,m} = \begin{cases} \min\left(1, Q^{+}_{n,m} / P^{+}_{n,m}\right) & P^{+}_{n,m} > 0 \\ 0 & P^{+}_{n,m} = 0 \end{cases} \tag{V.47}$$

$$R^{-}_{n,m} = \begin{cases} \min\left(1, Q^{-}_{n,m} / P^{-}_{n,m}\right) & P^{-}_{n,m} > 0 \\ 0 & P^{-}_{n,m} = 0 \end{cases} \tag{V.48}$$

The limiting coefficients are then given by

$$C_{n+1/2,m} = \begin{cases} \min\left(R^{+}_{n+1,m}, R^{-}_{n,m}\right) & A_{n+1/2,m} \geq 0 \\ \min\left(R^{+}_{n,m}, R^{-}_{n+1,m}\right) & A_{n+1/2,m} < 0 \end{cases} \tag{V.49}$$

$$C_{n,m+1/2} = \begin{cases} \min\left(R^{+}_{n,m+1}, R^{-}_{n,m}\right) & A_{n,m+1/2} \geq 0 \\ \min\left(R^{+}_{n,m}, R^{-}_{n,m+1}\right) & A_{n,m+1/2} < 0 \end{cases}$$

47. The antidiffusive fluxes in Equations V.38 and V.39 are limited by multiplying by the limiting coefficients and the solution is advanced to the next time level.

$$S^{k+1}_{n,m} = S^{L}_{n,m} - \left[A_1 (\mu_1)_m A_2 (\mu_2)_n d^{k+1}_{n,m}\right]^{-1} (C_{n+1/2,m} A_{n+1/2,m}$$

$$- C_{n-1/2,m} A_{n-1/2,m} + C_{n,m+1/2} A_{n,m+1/2} - C_{n,m-1/2} A_{n,m-1/2}) \tag{V.50}$$

48. The coding of the flux-corrected transport procedures is contained in Subroutine CONC in the numerical model.

Three Time Level Explicit scheme

49. In order to avoid the averaging of hydrodynamic quantities which is performed when employing a two time level transport scheme, with a three time level velocity scheme, a three time level explicit scheme is considered.

50. It is instructive to observe the form of the continuity equation employed in the multioperational (alternating direction) hydrodynamic scheme.

X - Sweep

$$\frac{1}{2\Delta t}\left(\eta^{k+1} - \eta^{k-1}\right)_{n,m} + 2\left(\mu_1\right)_m^{1}\Delta\alpha_1\left[\left(u^{k+1} + u^{k-1}\right)\overline{\overline{d}}^{\alpha_1 k}\Big|_{n,m+1/2} - \left(u^{k+1} + u^{k-1}\right)\overline{\overline{d}}^{\alpha_1 k}\Big|_{n,m-1/2}\right]$$

$$+ \left(\mu_2\right)_n^{1}\Delta\alpha_2\left[v^{k-1}\overline{\overline{d}}^{\alpha_2 k}\Big|_{n+1/2,m} - v^{k-1}\overline{\overline{d}}^{\alpha_2 k}\Big|_{n-1/2,m}\right] = 0 \quad \text{at } (n,m) \qquad \text{(V.51)}$$

with

$$\overline{\overline{d}}^{\alpha_1}_{n,m\pm1/2} = d^k_{n,m\pm1} + d^k_{n,m}$$

$$\overline{\overline{d}}^{\alpha_2}_{n\pm1/2,m} = d^k_{n\pm1,m} + d^k_{n,m}$$

and

$$d^k_{n,m} = \eta^k_{n,m} - h_{n,m}$$

Y - Sweep:

$$\frac{1}{2\Delta t}\left(\eta^{k+1}_{n,m} - \eta^{k-1}_{n,m}\right) + 2\left(\mu_2\right)_n^{1}\Delta\alpha_2\left[\left(v^{k+1} + v^{k-1}\right)\overline{\overline{d}}^{\alpha_2 k}\Big|_{n+1/2,m} - \left(v^{k+1} + v^{k-1}\right)\overline{\overline{d}}^{\alpha_2 k}\Big|_{n-1/2,m}\right] = 0$$

$$\text{at } (n,m) \qquad \text{(V.52)}$$

where

Δt = time step length

η^* = water surface elevation at intermediate time level*

$\eta^{k-1}_{n,m}$ = water surface elevation at time level k - 1 at cell (n,m)

$\Delta\alpha_1 = \alpha_1$ space increment

$\Delta\alpha_2 = \alpha_2$ space increment

$u^{k+1}_{n,m+1/2} = x - \alpha_1$ velocity component at time level k + 1 at cell (n,m)

$u^{k-1}_{n,m+1/2} = x - \alpha_1$ velocity component at time level k - 1 at cell (n,m)

$v^{k+1}_{n+1/2,m} = y - \alpha_2$ velocity component at time level k + 1 at cell (n,m)

$v^{k-1}_{n+1/2,m} = y - \alpha_2$ velocity component at time level k - 1 at cell (n,m)

$d^k_{n,m}$ = water depth at time level k at cell n,m

If we eliminate the intermediate level η^* ; e.g., solve for η^* in Equation V.51 and substitute in V.52, we obtain:

$$\frac{\left(\eta^{k+1}_{n,m} - \eta^{k-1}_{n,m}\right)}{2\Delta t} + \frac{1}{2(\mu_1)_m \Delta\alpha_1}\left[(u^{k+1} + u^{k-1})\, d^k\Big|_{n,m+1/2} - (u^{k+1} + u^{k-1})\, d^k\Big|_{n,m-1/2}\right]$$

$$+ \frac{1}{2(\mu_2)_n \Delta\alpha_2}\left[(v^{k+1} + v^{k-1})\, d^k\Big|_{n+1/2,m} - (v^{k+1} + v^{k-1})\, d^k\Big|_{n-1/2,m}\right] = 0 \qquad \text{(V.53)}$$

at (n,m)

Since $d^k_{n,m} = \eta^k_{n,m} - h_{n,m}$ Equation V.53 is a full three time level scheme. In order to develop a three time level volume consistent transport scheme, we replace $d^k_{n,m}$ in Equation V.53 with $d^k_{n,m} S^k_{n,m}$ and thereby obtain:

$$\frac{\left(\eta^{k+1}_{n,m} S^{k+1}_{n,m} - \eta^{k-1}_{n,m} S^{k-1}_{n,m}\right)}{2\Delta t} + \frac{1}{2(\mu_1)_m \Delta\alpha_1}\left[(u^{k+1} + u^{k-1})\, d^k S^k\Big|_{n,m+1/2} - (u^{k+1} + u^{k-1})\, d^k S^k\Big|_{n,m-1/2}\right]$$

$$+ \frac{1}{2(\mu_2)_n \Delta\alpha_2}\left[(v^{k+1} + v^{k-1})\, d^k S^k\Big|_{n+1/2,m} - (v^{k+1} + v^{k-1})\, d^k S^k\Big|_{n-1/2,m}\right] \qquad \text{(V.54)}$$

$$+ \frac{1}{(\mu_1)_m (\mu_2)_n}\left[u^{k-1} d^k S^k\Big|_{n,m+1/2} \frac{\left(\eta^{k+1}_{n+1,m} - \eta^{k-1}_{n-1,m}\right)}{(\mu_2)_{n+1}} - u^{k-1} d^k S^k\Big|_{n,m-1/2} \frac{\left(\eta^{k+1}_{n+1,m} - \eta^{k-1}_{n-1,m}\right)}{(\mu_2)_{n-1}}\right]$$

$$+ \frac{1}{(\mu_1)_m (\mu_2)_n}\left[v^{k-1} d^k S^k\Big|_{n+1/2,m} \frac{\left(\eta^{k+1}_{n,m+1} - \eta^{k-1}_{n,m-1}\right)}{(\mu_1)_{m+1}} - v^{k-1} d^k S^k\Big|_{n-1/2,m} \frac{\left(\eta^{k+1}_{n,m+1} - \eta^{k-1}_{n,m-1}\right)}{(\mu_1)_{m-1}}\right]$$

The scheme in Equation V.54 employs centered space differencing of the advective terms (FTCS). Alternatively, one may employ upwind differencing (FTUS). The two schemes FTCS and FTUS might then be employed in a flux-corrected transport procedure.

51. In order to analyze the stability of these schemes, we consider the linear case, $d^k_{n,m} = d$, $u^k_{n,m\pm1/2} = u$, $v^k_{n\pm1/2,m} = v$, $K^{k-1}_{\alpha_1} = K_x$, and $K^{k-1}_{\alpha_2} = K_y$. Also $(\mu_1)_m = (\mu_2)_m = 1$.

52. Let us consider the following general three time level transport scheme written in operator form, where

$$\delta_{2t}\left(S^k_{n,m}\right) = \left(S^{k+1}_{n,m} - S^{k-1}_{n,m}\right)/2\Delta t$$

$$\delta_x\left(S^k_{n,m}\right) = \left(S^k_{n,m+1} - S^k_{n,m-1}\right)/2\Delta x$$

$$\delta_y\left(S^k_{n,m}\right) = \left(S^k_{n+1,m} - S^k_{n-1,m}\right)/2\Delta y$$

$$\delta^2_x\left(S^k_{n,m}\right) = \left(S^k_{n,m+1} + S^k_{n,m-1} - 2S^k_{n,m}\right)/\Delta x^2$$

$$\delta^2_y\left(S^k_{n,m}\right) = \left(S^k_{n+1,m} + S^k_{n-1,m} - 2S^k_{n,m}\right)/\Delta y^2$$

$$\delta_{2t}\left(S^k_{n,m}\right) + u\overbrace{\left(\delta_x + g\,\frac{\Delta x}{2}\,\delta^2_x\right)}^{T_x}\left(S^k_{n,m}\right) + v\overbrace{\left(\delta_y + g\,\frac{\Delta y}{2}\,\delta^2_y\right)}^{T_y}\left(S^k_{n,m}\right)$$
$$- K_x\delta^2_x\left(S^{k-1}_{n,m}\right) - K_y\delta^2_y\left(S^{k-1}_{n,m}\right) = 0 \quad \text{at} \quad (n,m) \qquad (V.55)$$

with $g\varepsilon(-1\ ,\ 0\ ,\ 1)$

Note: If $g = o$, central differencing of the advective terms is affected. If $u,v > o$ $g = -1$ (backward differencing) is employed. If $u,v < o$, $g = +1$ (forward differencing) is employed. This method constitutes upwind differencing.

53. We note that Equation V.55 is a three time level scheme, thus in order to perform a stability analysis we set up a second variable $V^k_{n,m}$ and

set $V^{k+1}_{n,m} = S^{k}_{n,m}$, then Equation V.55 may be written in matrix form as follows:

$$\begin{bmatrix} S^{k+1}_{n,m} \\ V^{k+1}_{n,m} \end{bmatrix} = \begin{bmatrix} -2\Delta t(uT_x + vT_y) + 2\Delta t\left(K_x\delta_x^2 + K_y\delta_y^2\right) + 1 \\ 1 \qquad\qquad\qquad 0 \end{bmatrix} \begin{bmatrix} S^{k}_{n,m} \\ V^{k}_{n,m} \end{bmatrix} \tag{V.56}$$

54. Equation V.56 is in the required format for a stability analysis. Following standard practice, assume $S^{k}_{n,m} = e^{k\alpha\Delta t}e^{n\gamma\Delta y}e^{m\beta\Delta x}$

55. Thus we may develop the following supplemental relations:

$$\begin{aligned} T_x(S^{k}_{n,m}) &\equiv \left(\frac{i}{\Delta x}\sin\beta\Delta x - \frac{2g}{\Delta x}\sin^2\frac{\beta\Delta x}{2}\right)S^{k}_{n,m} \\ T_y(S^{k}_{n,m}) &\equiv \left(\frac{i}{\Delta y}\sin\gamma\Delta y - \frac{2g}{\Delta y}\sin^2\frac{\gamma\Delta y}{2}\right)S^{k}_{n,m} \\ \delta_x^2(S^{k}_{n,m}) &\equiv \frac{-4}{\Delta x^2}\sin^2\frac{\beta\Delta x}{2} \\ \delta_y^2(S^{k}_{n,m}) &\equiv \frac{-4}{\Delta y^2}\sin^2\frac{\beta\Delta x}{2} \end{aligned} \tag{V.57}$$

Thus we obtain for Equation V.56, the following matrix equation:

$$\begin{bmatrix} S^{k+1}_{n,m} \\ V^{k+1}_{n,m} \end{bmatrix} = \overbrace{\begin{bmatrix} -2\left[C_x\left(i\sin\beta\Delta x - 2g\sin^2\frac{\beta\Delta x}{2}\right) + \left(-8\left(D_x\sin^2\frac{\beta\Delta x}{2} + D_y\sin^2\frac{\gamma\Delta y}{2}\right) + 1\right) + C_y\left(i\sin\gamma\Delta y - 2g\sin^2\frac{\gamma\Delta y}{2}\right)\right] \\ 1 \qquad\qquad\qquad 0 \end{bmatrix}}^{A} \begin{bmatrix} S^{k}_{n,m} \\ V^{k}_{n,m} \end{bmatrix} \tag{V.58}$$

with

$$C_x = u\Delta t/\Delta x \qquad C_y = v\Delta t/\Delta t \qquad D_x = \frac{K_x\Delta t}{\Delta x^2} \qquad D_y = \frac{K_y\Delta t}{\Delta y^2}$$

In order to achieve stability all the eigenvalues of A must be less than 1 in magnitude. To compute the eigenvalues, the following charactertistic equation is used.

$$|A - \lambda I| = 0$$

$$\lambda^2 + \lambda\left[C_x\left(2i \sin \beta\Delta x - 4g \sin^2 \frac{\beta\Delta x}{2}\right) + C_y\left(2i \sin \gamma\Delta y - 4g \sin^2 \frac{\gamma\Delta y}{2}\right)\right] \qquad (V.59)$$

$$-1 + \left(8D_x \sin^2 \frac{\beta\Delta x}{2} + 8D_y \sin^2 \frac{\gamma\Delta y}{2}\right) = 0$$

In considering Equation V.59, let us introduce the following supplemental variables:

$$a = C_x\left(2i \sin \beta\Delta x - 4g \sin^2 \frac{\beta\Delta x}{2}\right) + C_y\left(2i \sin \gamma\Delta y - 4g \sin^2 \frac{\gamma\Delta y}{2}\right)$$

$$b = 8D_x \sin^2 \frac{\beta\Delta x}{2} + D_y \sin^2 \frac{\gamma\Delta y}{2} \qquad (V.60)$$

Then Equation V.59 becomes

$$\lambda^2 + 2a + (b - 1) = 0 \qquad (V.61)$$

Using the quadratic equation formula:

$$\lambda_{1,2} = \frac{-a \pm \sqrt{a^2 - 4(b - 1)}}{2} = \frac{-a}{2} \pm \sqrt{\left(\frac{a}{2}\right)^2 + 1 - b} \qquad (V.62)$$

56. To find restrictions on C_x C_y, D_x, and D_y such that $|\lambda_{1,2}| < 1$ appears to be difficult for this case.

57. Instead, we consider the ranges of C_x, C_y, D_x, and D_y for the Mississippi Sound case. Consider the following maximum velocity and dispersion conditions in Mississippi Sound: $u = v = 3$ fps, $K_x = K_y = 100$ ft^2/sec. Since on the global grid the minimum cell dimensions are $\Delta x = \Delta y = 3500$ ft and a time step $\Delta t = 360$ sec is employed, bounds on the supplemental relations in Equation V.53 become C_x, $C_y < 0.3$ and D_x, $D_y < 0.003$.

58. Let us introduce $\beta_m = 2\pi/m\Delta x$ and $\gamma_n = 2\pi/n\Delta y$ and consider the wave numbers n and m to vary from 2-9 over 3 log cycles. We compute the eigenvalue for each set of wave numbers n and m as follows:

$$a = C_x\left(2i \sin \frac{2\pi}{m} - 4g \sin^2 \frac{\pi}{m}\right) + C_y\left(2i \sin \frac{2\pi}{n} - 4g \sin^2 \frac{\pi}{n}\right)$$

$$b = 8\left(D_x \sin^2 \frac{\pi}{m} + D_y \sin^2 \frac{\pi}{n}\right) \qquad \text{(V.63)}$$

$$\lambda_{1,2} = -\frac{a}{2} \pm \sqrt{\left(\frac{a}{2}\right)^2 + 1 - 6}$$

59. The computer program employing Equation V.62 shown in Table V-3 was used to compute the eigenvalues for the general transport scheme. The results are shown in Table V-4 for the cases considered. Case III represents the conditions to be considered within Mississippi Sound. Since the upward scheme is unstable, it may not be employed as the lower order scheme in the flux-corrected transport method.

60. Although it is possible to flux-correct the three time level centering of the advective terms scheme, this was not undertaken in this study. This three level scheme with the advective terms centered in time was coded as Subroutine CONCE within the model, thereby allowing the model user an alternate scheme to employ in the transport calculations. This scheme may be employed for transport simulations in which the constituent levels are reasonably uniform. For sharp front problems, the Flux-Corrected Transport Scheme should be used.

Dispersion Coefficient Formulation

61. To close the numerical approximations to the two-dimensional depth averaged transport equation, relations for the effective dispersion coefficients must be developed in terms of flow field properties.

62. The effective dispersion coefficients are assumed to have the following forms:

$$K_x^* = C_x\sqrt{g}\,\frac{|u|h}{C} + D_x \; ; \quad K_y^* = C_y\sqrt{g}\,\frac{|v|h}{C} + D_y \qquad \text{(V.64)}$$

where

K_x^* , K_y^* = effective dispersion coefficients in the x and y directions

g = acceleration due to gravity

u , v = velocity components in the x and y directions, respectively

Table V-3

Computer Program for Determination of the Eigenvalues

for the General Three Time Level Explicit Scheme

```
      PROGRAM EIGEN
      PARAMETER (ND=5,N6=6)
      COMPLEX A,B,LM1,LM2
      DATA  PI/3.141592654/
5000  READ(ND,1)ICYC,CX,CY,DX,DY
1     FORMAT(I5,4F10.0)
      IF(ICYC.LE.0)STOP
      WRITE(N6,250)ICYC,CX,CY,DX,DY
250   FORMAT(1H1),56X,*THREE .IME LEVEL TRANSPORT SCHEMES*,////,
     1  25X,I5,* WAVE NUMBER CYCLES*,/,
     2  25X,G8.3,* X COURANT NUMBER*,/,
     2  25X,G8.3,* Y COURANT NUMBER*,/,
     2  25X,G8.3,* X DIFFUSION NUMBER *,/,
     2  25X,G8,3m* Y DIFFUSION NUMBER*,/)
      IF(CY+DY)3,3,4
3     ICYC1=1
      LIM1=1
      LIM2=1
      GO TO 5
4     ICYC1=ICYC
      LIM1=2
      LIM2=9
5     G=-1.
5005  WRITE(N6,56)G
56    FORMAT(1H1,20X,*G=*,F6.3,/)
      DO 200 I=1,ICYC1
      DO 200 J=LIM1,LIM2
      N=J*10**(I-1)
      DO 200 K=1,ICYC
      DO 200 L=2,9
      M=L*10**(K-1)
      A=CMPLX(-4,*G*(CX*SIN(PI/M)*SIN(PI/M)+CY*SIN(PI/N)*SIN(PI/N)),
     1  2,*CX*SIN(2.*PI/M)+CY*SIN(2*PI/N)))
      B=CMPLX(1.-8.*(DX*SIN(PI/M)*SIN(PI/M)*DY*SIN(PI/N)*SIN(PI/N)),0.)
      LM1=CSQRT((A/2.)*(A/2.)+B)
      LM2=-A/2.-LM1
      LM1=-A/2,+LM1
      AMAG1=CABS(LM1)
      AMAG2=CABS(LM2)
200   WRITE(N6.55)N,M,AMAG1,AMAG2
55    FORMAT(20X,2I6,9X,F6,3,14X,F6.3)
      IF(G.GT..5)GO TO 5000
      G=G+1.
      GO TO 5005
      END
```

Table V-4

Eigenvalue Analysis Results for the General Three Time Level Explicit Scheme

Advective Term	Magnitude of Largest Eigenvalue
Case I: $C_x = C_y = 0.$ $D_x = D_y = 0.125$ (Diffusion Only)	
Centered (g = 0)	<1
Upwind (g = -1)	<1
Forward (g = +1)	<1
Case II: $C_x = C_y = 0.5$ $D_x = D_y = 0.125$	
Centered (g = 0)	>1
Upwind (g = -1)	>1
Forward (g = +1)	>1
Case III: $C_x = C_y = 0.3$ $D_x = D_y = 0.003$	
Centered (g = 0)	<1
Upwind (g = -1)	>1
Forward (g = +1)	>1

h = water depth

C = Chezy coefficient

C_x , C_y = dispersion factors in the x and y directions, respectively

D_x , D_y = dispersion offsets due to wind effects in the x and y directions, respectively, (D_x , $D_y \geq 0$)

63. Elder (1959) has determined the longitudinal and lateral dispersion coefficients in open channel flow experiments to be given by the following relations

$$K_L = 5.93\ hu^* \qquad K_{LA} = 0.23\ hu^* \tag{V.65}$$

where

K_{LA} ≡ lateral dispersion coefficient

K_L ≡ longitudinal dispersion coefficient

h ≡ water depth (hydraulic radius)

u* ≡ shear (friction) velocity

For open channel flow, the following relations hold:

$$u^* = \sqrt{ghS_e} \qquad u = C\sqrt{hS_e} \tag{V.66}$$

where

u* ≡ friction velocity

g ≡ acceleration of gravity

h ≡ water depth

S_e ≡ slope of energy grade line

C ≡ Cheźy coefficient

As a result, we obtain:

$$u_* = \sqrt{g}\ \frac{u}{C} \tag{V.67}$$

where

u ≡ velocity

g ≡ gravity

C ≡ Cheźy coefficient

Therefore, Equation V.65 becomes

$$K_L = 5.93\sqrt{g}\ \frac{uh}{C} \qquad K_{LA} = 0.23\sqrt{g}\ \frac{uh}{C} \tag{V.68}$$

64. Taylor (1954) has conducted pipe flow experiments to determine the longitudinal dispersion coefficient. By assuming the hydraulic radius as half the pipe radius in the pipe experiments and equal to the water depth in a uniform steady flow open channel, the coefficient in the longitudinal dispersion coefficient equation (V.68) is determined to be 20.2 rather than 5.93.

65. For one-dimensional flow in the x direction, $C_x \in (5.93, 20.2)$ and $C_y = 0.23$. In order to extrapolate these results to a two-dimensional flow as occurs in Mississippi Sound C_x, C_y, D_x, D_y are specified for each grid cell. The cell face conditions for each cell are examined independently in each coordinate direction. For a no-flow cell face condition, C_x and D_x or C_y and D_y are set to zero. (No dispersion may occur across a solid boundary.) For a flow cell face condition on the u-velocity cell face (see Figure A-1), the second digit in the u-velocity cell face flag is examined. If advection is not allowed, C_x is reduced by a user specified factor, F. For a flow cell face condition on the v-velocity cell face (see Figure A-1), analogous procedures are employed.

66. In order to calibrate the effective dispersion coefficients, C_x, D_x, C_y, D_y, specified on a cell-by-cell basis, and F are adjusted until simulated salinity levels correspond to measured salinity levels. Based upon experimental results, C_x, $C_y \in (5.93, 20.2)$ $F \sim 0.23/5.93 = 0.0388$. The wind effect terms D_x and D_y are more difficult to determine. Leendertse (1970, 1971) in a simulation of Jamaica Bay suggested D_x, $D_y \in (25, 45)$ ft^2/sec. Since the velocity magnitudes u and v in Equation V.64 will increase with increasing wind speeds, the effective dispersion coefficients will increase without considering D_x and D_y. For this reason, D_x and D_y will be set to zero, and C_x, C_y, and F will be adjusted during the calibration process.

PART VI: DEVELOPMENT OF A GLOBAL GRID FOR MISSISSIPPI SOUND

67. The hydrodynamic salinity model developed in this study employs a variable (exponentially stretched) computational grid. In transforming real space to computational space, each coordinate axis is mapped independently using Program MAPIT. This enables the specification of partition points along each axis. These partition points coincide with the location of barrier island passes and the shoreline.

68. The grid spacing along the southern and eastern extents of the global grid as shown in Figure VI-1 was set to correspond to the 15-min latitude and longitude uniform grid employed in the GTM. In this manner, interpolation in only one space dimension is required in developing the global grid boundary conditions. This consideration established an upper bound on the grid spacing in each direction. The lower bound in grid spacing was obtained such that grid cell aspect ratios would be no larger than 20 and explicit time-step limitations would not be severe. Considerable engineering judgment and consultation with the Mobile District was exercised in developing the global grid.

69. The grid developed extends in geographical extent from the western end of Lake Borgne to Santa Rosa Island in the west-east orientation and from the Mississippi River Delta to above Mobile Bay in the north-south orientation. The east-west extent employs 116 lines and the north-south 60 lines, resulting in a grid of 6785 (115 × 59) computational cells as shown in Figure VI-2. Minimum spatial resolution of approximately 3500-4000 ft is obtained within the passes into Mississippi Sound and within the Sound itself. Depths within Mississippi Sound are relatively shallow (10-20 ft), except in the navigation channels, which are normally maintained at 30-35 ft. As a result, the gravity wave speed within the sound is <38 fps, resulting in an explicit time-step limitation of approximately 100 sec. All numerical simulations employ a 360-sec (6 min) time step, resulting in a maximum spatial Courant number of less than 4 within the Sound. The mapping for the horizontal (east-west) orientation is presented in Table VI-1. The mapping for the vertical (north-south) orientation is given in Table VI-2. The grid obtained is presented in Figure VI-2. In Tables VI-1 and VI-2, the real space values are in map inches as measured from the maps shown in Table VI-3 below.

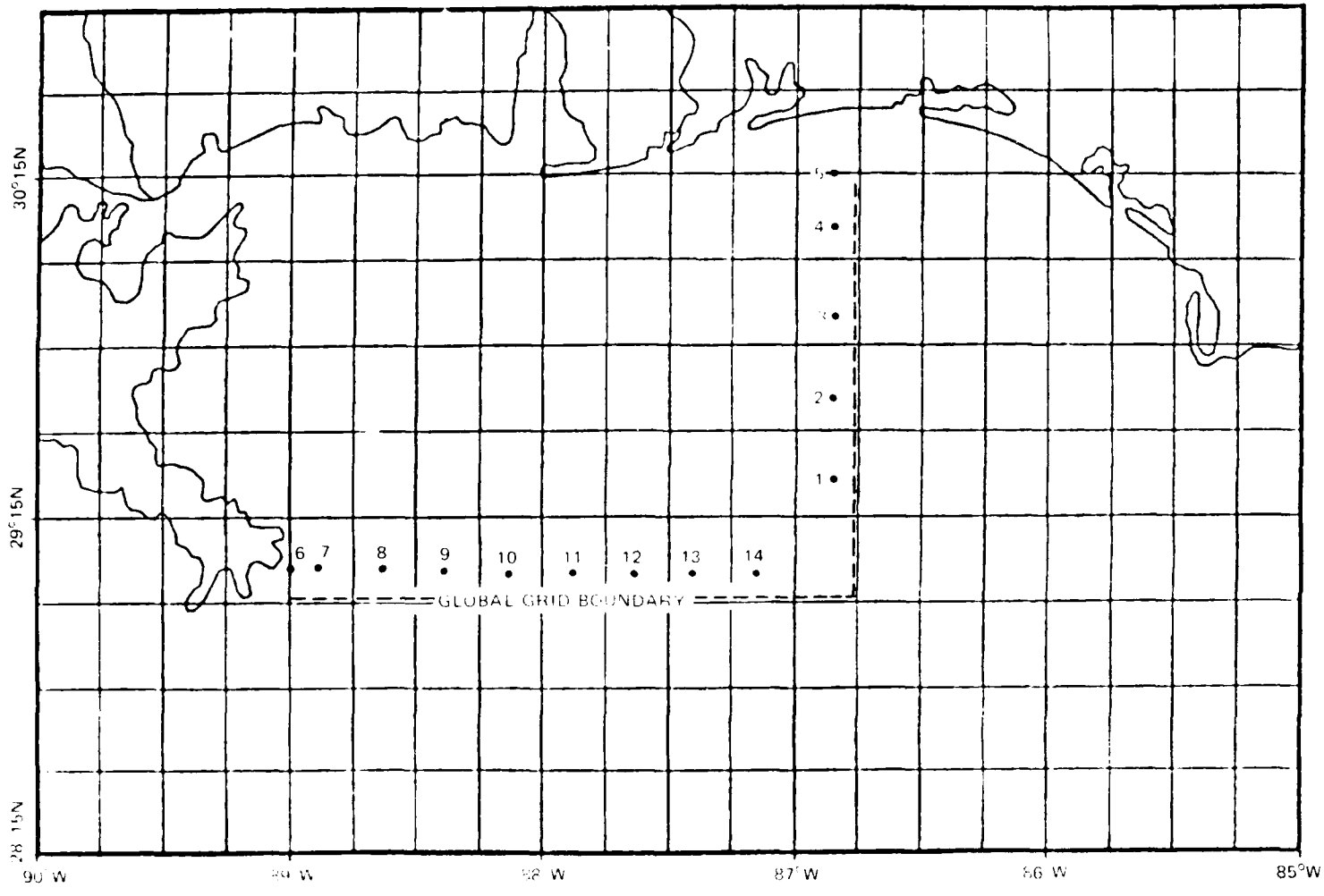

Figure VI-1. Global grid, GTM boundary orientation

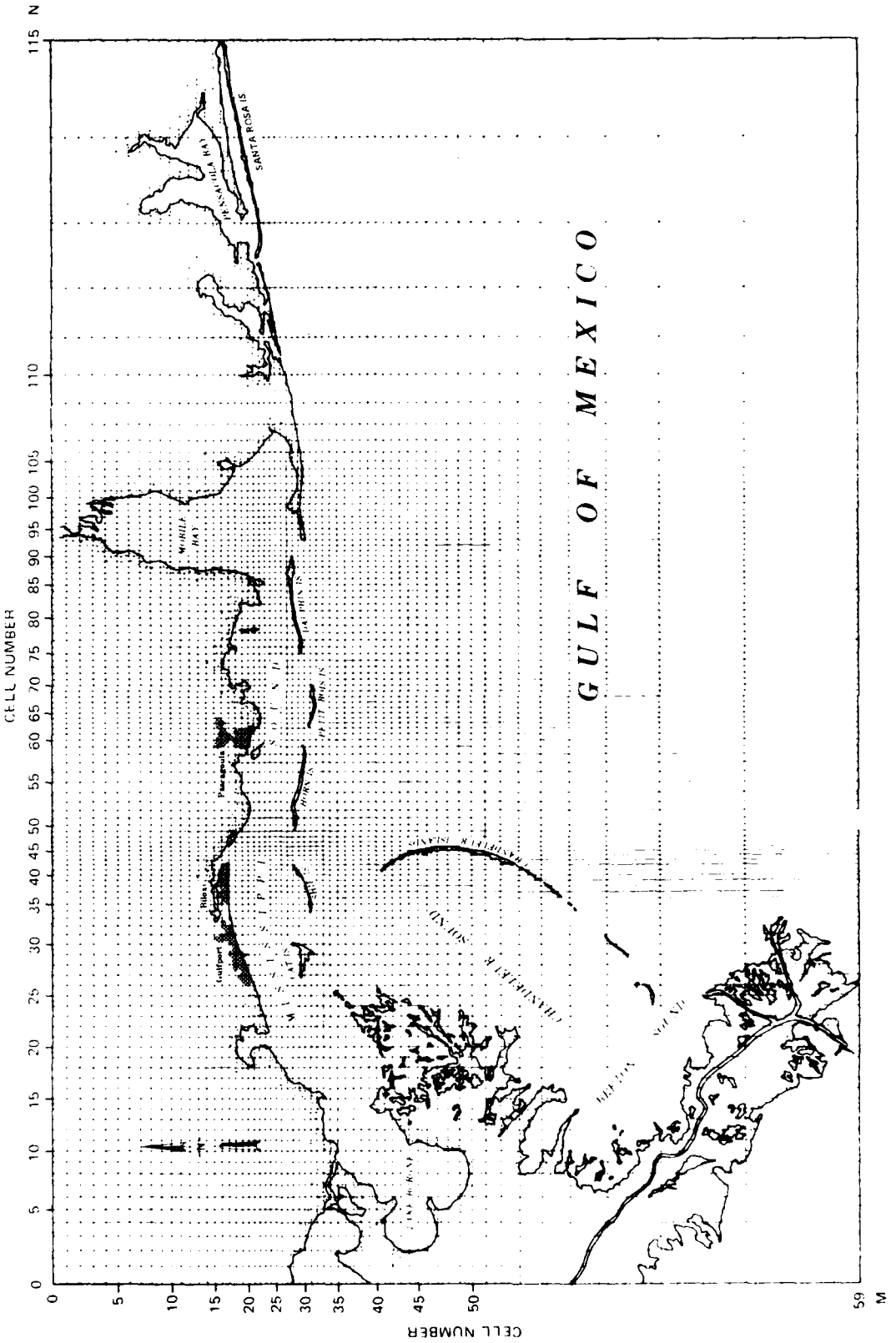

Figure VI-2. Mississippi Sound global grid

Table VI-1

Horizontal Mapping Results

Region No.	Cells per Region	Real Space	Alpha Space	Mu	A	B	C
1	5	0.10000E+01	1.0	0.75000E+00	0.22721E-01	0.97728E+00	0.76744E+00
2	8	0.38882E+01	6.0	0.49442E+00	0.67690E-01	0.10321E+01	0.74990E+00
3	17	0.74000E+01	14.0	0.40000E+00	0.18000E+01	0.40000E+00	0.10000E+01
4	4	0.14200E+02	31.0	0.40000E+00	0.19213E+02	0.24496E+05	0.24736E+01
5	12	0.15500E+02	35.0	0.26241E+00	0.32246E+02	0.11769E+03	0.54844E+00
6	9	0.18000E+02	47.0	0.16624E+00	0.16760E+02	0.36076E-10	0.63012E+01
7	8	0.20500E+02	56.0	0.42082E+00	0.25243E+02	0.23061E+10	0.49691E+01
8	16	0.22800E+02	64.0	0.18965E+00	0.18588E+02	0.26310E-04	0.28814E+01
9	12	0.26600E+02	80.0	0.28859E+00	0.41441E+02	0.13548E+05	0.15556E+01
10	14	0.29500E+02	92.0	0.20191E+00	0.24629E+02	0.15824E-06	0.38132E+01
11	9	0.32989E+02	106.0	0.30076E+00	0.31997E+02	0.85978E-65	0.32125E+02
12	1	0.45600E+02	115.0	0.38000E+01	0.39140E+03	0.38000E+01	0.10000E+01
13	0	0.49400E+02	116.0	0.38000E+01	0.	0.	0.

Table VI-2

Vertical Mapping Results

Region No.	Cells per Region	Real Space	Alpha Space	Mu	A	B	C
1	1	0.10000E+01	1.0	0.43500E+01	0.33500E+01	0.43500E+01	0.10000E+01
2	7	0.53500E+01	2.0	0.43500E+01	0.28318E+02	0.29864E+02	0.37879E+00
3	9	0.15325E+02	9.0	0.54682E+00	0.21432E+02	0.27389E+02	0.13389E+00
4	7	0.18900E+02	18.0	0.30000E+02	0.13500E+02	0.30000E+00	0.10000E+01
5	3	0.21000E+02	25.0	0.30000E+00	0.27943E+02	0.22470E+03	0.10802E+01
6	10	0.21800E+02	28.0	0.23699E+00	0.93014E+01	0.21307E+01	0.53093E+00
7	22	0.24000E+02	38.0	0.20537E+00	0.21534E+02	0.24660E-04	0.31650E+01
8	0	0.32000E+02	60.0	0.55206E+00	0.	0.	0.

Table VI-3

Global Grid Charts

No.	Description	Scale
NH 15-6	Baton Rouge	1:250000
NH 15-9	New Orleans	1:250000
NH 16-4	Mobile	1:250000
NH 16-7	Breton Sound	1:250000
NH 16-5	Pensacola	1:250000

Initial Depth Assignment

70. Program TGRID was employed to plot subgrids corresponding to grid areas shown on the individual nautical charts as shown in Table VI-4. Each subgrid was next overlaid on its corresponding nautical chart. For most grid cells, the assigned depth represented an average depth over the cell. In order to represent flow restrictions in some cells, the minimum depth in the cell was more heavily considered in the averaging process. The assigned depths are presented in Table VI-5, which were directly output from WIFM. In interpreting Table VI-5, all water depths are in feet, preceded by a minus sign, and are with respect to local mean sea level (LMSL), which was taken 1 ft above MLLW. (Land elevations were assigned a value of +10.)

Incorporation of Hydrographic Survey Information

71. In order to properly model circulation within Mississippi Sound, the depth field must be accurately specified along transects across barrier island passes and bay entrances. Raytheon Ocean Systems was contracted by the Mobile District to obtain soundings at 50-ft intervals for the transects shown in Figure II-5. Shallow water areas and land obstructions were avoided and soundings were plotted in state (Louisiana, Mississippi, and Alabama) coordinate systems at a scale of 1:8000.

72. The method of incorporating the hydrographic survey data into the previously developed depth field is developed in the context of a journal as presented below.

Journal setup

73. Plots of transects were identified and labeled with respect to the general location map (Figure II-5). Requested transects, noted on small craft charts 11367, 72, 74, and 78, were contrasted to actual transects by checking beginning and ending points in state coordinates of transects on the plots and on the charts. In cases where differences did exist, actual transects were added to the charts. Latitude and longitude of end points of the surveys were then interpolated from the small craft charts.

74. A journal was prepared (Table VI-6) identifying assigned labels for the various transects, giving latitude/longitude and state coordinates of the end points of each transect, and identifying pertinent nautical charts.

Table VI-4

Program TGRID Subgrid Plots

Grid Indices			
M	N	Nautical Chart	Scale
15-35	1-30	11371 22nd Ed. 4/80	1:80000
36-56	1-30	11371 22nd Ed. 4/80	1:80000
		11363 20th Ed. 1/80	1:80000
		11364 23rd Ed. 2/80	1:80000
57-59	1-30	11361 40th Ed. 6/78	1:80000
		11363 20th Ed. 1/80	1:80000
		11364 23rd Ed. 2/80	1:80000
15-36	31-78	11373 25th Ed. 6/80	1:80000
37-59	31-115	11360 24th Ed. 2/80	1:456394
37-56	29-45	11363 20th Ed. 1/80	1:80000
1-36	79-109	11376 33rd Ed. 9/79	1:80000
15-36	110-115	11382 23rd Ed. 11/77	1:80000

Table VI-5

Global Grid Depth Field

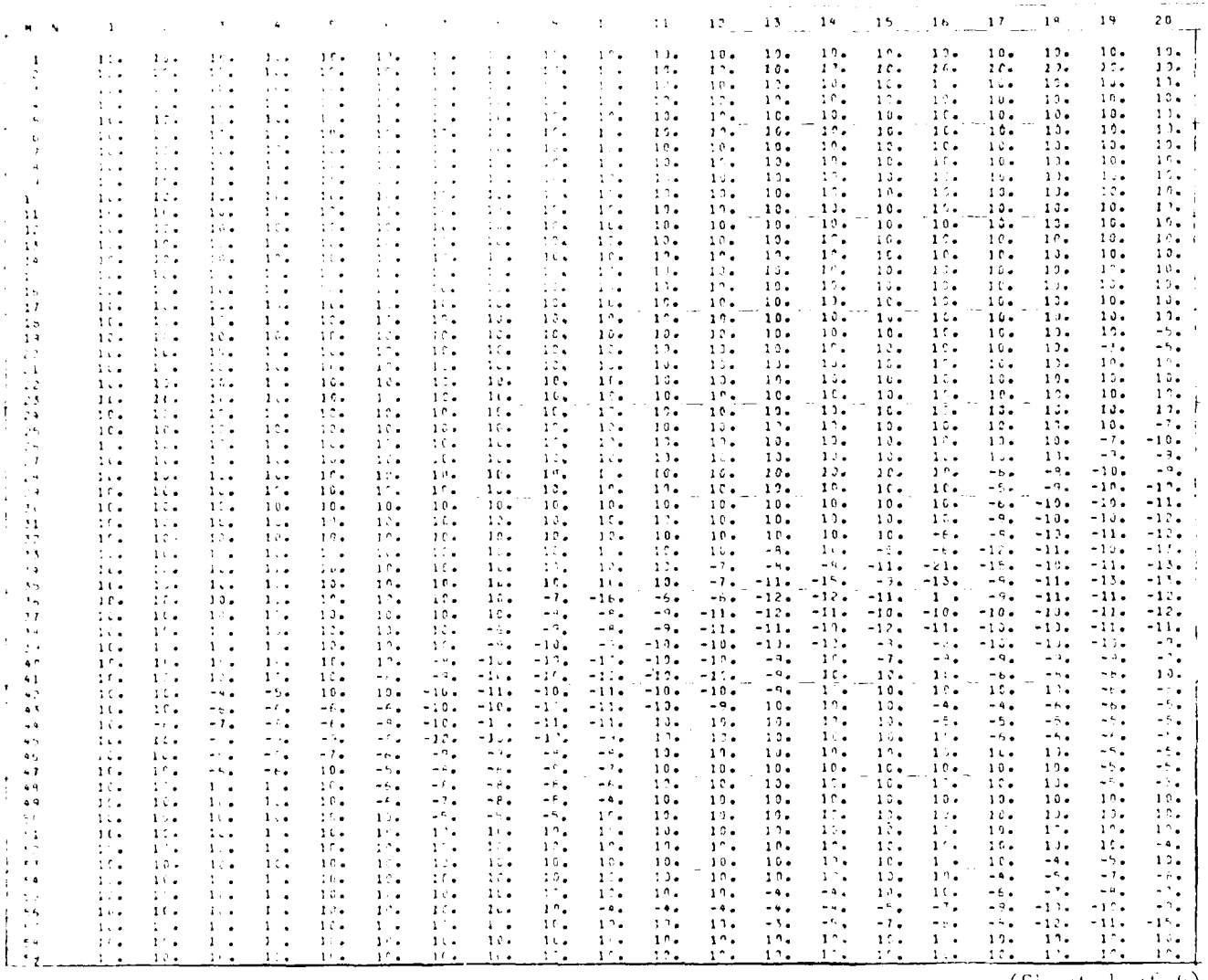

(Continued)

(Sheet 1 of 6)

Table VI-5 (Continued)

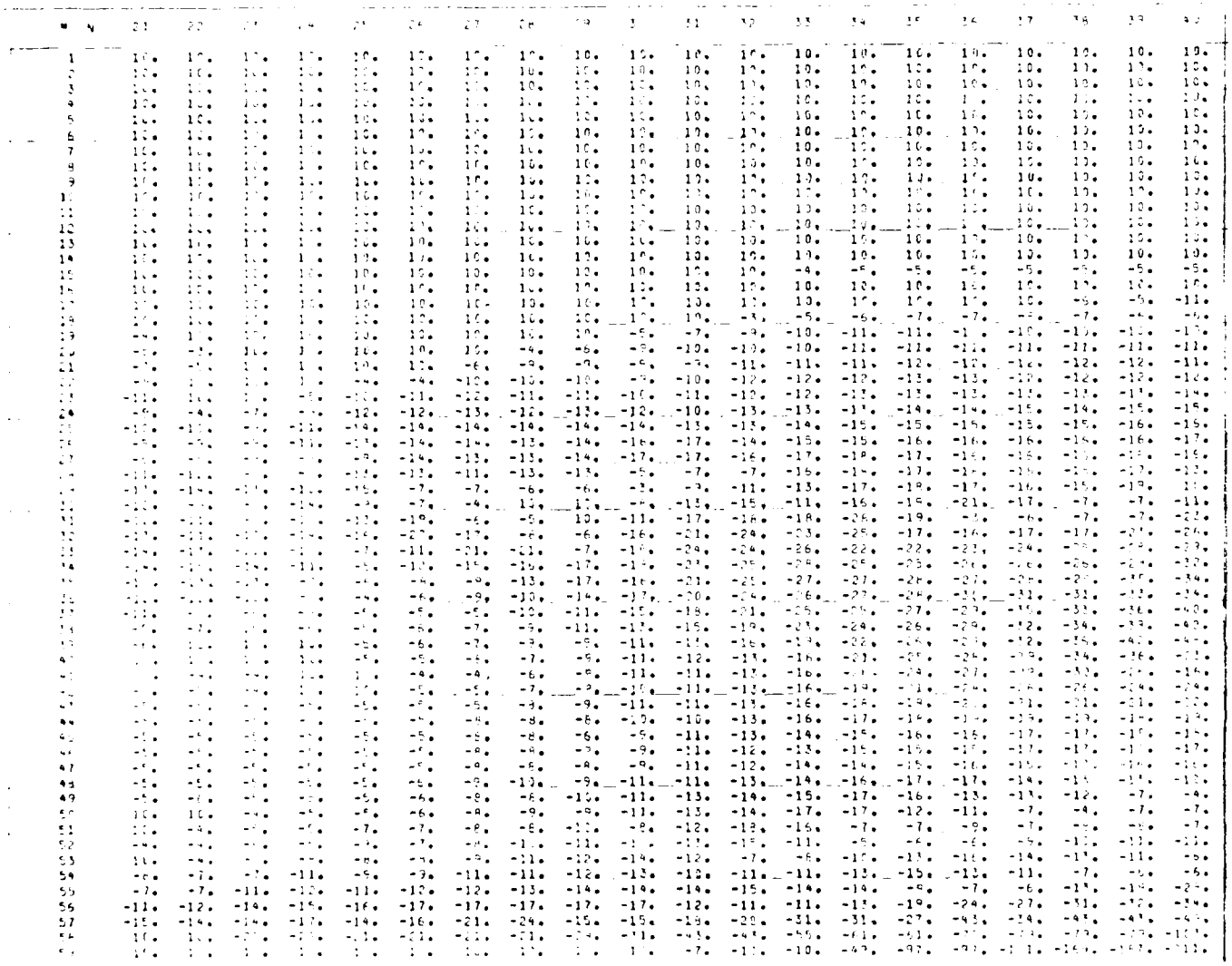

(Continued)

Table VI-5 (Continued)

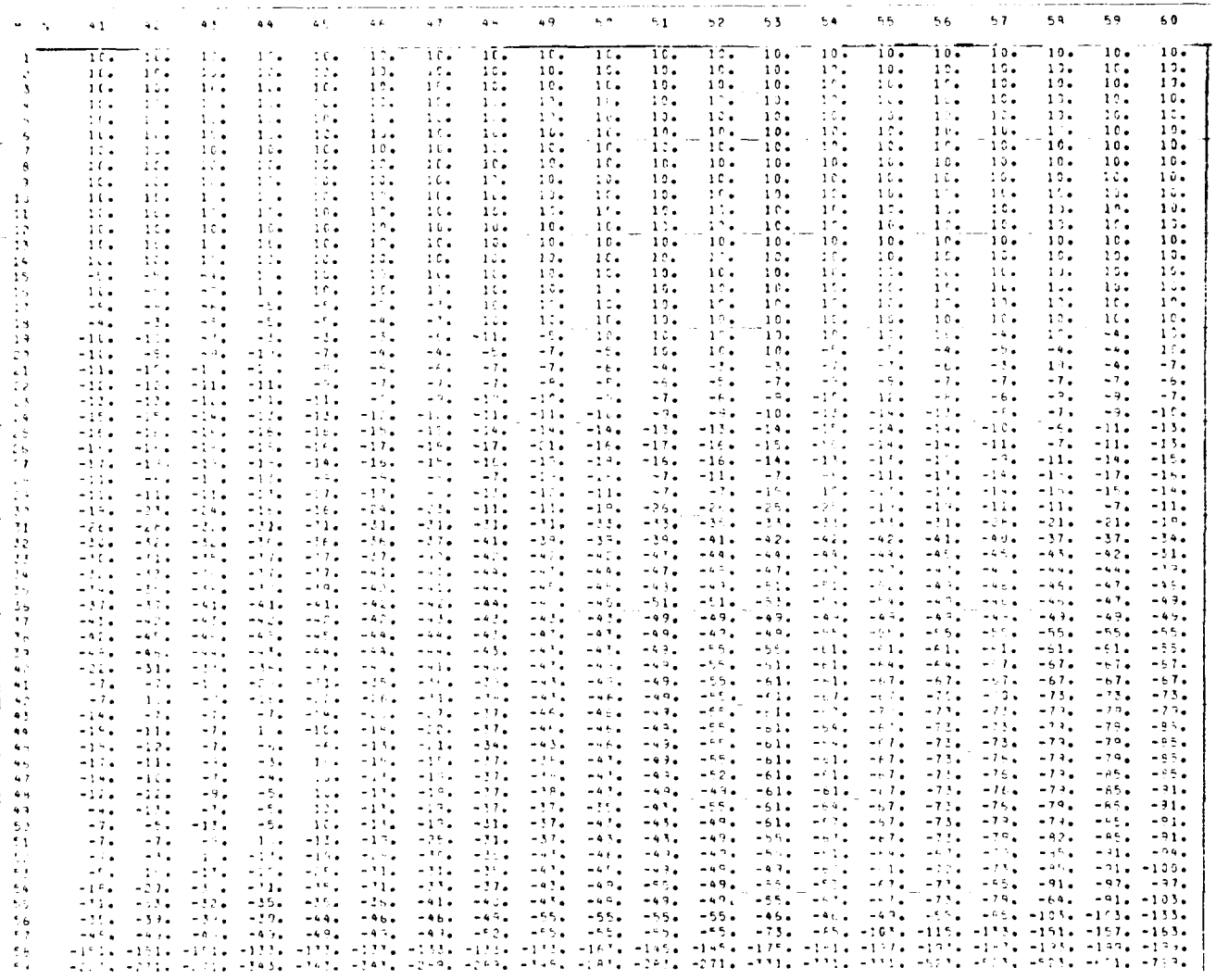

(Continued)

Table VI-5 (Continued)

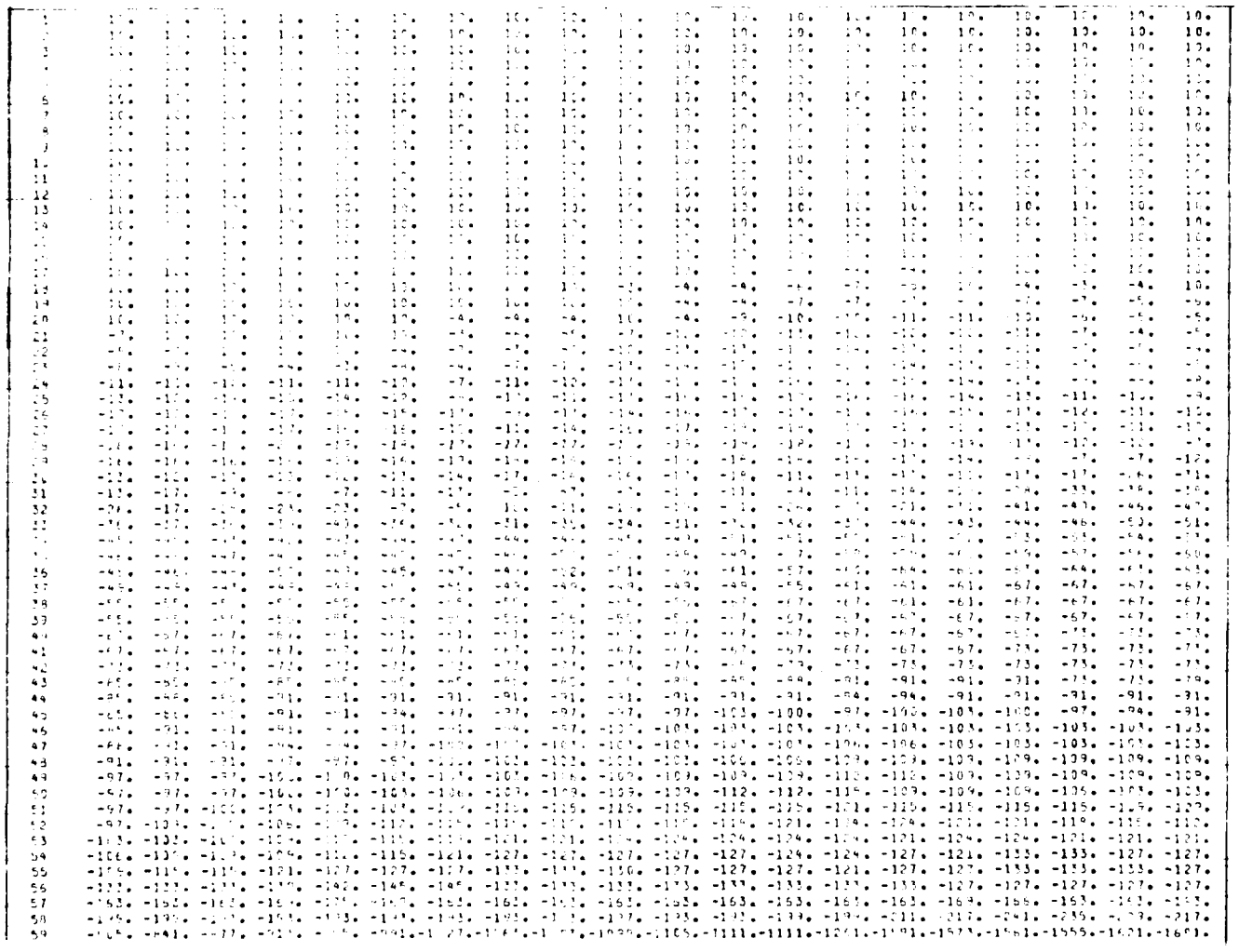

(Continued)

Table VI-5 (Continued)

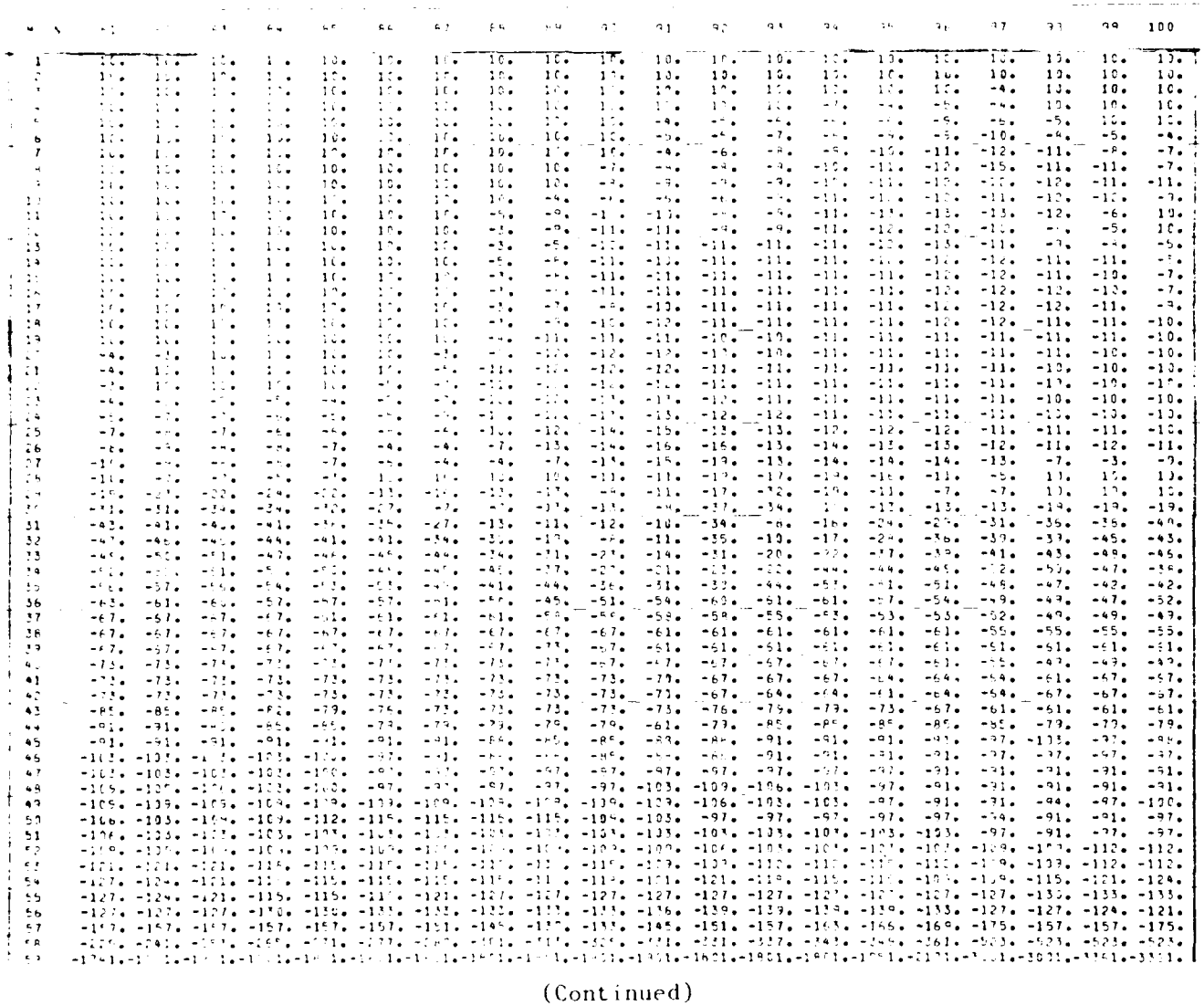

(Continued)

Table VI-5 (Concluded)

M	K	I 1	I02	I 3	I04	I05	I06	I 7	I0-	I09	I1	I11	I12	I13	I14	I15
1		10.	1 .	1 .	1 .	10.	1 .	1 .	1 .	1 .	1 .	1 .	1 .	1 .	1 .	1 .
2		1 .	1 .	1 .	1 .	1 .	1 .	1 .	1 .	1 .	1 .	1 .	1 .	1 .	1 .	1 .
3		1 .	1 .	1 .	1 .	1 .	1 .	1 .	1 .	1 .	1 .	1 .	1 .	1 .	1 .	1 .
4		1 .	1 .	1 .	1 .	1 .	1 .	1 .	1 .	1 .	1 .	1 .	1 .	1 .	1 .	1 .
5		1 .	1 .	1 .	1 .	1 .	1 .	1 .	1 .	1 .	1 .	1 .	1 .	1 .	1 .	1 .
6		1 .	1 .	1 .	1 .	1 .	1 .	1 .	1 .	1 .	1 .	1 .	1 .	1 .	1 .	1 .
7		1 .	1 .	1 .	1 .	1 .	1 .	1 .	1 .	1 .	1 .	1 .	1 .	1 .	1 .	1 .
8		1 .	1 .	1 .	1 .	1 .	1 .	1 .	1 .	1 .	1 .	1 .	1 .	1 .	1 .	1 .
9		1 .	1 .	1 .	1 .	1 .	1 .	1 .	1 .	1 .	1 .	1 .	1 .	1 .	1 .	1 .
10		1 .	1 .	1 .	1 .	1 .	1 .	1 .	1 .	1 .	1 .	1 .	1 .	1 .	1 .	1 .
11		1 .	1 .	1 .	1 .	1 .	1 .	1 .	1 .	1 .	1 .	1 .	1 .	1 .	1 .	1 .
12		1 .	1 .	1 .	1 .	1 .	1 .	1 .	1 .	1 .	1 .	1 .	1 .	1 .	1 .	1 .
13		1 .	1 .	1 .	1 .	1 .	1 .	1 .	1 .	1 .	1 .	1 .	1 .	1 .	1 .	1 .
14		1 .	1 .	1 .	1 .	1 .	1 .	1 .	1 .	1 .	1 .	1 .	1 .	1 .	1 .	1 .
15		1 .	1 .	1 .	1 .	1 .	1 .	1 .	1 .	1 .	1 .	1 .	1 .	1 .	1 .	1 .
16		1 .	1 .	1 .	1 .	1 .	1 .	1 .	1 .	1 .	1 .	1 .	1 .	1 .	1 .	1 .
17		-7.	-4.	1 .	1 .	1 .	1 .	1 .	1 .	1 .	1 .	1 .	1 .	1 .	1 .	1 .
18		-10.	-9.	-6.	1 .	1 .	1 .	1 .	1 .	1 .	1 .	1 .	1 .	1 .	1 .	1 .
19		-11.	-10.	-8.	-4.	1 .	1 .	1 .	1 .	1 .	1 .	1 .	1 .	1 .	1 .	1 .
20		-11.	-11.	-9.	-8.	-4.	1 .	1 .	1 .	1 .	1 .	1 .	1 .	1 .	1 .	1 .
21		-12.	-12.	-11.	-9.	-8.	1 .	1 .	1 .	1 .	1 .	1 .	1 .	1 .	1 .	1 .
22		-12.	-12.	-11.	-9.	-8.	-5.	1 .	1 .	1 .	1 .	1 .	1 .	1 .	-4.	-7.
23		-12.	-9.	-9.	-9.	-8.	-6.	-6.	1 .	1 .	1 .	1 .	1 .	-16.	-57.	-76.
24		-9.	-8.	-8.	-8.	-8.	-8.	-7.	1 .	1 .	1 .	1 .	1 .	-23.	-61.	-79.
25		-9.	-9.	-9.	-9.	-9.	-8.	-7.	-4.	1 .	1 .	1 .	-13.	-35.	-61.	-87.
26		-8.	-8.	-8.	-8.	-8.	-8.	-7.	1 .	1 .	1 .	1 .	-25.	-41.	-71.	-79.
27		-8.	-8.	-8.	-8.	-7.	-7.	-6.	1 .	1 .	1 .	-13.	-39.	-49.	-71.	-85.
28		-8.	-8.	-7.	-7.	-7.	-5.	1 .	1 .	1 .	1 .	-11.	-36.	-55.	-74.	-84.
29		1 .	1 .	1 .	1 .	1 .	1 .	1 .	1 .	-11.	-29.	-51.	-45.	-61.	-78.	-84.
30		-12.	-12.	-11.	-12.	-14.	-15.	-16.	-35.	-3 .	-34.	-53.	-57.	-68.	-83.	-87.
31		-40.	-39.	-31.	-27.	-26.	-31.	-31.	-34.	-31.	-35.	-46.	-55.	-67.	-91.	-93.
32		-36.	-25.	-2 .	-29.	-3 .	-33.	-38.	-37.	-36.	-35.	-48.	-61.	-71.	-91.	-94.
33		-31.	-26.	-31.	-33.	-35.	-33.	-37.	-39.	-39.	-43.	-53.	-76.	-69.	-91.	-92.
34		-31.	-3 .	-31.	-35.	-37.	-41.	-41.	-42.	-41.	-47.	-53.	-61.	-75.	-91.	-1 .
35		-40.	-3 .	-37.	-3 .	-43.	-47.	-47.	-44.	-45.	-5 .	-56.	-61.	-75.	-91.	-11 .
36		-42.	-43.	-49.	-46.	-47.	-49.	-46.	-46.	-46.	-54.	-75.	-61.	-80.	-91.	-1 .
37		-49.	-44.	-46.	-49.	-49.	-49.	-47.	-5 .	-5 .	-61.	-73.	-85.	-91.	-79.	-211.
38		-55.	-5 .	-55.	-55.	-55.	-55.	-5 .	-55.	-55.	-73.	-73.	-67.	-163.	-91.	-277.
39		-61.	-61.	-61.	-61.	-61.	-61.	-61.	-61.	-61.	-7 .	-55.	-55.	-97.	-91.	-313.
40		-49.	-49.	-49.	-49.	-49.	-47.	-73.	-7 .	-7 .	-7 .	-7 .	-7 .	-41.	-121.	-305.
41		-7 .	-73.	-7 .	-61.	-6 .	-67.	-73.	-64.	-6 .	-91.	-73.	-73.	-91.	-115.	-331.
42		-67.	-67.	-73.	-73.	-64.	-73.	-79.	-85.	-61.	-85.	-91.	-65.	-91.	-115.	-361.
43		-61.	-61.	-61.	-67.	-7 .	-7 .	-79.	-85.	-97.	-91.	-97.	-91.	-91.	-151.	-395.
44		-79.	-7 .	-7 .	-73.	-79.	-79.	-85.	-6 .	-6 .	-55.	-97.	-91.	-97.	-169.	-433.
45		-79.	-79.	-79.	-79.	-6 .	-85.	-6 .	-91.	-97.	-91.	-97.	-97.	-91.	-181.	-457.
46		-97.	-97.	-97.	-97.	-1 .	-1 .	-1 .	-1 .	-97.	-97.	-97.	-97.	-91.	-181.	-481.
47		-91.	-91.	-91.	-91.	-91.	-91.	-91.	-1 .	-97.	-97.	-1 .	-1 .	-1 .	-199.	-475.
48		-91.	-91.	-91.	-97.	-97.	-97.	-163.	-1 .	-1 .	-97.	-1 .	-1 .	-115.	-373.	-517.
49		-1 .	-1 .	-1 .	-97.	-1 .	-1 .	-1 .	-97.	-97.	-97.	-1 .	-97.	-157.	-391.	-517.
50		-1 .	-1 .	-1 .	-1 .	-1 .	-1 .	-1 .	-1 .	-1 .	-1 .	-1 .	-1 .	-181.	-4 .	-611.
51		-1 .	-1 .	-1 .	-1 .	-1 .	-1 .	-1 .	-1 .	-1 .	-1 .	-1 .	-1 .	-253.	-6 .	-547.
52		-1 .	-1 .	-1 .	-1 .	-1 .	-1 .	-1 .	-1 .	-1 .	-1 .	-1 .	-1 .	-271.	-6 .	-6 .
53		-1 .	-1 .	-1 .	-1 .	-1 .	-1 .	-1 .	-1 .	-1 .	-1 .	-1 .	-145.	-427.	-715.	-6 .
54		-1 .	-1 .	-1 .	-1 .	-1 .	-1 .	-1 .	-1 .	-1 .	-1 .	-1 .	-163.	-451.	-733.	-619.
55		-1 .	-1 .	-1 .	-1 .	-1 .	-1 .	-1 .	-1 .	-1 .	-1 .	-1 .	-181.	-601.	-799.	-733.
56		-1 .	-1 .	-1 .	-1 .	-1 .	-1 .	-1 .	-1 .	-1 .	-1 .	-1 .	-253.	-601.	-925.	-829.
57		-1 .	-1 .	-1 .	-1 .	-1 .	-1 .	-1 .	-1 .	-1 .	-1 .	-1 .	-511.	-1387.	-1261.	-1493.
58		-1 .	-1 .	-1 .	-1 .	-1 .	-1 .	-1 .	-1 .	-1 .	-1 .	-1 .	-1471.	-1891.	-2159.	-1621.
59		-1 .	-1 .	-1 .	-1 .	-1 .	-1 .	-1 .	-1 .	-1 .	-1 .	-1 .	-4183.	-4 .	-3021.	-2971.

(Sheet 6 of 6)

Table VI-6

Hydrographic Survey Journal

TRANSECT NO.	GENERAL DESCRIPTION	STARTING POINT LATITUDE	STARTING POINT LONGITUDE	ENDING POINT LATITUDE	ENDING POINT LONGITUDE	STATE COORDINATES START		STATE COORDINATES END	GRIDCELLS	NOAA CHARTS	NO.
1A	PASS HEUREUX PT LE PETIT PASS ISLAND	30°09'¾	89°29'	30°05'	89°28'½	2585 518	LA	2587 521	(15,39)p	113 11	1A
1B	LE PETIT PASS ISLAND TO HALF MOON ISLAND	30°05'½	89°28'¼	30°07'¾	89°27'	2589 524	LA	2597 536	(15,38) (16,37)	11	1B
1C	HALF MOON ISLAND TO LIGHTHOUSE PT	30°08'½	89°26'¾	30°10'½	89°27'½	2591 543	LA	2593 553	(15,34)//(16,34) (16,35)	11 & 67	1C
2	CAILLOU BOAD BRIDGE, BAY ST LOUIS TO HELICOPTER PT	30°18'1/10	89°19'¾	30°18'1/10	89°18'	2634 600	LA	2643 600	(21,24)	11 & 12	2
3	ISLE AU PITRE TO WEST PT. CAT ISLAND	30°09'¾	89°11'½	30°13'½	89°10'¾	2677 550	LA	2680 573	(25,34)p (26,30)p (26,31) (26,32) (26,33)	11 & 12	3
4	ISLE AU PITRE TO SOUTH SPIT CAT ISLAND	30° 9'¾	89°11'½	30°11'	89°07'	2677 550	LA	2702 557	(24,34) (27,34) (28,35)	113 11 & 12	4
5	SHIP ISLAND PASS	30°19'¼	89°03'¾	30°12'¾	89°19'¼	427 207	MS	452 198	(31,29)/(31,30) (32,30) (33,31) (34,31)	113 73 & 12	5
6	GULFPORT CHANNEL AT SHIP ISLAND PASS	30°13'	89°00'½	30°12'	88°58'¼	495 199	MS	457 199	(33,32) (34,32)	73 & 12	6
7	CAMILLE CUT	30°13'	88°55'½	30°13'¼	88°54'⅔	470 201	MS	475 202	(34,30) (38,31) (39,30)* (39,31)*	73 & 12	7
8	BILOXI BAY BRIDGE BILOXI TO FLEMMER PT	30°23'⅔	88°51'¼	30°24'½	88°50'¼	494 266	MS	497 269	(42,16) (43,16) SPECIAL CASE; data divided equally between adjacent cells	73 & 12	8
9	BILOXI BAY SOUTH DEER ISLAND TO DAVIS BAYOU	30°21'½	88°48'	30°22'¼	88°47'⅔	510 254	MS	512 257	SURVEY TOO SHORT TO BE OF USE; DISREGARD	73 & 12	9
10A	DOG KEYS PASS (SOUTH TRANSECT)	30°19'⅛	88°52'½	30°19'⅔	88°46'¼	488 209	MS	520 209	(42,29) (43,29) (44,29) (45,29) (46,29) (47,29) (48,29) (49,29)	73 & 12	10A
10B	PASS DE L'OUEST BETWEEN HORN ISLAND AND PETIT BOIS ISLAND	30°14'¾	88°52'¼	30°14'¾	88°46'⅓	489 211	MS	517 211	(42,28) (43,28) (44,28) (45,28) (46,28) (47,28) (48,28) (49,28)	73 & 12	10B
10C	DOG KEYS PASS (NORTH TRANSECT)	30°15'	88°52'½	30°15'	88°46'½	458 213	MS	520 213	(42,28) (43,28) (44,28) (45,28) (46,28) (47,28) (48,28) (49,28)	73 & 12	10C
11A	HORN ISLAND PASS (SOUTH TRANSECT)	30°13'	88°34'	30°12'½	88°30'	589 201	MS	605 191	(59,31) (60,31) (61,31) (62,31)	73 & 11	11A
11B	HORN ISLAND TO PETIT BOIS ISLAND	30°13'½	88°33'¼	30°12'¼	88°30'½	596 202	MS	603 199	(59,30) (60,30) (61,31) (62,31)	73 & 11	11B
11C	HORN ISLAND PASS (NORTH TRANSECT)	30°13'¾	88°33'½	30°13'½	88°30'	595 205	MS	604 209	(59,30) (60,30) (61,30) (62,30)	73 & 11	11C
12A	PETIT BOIS PASS (SOUTH TRANSECT)	30°12'½	88°23'½	30°13'	88°18'½	639 197	MS	665 210	(71,31) (72,31) (73,31) (74,31) (75,31) (76,31)	73 & 74	12A
12B	PETIT BOIS ISLAND TO DAUPHIN ISLAND	30°12'¼	88°24'	30°13'½	88°18'¼	627 197	MS	664 209	(71,31) (72,31) (73,31) (74,31) (75,31)	73 & 74	12B
12C	- - - -	30°12'½	88°24'¾	30°14'	88°19'½	618 198	MS	660 206	(71,31) (72,31) (73,30) (74,30) (75,30)	73 & 74	12C
12D	NORTH TRANSECT	30°12'¾	88°24'	30°14'½	88°19'¾	635 199	MS	640 209	(70,31) (71,31) (72,30) (73,30) (74,30) (75,30)	113 73 & 74	12D
13	DAUPHIN ISLAND TO BARRAN PT	30°15'	88°11'½	30°19'	88°11'¼	282 92	AL	282 115	(82,27) (83,27) (83,26) (82,26) (82,25) (82,24)	113 76 & 78	13
14	GRANTS PASS, PASS AUX HERONS	30°18'	89°08'¼	30°17'¼	88°07'¼	299 109	AL	331 105	(96,25)	76 & 78	14
15	MOBILE BAY ENTRANCE FT GAINES TO MOBILE PT	30°15'	88°04'½	30°13'⅔	88°01'¼	319 91	AL	334 89	(90,28) (91,29) (92,29) (93,30)	76 & 78	15
16	MOBILE BAY MIDDLE TRANSECT	30°12'¼	88°04'	30°12'	88°00'⅔	320 74	AL	344 73	(91,32) (92,32) (93,32)	76 & 78	16
17	MOBILE BAY (SOUTH TRANSECT)	30°10'	88°04'	30°10'	88°01'½	320 61	AL	334 61	(91,34) (92,34) (93,34)	113 76 & 78	17

p indicates partial transect of cell / indicates whose cells were considered together. * indicates 'related' cells.

Procedure for transferring
grid lines to sounding plots

75. The various documents used and their scales are: (a) small craft charts - 1:40000; (b) nautical charts - 1:80000; (c) sounding plots - 1:8000; and (d) subgrids - 1:80000. All measurements were taken using a scale divided into sixtieths (1/60) of an inch.

76. The transects as actually surveyed were transferred to the nautical charts from the small craft charts using latitude/longitude in combination with common land feature identification, the 2:1 scale relationship serving as a control for accurate placement.

77. The nautical charts were overlaid with the corresponding subgrid to identify the affected cells. A 1:10 scale factor was used to transfer the grid lines to the sounding plots. Each cell was then identified and labeled by its grid coordinates. As each nautical chart contained several transects, it was possible to identify in terms of state coordinates at least one lateral grid line to serve as a control for consistent lateral line placement. Vertical line placement was controlled by visual comparison of the chart and sounding plot.

Comparison of Previously Assigned Depths to Surveyed Depth

78. The nautical chart with subgrid overlay and depth grid (Table VI-5) was used to refine cell identification with regard to model features to account for related cells and special cases.

79. The overlaid nautical charts had been used in assigning initial cell depths, thus their use in comparing survey depths with previously assigned depths would serve as a control so that the whole cell could be viewed in conjunction with the transect.

80. The depth grid (Table VI-5) was used to list individual cell depths along each transect. Then each sounding plot was examined to determine a representative depth range in each cell. The representative range was compared with the previously assigned depth together with the specific cell on the overlaid nautical chart to determine if a cell depth needed to be corrected. A table was prepared to show the results of these comparisons (Table VI-7).

Table VI-7

Comparison of Initial Cell to

Survey Range Depths (ft)

Transect	Grid Cell	Initial Depth (MLLW)	Depth Range Survey	Revised Depth (MLLW)
1A	(15,39)	7	7.0-31.6- 5.7 (P)	+
1B	(15,38)	9	11.1-12.4-13.1	11
1B	(16,37)	9	7.1-12.4	+
1C	(15,34)*	10	9.0-35.0	+
1C	(16,34)*	14	9.0-35.0	20
1C	(16,35)	11	9.5-16.0-14.2	12
2	(21,24)	8	4.9- 8.2	+
3	(25,34)	4	9.6-15.0- 9.0 (P)	+
3	(26,33)	10	18.4- 7.0- 9.6	+
3	(26,32)	19	17.1-22.0-18.4	+
3	(26,31)	13	13.7-21.0-16.7	18
3	(26,30)	6	11.0-13.7 (P)	+
4	(26,34)	10	6.6-13.4-10.6	11
4	(27,34)	13	10.8-16.0-13.0-17.0	14
4	(28,33)	20	6.3-30.0	+
5	(31,29)*	8	9.5-11.2 (P)	+
5	(31,30)*	12	11.4-14.7	+
5	(32,30)	11	14.5-16.9	14.5
5	(33,31)	17	18.0-24.3	+
5	(34,31)	27	24.4-36.8-32.7 (P)	+
6	(33,32)	20	24.1-32.5	22.5
6	(34,32)	24	32.2-21.4	+
7	(38,30)	16	3.9- 9.3- 2.8	6
7	(38,31)	10	3.9- 9.3- 2.8	6
	(39,30)**	2	3.9- 9.3- 2.8	6
	(39,31)**	18	3.9- 9.3- 2.8	6
8†	(42,16)	4	3.9- 7.8	+
8†	(43,16)	4	7.3-16.7- 5.5	8
10A	(42,29)	10	7.2-13.6	+
	(43,29)	10	7.8- 9.7	+
	(44,29)	10	8.6-26.3	12
	(45,29)	16	25.5- 7.0-16.8	+

(Continued)

Note: MLLW - Model Depth +1; (P) - Partial transect of cell; + - Indicates no revision in previously assigned model depth.

* Indicates cells considered together.

** Related cells.

† Special case, transect 8; survey halved.

(Sheet 1 of 3)

Table VI-7 (Continued)

Transect	Grid Cell	Initial Depth (MLLW)	Depth Range Survey	Revised Depth (MLLW)
10A	(46,29)	18	17.0-19.0- 9.8- 5.8	16
(Cont'd)	(47,29)	8	5.8-10.7	+
	(48,29)	11	11.0-23.1	12
	(49,29)	11	11.3-23.3	+
10B&C	(42,28)	11	4.1- 6.5 (B)	5
			5.9-14.6 (C)	
	(43,28)	6	7.2-18.9- 9.4 (B)	9.5
			5.9- 4.5-16.9-13.4 (C)	
	(44,28)	12	17.1-34.3- 7.1	+
			8.5-20.7-13.5 (C)	
	(45,28)	10	16.2- 6.8-10.1 (B)	
			8.1- 8.7	7.5
10B&C	(46,28)	6	8.1-10.2 (B)	8
			8.2- 8.5 (C)	
10C	(47,28)	7	6.1- 8.1	+
	(48,28)	4	6.2- 4.1- 6.6	5.5
	(49,28)	18	6.9-32.7-17.6	+
11A	(59,31)	20	13.6-16.4 (P)	+
	(60,31)	18	16.4- 9.6	+
	(61,31)	12	6.9-10.8	+
	(62,31)	16	6.5-46.5	+
11B	(59,30)	10	4.0- 8.0- 5.0	6
	(60,30)	10	5.8-13.9-10.0	+
	(61,31)	12	6.9-10.8	+
	(62,31)	16	6.5-46.5	+
11C	(59,30)	10	4.0- 8.0- 5.0	6
	(60,30)	10	5.8-13.9-10.0	+
	(61,30)	12	11.9-12.9-11.9	+
	(62,30)	11	5.1-11.4 13.9-30.7	+
12A	(71,31)	9	3.2-11.5 13.7-16.4	+
	(72,31)	7	7.3-11.5	10
	(73,31)	6	8.9-17.0	8
	(74,31)	5	8.3-10.9	10
	(75,31)	10	11.5-19.9- 9.0	13
	(76,31)	18	11.4-20.8 (P)	+
12B	(71,31)	9	3.2-11.5 13.7-16.4	+
	(72,31)	7	7.3-11.5	10
	(73,31)	6	8.9-17.0	8
	(74,31)	5	8.3-10.9	10
	(75,30)	12	10.4-19.0	+

(Continued)

Table VI-7 (Concluded)

Transect	Grid Cell	Initial Depth (MLLW)	Depth Range Survey	Revised Depth (MLLW)
12A	(71,31)	9	3.2-11.5 13.7-16.4	+
	(72,31)	7	7.3-11.5	10
	(73,30)	12	17.6-17.8 9.0-10.6	10
	(74,30)	12	9.8-13.0	+
	(75,30)	12	10.4-19.0	+
12D	(70,31)	6	7.0- 8.1	+
	(71,31)	9	3.2-11.5 13.7-16.4	+
	(72,30)	15	14.9-17.7	17
	(73,30)	12	17.6-17.8 9.0-10.6	10
	(74,29)	17	16.5-17.5	+
	(75,29)	16	7.7-18.3 (P)	+
13	(82,23)	4	3.7- 6.4 (P)	+
	(82,24)	6	6.3- 7.3	+
	(82,25)	6	7.2- 8.3	7
	(82,26)	7	7.9- 8.5	8
	(82,27)	8	8.4-10.0	+
	(82,28)	6	3.9-11.0	+
14	(86,25)	4	5.5-14.8	7
15	(90,28)	6	9.7-13.4 (P)	10
	(91,29)	8	9.6-12.6	10
	(92,29)	21	12.6- 9.9 14.1-41.2	16
	(93,30)	19	20.6-42.2	33
	(91,32)	7	8.6-15.0-10.0	10
	(92,32)	34	10.5- 4.0-14.8	+
	(93,32)	8	14.0- 9.0-15.8	9.5
17	(91,34)	17	23.5-20.0-42.6	20
	(92,34)	22	44.5-17.7-20.8	+
	(93,34)	21	20.0-31.5 (P)	+

Barrier Island Configuration

81. All barrier islands were located on cell faces with a land elevation of 10 ft. The barriers were modeled as exposed barriers; no overtopping occurred at any barriers in any of the simulations. The barrier islands are given in Table VI-8. The orientation labeled 1 indicates a u-face barrier, while the orientation labeled 2 represents the barrier obstruction to be along the v-face of the cell as shown in Figure A-1.

Flow Inputs

82. The major flow inputs (see Table VI-9) and their locations in the grid will be considered. Average daily flow values as obtained from the United States Geological Survey (USGS) are employed in the numerical model.

Calibration/Verification Stations

83. In order to compare simulated water surface elevations with the observed values, the location of the water surface elevation stations must be located on the grid. Results are shown in Table VI-10.

84. The placements of the meteorological and velocity/salinity stations are given in Tables VI-11 and VI-12, respectively.

Table VI-8

Barrier Configuration

No.	Orientation	Location N	Location M
1	1	41	17
2	2	41	18
3	1	42	18
4	1	43	18
5	1	44	18
6	1	45	18
7	2	45	19
8	1	34	31
9	1	35	31
10	1	36	31
11	1	36	1
12	1	37	30
13	1	41	28
14	1	50	28
15	1	51	28
16	1	52	28
17	1	53	28
18	1	55	29
19	1	56	29
20	2	56	30
21	1	57	30
22	1	58	30
23	1	58	24
24	2	57	24
25	1	74	17
26	1	63	31
27	1	64	31
28	1	65	31
29	2	65	32
30	1	66	32
31	1	67	32
32	1	69	31
33	2	78	19
34	2	78	20
35	2	78	21
36	2	78	22
37	2	41	41
38	1	43	43
39	2	44	45
40	1	42	50

(Continued)

Table VI-8 (Continued)

No.	Orientation	Location N	Location M
41	1	41	49
42	2	40	49
43	1	39	49
44	2	38	59
45	2	15	33
46	1	30	29
47	2	30	28
48	2	30	29
49	2	17	43
50	1	19	43
51	2	19	45
52	2	19	46
53	2	19	47
54	2	19	48
55	1	21	44
56	2	21	44
57	2	22	41
58	2	22	42
59	2	22	45
60	2	22	46
61	2	21	47
62	2	21	48
63	1	21	48
64	1	22	47
65	1	23	47
66	1	24	47
67	1	22	46
68	1	23	49
69	1	24	49
70	1	25	49
71	1	24	45
72	1	25	35
73	2	24	37
74	2	24	43
75	2	24	44
76	2	23	44
77	2	23	45
78	2	23	46
79	2	23	47
80	1	76	29

(Continued)

AD-A156 616 NUMERICAL MODEL INVESTIGATION OF MISSISSIPPI SOUND AND ADJACENT AREAS(U) COASTAL ENGINEERING RESEARCH CENTER VICKSBURG MS R A SCHMALZ FEB 85 CERC-MP-85-2 2/3

UNCLASSIFIED F/G 8/8 NL

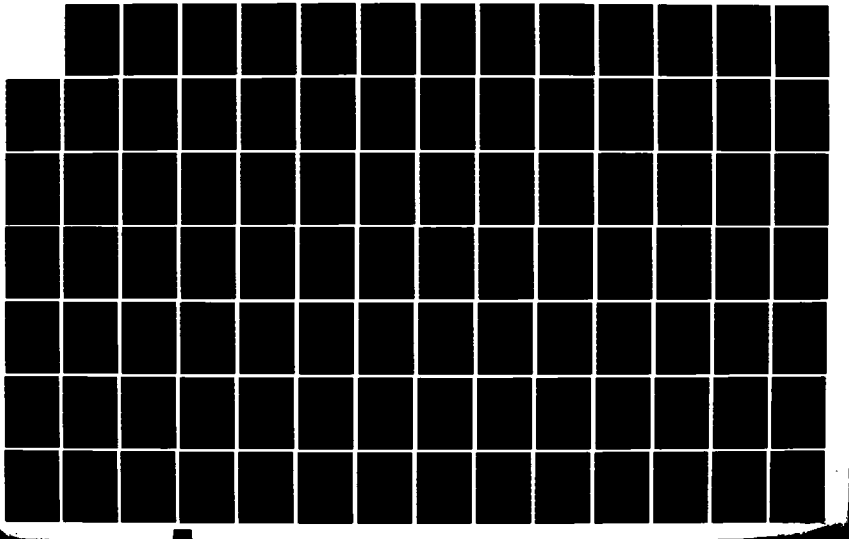

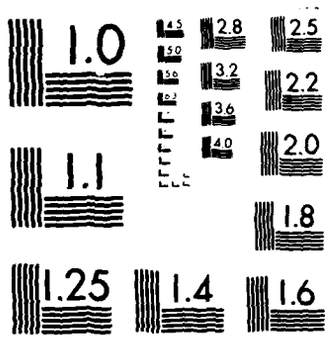

MICROCOPY RESOLUTION TEST CHART
NATIONAL BUREAU OF STANDARDS 1963 A

Table VI-8 (Concluded)

No.	Orientation	Location N	Location M
81	1	77	29
82	1	78	29
83	1	79	29
84	2	79	29
85	1	80	28
86	1	81	28
87	1	82	28
88	1	83	28
89	1	84	28
90	1	85	28
91	2	88	27
92	1	87	26
93	1	88	26
94	2	86	26
95	1	86	25
96	2	85	23
97	2	88	31
98	1	89	31
99	1	95	29
100	1	96	29
101	1	97	29
102	2	25	35
103	1	27	30
104	1	40	54
105	2	40	54
106	1	37	54
107	1	38	54
108	2	36	55
109	2	39	30
110	1	90	31
111	2	90	32

Table VI-9

Flow Inputs in the Global Grid

Inflow	Grid Cell
Mobile River System	(97,3)
East Pascagoula River	(59,19)
Pascagoula River	(59,17)
Pearl River	(13,33)
Jourdan and Wolf Rivers	(19,20)
Biloxi River System	(34,15)

Table VI-10

Water Surface Elevation Stations

Station No.	Type	WIFM Grid Coordinates
T8*	S	(110,28)
T12	S	(107,24)
T13	S	(90,28)
T10	S	(88,14)
T9	S	(87,27)
T11	S	(92, 5)
T7	S	(70,21)
T6	S	(67,32)
T5	S	(61,21)
T4	S	(55,29)
T21	S	(47,17)
T20	S	(43,15)
T15	S	(43,17)
T16	S	(35,18)
T19	S	(34,15), (35,15)
T14	S	(35,31)
T17	S	(24,23)
T18	S	(21,22)
T22	S	--
T1	S	(32,59)
T2	S	(26,57)
T3	S	(22,51), (23,51)
P22	DSP	(67,49)
P23	DSP	(89,49), (90,49)
P24	DSP	(108,49)

Note: S = Standard Gage; DSP = Deep Sea Pressure Gage.

* Refer to Figure II-3 for station locations.

Table VI-11

Meteorological Stations

Station No.	WIFM Grid Coordinates
M1	(22,23)
M2	(34,31)
M3	(42,17)
M4	(55,29)
M5	(89,28)

Table VI-12

Velocity/Salinity Continuous Stations

Station No.	Type	WIFM Grid Coordinates
V1	V	(15,39)*
V2	V	(16,37), (16,38)
V3	V	(16,35)
V4	V	(27,32), (26,31)
V5	V	(29,22)
VS6	VS	(28,27), (27,27)
V7	V	(32,25)
V8	V	(34,32)
V9	V	(45,29)
VS10	VS	(49,29), (49,28)
V11	V	(49,23)
VS12	VS	(54,27)
V13	V	(62,27)
V14	V	(60,30)
VS15	VS	(62,31), (62,32)
V16	V	(67,28), (68,28)
V17	V	(72,30), (72,31)
VS18	VS	(75,30)
V19	V	(76,25)
VS20	VS	(87,25)
V21	V	(93,30)

Note: V = Velocity; VS = Velocity and Salinity.
* Refer to Figure II-1 for station locations.

PART VII: SELECTION OF THE CALIBRATION AND VERIFICATION PERIODS

85. In order to understand the general behavior of the hydrodynamics and salinity distribution in Mississippi Sound over the sampling period, river inflows, meteorological station wind information, and salinity transect data were tabulated. A brief discussion of the significant findings and the tables themselves are presented in turn for each data group. Periods for numerical study are selected based upon these findings and on modeling requirements. The selection process is presented in detail in the final section.

River Inflows

86. United States Geological Survey (USGS) daily average streamflows were tabulated from April-September 1980 for the major streams to be considered in the numerical model as shown in Table VII-1. Flow for the Biloxi River System consisted of flows in the Tchoutacabouffa and Biloxi Rivers and Bayou Bernard. Total drainage areas for these three systems totaled 588.68 square miles (Bettandorff 1972). Daily mean flows for the Biloxi River at Wortham, Miss., (Station 02481000) were obtained from the USGS. The drainage area at Wortham, Miss., was given as 96.11 square miles. The total flow for the Biloxi River System was estimated by multiplying the Wortham, Miss., gage reading by 6.1251 = 588.68/96.11. The flow for the Jourdan and Wolf System was obtained similarly. The drainage areas totaled 759.20 square miles for the two rivers at Mississippi Sound (Bettandorff 1972). Daily mean flows at Station 02481510 on the Wolf River near Landon, Miss., (drainage area 308.28 square miles) were multiplied by 2.4627 = 759.20/308.28 to estimate the total inflow to the Sound.

87. The total drainage area of the Pascagoula River System as given by the USGS is 9498 square miles. Daily mean flows at Station 02479000 at Merrill, Miss., gage (drainage area 6590 square miles) were multiplied by 1.4413 = 9498/6590 to estimate the total inflow into Mississippi Sound. Based upon USGS Water Supply Paper No. 1763 (Harvey et al. 1965), this flow was divided between the West Pascagoula and Pascagoula Rivers as follows. The West Pascagoula River received 0.6 of the flow with the remaining 0.4 of the flow being assigned to the Pascagoula River.

Table VII-1

Daily Discharges (USGS) into Mississippi Sound, in Cfs

April-September 1980

Date	River Systems					
	Pearl	Jourdan Wolf	Biloxi	West Pascagoula	Pascagoula	Mobile
April						
1	122,929	8,422	4,753	85,476	57,651	369,150
2	117,286	8,472	7,656	93,395	62,263	385,200
3	116,633	13,816	12,985	99,448	66,299	354,170
4	111,403	8,644	8,085	95,124	63,416	372,360
5	102,904	5,566	3,957	85,093	56,729	395,900
6	93,489	4,137	2,437	73,678	49,119	396,970
7	85,252	4,014	2,499	64,252	42,835	395,900
8	80,152	4,039	2,536	56,988	37,992	383,060
9	78,976	4,014	2,413	49,464	32,976	325,280
10	72,176	4,261	1,611	42,114	28,076	300,349
11	67,600	3,817	1,255	35,715	23,810	329,560
12	66,423	9,087	11,944	34,936	23,291	315,650
13	71,784	31,769	38,955	45,054	30,036	297,353
14	87,082	31,276	33,627	55,172	36,781	239,573
15	105,519	24,405	10,045	62,868	41,912	247,384
16	110,095	7,782	4,269	77,051	51,367	247,170
17	105,519	4,531	2,854	94,259	62,840	212,609
18	102,250	3,546	2,144	98,583	65,722	209,720
19	101,596	3,325	1,960	91,665	61,110	225,235
20	97,673	2,980	1,838	80,683	53,788	261,080
21	89,959	2,487	1,531	69,959	46,640	278,200
22	74,268	2,066	1,103	60,793	40,529	294,250
23	77,668	1,822	919	49,378	32,919	328,490
24	74,268	1,625	796	39,693	26,462	339,190
25	72,176	1,478	735	31,910	21,273	243,470
26	78,976	4,728	7,963	28,796	19,198	347,750
27	82,114	8,373	6,125	32,342	21,561	342,400
28	70,607	6,009	3,063	34,072	22,714	322,070
29	63,416	3,497	1,838	33,985	22,657	304,950
30	59,362	2,266	1,225	33,120	22,080	271,887
May						
1	57,532	1,899	919	32,342	21,561	246,742
2	54,786	1,675	735	29,748	19,832	234,437
3	51,779	2,194	1,531	27,067	18,045	218,280
4	46,548	1,877	980	24,040	16,027	205,012
5	42,364	1,428	735	19,890	13,260	186,822
6	38,703	1,133	613	17,468	11,645	161,784

(Continued)

Table VII-1 (Continued)

Date	River Systems					
	Pearl	Jourdan Wolf	Biloxi	West Pascagoula	Pascagoula	Mobile
May (Continued)						
7	35,826	1,034	551	15,912	10,608	160,179
8	33,473	1,010	521	14,269	9,512	190,032
9	30,204	985	502	12,712	8,475	110,531
10	25,366	948	490	11,501	7,668	86,991
11	20,136	886	465	10,377	6,918	80,143
12	16,867	837	441	9,512	6,342	65,056
13	14,644	788	416	8,648	5,765	68,694
14	12,369	776	392	8,025	5,350	70,620
15	10,604	788	368	8,189	5,460	65,591
16	13,598	2,857	1,225	9,512	6,342	55,961
17	28,766	16,401	15,313	21,879	14,586	42,265
18	45,241	16,254	9,188	36,234	24,156	43,763
19	57,793	23,790	27,563	43,152	28,768	41,409
20	73,876	36,694	24,500	52,837	35,225	44,619
21	65,769	30,784	12,250	61,831	41,220	53,179
22	59,362	17,608	4,288	61,571	41,047	121,445
23	53,609	6,009	2,756	60,447	40,298	199,662
24	48,510	4,113	1,838	57,853	38,569	214,749
25	46,287	2,931	1,347	54,913	36,608	228,124
26	44,587	2,327	1,041	53,269	35,513	263,220
27	42,364	1,963	796	53,010	35,340	280,340
28	37,526	1,675	674	49,983	33,322	295,320
29	31,381	1,478	551	43,584	29,056	294,250
30	24,974	1,305	490	37,271	24,848	276,060
31	20,921	1,157	453	30,786	20,524	278,200
June						
1	18,698	1,071	416	21,879	14,586	273,920
2	16,998	960	367	14,009	9,339	260,010
3	14,383	874	331	10,291	6,860	136,318
4	11,716	808	306	8,994	5,995	111,815
5	9,624	739	282	8,189	5,460	95,444
6	7,924	690	263	7,498	4,998	76,933
7	6,982	640	251	6,961	4,641	66,233
8	6,904	566	239	6,425	4,283	57,673
9	7,165	591	220	6,399	4,266	52,216
10	6,825	566	233	7,160	4,774	52,216

(Continued)

Table VII-1 (Continued)

Date	River Systems					
	Pearl	Jourdan Wolf	Biloxi	West Pascagoula	Pascagoula	Mobile
June (Continued)						
11	6,015	566	208	6,797	4,531	50,183
12	5,570	520	190	7,281	4,854	37,022
13	5,269	475	172	7,169	4,779	33,919
14	5,086	446	159	6,685	4,456	23,273
15	4,890	419	147	6,053	4,036	23,112
16	4,773	406	135	5,318	3,546	19,945
17	4,655	389	129	4,817	3,211	17,302
18	4,576	387	123	4,566	3,044	16,820
19	4,642	419	153	4,479	2,986	18,115
20	4,668	431	135	4,436	2,957	17,923
21	4,576	441	123	4,454	2,969	21,956
22	4,472	414	110	4,687	3,125	21,828
23	4,472	458	116	5,085	3,390	23,925
24	4,655	677	214	4,869	3,246	27,360
25	4,838	857	184	4,211	2,808	25,894
26	4,579	823	153	4,635	3,090	30,281
27	4,576	754	123	5,422	3,615	37,236
28	4,943	549	110	5,967	3,978	24,396
29	5,871	468	98	6,884	4,589	29,853
30	7,924	468	92	6,754	4,503	63,986
July						
1	9,022	539	123	5,578	3,718	73,509
2	9,218	529	98	4,817	3,211	57,994
3	9,676	396	86	4,255	2,836	37,450
4	10,434	342	73	3,943	2,629	29,746
5	11,519	313	67	3,701	2,467	21,775
6	12,212	296	61	3,494	2,329	22,342
7	11,964	278	59	3,364	2,243	28,783
8	10,447	276	56	3,563	2,375	29,960
9	7,963	320	86	4,099	2,733	23,439
10	6,642	362	80	3,753	2,502	21,689
11	5,975	335	67	3,442	2,295	18,768
12	5,243	288	61	3,191	2,127	19,314
13	4,603	264	58	3,035	2,024	23,198
14	4,250	244	53	2,888	1,926	26,108
15	4,067	236	51	2,759	1,839	26,483
16	3,923	229	50	2,672	1,781	27,595

(Continued)

Table VII-1 (Continued)

Date	River Systems					
	Pearl	Jourdan Wolf	Biloxi	West Pascagoula	Pascagoula	Mobile
July (Continued)						
17	3,949	229	50	2,629	1,753	18,821
18	3,923	288	51	2,689	1,793	18,211
19	4,001	328	61	2,854	1,902	16,221
20	4,406	406	80	3,277	2,185	18,425
21	5,034	1,953	484	3,727	2,485	16,275
22	5,544	2,931	1,323	5,906	3,938	15,857
23	6,015	1,832	1,023	7,212	4,808	17,441
24	6,629	1,271	606	7,722	5,148	15,665
25	7,061	798	331	7,964	5,310	15,697
26	7,845	589	208	6,711	4,474	14,541
27	7,871	475	184	5,768	3,845	15,943
28	7,715	426	178	5,223	3,482	17,559
29	8,028	589	196	5,748	3,165	19,442
30	6,211	525	159	4,661	3,107	17,366
31	5,479	480	141	4,782	3,188	21,817
August						
1	5,243	406	110	4,514	3,009	23,208
2	4,851	340	98	3,935	2,623	21,871
3	4,406	305	92	3,468	2,312	23,273
4	4,119	313	129	3,200	2,133	21,421
5	3,962	414	172	3,070	2,047	24,781
6	3,844	335	123	3,234	2,156	26,140
7	3,753	325	92	2,958	1,972	16,628
8	3,635	278	86	2,733	1,822	16,425
9	3,687	268	80	2,560	1,706	14,167
10	3,687	241	73	2,404	1,603	14,370
11	3,596	236	67	2,776	1,851	18,693
12	3,517	251	92	2,724	1,816	17,527
13	3,465	310	135	2,473	1,649	13,439
14	3,347	340	220	2,352	1,568	14,830
15	3,282	362	263	2,447	1,632	15,215
16	3,269	394	245	2,292	1,528	12,594
17	3,334	397	190	2,153	1,436	12,487
18	3,308	328	129	2,058	1,372	14,049
19	3,217	278	153	1,946	1,297	12,669
20	3,138	239	104	1,851	1,234	13,568
21	3,073	256	86	1,807	1,205	13,150

(Continued)

Table VII-1 (Concluded)

Date	River Systems					
	Pearl	Jourdan Wolf	Biloxi	West Pascagoula	Pascagoula	Mobile
August (Continued)						
22	3,033	239	92	1,816	1,210	14,905
23	2,981	214	80	1,747	1,165	12,487
24	2,916	209	67	1,626	1,084	13,857
25	2,877	195	61	1,565	1,043	15,322
26	2,864	190	55	1,522	1,015	13,568
27	2,850	187	49	1,557	1,038	15,111
28	2,824	185	45	1,894	1,263	14,167
29	2,811	182	40	2,119	1,412	12,605
30	2,890	180	38	2,274	1,516	12,112
31	2,994	244	37	2,361	1,574	12,326
September						
1	3,491	239	43	2,335	1,557	12,380
2	3,387	251	39	2,473	1,649	12,498
3	3,203	303	34	2,274	1,516	11,652
4	3,073	293	33	2,050	1,366	11,042
5	3,034	342	32	1,903	1,268	11,577
6	2,968	313	45	1,799	1,199	10,411
7	2,929	276	45	1,730	1,153	10,326
8	2,929	232	39	1,669	1,113	10,647
9	2,877	209	38	1,643	1,095	13,247
10	2,811	197	36	1,565	1,043	11,920
11	2,733	192	35	1,513	1,009	12,080
12	2,720	187	33	1,479	986	11,941
13	2,759	182	32	1,453	969	10,229
14	2,772	177	35	1,418	945	9,587
15	2,694	175	55	1,401	934	11,149
16	2,615	172	44	1,410	940	13,857
17	2,628	197	39	1,384	922	13,899
18	2,667	261	39	1,444	963	10,721
19	2,733	273	67	1,626	1,084	10,219
20	2,759	241	60	1,730	1,153	10,572
21	2,733	214	53	1,660	1,107	9,780
22	2,746	204	47	1,626	1,084	10,486
23	2,707	195	44	1,548	1,032	11,235
24	2,654	185	39	1,444	963	11,107
25	2,628	180	36	1,401	934	10,529
26	2,837	214	45	1,349	899	9,213
27	2,942	227	41	1,444	963	9,309
28	2,798	204	38	1,427	951	9,512
29	2,680	192	38	1,384	922	10,112
30	2,837	190	39	2,067	1,378	11,010

(Sheet 5 of 5)

88. The development of the Mobile River System was treated as described by Schroeder (1979). The total inflow to Mobile Bay was assumed to be equal to 1.07 times the sum of the gage readings for the Tombigbee River at Coffeeville, Ala., Station 02429761 and the Alabama River at Clairborne, Ala., Station 02429500. To allow for the travel time, the resulting inflow time series was lagged by 5 days to estimate the inflow time series at Mobile Bay.

89. The total drainage area reported by the USGS for the Pearl River at its mouth is 8669 square miles. To estimate flow into Mississippi Sound, daily mean values at Station 02489500 near Bogalusa, La. (drainage area 6630 square miles) were multiplied by 1.3075 = 8669/6630.

90. River inflows were high in the spring months (April and May) and receded during June and were relatively low in July, August, and September. Total average daily inflows for all six river systems were 518,000 cfs, 258,000 cfs, 77,500 cfs, 39,150 cfs, 23,900 cfs, and 16,900 cfs for April, May, June, July, August, and September, respectively.

Meteorological Station Wind Data

91. Daily maximum hourly averaged wind speeds and daily maximum (2-sec gust) wind speeds were tabulated over the survey period at Station 4 on Horn Island as shown in Table VII-2. For periods in which data at Station 4 were not available, data were tabulated for Station 2 at Ship Island as shown in Table VII-3 to provide a record of wind information as complete as possible. The range of daily maximum hourly averaged wind speed was 5.6 (July 10) to 31.7 (April 13) mph. The range of daily maximum winds speed was 10.7 (July 10) to 45.4 (April 13) mph. Typical daily maximum hourly averaged windspeeds were 20, 12, 10, 15, 13, 8-28, and 8-24 mph for April, May, June, July, August, September, and October 1980. April and early May constituted a period of relatively high winds. Fall storms occurred in September and October. The gages were removed during Hurricane Allen (7 August-17 August).

Salinity Transect Data

92. Throughout the 180-day survey period at approximately 3-week intervals, salinity transects were obtained at locations shown in Figure II-4. Salinity values were measured at 5-ft-depth intervals. In order to characterize

Table VII-2

Wind Characteristics for Meteorological Station 4, Horn Island

Date	Julian Day	Maximum Hourly Average Speed mph	Maximum Gust mph
May 8	129	12.6	20.0
9	130	24.0	31.4
10	131	10.6	18.7
11	132	11.5	22.0
12	133	10.8	18.7
13	134	10.8	20.0
14	135	9.9	18.0
15	136	18.3	38.1
16	137	31.9	43.4
17	138	26.7	38.7
18	139	10.0	16.0
19	140	13.4	26.7
20	141	17.6	31.4
21	142	11.9	29.4
22	143	14.0	21.4
23	144	9.5	17.4
24	145	9.8	18.0
25	146	10.2	18.0
26	147	10.3	34.7
27	148	12.1	17.4
28	149	9.7	16.7
29	150	13.2	21.4
30	151	9.6	17.4
31	152	8.8	15.4
Jun 1	153	8.2	14.0
2	154	9.7	17.4
3	155	6.1	12.0
4	156	6.2	11.4
5	157	13.4	19.4
6	158	6.8	15.4
7	159	9.2	18.7
8	160	11.3	19.4
9	161	20.9	29.4
10	162	17.6	22.7
11	163	11.3	14.7
12	164	16.1	20.7
13	165	11.4	16.7
14	166	7.1	13.4
15	167	7.2	13.4
16	168	7.6	15.4
17	169	8.3	16.0
18	170	11.4	21.4
19	171	9.9	22.7
20	172	10.8	16.0
21	173	10.1	18.7
22	174	10.0	20.7
23	175	10.0	25.4
24	176	10.0	32.7
25	177	11.3	23.4
26	178	15.0	36.1
27	179	9.2	21.4
28	180	9.3	16.7
29	181	9.6	18.7
30	182	13.4	21.4
Jul 1	183	14.3	28.7
2	184	11.3	19.4
3	185	11.2	20.7
4	186	8.3	13.4
5	187	8.7	15.4
6	188	8.8	15.4
7	189	21.1	46.8
8	190	19.2	34.7
9	191	7.6	14.8
10	192	5.6	10.7
		Out of Service	
31	213	8.0	14.0
Aug 1	214	7.7	14.0
2	215	8.8	17.4
3	216	9.1	28.1
4	217	8.4	16.7
5	218	8.3	15.4
6	219	13.4	18.7
Out of Service (Hurricane Allen)			
18	231	6.3	12.0
19	232	7.9	12.0
20	233	8.6	12.7
21	234	8.8	20.7
22	235	12.3	22.7

(Continued)

Table VII-2 (Concluded)

Date	Julian Day	Maximum Hourly Average Speed mph	Maximum Gust mph
Aug 23	236	19.1	25.4
24	237	18.4	23.4
25	238	10.5	20.0
26	239	12.7	16.7
27	240	13.3	18.0
28	241	13.8	22.0
29	242	8.8	16.7
30	243	7.4	16.0
31	244	8.7	16.7
Sep 1	245	10.2	16.0
2	246	17.1	25.4
3	247	24.0	32.1
4	248	28.6	38.1
5	249	20.0	32.7
6	250	12.6	18.7
7	251	12.2	15.4
8	252	7.9	17.7
9	253	8.3	14.0
10	254	8.6	14.7
11	255	14.5	18.0
12	256	10.0	18.7
13	257	9.6	14.7
14	258	12.3	18.7
15	259	8.1	14.0
16	260	8.0	15.4
17	261	10.3	32.7
18	262	15.6	18.4
19	263	13.3	23.4
20	264	8.9	19.4
21	265	8.8	15.4
22	266	7.2	13.4
23	267	9.1	14.7
24	268	6.6	16.7
25	269	7.5	15.4
26	270	17.2	22.0
27	271	19.3	24.7
28	272	17.1	22.0
29	273	9.8	19.4
30	274	20.2	32.7

Date	Julian Day	Maximum Hourly Average Speed mph	Maximum Gust mph
Oct 1	275	18.3	24.0
2	276	10.4	14.0
3	277	22.6	30.1
4	278	19.1	26.1
5	279	9.6	29.4
6	280	23.7	30.1
7	281	17.2	21.4
8	282	8.8	11.4
9	283	6.2	11.4
10	284	10.9	14.0
11	285	12.7	19.4
12	286	21.1	27.4
13	287	17.0	21.4
14	288	9.9	12.7
15	289	15.1	19.4
16	290	15.1	26.7
17	291	10.2	18.0
18	292	7.9	15.4
19	293	18.5	22.7
20	294	24.0	32.7
21	295	18.8	24.7
22	296	11.5	14.7
23	297	13.3	20.0
24	298	20.7	34.1
25	299	23.6	36.1
26	300	11.8	18.0
27	301	15.8	28.1
28	302	17.0	31.4
29	303	23.7	30.7
30	304	21.7	28.1
31	305	20.8	26.1
Nov 1	306	11.2	14.7
2*	307	7.2	10.7
3*	308	7.3	15.4
4*	309	19.5	20.7
5*	310	15.8	31.4
6*	311	12.5	16.0
7*	312	7.7	20.0

* Gage possibly malfunctioning.

Table VII-3

Wind Characteristics for Meteorological Station 2, Ship Island

Date	Julian Day	Maximum Hourly Average Speed mph	Maximum Gust mph
Apr 10	101	13.1	16.7
11	102	21.9	28.1
12	103	30.5	44.8
13	104	31.7	45.4
14	105	29.5	40.1
15	106	23.1	30.7
16	107	10.3	14.0
17	108	10.4	14.7
18	109	18.4	34.7
19	110	26.6	37.4
20	111	13.0	16.7
21	112	14.7	20.0
22	113	18.0	24.7
23	114	16.1	20.7
24	115	17.6	22.7
25	116	20.8	28.7
26	117	25.8	44.1
27	118	24.1	32.1
28	119	26.0	28.1
29	120	21.5	28.1
30	121	18.9	24.0
May 1	122	14.8	19.4
2	123	15.8	20.0
3	124	15.8	28.7
4	125	15.5	20.7
5	126	14.8	18.7
6	127	18.0	24.0
7	128	18.5	24.0
8	129	17.7	29.4
Out of Service			
Jul 9	191	10.3	14.0
10	192	10.5	14.0
11	193	14.3	18.7
12	194	19.5	24.0
13	195	18.7	24.0
14	196	18.8	22.7
15	197	16.6	20.7
16	198	14.9	21.4
17	199	15.1	23.4
18	200	16.7	38.1
19	201	12.5	28.7
20	202	22.3	28.1
21	203	20.3	27.4
22	204	15.9	24.7
23	205	16.6	33.4
24*	206	23.6	26.1
25*	207	20.5	23.4
26*	208	25.3	24.7
27*	209	28.9	30.7
28*	210	29.6	31.4
29*	211	34.1	17.4
30	212	14.8	18.7
31	213	12.4	18.7
Aug 1	214	11.6	15.1
2	215	17.1	30.1
3	216	21.7	36.7
4	217	15.8	20.0
5	218	17.3	22.0
6	219	14.3	20.0

* Gage possibly malfunctioning.

the general horizontal salinity distribution, middepth salinity conditions for 11 stations are shown in Table VII-4 with the range over depths listed underneath the middepth value. Stations T26, T28, T30, T36, and T42 characterize the western portion of the Sound. Stations T2, T52, and T54 represent the central portion of the Sound, while stations T60, T70, and T80 portray conditions in the eastern section of the Sound. In referencing the table, if one goes across the table at any one date, the horizontal salinity distribution is obtained. If one goes down a column, the change in conditions over time are represented for each station, group, or for the entire Sound. In April and May 1980, the entire Sound, particularly the western end and the entrance to Mobile Bay, exhibited very low salinity. As June progressed, salinity levels increased overall. This trend continued through July. By August, conditions in the Sound had stabilized to a summer pattern. Note that the 8/22-23 transect values correspond very closely to the 9/24-25 values.

93. Horizontal salinity gradients are largest in the Spring. However, local gradients may be found throughout the period in the highly transient Lake Borgne (T26) and Mobile Bay (T80) entrances.

Calibration and Verification Periods

94. It is desirable to calibrate and verify the hydrodynamic parameters (bottom stress) and salinity parameters (dispersion coefficients) separately but over the same periods. The following criteria are used to select the calibration and verification periods:

a. Streamflow must remain relatively constant. Storm or flood periods exhibiting time-varying flow characteristics are discarded from consideration.

b. In order to minimize wind effects, periods for which wind speeds are minimum are to be considered.

c. Since continuous salinity levels are available at only six stations (VS stations in Figure II-1), it will be necessary to employ salinity transect values in defining the initial conditions. Therefore, these periods must begin in a transect day.

95. By considering river inflows (Table VII-1), wind conditions (Tables VII-2 and VII-3), and salinity transect conditions in Table VII-4, a general understanding of the dynamics of the Sound may be obtained.

96. In the numerical study of the Sound, it is necessary (for reasons of computational cost) to consider a 5- to 6-day period. This constraint

Table VII-4

Representative Spatial Salinity Transect Data, 1980 (ppt)

Date	West Group Stations					Mid Group Stations			East Group Stations		
	T26	T28	T30	T36	T42	T2	T52	T54	T60	T70	T80
4/28-29	2.4	1.0	0.4	3.3	8.6	12.9	16.3	14.7	34.6	15.4	2.1
	NA	NA	0.4-0.5	3.3-3.5	8.6-8.5	12.9-13.0	NA	14.7-14.7	11.8-35.1	14.7-16.3	2.0-2.2
5/21-22	1.9	2.0	1.5	7.7	13.5	16.1	12.3	14.9	22.3	20.3	9.8
	1.8-1.9	2.0-2.0	1.5-1.6	7.7-7.7	12.3-15.5	14.2-18.8	6.8-15.2	10.9-19.0	10.7-28.0	17.5-23.9	4.6-11.6
6/12-13	5.16	7.66	6.08-6.03	11.88	16.23	16.55	20.60	17.38	27.1	18.63	14.09
	4.39-5.16	7.56-8.14	5.16-6.51	11.11-12.36	15.51-16.65	16.65-18.11	13.61-22.58	17.38-18.52	18.11-28.8	16.13-25.90	9.0-17.9
7/23-24	17.17	20.25	20.19	26.96	28.37	28.42	24.96	28.84	27.05	30.14	34.37
	17.17-17.17	20.18-20.21	20.1-20.2	26.9-27.16	28.38-28.48	28.41-28.42	24.96-24.96	29.04-28.84	21.75-29.44	30.34-30.14	23.97-24.57
8/22-23	14.2	16.30	17.8	21.3	23.2	27.2	24.3	24.3	29.6	27.10	17.7
	14.2-14.1	16.4-17.2	16.7-17.8	21.2-22.4	21.6-27.0	27.1-27.4	23.9-24.6	24.4-24.5	27.3-31.3	26.3-30.6	16.4-19.00
9/2-3	18.3	17.3	17.1	38.9	26.8	28.8	NA	NA	NA	NA	NA
	18.4-18.6	17.2-17.8	17.2-17.4	39.0-39.6	26.3-26.6	28.7-28.9	NA	NA	NA	NA	NA
9/8-9-10	14.3	14.8	14.6	22.5	23.8	25.8	27.0	25.4	30.7	26.9	23.6
	13.9-14.6	14.8-15.1	14.0-15.1	21.8-22.6	23.5-23.9	25.6-27.8	26.7-27.4	25.2-26.1	27.6-31.4	26.7-30.0	21.4-24.0
9/20-21	16.0	17.3	17.0	21.9	23.7	26.0	26.3	27.3	28.1	28.5	22.9
	15.5-16.2	16.9-17.3	16.0-17.1	22.1-21.4	23.5-23.8	26.1-26.3	26.1-26.2	27.4-27.5	27.3-28.7	27.9-28.9	22.2-23.4
9/24-25-28	14.2	15.1	17.2	21.1	23.0	25.7	26.7	27.6	29.1	29.9	NA
	11.3-16.0	16.3-18.2	16.5-17.0	21.4-22.2	23.0-23.0	25.6-26.3	26.9-27.9	27.5-27.6	27.0-30.7	29.9-30.0	NA
11/6-7	11.3	11.14	10.65	22.41	29.71	28.07	28.92	27.62	31.08	29.82	24.88
	11.47-11.30	11.26-11.13	10.26-12.79	22.27-22.63	29.35-29.39	28.0-28.12	27.69-29.44	26.23-29.10	28.96-32.10	29.34-30.53	20.77-24.29

Note: First line of horizontal readings for each date indicates middepth salinity, ppt, and second line indicates range surface-bottom, ppt.

coupled with the previous three criteria is sufficient to determine the periods for numerical study.

97. Consider Table VII-4; the 4/28-4/29 period is eliminated due to excessive wind and highly transient flood flow conditions. The 5/21-5/22 period, although relatively calm, exhibits transient flow conditions and is discarded. The 7/23-24, 8/22-23, and 9/8-9 periods exhibit excessive wind and are eliminated. The 9/2-3 transect is incomplete and therefore this period is not considered.

98. The 6-day period, 9/20-9/25, was selected for further study as a potential calibration period for both hydrodynamics and salinity mechanisms. From the hydrodynamic perspective, the astronomic tide characteristics at Pascagoula as shown by Outlaw (1983, Plate 42) indicate that during 9/23 and 9/24 the semidiurnal constituents M_2 and S_2 assume increasing importance as the tidal range is reduced on entering a neap tide period. From the salinity perspective, values are relatively constant in time over this period. Therefore, salinity transect values obtained over the 2-day period, 20-21 September may be used to define initial conditions. In addition, the 24-25 September values may be used as values to compare with the numerical results. Maximum daily hourly averaged wind speeds are less than 9.0 mph over the entire period. Therefore, wind effects should be small.

99. The 5-day period, 6/12-6/16, was selected for further study as a potential verification period for both hydrodynamic and salinity mechanisms. From the hydrodynamic viewpoint, the astronomic tide characteristics at Pascagoula as shown in Outlaw (1983, Plate 39) indicate that the diurnal constituents O_1, K_1, P_1 dominate and determine the character of the tide. The tide range is characteristic of a Spring tide. From the salinity viewpoint, this period exhibits a relatively large horizontal gradient. Vertical salinity gradients are significant in the middle and eastern station groups in Table VII-4. The maximum daily hourly averaged wind speed declines from 16.1 to 11.4 mph from 6/12-6/13 and to less than 8.0 mph for the 6/14-6/16 period. The vertical salinity gradients indicate that the middle and eastern sections of Mississippi Sound are partially mixed, while the western section is reasonably well mixed. The vertically integrated two-dimensional modeling concept employed for salinity may not be applicable during this period. As a result, salinity was not considered. The hydrodynamic mechanisms were verified using this Spring tide period.

PART VIII: CALIBRATION PERIOD 20-25 SEPTEMBER 1980

100. In order to obtain a more detailed understanding of the dynamics of the Sound prior to simulating this period, hourly values of wind speed and direction and salinity are considered in turn below. A complete set of salinity transect values are presented in order to investigate the degree of stratification. Based upon the results of the harmonic analysis, the predicted values of water surface elevation and currents are developed and compared versus the unfiltered (raw) data.

Wind Information

101. Hourly wind speeds and directions are as shown in Table VIII-1. At most stations average hourly wind speeds are below 10 mph, with daily maximum wind speeds (2-sec gust) below 20 mph. Wind direction and velocity are relatively uniform spatially at each hour over the period. The wind effects should be relatively small on water surface displacements over this period.

Instantaneous Salinity Information

102. Hourly values of salinity meters nearest middepth were considered. Middepth locations were selected as being the most appropriate to compare with the vertical averaged model results. The range for each day at each station as located in Figure II-1 is given in Table VIII-2. Salinity levels are normally within a range of approximately 1-2 parts per thousand for all days. The maximum spatial difference over the Sound is approximately 5-6 parts per thousand.

Salinity Transect Information

103. Representative middepth salinity values are shown in Figure VIII-1. The salinity range over depth is given to indicate the degree of stratification. Stratification effects even within the navigation channels were not significant during this period. Therefore, the well-mixed assumption appeared to be valid during this period.

104. In order to investigate the reliability of the instantaneous

Table VIII-1

Hourly Meteorological Data (Wind Speed and Direction), 20-25 September 1980, Stations M1-M5

Date/ Julian Day	Hour	Station M1			Station M3			Station M4			Station M5		
		Speed mph	Direction MAG	24-hr Max Speed mph	Speed mph	Direction MAG	24-hr Max Speed mph	Speed mph	Direction MAG	24-hr Max Speed mph	Speed mph	Direction MAG	24-hr Max Speed mph
9/20-264	1	5.7	142	14.0	13.9	117	18.0	8.6	115		10.4	106	
	2	6.5	148	14.0	11.8	121		8.3	119		10.6	140	
	3	5.4	144	14.0	11.0	129		8.2	135		13.1	146	
	4	5.7	150		9.9	132		7.6	139		13.4	150	
	5	5.1	155		7.5	155		6.2	149		13.0	151	19.4
	6	4.3	156		4.6	154		7.4	162		12.8	156	
	7	5.9	170		6.6	164		5.8	157		10.1	165	
	8	1.9	147		3.4	103		5.2	151		8.2	149	
	9	1.3	122		3.3	32		5.2	153		5.8	112	
	10	3.6	156		3.3	39		4.0	154		5.0	74	
	11	3.6	162		3.2	53		3.8	151		10.2	103	
	12	4.1	154		3.4	46		3.1	122		10.3	100	
	13	3.6	150		5.9	76		6.8	157	19.4	8.8	104	
	14	3.6	148		6.8	88		3.3	124		7.6	110	
	15	4.5	134		5.0	98		5.8	134		7.4	131	
	16	4.2	130		7.3	119		8.9	141		9.1	136	
	17	4.3	142		8.6	133		8.7	132		10.1	129	
	18	5.1	135		8.3	152		7.4	142		9.7	134	
	19	5.1	150		8.7	155		7.3	141		9.9	133	
	20	5.1	151		8.7	151		7.7	149		10.1	137	
	21	4.9	154		8.2	157		7.0	149		9.6	139	
	22	5.3	143		8.3	160		6.7	145		8.4	144	
	23	5.0	160		7.5	161		6.3	164		8.0	137	
	24	4.7	145		6.8	156		4.5	157		7.3	152	

(Continued)

Note: No data recorded at station M2 because of tape drive malfunction.

Table VIII-1 (Continued)

Date/ Julian Day	Hour	Station M1 Speed mph	Station M1 Direction MAG	Station M1 24-hr Max Speed mph	Station M3 Speed mph	Station M3 Direction MAG	Station M3 24-hr Max Speed mph	Station M4 Speed mph	Station M4 Direction MAG	Station M4 24-hr Max Speed mph	Station M5 Speed mph	Station M5 Direction MAG	Station M5 24-hr Max Speed mph
9/21-265	1	4.3	151		6.2	153		4.5	157		6.8	151	
	2	4.6	145		6.8	151		4.7	146		7.0	132	
	3	4.1	143		7.6	136		5.8	138		10.0	136	
	4	5.2	138		9.0	146		6.3	136		12.4	150	
	5	5.4	155		8.6	145		6.4	141		14.3	154	18.0
	6	4.7	141		9.3	148		7.8	142		13.3	163	
	7	5.3	149		10.6	151		7.7	148	15.4	11.6	159	
	8	6.8	157	15.4	10.6	156		8.0	160		9.7	183	
	9	8.9	167		9.7	167		6.6	166		7.4	187	
	10	9.7	170		7.8	171		5.0	169		7.4	166	
	11	7.5	173		8.4	192	34.7	3.9	178		6.7	162	
	12	6.1	192		3.7	198	18.7*	3.2	160		6.6	138	
	13	3.6	210		3.4	174		3.7	146		7.0	137	
	14	2.3	337		1.9	89		4.9	147		6.3	138	
	15	0.9	238		3.0	173		4.9	135		6.8	135	
	16	2.4	186		7.2	161		6.7	129		6.4	144	
	17	3.5	159		8.4	156		6.1	153		6.1	140	
	18	4.8	130		8.1	158		6.5	135		6.6	144	
	19	5.0	138		8.3	164		7.3	146		6.1	150	
	20	4.8	160		8.7	169		6.6	154		7.1	149	
	21	4.8	146		8.2	173		6.6	137		8.1	149	
	22	5.5	144		8.2	163		6.8	160		8.7	151	
	23	5.5	151		8.6	150		7.5	158		9.8	148	
	24	5.8	153		9.0	153		6.3	160		7.9	168	

(Continued)

* Next larger value.

Table VIII-1 (Continued)

Date/ Julian Day	Hour	Station M1			Station M3			Station M4			Station M5		
		Speed mph	Direc-tion MAG	24-hr Max Speed mph	Speed mph	Direc-tion MAG	24-hr Max Speed mph	Speed mph	Direc-tion MAG	24-hr Max Speed mph	Speed mph	Direc-tion MAG	24-hr Max Speed mph
9/22-266	1	5.1	154		7.6	152		6.0	150		8.1	158	
	2	6.3	159		8.2	166		6.9	150	13.4	9.7	171	12.7
	3	5.9	161		9.2	164		6.4	157		9.7	161	12.7
	4	6.1	158		9.1	164	14.0	5.3	161		9.2	151	12.7
	5	9.0	162	15.4	8.6	158		5.4	166		8.1	152	
	6	11.1	167	15.4	8.1	160		5.0	163		8.1	153	
	7	7.3	166		7.7	176		5.0	153		7.2	163	
	8	7.5	167		7.2	170		4.4	160		7.1	171	
	9	9.7	173		7.7	167		5.5	166		6.4	178	
	10	8.1	171		7.4	179		4.6	179		5.8	172	
	11	7.0	176		4.9	184		3.2	173		4.7	158	
	12	7.1	176		4.0	184		3.7	162		7.3	148	
	13	5.1	183		0.9	59		3.4	161		7.1	149	
	14	3.7	161		2.4	47		4.4	156		5.9	149	
	15	4.4	171		2.0	143		4.1	157		4.6	138	
	16	4.2	175		3.7	158		3.9	131		4.7	134	
	17	3.9	141		5.3	166		5.6	86		5.3	127	
	18	4.6	153		7.0	170		6.0	102	13.4	6.2	143	
	19	4.8	152		8.2	177		7.2	137		5.8	143	
	20	5.1	152		8.5	175		6.9	148		6.3	135	
	21	5.5	147		7.6	166		7.1	151		6.7	146	
	22	6.0	157		9.1	166	14.0	7.3	145		6.5	160	
	23	5.6	155		9.9	165	14.0	7.2	156		7.2	158	
	24	6.9	154		8.9	165		6.6	167		8.0	177	

(Continued)

Table VIII-1 (Continued)

Date/ Julian Day	Hour	Station M1 Speed mph	Station M1 Direction MAG	Station M1 24-hr Max Speed mph	Station M3 Speed mph	Station M3 Direction MAG	Station M3 24-hr Max Speed mph	Station M4 Speed mph	Station M4 Direction MAG	Station M4 24-hr Max Speed mph	Station M5 Speed mph	Station M5 Direction MAG	Station M5 24-hr Max Speed mph
9/23-267	1	8.1	169		8.4	176		5.8	162		7.4	179	
	2	8.0	164	16.7	8.5	171		4.9	166		7.7	176	
	3	6.0	162		7.1	179		4.1	174		6.4	182	
	4	8.7	168		5.8	188		4.5	171		6.8	181	
	5	8.8	169		5.9	179		4.0	173		6.2	178	
	6	7.0	172		4.9	181		3.0	164		3.8	171	
	7	5.5	166		4.3	179		1.9	162		0.7	210	
	8	5.8	187		4.2	188		1.7	159		2.0	191	
	9	5.0	178		3.1	197		1.7	176		1.2	290	
	10	3.3	197		1.4	327		0.5	198		0.9	319	
	11	3.4	21		4.4	359		0.2	232		1.3	339	
	12	3.4	35		6.2	357		2.8	15		1.4	31	
	13	3.2	32		6.1	7	17.4	6.7	24		3.3	21	
	14	3.5	30		5.3	7		7.9	37		7.1	48	
	15	2.8	76		4.0	31		7.6	44		8.3	57	
	16	4.1	105		2.7	97		6.7	62		7.7	60	
	17	4.9	115		5.0	166		7.4	73		5.4	50	
	18	4.7	123		8.7	147		9.1	87		3.9	77	
	19	4.1	141		9.5	144		8.7	119	14.7	8.6	133	15.4
	20	4.6	132		10.0	148		7.2	140		9.2	139	
	21	4.8	138		9.6	146		8.3	138	14.7	8.7	151	
	22	4.5	141		8.8	157		7.1	147		8.1	154	
	23	4.6	152		9.2	152		6.9	157		9.3	154	
	24	5.6	159		7.5	163		5.7	162		8.2	157	

(Continued)

Table VIII-1 (Continued)

Date/ Julian Day	Hour	Station M1 Speed mph	Station M1 Direction MAG	Station M1 24-hr Max Speed mph	Station M3 Speed mph	Station M3 Direction MAG	Station M3 24-hr Max Speed mph	Station M4 Speed mph	Station M4 Direction MAG	Station M4 24-hr Max Speed mph	Station M5 Speed mph	Station M5 Direction MAG	Station M5 24-hr Max Speed mph
9/24-268	1	5.8	174		6.2	175		3.7	154		6.9	159	
	2	5.3	158		5.2	163		3.8	160		6.7	151	
	3	2.5	152		4.7	145		2.9	136		5.4	137	
	4	3.0	148		5.1	150		3.7	149		4.7	152	
	5	4.7	159		5.6	160		4.5	153		7.3	161	
	6	8.2	180		6.8	176		5.1	166		9.6	158	
	7	5.5	168		5.6	168		5.1	158		8.9	158	
	8	6.2	173		6.4	161		4.4	168		7.6	175	
	9	5.6	172		6.2	149		4.7	148		5.6	168	
	10	5.0	181		3.8	167		4.2	152		7.4	158	
	11	2.4	126		3.3	15		4.3	169		8.9	153	14.0
	12	2.9	147		4.1	73		3.7	161		6.2	166	
	13	7.5	185	12.0*	4.4	67		4.1	176		7.2	155	
	14	5.1	181		2.7	18		4.9	166		6.4	163	
	15	11.1	213	22.7	2.0	18		4.1	185		5.6	172	
	16	4.8	210		2.7	171		3.6	165		4.0	178	
	17	4.1	194		5.6	173		6.6	212	16.7	4.2	201	
	18	3.6	188		8.3	184	15.4	4.5	238		4.3	193	
	19	4.3	156		5.1	187		4.5	183		4.2	171	
	20	4.2	145		6.6	180		4.6	169		4.9	151	
	21	4.2	151		7.5	164		5.4	178		5.7	162	
	22	5.4	144		8.0	167		5.4	153		6.7	146	
	23	5.1	153		8.1	169		5.8	153		7.3	150	
	24	5.2	154		7.5	156		5.4	145		8.9	156	

(Continued)

* Next larger value.

Table VIII-1 (Concluded)

Date/ Julian Day	Hour	Station M1 Speed mph	Station M1 Direction MAG	Station M1 24-hr Max Speed mph	Station M3 Speed mph	Station M3 Direction MAG	Station M3 24-hr Max Speed mph	Station M4 Speed mph	Station M4 Direction MAG	Station M4 24-hr Max Speed mph	Station M5 Speed mph	Station M5 Direction MAG	Station M5 24-hr Max Speed mph
9/25-269	1	5.2	150		7.7	140		3.7	141		9.2	146	
	2	4.9	139		8.3	142		6.3	141		8.7	154	
	3	4.4	148		7.4	147		5.2	138		9.2	149	
	4	3.5	141		7.5	148		6.7	147		8.4	166	
	5	3.7	145		9.1	151		6.9	156		9.8	162	
	6	5.8	159		9.1	151		7.5	153		11.3	162	
	7	7.2	162		9.2	162		8.2	153		11.2	161	15.4
	8	9.5	167	16.7	10.0	173	15.4	7.3	162		11.4	159	15.4
	9	9.4	161		9.8	174		6.7	165		11.6	163	15.4
	10	9.4	171		8.0	175		6.0	180		10.1	156	
	11	11.2	171		8.4	166		5.6	165		9.1	155	
	12	9.5	179		7.1	173		5.6	165		8.1	160	
	13	6.7	172		5.2	173		5.4	153		9.0	139	
	14	4.8	177		1.4	246		5.1	160		8.7	145	
	15	4.6	187		0.6	231		5.0	173		7.7	142	
	16	3.4	191		4.4	174		6.1	163		8.2	144	
	17	5.0	163		2.8	193		3.5	213	15.4	8.4	169	
	18	5.7	162		6.5	196		1.2	221		8.1	173	
	19	5.5	151		5.7	178		6.2	182		9.0	175	
	20	5.3	157		2.4	144		5.2	182		6.8	163	
	21	4.9	149		4.7	34		3.0	190		6.0	148	
	22	4.1	145		2.8	112		3.6	69		6.5	144	
	23	3.7	138		4.8	127		5.6	67		6.3	140	
	24	2.4	131		4.5	125		3.1	95		5.2	156	

Table VIII-2

Range of Hourly Salinity Data (ppt) for CT Stations,

20-25 September 1980

Date/Julian Day	6S	10S	12S	15M*	18M	20M
9/20-264	19.67-21.25	24.83-25.99	19.5-25.11	23.09-26.67	23.79-25.76	17.79-19.95
9/21-265	18.18-20.94	24.70-25.53	24.57-24.95	25.56-26.41	23.65-26.15	18.32-21.71**
9/22-266	20.38-20.95	24.28-25.40	24.49-25.37	23.97-26.79	22.36-25.09**	17.29-21.62**
9/23-267	20.37-21.11	23.71-25.15	24.50-24.84	23.17-25.17	12.57-24.28	17.80-20.31
9/24-268	20.35-21.07	23.91-24.69	23.70-24.54	21.96-23.65	21.31-22.98	17.71-20.69**
9/25-269	20.61-21.66	23.61-24.45	23.64-23.93	21.37-23.66	19.76-21.68	17.64-20.69

* Station 15B was used.

** Some spurious data points were discovered.

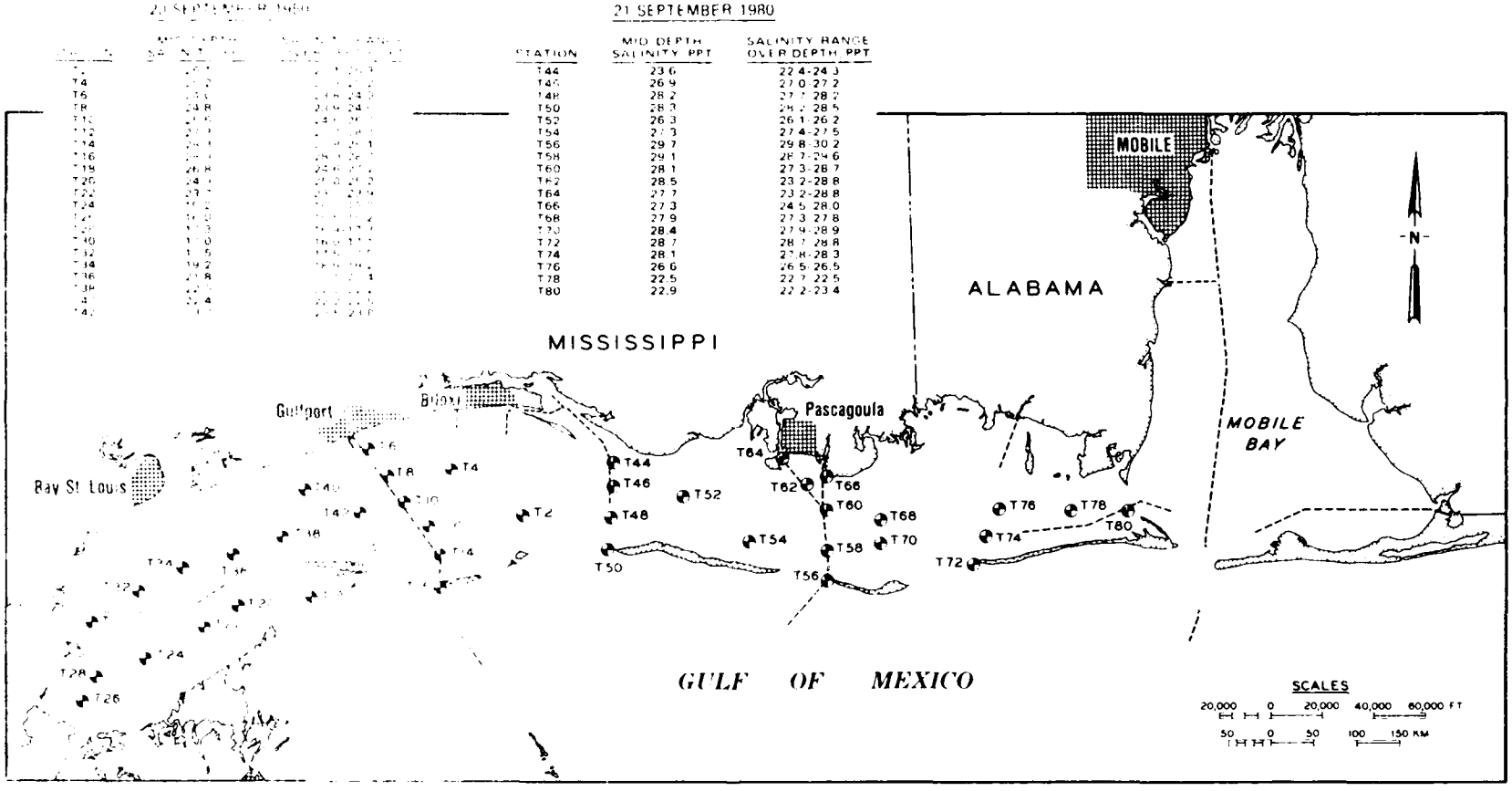

Figure VIII-1. September 20-21 salinity transect data

salinity and temperature data obtained using the deployed conductivity-temperature sensors, the salinity and temperature transect values obtained using a field salinometer were compared at common times and spatial locations as shown in Table VIII-3.

105. In most instances, temperature values were extremely close. However, the salinity values obtained from the conductivity-temperature sensors tended to be 2-3 parts per thousand lower than the field salinometer values. Raytheon Ocean Systems Company (Parker 1981) indicated that there were biological fouling problems with the conductivity probe. Antifouling paints cannot be used on the sensor because the metal ions released by such paints affect the conductivity readings. Therefore, in analyzing the salinity data, the instantaneous salinity data should be considered less reliable then the salinity transect data. Since salinity transect data were available for 20-21 September and 24-25 September these data were used to establish initial conditions and as calibration data, respectively.

Water Surface Elevation Information

106. Program TIDE (Appendix B) was developed to predict the tidal elevations presented in Part III after Schureman (1940) based upon the constituent amplitudes and phases. Astronomic data are calculated in order to determine constituent node factors and equilibrium arguments at the start of the prediction period. Based upon specified amplitudes and local epochs for the O_1, K_1, P_1, M_2, and S_2 constituents, as given previously in Tables III-2 and III-3, the program reconstructs the water surface elevation for each station. Subroutine TAPE accesses the edited hourly elevations as provided by NOAA and the filtered elevations input to the harmonic analysis so that these elevations may be printed next to the reconstructed elevation at each hour of the prediction period.

107. Table VIII-4 presents the astronomic data with reference to Greenwich Mean Time (GMT). By employing local epochs, the time reference is transformed directly to Central Standard Time (CST). Consider the Pascagoula station, 874-1196; tidal constituents are given in Table VIII-5. Since local epochs are used, the water surface elevations given in Table VIII-6 are in CST beginning at 20 September, hour 00. Elevations are given for the first 2 days of the 5-day period. The unfiltered (UF) and filtered (F) columns present the

Table VIII-3

Comparison of 20-21 September Salinity Transect Data with Instantaneous Salinity Data

Station	Date-Julian Day	CST Time	Location Latitude deg	Location Longitude deg	Water Depth ft	Measurement Depth ft	Salinity ppt	Temperature °C
T42	20 Sep (264)	2222	3016.6	8905.2	13	5.0 10.0	23.70 23.8	27.80 27.90
6S	20 Sep (264)	2230	3015.6	8908.54	13	5.0 8.0	20.42 18.68	28.70 28.58
T50	21 Sep (265)	1500	3014.55	8846.6	42	5.0 20.0	28.20 28.20	28.10 28.10
10S B	21 Sep (265)	1500	3014.90	8846.4	24	5.0 19.0	25.40 25.72	28.45 28.41
T54	21 Sep (265)	1608	3015.3	8836.25	13	5.0 10.0	27.20 27.40	28.1 28.0
12S B	21 Sep (265)	1600	3016.14	8840.8	14	5.0 9.0	24.76 25.14	28.27 28.25
T56	21 Sep (265)	1728	3012.42	8830.7	42	5.0 15.0	29.6 29.5	28.7 28.6
15S B	21 Sep (265)	1730	3012.00	8831.00	28	5.0 [illegible]	[illegible]	[illegible]
[illegible]	[illegible]	[illegible]	[illegible]	[illegible]	[illegible]	[illegible]	[illegible]	[illegible]
[illegible]	[illegible]	2100	3013.73	8819.[illegible]	15	[illegible]	[illegible]	[illegible]
T80	21 Sep (265)	2222	3017.1	8803.2[illegible]	16	5.0 10.0	22.6 22.9	29.3 28.2
20	21 Sep (265)	2230	3017.64	8807.3	10	5.0	20.46	29.33

Table VIII-4

Verification Period, Astronomic Tide Conditions,

20 September 1980, Hour 0000

a. Astronomic Terms at Greenwich:

Term	Degrees
Longitude of lunar node	137.96955
Mean longitude of sun	179.04444
Longitude of solar perigee	282.60883
Mean longitude of moon	303.55682
Longitude of lunar perigee	18.79060
Intersection of lunar orbit and equator	19.91312
Longitude in the lunar orbit	9.44233
Longitude in the celestial orbit	10.15299
V prime	6.67200
V double prime	12.80633
Solar hour angle	180.00000

b. Node Factors and Equilibrium Arguments:

Tidal Constituent	Node Factor	Equilibrium Argument (V + U)	Components V	Components U
M2	1.028	179.55	110.98	358.58
S2	1.000	180.00	180.00	0.00
N2	1.028	184.79	186.21	358.58
K1	.728	262.37	269.94	353.33
M4	1.057	219.11	221.95	357.16
O1	.870	217.66	291.93	8.73
M6	1.087	328.66	332.93	356.74
MK3	.946	11.93	20.02	351.91
S4	1.000	0.00	0.00	0.00
MN4	1.057	294.34	297.18	357.16
V2	1.028	145.30	146.72	359.58
S6	1.000	0.00	0.00	0.00
U2	1.028	220.53	221.95	358.58
2N2	1.028	262.85	261.44	359.58
OO1	.621	127.12	156.16	330.96
LP2	1.028	253.91	255.23	359.58
S1	1.000	180.00	180.00	0.00
M1	1.666	329.32	325.49	3.84
J1	.888	183.66	193.81	349.85
MM	1.057	264.77	264.77	0.00
SSA	1.000	358.08	358.08	0.00
SA	1.000	179.04	179.04	0.00
MSF	1.057	249.02	249.02	0.00
MF	.735	228.23	247.11	341.12
RHO1	.870	246.40	237.67	8.73
Q1	.870	285.93	277.16	8.73
T2	1.000	183.56	183.56	0.00
R2	1.000	76.44	76.44	0.00
2Q1	.870	1.13	352.40	8.73
P1	1.000	90.96	90.96	0.00
2SM2	1.028	251.45	249.02	1.42
M3	1.542	164.33	166.46	357.57
L2	.657	217.21	215.74	354.47
2MK3	.773	316.74	312.91	3.83
K2	.910	345.55	355.08	347.49
M8	1.117	76.22	83.90	354.31
MS4	1.057	109.55	110.98	358.58

Table VIII-5

Tidal Constituents at Pascagoula (874-1196)

Constituent	NGVD = +0.58 Ft Above MSL Amplitude, ft	Local Epoch, deg
O1	0.49	295.9
K1	0.47	306.6
P1	0.14	309.4
M2	0.09	323.6
S2	0.05	339.5

Table VIII-6

Pascagoula 874-1196 NGVD (1929) Water Surface Elevation (ft), 20 September 1980, Hour 00

Hour	Unfiltered	Filtered	Reconstructed
0	1.11000	.94[illegible]	.78[illegible]
1	1.2[illegible]000	1.[illegible]000	.[illegible]
2	1.3[illegible]000	1.1[illegible]	1.[illegible]1442
3	1.44000	1.17000	1.[illegible]
4	1.5[illegible]000	1.2[illegible]	1.[illegible]
5	1.[illegible]000	1.25000	1.2322[illegible]
6	1.[illegible]	1.2400[illegible]	1.24[illegible]
7	1.4[illegible]000	1.1[illegible]	1.[illegible]7
8	1.[illegible]	1.[illegible]	1.[illegible]
9	1.3[illegible]	.9[illegible]	.[illegible]
10	1.14[illegible]	.76[illegible]	.[illegible]527
11	.[illegible]	.[illegible]40000	.[illegible]
12	.[illegible]7[illegible]	.31[illegible]	.41[illegible]
13	.4[illegible]000	.11[illegible]	.227[illegible]
14	.2[illegible]	-.[illegible]E-01	.7[illegible]E-01
15	.[illegible]000	-.1[illegible]	-.[illegible]41[illegible]E-01
16	.2[illegible]000	-.2[illegible]000	-.[illegible]78[illegible]E-01
17	.2[illegible]000	-.17[illegible]	-.[illegible]61945E-01
18	.2[illegible]000	-.9[illegible]000E-01	-.32[illegible]78E-01
19	.37[illegible]000	.3[illegible]E-01	.5[illegible]5356E-01
20	.3[illegible]	.1[illegible]	.172[illegible]
21	.72[illegible]000	.36000[illegible]	.294413
22	.9[illegible]	.52[illegible]	.415[illegible]4
23	1.0[illegible]	.[illegible]000	.[illegible]9[illegible]58
24	1.12[illegible]	.79[illegible]	.[illegible]35[illegible]
25	1.2[illegible]	.[illegible]	.73[illegible]
26	1.34000	.980000	.[illegible]
27	1.3[illegible]	1.[illegible]	.928[illegible]
28	1.4[illegible]	1.13000	1.01963
29	1.5[illegible]0	1.1[illegible]	1.09[illegible]4
30	1.5[illegible]	1.[illegible]	1.1[illegible]
31	1.54[illegible]	1.2100	1.1[illegible]
32	1.46[illegible]	1.1[illegible]	1.16[illegible]
33	1.4[illegible]	1.0400[illegible]	1.0[illegible]144
34	1.2[illegible]	.[illegible]	.[illegible]7[illegible]147
35	1.03000	.6[illegible]	.[illegible]7544
36	.93[illegible]	.46[illegible]	.519[illegible]
37	.58[illegible]	.240000	.427834
38	.43[illegible]	.6[illegible]E-01	.254017
39	.2[illegible]	-.7[illegible]E-01	.117[illegible]07
40	.2[illegible]	-.12[illegible]	.324[illegible]E-01
41	.27[illegible]	-.1[illegible]	.2[illegible]73[illegible]E-02
42	.3[illegible]000	-.2[illegible]E-01	.244139E-01
43	.[illegible]	.1[illegible]E+00	.[illegible]79[illegible]E-01
44	.6[illegible]	.2[illegible]	.174[illegible]
45	.[illegible]	.3[illegible]	.271[illegible]
46	.94[illegible]	.4[illegible]	.3[illegible]091
47	1.[illegible]	.5[illegible]000	.44[illegible]
48	1.13[illegible]	.6[illegible]	.52241[illegible]

unfiltered (edited NOAA) and filtered (harmonic analysis input) data, respectively. All elevations are with respect to NGVD (1929). Information analogous to that shown in Table VIII-6 for station 874-1196 is developed by the program for all other stations shown in Table II-3.

108. In interpreting the elevation table, it should be noted that predicted levels are based upon the five major tidal constituents (O_1, K_1, P_1, M_2, and S_2), whereas the unfiltered levels contain all tidal energy. Reid and Whitaker (1981) note that these five tidal constituents contain approximately 95 percent of the tidal energy.

109. The unfiltered levels contain meteorological input in addition to all the tidal energy. In examining Table VIII-6, the filtered and reconstructed levels are usually very close (less than 0.1 ft). Unfiltered levels are 0.4-0.6 ft higher at each hour. The winds shown in Table VIII-1 do not appear to be of sufficient strength to account for all of the difference. In addition, this pattern in elevations holds at all other tidal stations as well. The majority of the 0.4- to 0.6-ft difference between unfiltered and reconstructed levels is believed to constitute a measure of the forerunner and far field surge of tropical storm Hermine, which passed through the Carribean over the Yucatan Peninsula and through the lower Gulf of Mexico during 20-25 September as shown in the 1980 supplement to Cry (1977). The magnitude of this effect as noted from the data is less than 0.6 ft, which is within the range of magnitudes of these effects observed for other tropical storms and hurricanes.

Current Component Information

110. Program TIDE may also be used to reconstruct tidal currents as well. Tidal currents are represented in E-W and N-S component form, with the E and N directions considered positive. The same astronomic data as given in Table VIII-4 are employed. The time reference is again CST since local epochs as shown in Table VIII-7 for station V10-S are used for each current component.

111. The unfiltered (edited), filtered (harmonic analysis input), and reconstructed currents for the first day of the 5-day period are given for station V10-S in Table VIII-8. Since a vertically integrated two-dimensional modeling approach is being employed, the meter nearest middepth was considered for stations shown in Table III-5, for which meters were placed at various

Table VIII-7

Station V10-S Tidal Constituents

V10-S E-W; Mean Amplitude = 0.01 fps

Constituents	Mean Amp. (ft)	Epoch (deg)
O1	.238	240.20
K1	.190	256.60
M2	.079	33.60
S2	.036	292.30

V10-S N-S; Mean Amplitude = -0.02 fps

Constituents	Mean Amp. (ft)	Epoch (deg)
O1	.236	239.60
K1	.210	266.80
M2	.080	39.90
S2	.046	350.3

Table VIII-8

Station V10-S Velocity (fps) Comparisons

Hour	-Unfiltered	Filtered	Predicted
	.5[illegible]E-01	.1[illegible]	.[illegible]
1	.14[illegible]	.1[illegible]	.743471
2	.18[illegible]	.1[illegible]	.[illegible]
3	.31[illegible]	.1[illegible]	.235128
4	.32[illegible]	.22[illegible]	.16[illegible]
5	.26[illegible]	.24[illegible]	.11[illegible]
6	.2[illegible]	.23[illegible]	.[illegible]E-01
7	.9[illegible]E-01	.16[illegible]	.[illegible]E-01
8	-.3[illegible]E-01	.5[illegible]E-01	-.[illegible]E-02
9	-.3[illegible]E-01	-.8[illegible]E-01	-.524593E-01
10	-.25[illegible]	-.23[illegible]	-.116658
11	-.31[illegible]	-.36[illegible]	-.192128
12	-.43[illegible]	-.4[illegible]	-.[illegible]
13	-.4-[illegible]	-.4[illegible]	-.336465
14	-.46[illegible]	-.47[illegible]	-.3[illegible]
15	-.26[illegible]	-.39[illegible]	-.396604
16	-.9[illegible]E-01	-.26[illegible]	-.356022
17	-.5[illegible]E-01	-.12[illegible]	-.28[illegible]
18	.1[illegible]E-01	.2[illegible]E-01	-.[illegible]
19	.5[illegible]E-01	.15[illegible]	-.[illegible]E-01
20	.32[illegible]	.23[illegible]	.[illegible]E-01
21	.39[illegible]	.28[illegible]	.210658
22	.44[illegible]	.28[illegible]	.296683
23	.12[illegible]	.27[illegible]	.345348
24	.5[illegible]E-01	.23[illegible]	.354[illegible]
25	.7[illegible]E-01	.2[illegible]	.331131
26	.17[illegible]	.1[illegible]	.295[illegible]
27	.12[illegible]	.17[illegible]	.231044
28	.16[illegible]	.17[illegible]	.17850[illegible]
29	.2[illegible]	.16[illegible]	.135[illegible]43
30	.11[illegible]	.14[illegible]	.1[illegible]163
31	.2[illegible]E-01	.11[illegible]	.761[illegible]23E-01
32	0.	.7[illegible]E-01	.49[illegible]E-01
33	-.76[illegible]E-01	.1[illegible]E-01	.147914E-01
34	-.5[illegible]E-01	-.7[illegible]E-01	-.341077E-01
35	-.16[illegible]	-.15[illegible]	-.981431E-01
36	-.15[illegible]	-.24[illegible]	-.172[illegible]65
37	-.29[illegible]	-.32[illegible]	-.247[illegible]
38	-.41[illegible]	-.3[illegible]	-.31[illegible]
39	-.46[illegible]	-.38[illegible]	-.34724[illegible]
40	-.22[illegible]	-.34[illegible]	-.348[illegible]11
41	-.8[illegible]E-01	-.23[illegible]	-.3[illegible]
42	.7[illegible]E-01	-.9[illegible]E-01	-.[illegible]
43	.13[illegible]	.6[illegible]E-01	-.[illegible]
44	.33[illegible]	.1[illegible]	-.[illegible]
45	.34[illegible]	.26[illegible]	.176645
46	.22[illegible]	.28[illegible]	.200942
47	.26[illegible]	.24[illegible]	.264376
48	.17[illegible]	.17[illegible]	.[illegible]

(Continued)

Table VIII-8 (Concluded)

Hour	Unfiltered	Filtered	Predicted
[illegible]	[illegible]	[illegible]	[illegible]
1	[illegible]	[illegible]	[illegible]
2	[illegible]	[illegible]	[illegible]
3	[illegible]	[illegible]	[illegible]
4	[illegible]	[illegible]	[illegible]
5	[illegible]	[illegible]	[illegible]
6	[illegible]	[illegible]	[illegible]
7	[illegible]	[illegible]	[illegible]
8	[illegible]	[illegible]	[illegible]
9	[illegible]	[illegible]	[illegible]
10	[illegible]	[illegible]	[illegible]
11	[illegible]	[illegible]	[illegible]
12	[illegible]	[illegible]	[illegible]
13	[illegible]	[illegible]	[illegible]
14	[illegible]	[illegible]	[illegible]
15	[illegible]	[illegible]	[illegible]
16	[illegible]	[illegible]	[illegible]
17	[illegible]	[illegible]	[illegible]
18	[illegible]	[illegible]	[illegible]
19	[illegible]	[illegible]	[illegible]
20	[illegible]	[illegible]	[illegible]
21	[illegible]	[illegible]	[illegible]
22	[illegible]	[illegible]	[illegible]
23	[illegible]	[illegible]	[illegible]
24	[illegible]	[illegible]	[illegible]
25	[illegible]	[illegible]	[illegible]
26	[illegible]	[illegible]	[illegible]
27	[illegible]	[illegible]	[illegible]
28	[illegible]	[illegible]	[illegible]
29	[illegible]	[illegible]	[illegible]
30	[illegible]	[illegible]	[illegible]
31	[illegible]	[illegible]	[illegible]
32	[illegible]	[illegible]	[illegible]
33	[illegible]	[illegible]	[illegible]
34	[illegible]	[illegible]	[illegible]
35	[illegible]	[illegible]	[illegible]
36	[illegible]	[illegible]	[illegible]
37	[illegible]	[illegible]	[illegible]
38	[illegible]	[illegible]	[illegible]
39	[illegible]	[illegible]	[illegible]
40	[illegible]	[illegible]	[illegible]
41	[illegible]	[illegible]	[illegible]
42	[illegible]	[illegible]	[illegible]
43	[illegible]	[illegible]	[illegible]
44	[illegible]	[illegible]	[illegible]
45	[illegible]	[illegible]	[illegible]
46	[illegible]	[illegible]	[illegible]
47	[illegible]	[illegible]	[illegible]
48	[illegible]	[illegible]	[illegible]

depths. The subsets of stations considered are indicated by asterisks in Table III-5.

112. Predicted currents are reconstructed from the five major tidal constituents (O_1, K_1, P_1, M_2, and S_2). The K_1 in Table III-7 contains both K_1 and P_1 energy. In order to separate K_1 and P_1, at least 182 days of record are necessary. Since current meters were removed during the shrimp season and during Hurricane Allen, a complete 182-day record was not available for any of the current stations. As a result the K_1 constituent reported in Tables III-6 through III-9 contains P_1 energy and is valid only during the analysis period. Therefore, the total tidal current signal may be predicted at a given station only during the period given in Table III-5.

PART IX: VERIFICATION PERIOD 12-16 JUNE 1980

113. In order to obtain a more detailed understanding of the behavior of the Sound prior to simulating this period, hourly values of wind speed and direction and salinity are considered. A complete set of salinity transect values is also presented in order to investigate stratification effects Sound-wide. Based upon the results of the harmonic analysis, the predicted values of water surface elevation and currents are developed and compared with the unfiltered (raw) data.

Wind Information

114. Hourly wind speeds and directions are as shown in Table IX-1. At most stations average hourly wind speeds are below 15 mph, while daily maximum wind speeds (2-sec gust) are below 20 mph. Wind direction and velocity are spatially uniform at any one hour over the period.

Instantaneous Salinity Information

115. Hourly values of salinity at meters nearest middepth appear to exhibit tidal variations at most stations. In order to investigate the temporal variations, the maximum and minimum values are given in Table IX-2, such that their difference (W) is maximum for the day given. Maximum daily variations in salinity range from 4.18 ppt at station 6S to 11.0 ppt at station 20M. The maximum spatial difference in salinity over the entire Sound is greater than 13 ppt as shown in Table IX-2. This period exhibits highly variable salinity conditions both in space and in time.

Salinity Transect Information

116. Representative middepth salinity values are shown in Figure IX-1. The range over depth is given to indicate the degree of stratification. Stratification effects are quite significant over the mid and eastern section of the Sound, even outside navigation channels during this period. The well-mixed assumption does not hold over these areas during this period. As a result, a two-dimensional vertically averaged approach may not hold for salinity.

Table IX-1

Hourly Meteorological Data (Wind Speed and Direction), 12-16 June 1980, Stations M1-M5

June 1980 Day	Julian Day	Hour	Station M1 Speed mph	Station M1 Direction MAG	Station M1 24-hr Max Speed mph	Station M2 Speed mph	Station M2 Direction MAG	Station M2 24-hr Max Speed mph	Station M3 Speed mph	Station M3 Direction MAG	Station M3 24-hr Max Speed mph	Station M4 Speed mph	Station M4 Direction MAG	Station M4 24-hr Max Speed mph	Station M5 Speed mph	Station M5 Direction MAG	Station M5 24-hr Max Speed mph
12	164	1	5.2	218		5.7	191		5.2	235		4.1	254		7.9	247	
		2	4.8	236		6.2	210		4.3	268		3.2	265		5.3	264	
		3	3.6	234		5.1	216		2.9	301		3.8	278		3.8	282	
		4	1.2	349		5.4	263		2.0	324		4.8	283		3.8	302	
		5	1.0	34		7.0	259		3.2	333		7.1	316		4.5	298	
		6	2.8	341		7.9	262		3.3	336		7.6	326		3.9	314	
		7	4.3	8		8.5	309		3.8	345		9.4	336		4.2	339	
		8	4.4	11		9.7	314		4.3	346		10.2	345		6.3	10	
		9	4.3	14		11.5	334		6.3	351		11.7	352		9.5	14	
		10	5.9	24		16.3	345		9.3	8		16.1	14	20.7	12.9	26	18.7
		11	8.4	43		18.0	5	22.7	10.4	10		15.5	28	20.2	11.6	35	
		12	9.9	49	17.4	18.0	11	22.7	11.4	19		14.8	34		12.5	32	
		13	10.3	56		18.6	17	22.7	11.8	24		14.2	36		12.1	35	
		14	8.4	54		16.5	20		10.7	30		12.3	45		9.3	33	
		15	7.2	65		12.8	19		7.7	35		9.8	48		7.8	33	
		16	4.2	112		9.3	27		5.4	53		7.0	52		7.7	31	
		17	4.5	147		6.6	20		2.6	139		5.8	69		6.7	22	
		18	4.7	164		4.0	25		3.2	36		4.0	72		6.5	12	
		19	5.5	170		4.0	117		8.0	12		3.9	82		7.4	16	
		20	6.8	177		6.1	121		6.6	4	17.4	4.9	96		6.2	26	
		21	7.4	179		6.5	127		7.6	29		6.2	158		6.4	28	
		22	5.0	167		6.8	134		3.4	144		6.8	157		6.7	28	
		23	4.4	168		6.4	141		7.3	184		6.2	157		1.6	6	
		24	4.7	180		6.5	151		6.5	192		4.9	189		6.4	203	
13	165	1	3.8	161		6.3	154		4.7	212		3.8	220		7.4	223	
		2	5.3	174		4.4	175		4.1	235		2.5	205		6.1	238	
		3	3.3	186		2.8	194		3.7	233		2.6	206		3.5	280	
		4	1.4	163		2.4	213		3.3	300		2.2	243		3.5	304	
		5	2.1	20		4.5	282		4.3	345		2.8	296		4.0	306	
		6	2.8	16		8.0	308		4.5	0		5.2	341		3.5	313	
		7	3.8	42		9.2	357		5.9	8		5.9	10		3.2	341	
		8	3.4	29		10.0	13		7.1	11		7.1	31		4.2	358	
		9	2.8	66		10.4	10		7.4	8		7.7	27		3.5	358	
		10	3.3	6		9.9	0		6.7	357		11.0	20		4.5	52	
		11	4.8	49		11.1	349		7.1	355		10.3	20		5.8	18	
		12	4.7	39		11.8	354	16.7	7.7/ 6.4*	353/ 47		9.0	30		7.4	13	
		13	4.5	17		10.8	352		8.6	7		11.4	22		7.6	54	
		14	6.2	41		10.4	358		7.7	3		10.1	22		8.5	69	

(Continued)

*Meter change.

Table IX-1 (Concluded)

Date 1980	Julian		Station M1			Station M2			Station M3			Station M4			Station M5		
				Direc-	24-hr		Direc-	24-hr		Direc-	24-hr		Direc-	24-hr		Direc-	24-hr
Day	Day	Hour	Speed mph	tion MAG	Max Speed mph	Speed mph	tion MAG	Max Speed mph	Speed mph	tion MAG	Max Speed mph	Speed mph	tion MAG	Max Speed mph	Speed mph	tion MAG	Max Speed mph
15	167	7	13.9	202		13.1	168	17.4	9.8	210		6.9	205	14.0	12.8	221	
(Continued)		8	12.6	209		13.0	181	17.4	8.6	224		7.1	217		13.0	222	
		9	13.4	215		11.6	174		10.5	217	18.0	6.7	212		12.4	227	
		10	13.4	212		11.3	176		9.6	216		6.9	211	14.0	12.2	231	
		11	13.0	210		12.8	179		8.8	215		6.3	217		10.2	230	
		12	12.2	216		11.6	181		8.3	225		5.3	225		9.2	342	
		13	11.4	203		10.8	168		7.7	217		5.8	211		9.6	228	
		14	10.7	197		10.7	167		7.3	212		6.8	204		9.4	215	
		15	8.9	199		9.8	160		7.5	205		6.0	202		7.8	214	
		16	6.4	205		7.8	167		6.6	208		6.1	198		8.5	195	
		17	5.2	196		7.5	161		6.1	211		6.0	193		7.1	196	
		18	8.1	178		8.2	151		7.6	197		6.0	192		7.7	189	
		19	8.9	173		8.8	149		7.8	195		7.0	186		8.0	194	
		20	8.2	163		9.0	148		8.4	194		6.3	191		8.4	200	
		21	9.6	161		9.5	141		8.7	193		7.2	186		8.4	202	
		22	12.2	175		10.5	144		8.6	176		7.0	182		8.0	199	
		23	10.9	175		10.2	141		8.9	177		6.5	184		9.5	185	
		24	9.4	168		10.1	136		8.3	174		6.0	172		9.0	188	
16	168	1	7.9	168		9.2	135		7.8	172		5.5	171		8.6	177	
		2	10.0	170		10.8	132		8.4	171		5.8	175		9.2	187	
		3	13.1	172		11.0	137		8.8	171		6.3	169		10.0	191	
		4	13.2	177		13.1	133		9.8	175		6.8	179		10.6	187	
		5	14.5	177	20.0	15.0	139		10.4	179		8.1	181	15.4	12.2	186	
		6	13.2	182		14.3	143		10.1	188		7.7	176		12.9	180	18.0
		7	13.9	187		14.1	137		10.1	189		7.9	181		13.2	182	
		8	12.2	194		12.2	136		9.1	178		8.1	176	15.4	14.1	184	
		9	8.6	209		11.5	146		7.8	192		7.2	184	15.4	14.0	196	
		10	6.3	244		12.8	142		8.9	190		7.2	200		13.2	208	18.0
		11	6.5	266		14.1	151	20.0	9.6	190	17.4	7.4	199		12.9	213	18.0
		12	5.4	269		12.9	170		9.7	195		7.6	210	15.4	11.6	224	
		13	3.9	314		9.4	173		4.3	252		6.2	216		9.7	235	
		14	4.1	339		5.8	192		5.7	353		5.9	216		7.8	235	
		15	1.2	262		4.5	209		4.9	31		6.0	230		7.0	231	
		16	4.1	198		2.9	171		3.9	179		5.1	216		4.5	212	
		17	5.1	162		5.5	136		5.0	177		5.4	185		5.4	212	
		18	5.4	162		4.4	133		6.1	166		5.9	185		6.5	199	
		19	6.3	162		7.5	125		9.3	170		6.7	178		6.9	204	
		20	6.3	168		9.0	149		9.1	180		7.8	187		8.5	180	
		21	7.7	172		9.9	150		9.3	182		7.9	175		9.5	178	
		22	8.5	179		9.5	159		9.6	206		7.0	185		9.3	180	
		23	9.3	178		10.0	152		8.5	190		6.4	108		10.2	201	
		24	9.9	178		10.6	198		9.0	193		6.3	195		10.3	197	

(Sheet 3 of 3)

Table IX-2

12-16 June 1980 Continuous Station Salinity Levels

Station	Temporal Variation				Spatial Variation	
	Salinity, ppt		Difference	Day Corresponding to These Conditions	Salinity	
	Minimum	Maximum	Δ , ppt		ppt	Date and Time
6S	11.84	16.02	4.18	12 June	12.52	14 June 1800 hours CST
10S	15.31	19.59	4.28	13 June	18.72	
12S	7.78	12.55	4.77	13 June	11.45	
15M	18.77	27.24	8.47	16 June	29.94	
18M	15.70	17.95	2.25	15 June	16.67	
20M	5.42	16.42	11.00	15 June	11.29	

12 JUNE 1980

STATION	MID DEPTH SALINITY, PPT	SALINITY RANGE OVER DEPTH, PPT
T2	16.6	16.1-18.1
T4	16.9	16.86-16.96
T6	22.3	14.5-26.1
T8	24.4	17.6-29.1
T10	19.9	17.7-24.7
T12	20.9	20.9-25.0
T14	21.2	18.3-27.0
T16	20.8	19.8-28.0
T18	20.5	20.4-20.9
T20	19.3	19.0-19.5
T22	17.6	16.4-18.2
T24	9.96	9.96-11.3
T26	4.4	4.4-5.2
T28	6.7	5.8-8.1
T30	6.0	5.2-6.5
T32	11.0	11.0-11.5
T34	12.4	11.1-12.5
T36	11.9	11.1-12.4
T38	12.9	12.9-14.6
T40	13.2	13.2-13.1
T42	16.2	15.5-16.7

13 JUNE 1980

STATION	MID DEPTH SALINITY, PPT	SALINITY RANGE OVER DEPTH, PPT
T44	13.5	13.3-15.9
T46	16.6	13.9-19.8
T48	21.5	16.6-21.9
T50	22.4	17.9-22.4
T52	20.6	13.6-22.6
T54	17.4	17.4-18.5
T56	28.7	21.9-30.3
T58	28.7	17.8-29.6
T60	27.1	18.1-28.8
T62	27.4	16.1-28.6
T64	25.0	14.7-28.1
T66	26.2	17.9-28.5
T68	16.4	16.0-17.6
T70	18.6	16.1-25.9
T72	24.8	23.6-24.8
T74	24.3	12.9-24.3
T76	15.4	13.3-24.6
T78	11.5	11.5-11.8
T80	14.1	9.0-17.9

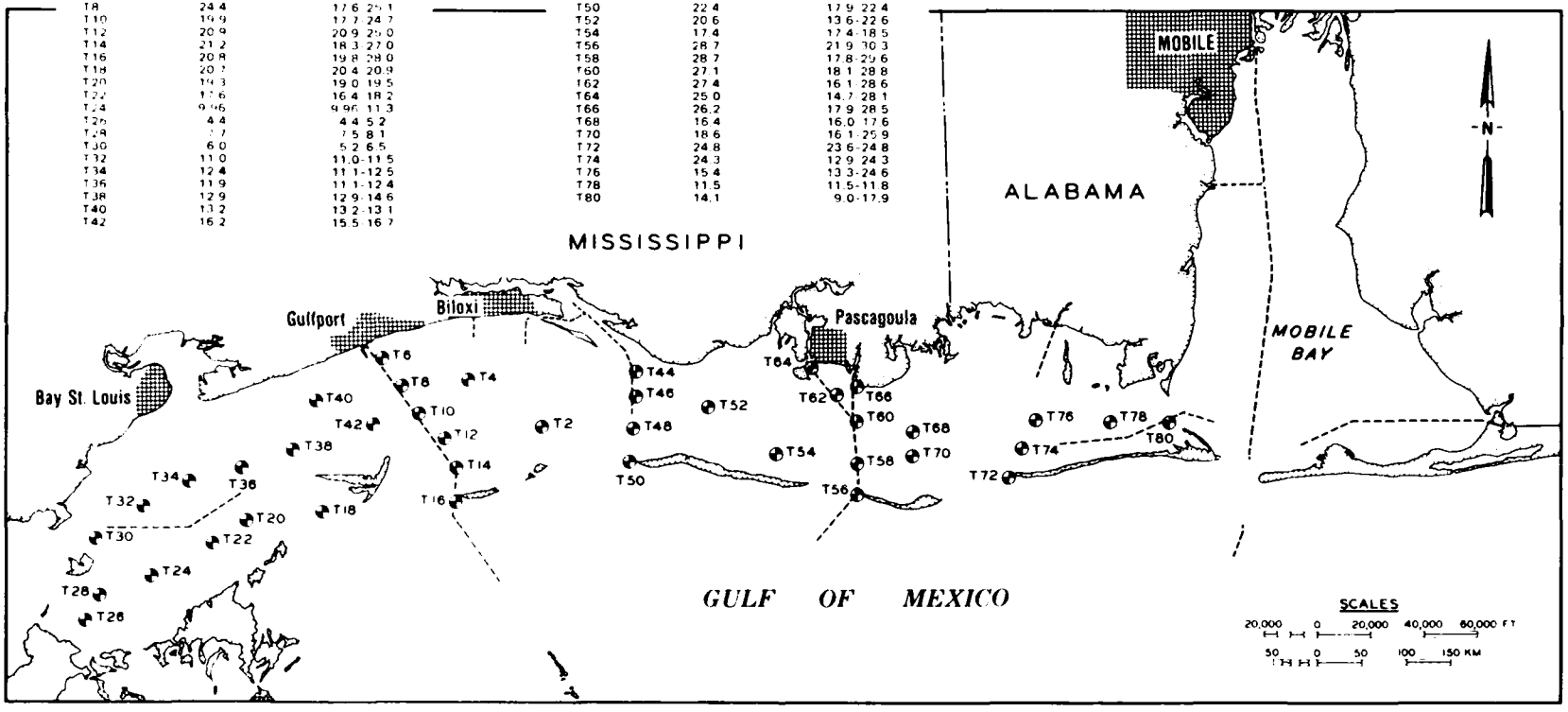

Figure IX-1. 12-13 June salinity transect data

117. It should also be mentioned that the biological fouling problem associated with the conductivity probe was also evident during this period. Instantaneous salinity values were consistently 2-3 ppt lower than corresponding salinity transect values. As a result, salinity transect values should be considered to be more reliable than the continuous salinity levels determined at the conductivity-temperature (CT) stations. However, the time and spatial variability characteristic of the continuous salinity data shown in Table IX-2 is considered valid. As a result, the initial salinity conditions cannot be specified using the transect data, since these data were obtained over 2 days and do not constitute a snapshot of the system. As a result salinity will not be simulated during this period.

Water Surface Elevation and Current Component Information

118. The astronomic data, constituent node factor, and equilibrium arguments are shown in Table IX-3 for conditions at the start of the verification period. The major constituents at Pascagoula station 874-1196 are as previously given. The water levels are presented for this station in Table IX-4 from 20 September, hr 0, CST, for the first 2 days of the verification period.

119. In interpreting the elevation table, predicted levels are based on the five major constituents (O_1, K_1, P_1, M_2, and S_2), whereas the filtered levels contain all tidal energy. The unfiltered levels contain meteorological input in addition to all the tidal energy. In examining Table IX-4, the filtered and predicted levels are usually within 0.1 ft. Unfiltered levels are within 0.3 ft of filtered levels. This difference is consistent with the wind information shown in Table IX-1. No tropical storms or hurricanes influenced Mississippi Sound during this period. Current data for station 10S were not available for this period; as a result station V10S was not considered.

Table IX-3

Verification Period Astronomical Tide Conditions, 6 June 1980, Hour 0000

a. Astronomic Terms at Greenwich:

Term	Degrees
Longitude of lunar node	143.26493
Mean longitude of sun	80.47970
Longitude of solar perigee	282.60412
Mean longitude of moon	65.91713
Longitude of lunar perigee	7.65024
Intersection of lunar orbit and equator	19.55813
Longitude in the lunar orbit	8.58509
Longitude in the celestial orbit	9.21961
V prime	6.02663
V double prime	11.20029
Solar hour angle	180.00000

b. Node Factors and Equilibrium Arguments:

Tidal Constituents	Node Factor	Equilibrium Argument (V + U)	Components V	Components U
M2	1.[illegible]	27.9[illegible]	29.13	358.73
S2	1.[illegible]	[illegible]	0.00	0.00
N2	1.[illegible]	329.5[illegible]	330.86	358.73
K1	.8[illegible]	164.45	170.49	353.97
M4	1.[illegible]2	55.71	58.25	357.46
O1	.85[illegible]	226.6[illegible]	218.65	7.95
M6	1.[illegible]4	83.57	87.38	356.19
MK3	.8[illegible]6	192.31	199.60	352.70
S4	1.0[illegible]	0.00	0.00	0.00
MN4	1.[illegible]62	357.45	353.98	357.46
V2	1.0[illegible]	115.25	116.52	358.73
S6	1.[illegible]0[illegible]	[illegible]	0.00	0.00
U2	1.0[illegible]3	56.98	58.25	358.73
2N2	1.0130	271.32	272.59	358.73
OO1	.[illegible]89	275.92	302.31	333.61
LDA2	1.[illegible]3[illegible]	12[illegible].46	121.73	358.73
S1	1.[illegible]02	180.00	180.00	0.00
M1	1.[illegible]55	103.45	104.56	359.91
J1	.[illegible]75	21[illegible].5[illegible]	228.75	350.78
MM	1.10[illegible]	[illegible]8.27	56.27	0.00
SSA	1.[illegible]0	180.9[illegible]	180.96	0.00
SA	1.[illegible]0	[illegible]0.4[illegible]	60.49	0.00
MSF	1.105	330.87	330.87	0.00
MF	.71[illegible]	114.66	131.83	342.83
RHO1	.[illegible]5[illegible]	31[illegible].9[illegible]	306.04	7.95
Q1	.[illegible]56	168.3[illegible]	160.38	7.95
T2	1.[illegible]0	2[illegible]2.12	302.12	0.00
R2	1.[illegible]0[illegible]	[illegible]37.8[illegible]	337.68	0.00
2Q1	.[illegible]56	11[illegible].0[illegible]	102.11	7.95
P1	1.000	1[illegible].9[illegible]	189.52	0.00
2SM2	1.[illegible]36	[illegible]30.14	330.87	1.27
M3	1.[illegible]46	2[illegible]1.7[illegible]	[illegible]23.69	358.10
L2	.947	266.5[illegible]	267.32	359.14
2MK3	.9[illegible]6	251.26	247.77	3.49
K2	.[illegible]95	149.7[illegible]	160.96	345.80
M8	1.127	111.42	116.59	354.92
MS4	1.062	27.86	29.13	358.73

Table IX-4

Pascagoula 874-1196 Water Surface Elevation*

Hour	Unfiltered	Filtered	Reconstructed

PART X: GLOBAL GRID HYDRODYNAMIC CALIBRATION AND VERIFICATION AND SYSTEM MODIFICATION

120. In this part, hydrodynamic simulation results over the global grid developed in Part VI are presented. Bottom friction mechanics (Manning's n versus stilled water depth) are calibrated considering the period 20-24 September 1980. The period 12-14 June 1980 was employed to verify the bottom friction. In order to consider the spatial extent of system induced changes in the hydrodynamics, a hypothetical system modification in the vicinity of Sand Island was made and a hydrodynamic simulation performed over the period 20-24 September. Salinity was not considered in any of these three simulations. As a result, meteorological effects (wind, surge setup, pressure anomaly) were not considered. The simulations corresponded to solely astronomic conditions.

121. Program TIDE (Appendix B) was incorporated in WIFM as a set of subroutines in order to develop water surface elevations at the boundary of the global grid. Harmonic constants (mean amplitude and Greenwich epoch) developed by the GTM were input. Astronomic arguments, node factors, and equilibrium arguments are computed at the start of the simulation period. Contributions from each of the five constituents (O_1, K_1, P_1, M_2, and S_2) are summed to produce the predicted or reconstructed tidal elevation at the boundary. Since GTM grid spacing did not correspond to global grid spacings, it was necessary to employ an interpolation procedure. The amplitudes (cm) and phases (°Greenwich) are shown in Table X-1 for the 14 tidal signals located on the GTM grid as shown in Figure VI-1. The convective acceleration and eddy dispersion terms in the motion equations were set to zero on the solid and open boundaries of the global grid, thereby linearizing the motion equations at locations around the boundary. The same approach was employed around barriers. Subroutine ADVBAR (Appendix D) was developed in order to perform this task for the model user automatically. For global grid boundary cells (115, 22-59), values were interpolated linearly on cell-centered distances between the appropriate signals 1-5. For global grid boundary cells (31-114, 59) values were interpolated linearly on cell-centered distances between the appropriate signals 6-14.

122. Zero offset was assumed so that the reconstructed tidal signal oscillated about local mean sea level (LMSL), which was selected as the model datum. Based upon Table III-1, 1 ft was added to all soundings to convert their reference Gulf Coast Low Water Datum (MLLW) to the model datum (LMSL).

Table X-1

Gulf Tide Model Boundary Inputs

Constituent	Amplitude, cm	Phase, °G	Ampl. Mult. Factor
	Signal 1, GTM Lat 1, Global Grid Cell (115, 59)		
O_1	12.4	18.1	1.15
P_1	3.6	24.2	1.19
K_1	12.6	25.4	1.12
M_2	1.8	136.4	0.72
S_2	0.7	120.6	1.00
	Signal 2, GTM Lat 2, Global Grid Cell (115,56)		
O_1	12.4	18.3	1.15
P_1	3.6	24.5	1.19
K_1	12.7	25.7	1.12
M_2	1.8	136.8	0.72
S_2	0.8	0.72	1.00
	Signal 3, GTM Lat 3, Global Grid Cell (115, 50)		
O_1	12.4	18.5	1.15
P_1	3.6	24.8	1.19
K_1	12.7	25.9	1.12
M_2	1.8	137.5	0.72
S_2	0.8	120.1	1.00
	Signal 4, GTM Lat 4, Global Grid Cell (115, 37)		
O_1	12.5	18.6	1.00
P_1	3.6	25.0	1.00
K_1	12.8	26.1	1.00
M_2	1.8	137.2	1.00
S_2	0.8	119.2	1.00
	Signal 5, GTM Lat 4, Global Grid Cell (115, 22)		
O_1	12.5	18.6	1.00
P_1	3.6	25.0	1.00
K_1	12.8	26.1	1.00
M_2	1.8	137.2	1.00
S_2	0.8	119.2	1.00

(Continued)

Table X-1 (Continued)

Constituent	Amplitude, cm	Phase, °G	Ampl. Mult. Factor
	Signal 6, GTM Long. 1, Global Grid Cell (31, 59)		
O_1	12.3	17.8	1.00
P_1	3.6	22.4	1.00
K_1	12.5	25.1	1.00
M_2	1.4	147.2	1.00
S_2	0.6	124.8	1.00
	Signal 7, GTM Long. 1, Global Grid Cell (42, 59)		
O_1	12.3	17.8	1.00
P_1	3.6	22.4	1.00
K_1	12.5	25.1	1.00
M_2	1.4	147.2	1.00
S_2	0.6	124.8	1.00
	Signal 8, GTM Long. 2, Global Grid Cell (57, 59)		
O_1	12.3	17.8	1.08
P_1	3.6	22.6	1.02
K_1	12.5	25.1	1.08
M_2	1.4	144.3	0.76
S_2	0.7	123.3	0.84
	Signal 9, GTM Long. 3, Global Grid Cell (73, 59)		
O_1	12.3	17.8	1.08
P_1	3.6	22.8	1.20
K_1	12.5	25.1	1.08
M_2	1.4	141.3	0.76
S_2	0.7	121.7	0.84
	Signal 10, GTM Long. 4, Global Grid Cell (87, 59)		
O_1	12.3	17.8	1.10
P_1	3.6	23.0	1.24
K_1	12.5	25.1	1.12
M_2	1.5	139.2	0.76
S_2	0.7	120.7	0.95

(Continued)

Table X-1 (Concluded)

Constituent	Amplitude, cm	Phase, °G	Ampl. Mult. Factor
	Signal 11, GTM Long. 5, Global Grid Cell (103, 59)		
O_1	12.3	17.9	1.10
P_1	3.6	23.2	1.24
K_1	12.5	25.1	1.12
M_2	1.5	137.5	0.76
S_2	0.7	119.9	0.95
	Signal 12, GTM Long. 6, Global Grid Cell (110, 59)		
O_1	12.3	17.9	1.15
P_1	3.6	23.4	1.19
K_1	12.5	25.2	1.12
M_2	1.6	136.2	0.72
S_2	0.7	119.4	1.00
	Signal 13, GTM Long. 7, Global Grid Cell (112, 59)		
O_1	12.3	17.9	1.15
P_1	3.6	23.6	1.19
K_1	12.5	25.2	1.12
M_2	1.6	133.5	0.72
S_2	0.7	119.4	1.00
	Signal 14, GTM Long. 8, Global Grid Cell (115, 58)		
O_1	12.3	18.0	1.15
P_1	3.6	23.8	1.19
K_1	12.5	25.2	1.12
M_2	1.7	135.2	0.72
S_2	0.7	119.7	1.00

123. All water surface elevations and velocity components were initialized to zero. A cubic polynomial feathering routine (Appendix C) was developed to smoothly transition the boundary elevations from zero to their reconstructed levels. The convective acceleration and eddy dispersion terms in the motion equations were set to zero on the solid and open boundaries of the global grid, thereby linearizing the motion equations at locations around the boundary. The same approach was employed around barriers. Subroutine ADVBAR (Appendix D) was developed in order to perform this task for the model user automatically.

124. During the calibration process, it was necessary to adjust the amplitudes of tidal constituents from the values tabulated in Table X-1. The GTM amplitudes were multiplied by the factors shown in the last column. Phases, as reported by the GTM, were used directly. In order to develop the appropriate amplitude multiplication factors, the harmonic analysis results obtained by Outlaw (1983) and those reported by Reid and Whitaker (1981) for the GTM were compared at the three deep sea pressure gages as shown in Table X-2. As can be observed, the Outlaw (1983) results were approximately 10-15 percent higher for the three major diurnal constituents. Pressure station 22 diurnal amplitude factors as reported in Table X-2 were used to modify the diurnal constituents of signals 8 and 9 in Table X-1. Pressure station 23 diurnal amplitude factors of Table X-2 were used to modify the diurnal constituents of signals 10 and 11 in Table X-1, while diurnal factors in Table X-2 for pressure station 24 were used to modify the diurnal constituents of signals 1-4, and 12-14 in Table X-1. Since simulation results employing the GTM results at the boundary are compared with the tide reconstructed from the O_1, K_1, P_1, M_2, and S_2 constituents given by Outlaw (1983) in Tables III-2 and III-3, the use of the multiplication factors to make the GTM results consistent with Outlaw's (1983) results is warranted.

125. Initial attempts at employing this same procedure for the semidiurnal factors resulted in simulated tide exceeding reconstructed tides during the last 2 days of the 5-day (20-24 Sep 1980) calibration period, when the semidiurnal components were most important in determining the structure of the tide. In order to obtain the best fit between simulated and reconstructed tides during this period of the simulation, it was necessary to reduce the amplitudes of these constituents as shown in Table X-1 slightly below the levels reported by Reid and Whitaker (1981). The M_2 constituent was effectively reduced by 25 percent, while the S_2 component was essentially unchanged. In

Table X-2

Comparison of Outlaw (1983) Analysis and

Reid and Whitaker (1981) GTM Results

Constituent	Amplitude, ft			Phase, °G		
	Outlaw	Reid	Factor	Outlaw	Reid	Difference
			Deep Sea Pressure Station 22			
O_1	0.46	0.427	1.0785	299.1	295.36	3.7
K_1	0.47	0.436	1.0770	309.2	296.45	12.7
P_1	0.15	0.125	1.2029	305.3	294.65	10.6
M_2	0.09	0.059	1.5228	320.6	332.72	-12.1
S_2	0.05	0.030	1.6949	328.6	306.90	21.7
			Deep Sea Pressure Station 23			
O_1	0.46	0.420	1.0955	297.5	294.86	2.6
K_1	0.48	0.430	1.1168	308.1	295.75	12.3
P_1	0.15	0.121	1.2356	304.3	294.15	10.1
M_2	0.09	0.059	1.5228	312.0	328.22	-16.2
S_2	0.05	0.026	1.9084	321.9	302.90	19.0
			Deep Sea Pressure Station 24			
O_1	0.47	0.41	1.1463	296.4	294.86	1.5
K_1	0.47	0.420	1.1193	309.9	295.65	13.2
P_1	0.14	0.118	1.1854	300.5	295.25	5.2
M_2	0.09	0.062	1.4446	311.0	324.62	-13.6
S_2	0.06	0.026	2.2901	321.5	301.30	20.2

the immediate nearshore regions, the GTM results were used directly.

126. The depth versus Manning's n relationship shown in Table X-3 was calibrated. Simulation results employing the calibrated relationship are presented in Figures X-1 through X-11 for water surface elevations and in Figures X-12 through X-18 for u and v current components for 240 hr starting at 20 September hour 0000 CST. Results are presented from western to eastern Mississippi Sound. Simulated water surface elevations correspond more closely to predicted (reconstructed) values east of Gulfport. Although simulation results are acceptable in western Mississippi Sound, improvements could be made by including the effects of the Lake Pontchartrain system. The simulated depth averaged current components reveal the same structure, i.e., ebb and

Table X-3

Calibrated Depth Versus Manning's n Relationship

Category L	Depth Range, ft*		Manning's n Roughness Factor
	N_L	U_L	
1	0 -	5	0.022
2	5 -	10	0.021
3	10 -	20	0.020
4	20 -	25	0.019
5	25 -	30	0.018
6	30 -	35	0.017
7	35 -	40	0.016
8	40 -	50	0.015
9	50 -	100	0.014
10	100 -	200	0.013
11	200 -	500	0.012
12	500 -	1000	0.011
13	1000 -	5000	0.010

* If the cell water depth with respect to model datum is greater than or equal to N_L and less than U_L, the category L Manning's n value is assigned to that cell.

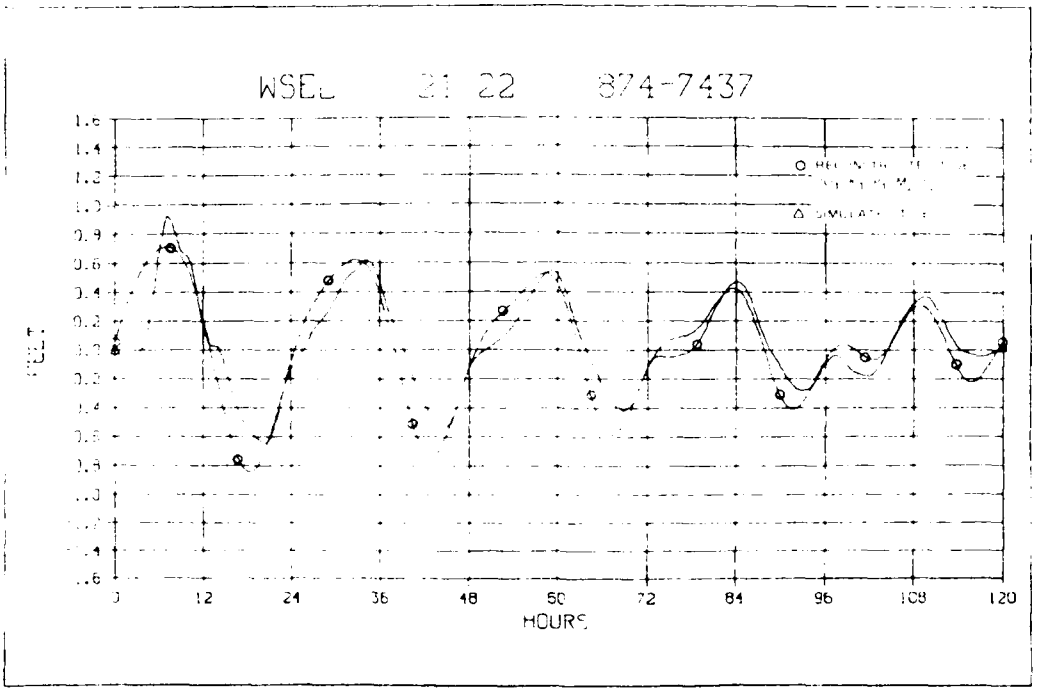

Figure X-1. Water surface elevations, simulated and predicted, at station 874-7437, 20-24 September 1980

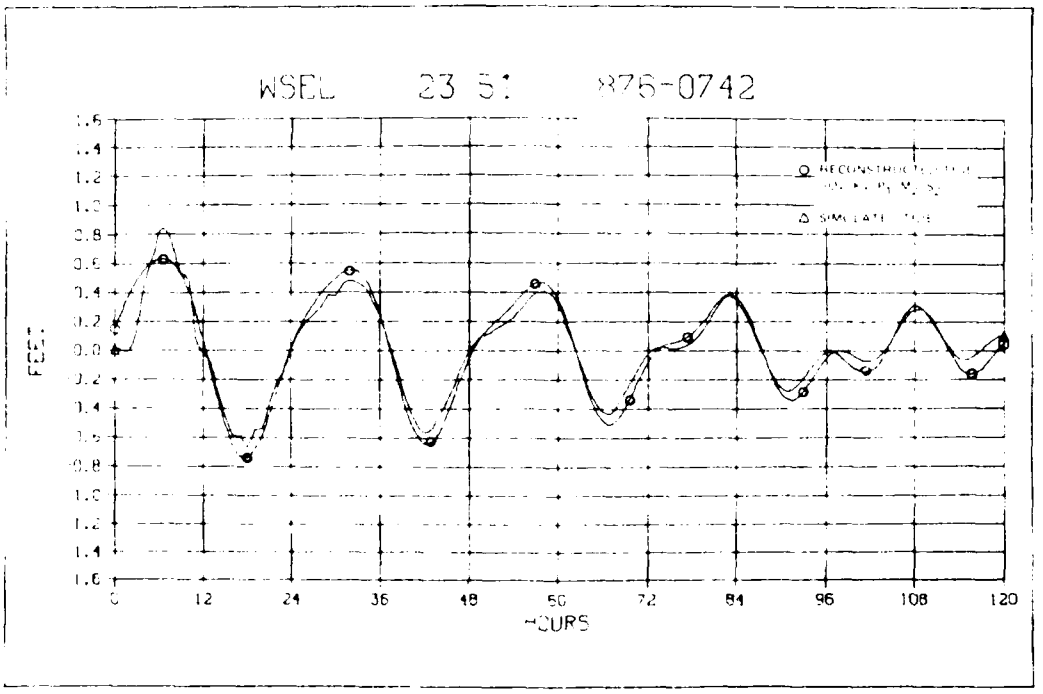

Figure X-2. Water surface elevations, simulated and predicted, at station 876-0742, 20-24 September 1980

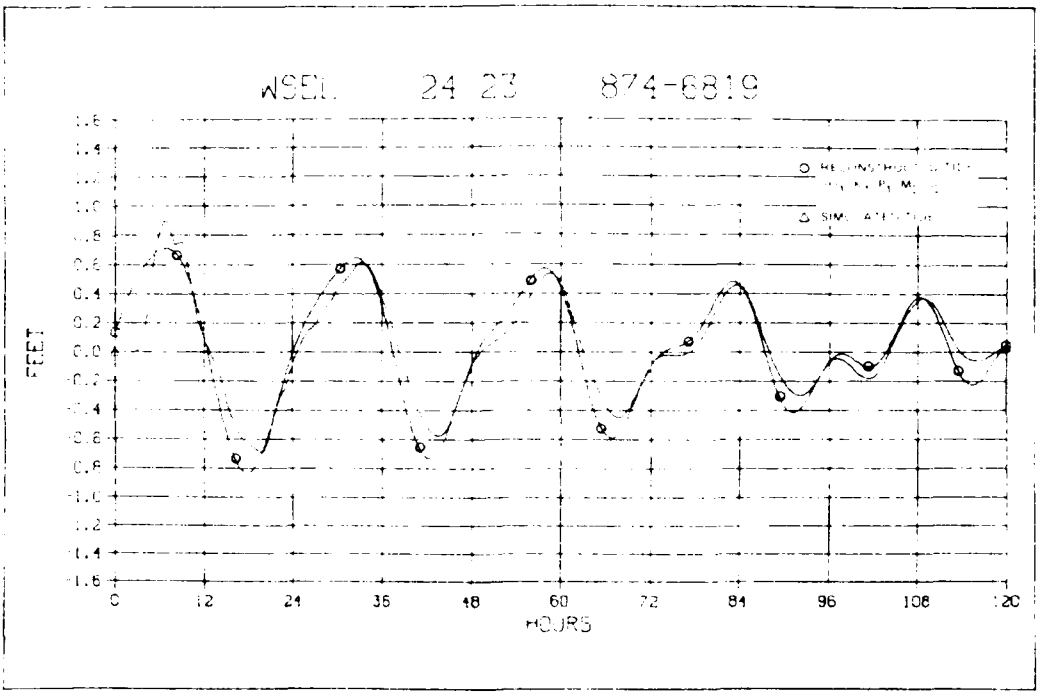

Figure X-3. Water surface elevations, simulated and predicted, at station 874-6819, 20-24 September 1980

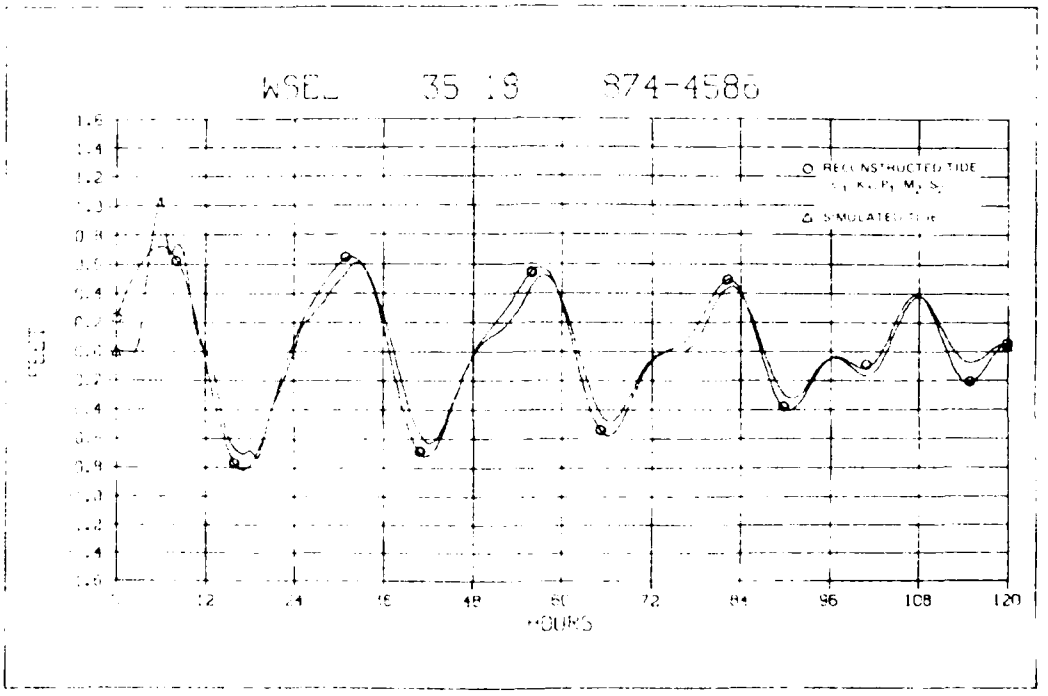

Figure X-4. Water surface elevations, simulated and predicted, at station 874-4586, 20-24 September 1980

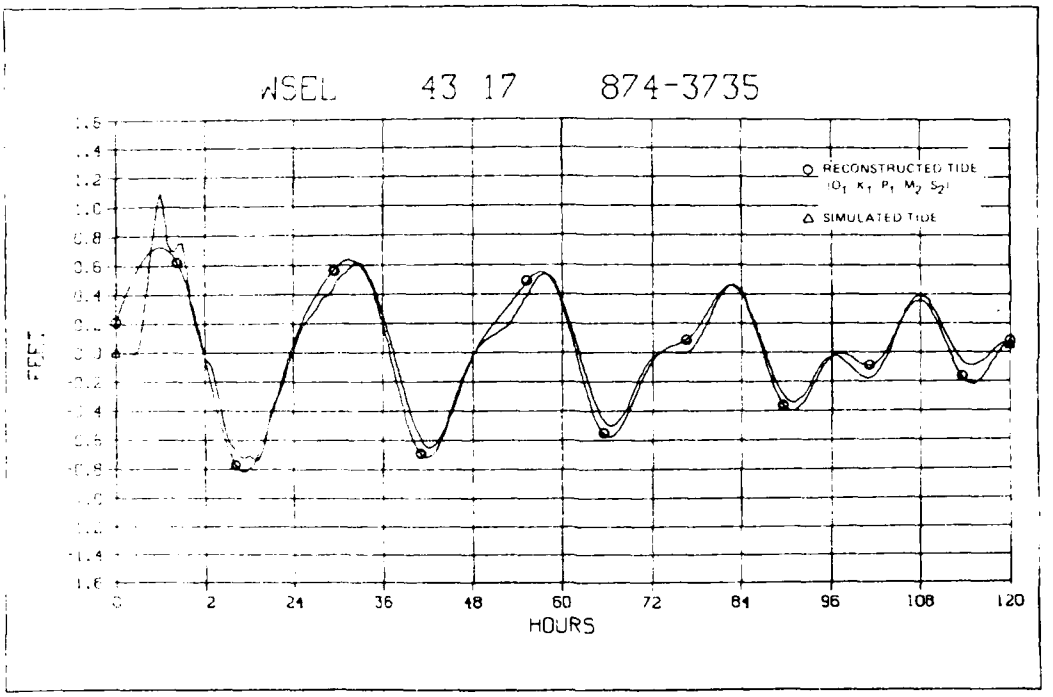

Figure X-5. Water surface elevations, simulated and predicted, at station 874-3735, 20-24 September 1980

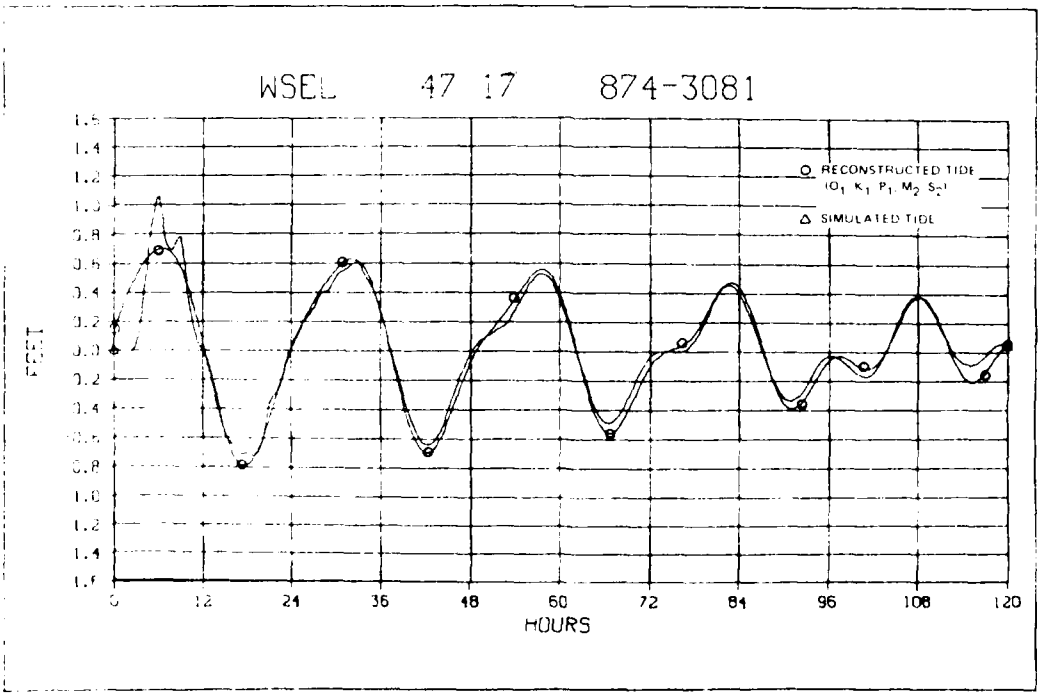

Figure X-6. Water surface elevations, simulated and predicted, at station 874-3081, 20-24 September 1980

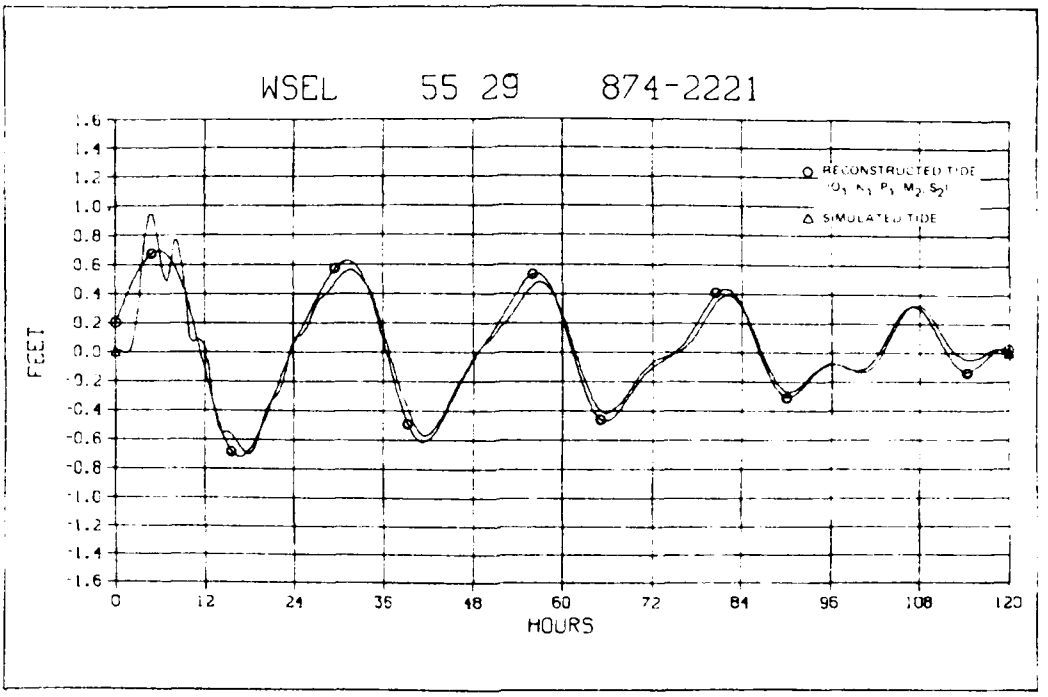

Figure X-7. Water surface elevations, simulated and predicted, at station 874-2221, 20-24 September 1980

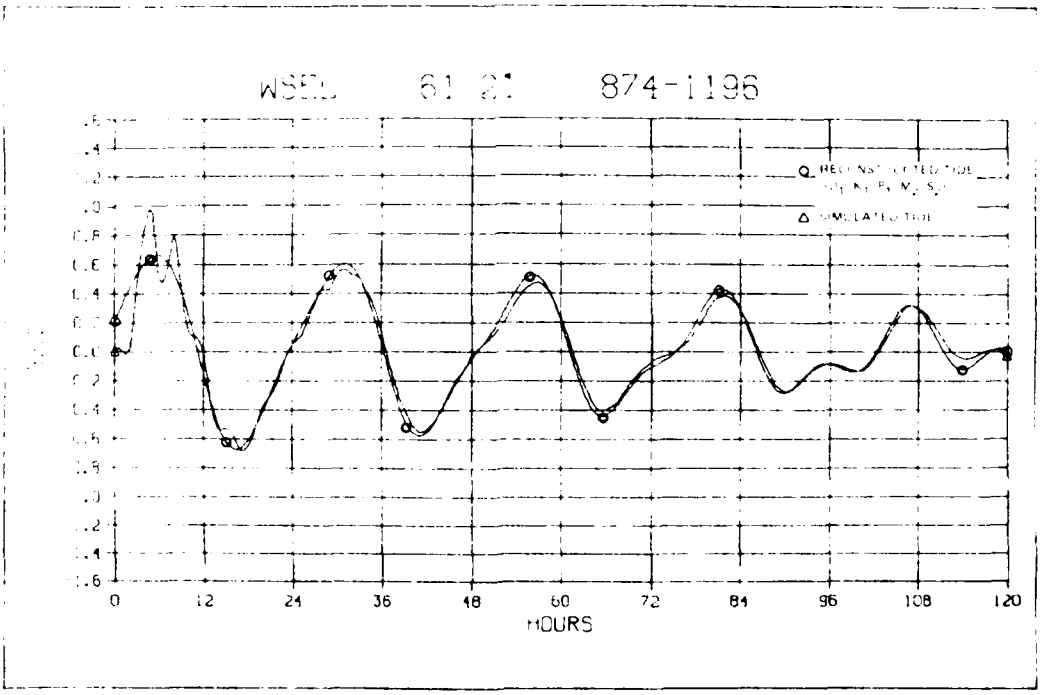

Figure X-8. Water surface elevations, simulated and predicted, at station 874-1196, 20-24 September 1980

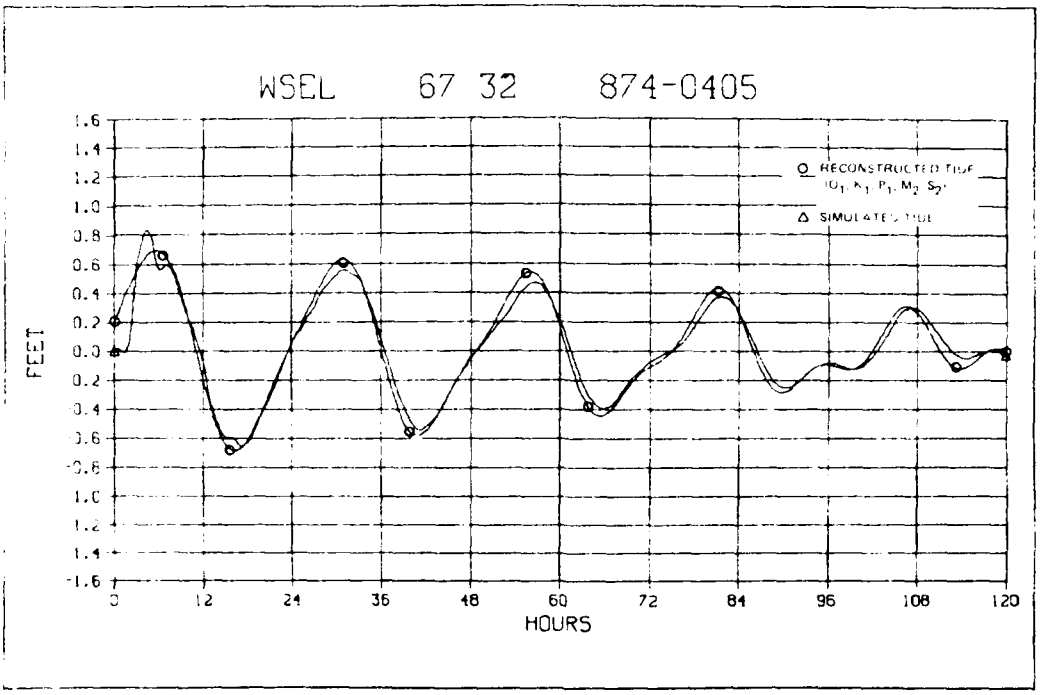

Figure X-9. Water surface elevations, simulated and predicted, at station 874-0405, 20-24 September 1980

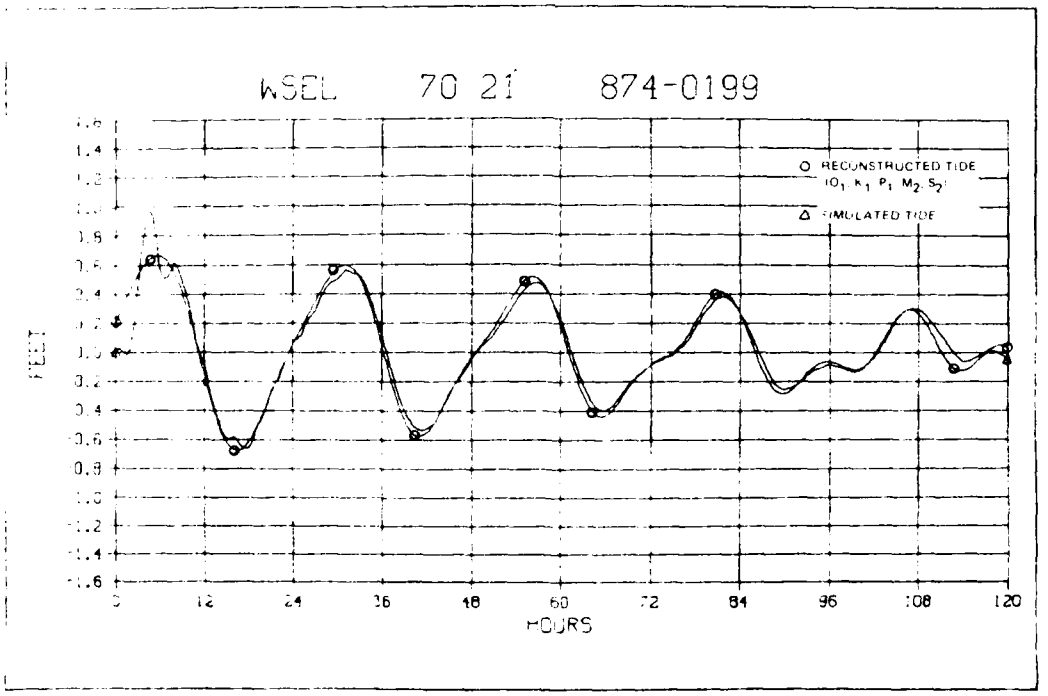

Figure X-10. Water surface elevations, simulated and predicted, at station 874-0199, 20-24 September 1980

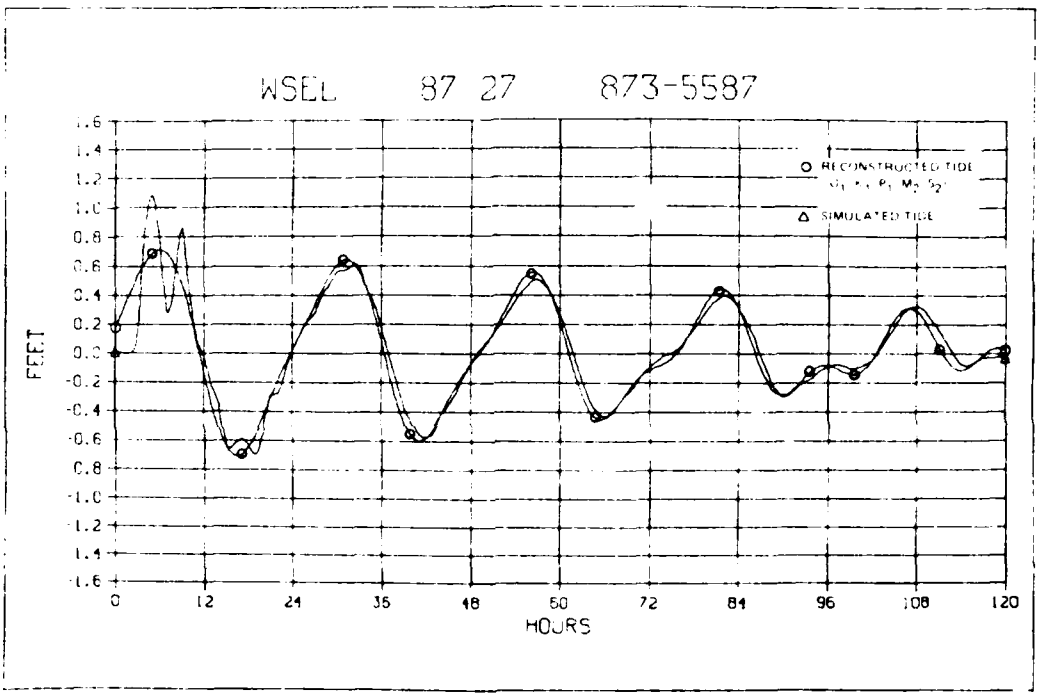

Figure X-11. Water surface elevations, simulated and predicted, at station 873-5587, 20-24 September 1980

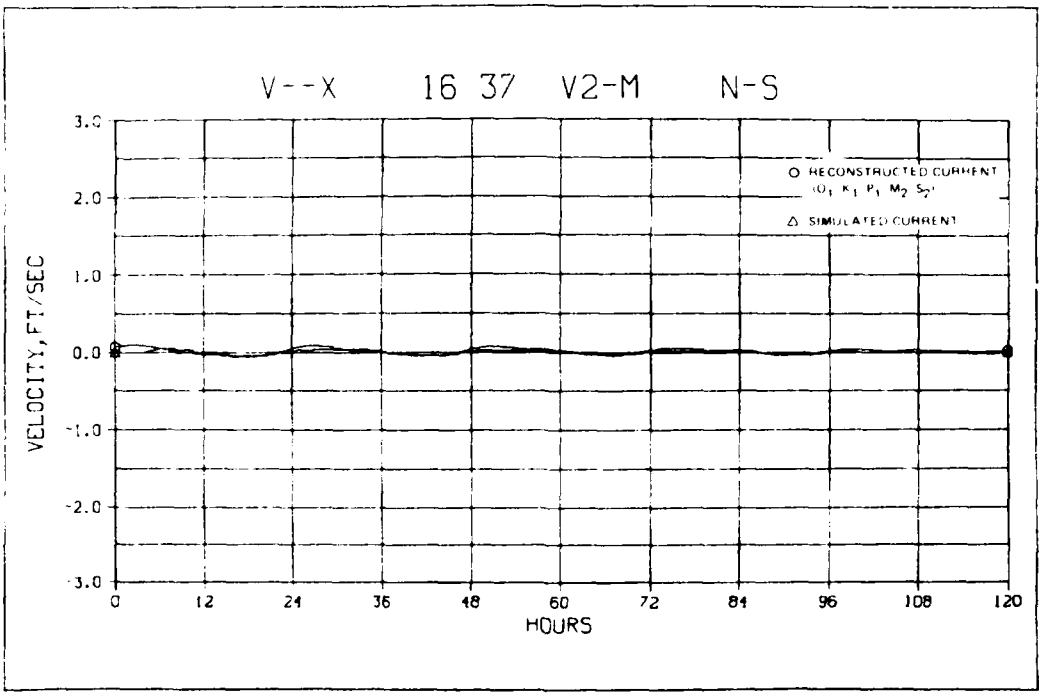

a. North-south

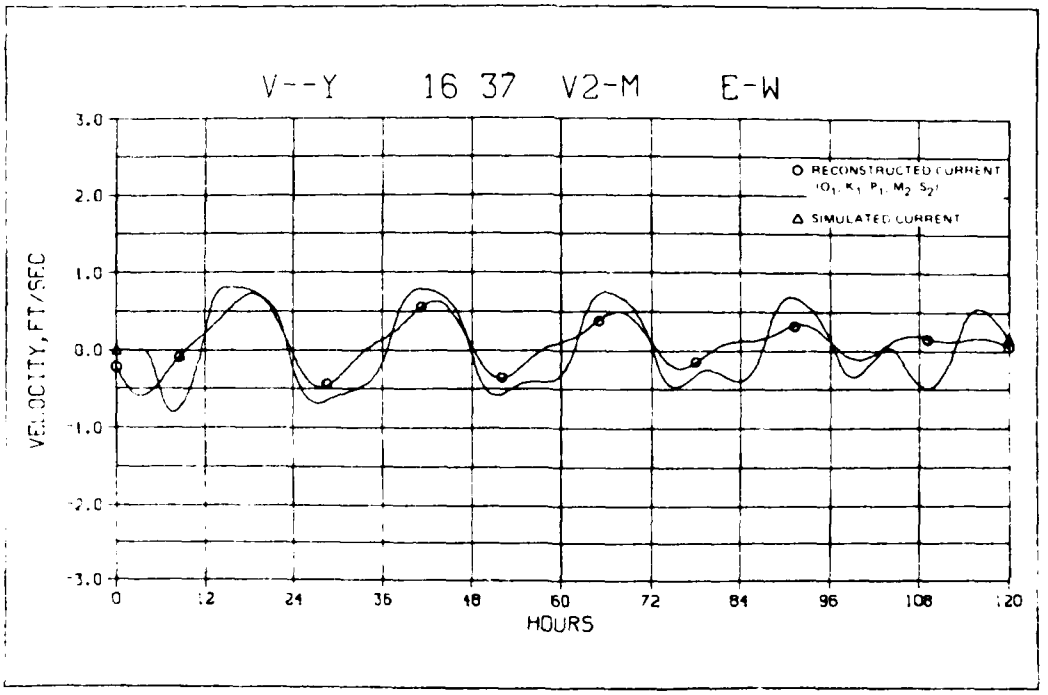

b. East-west

Figure X-12. Velocity components, simulated and predicted, at station V2-M, 20-24 September 1980

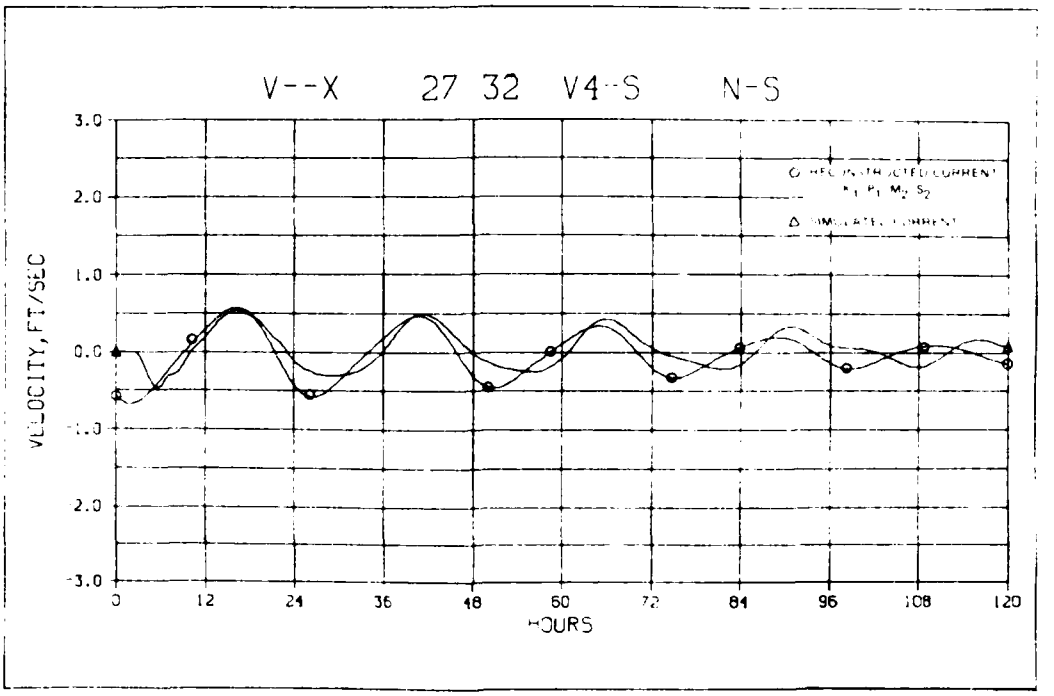

a. North-south

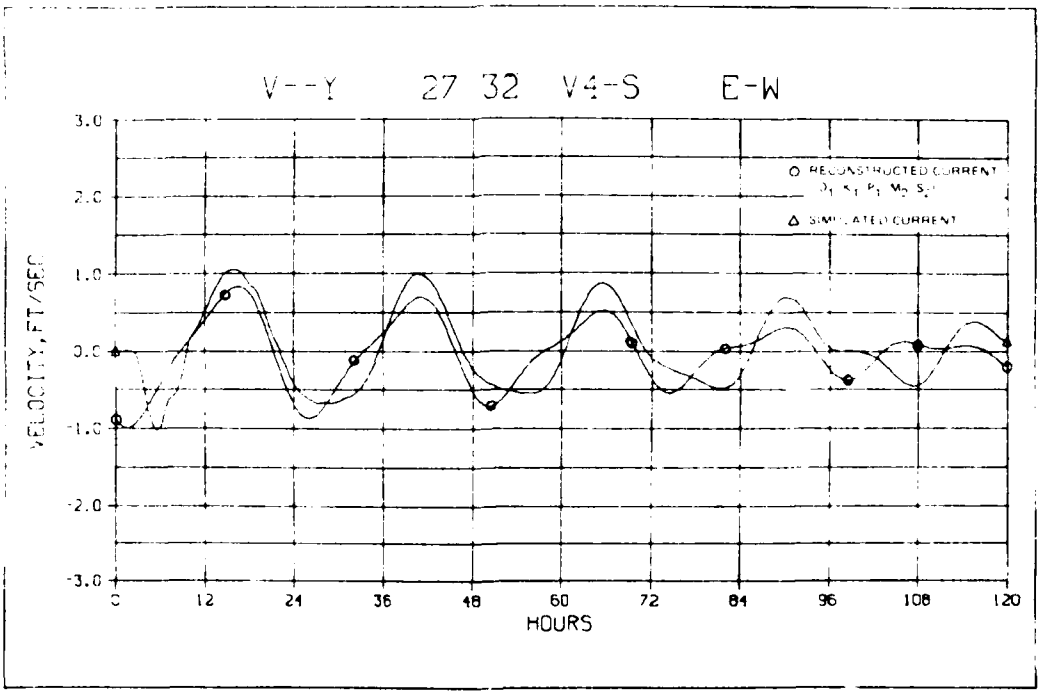

b. East-west

Figure X-13. Velocity components, simulated and predicted, at station V4-S, 20-24 September 1980

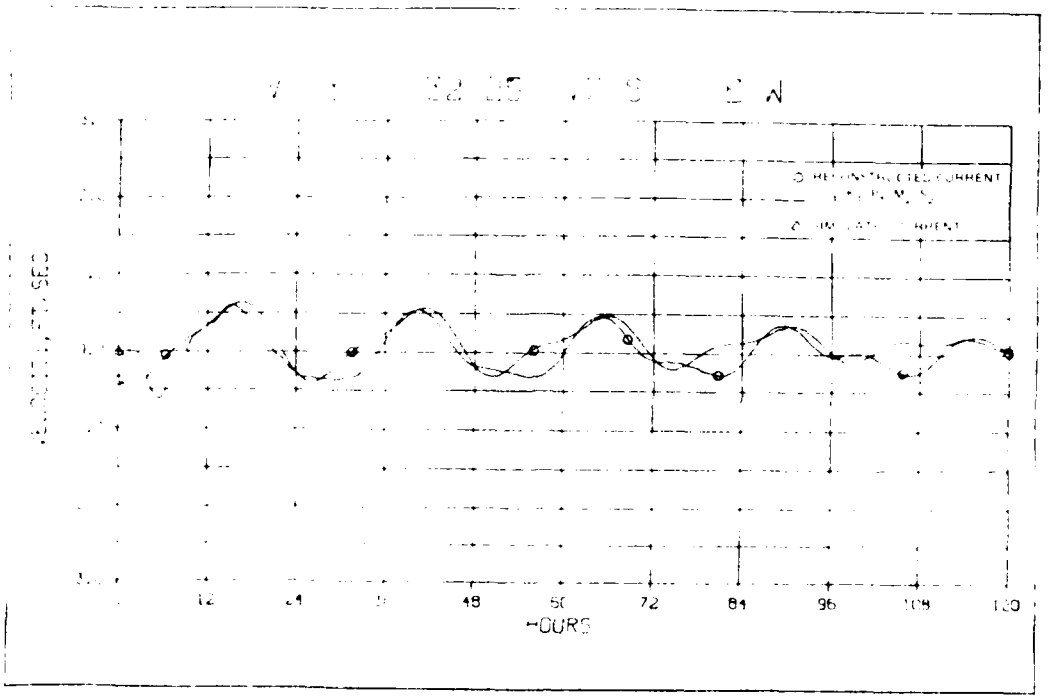

a. North-south

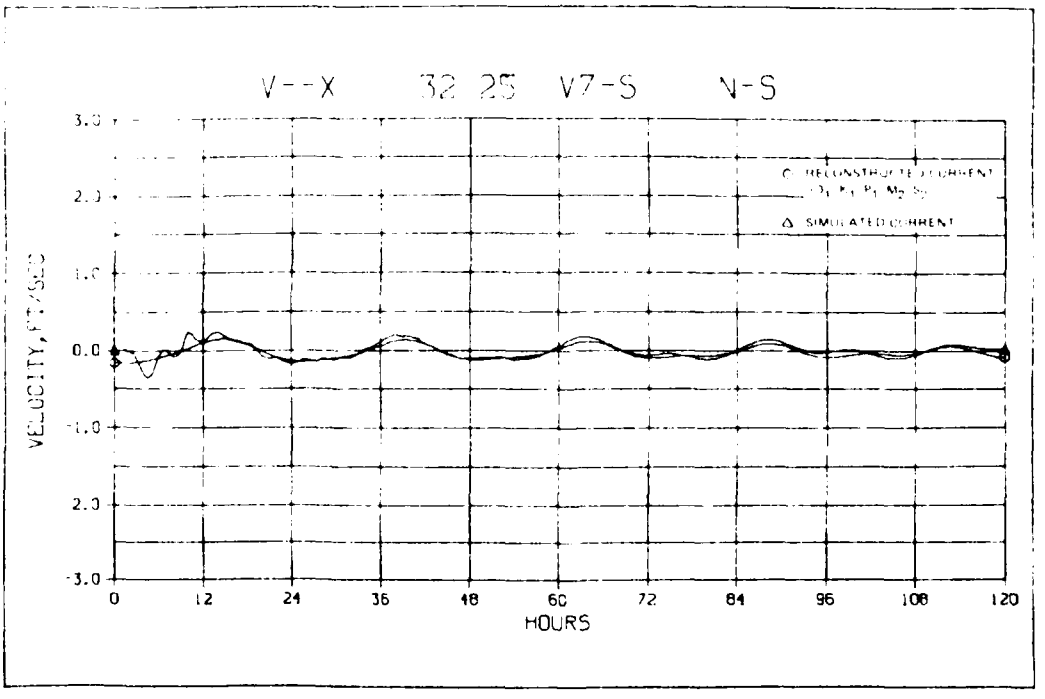

b. East-west

Figure X-14. Velocity components, simulated and predicted, at station V7-S, 20-24 September 1980

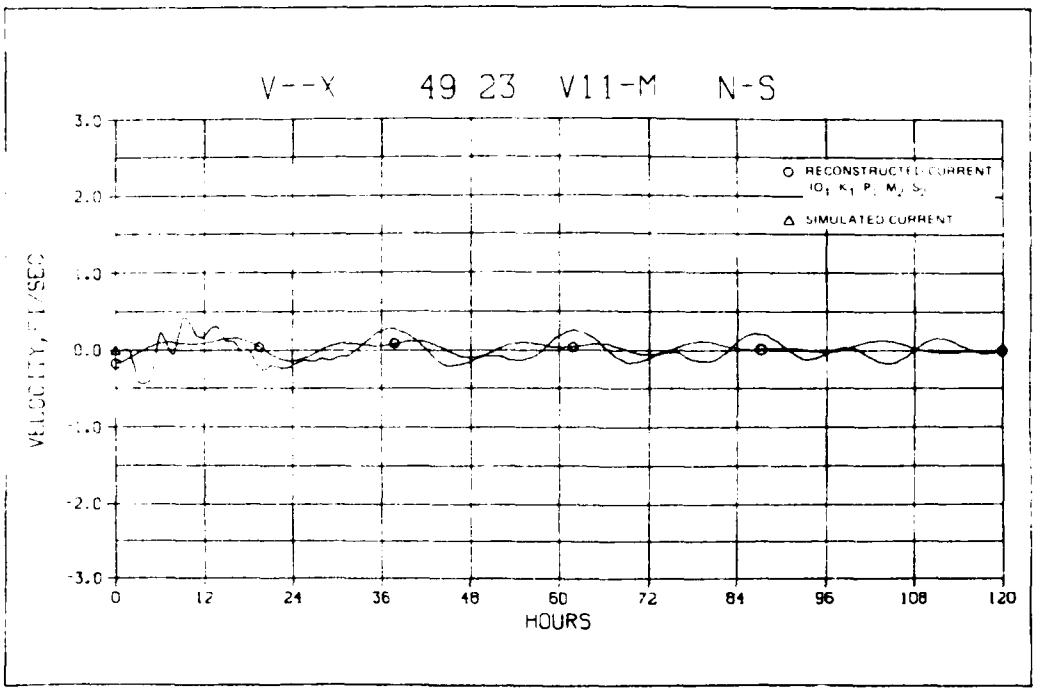

a. North-south

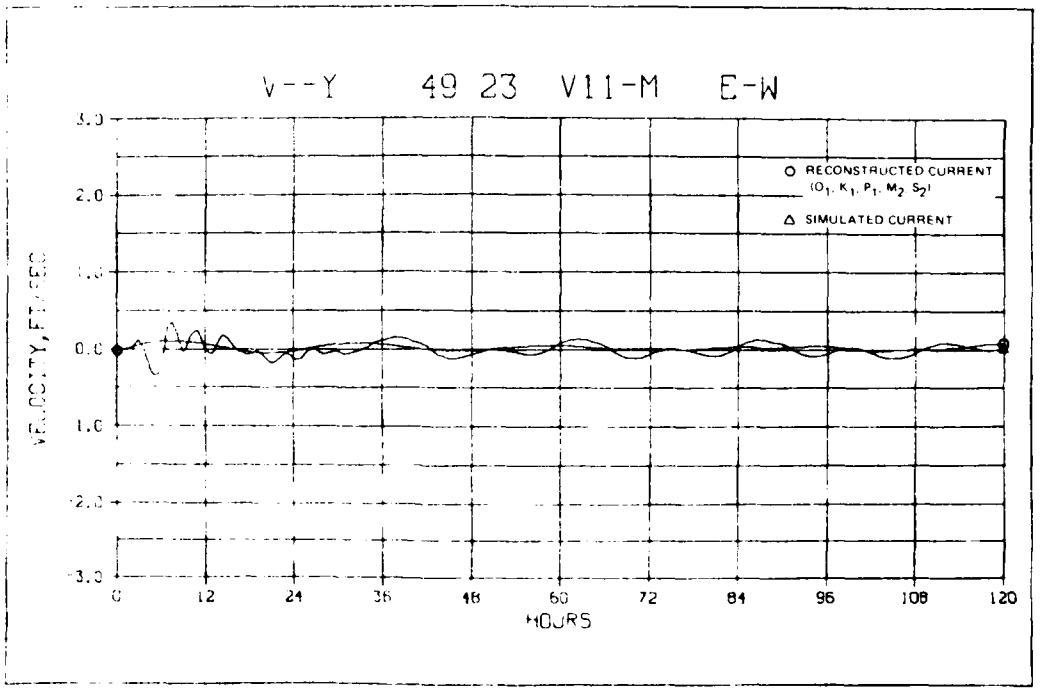

b. East-west

Figure X-15. Velocity components, simulated and predicted, at station V11-M, 20-24 September 1980

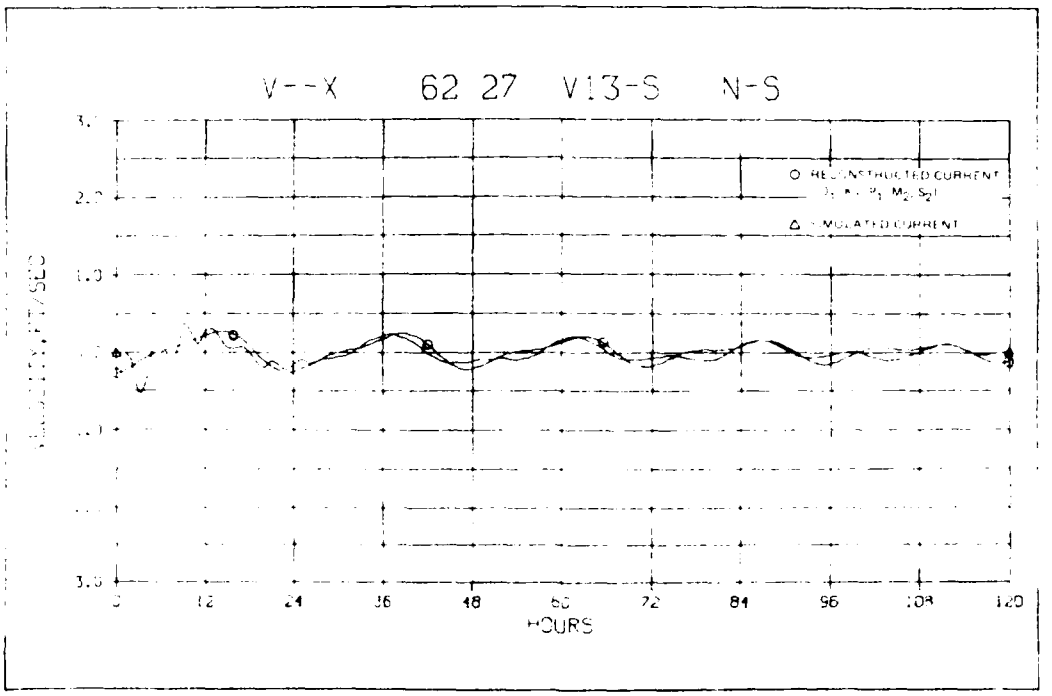

a. North-south

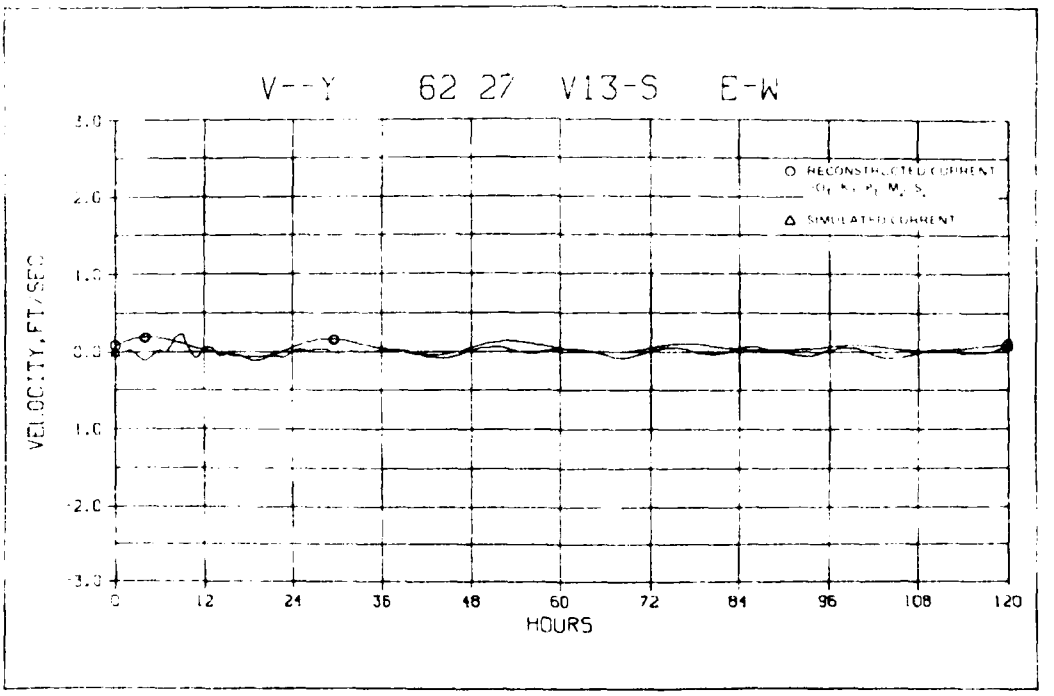

East-west

Figure X-16. Velocity components, simulated and predicted, at station V13-S, 20-24 September 1980

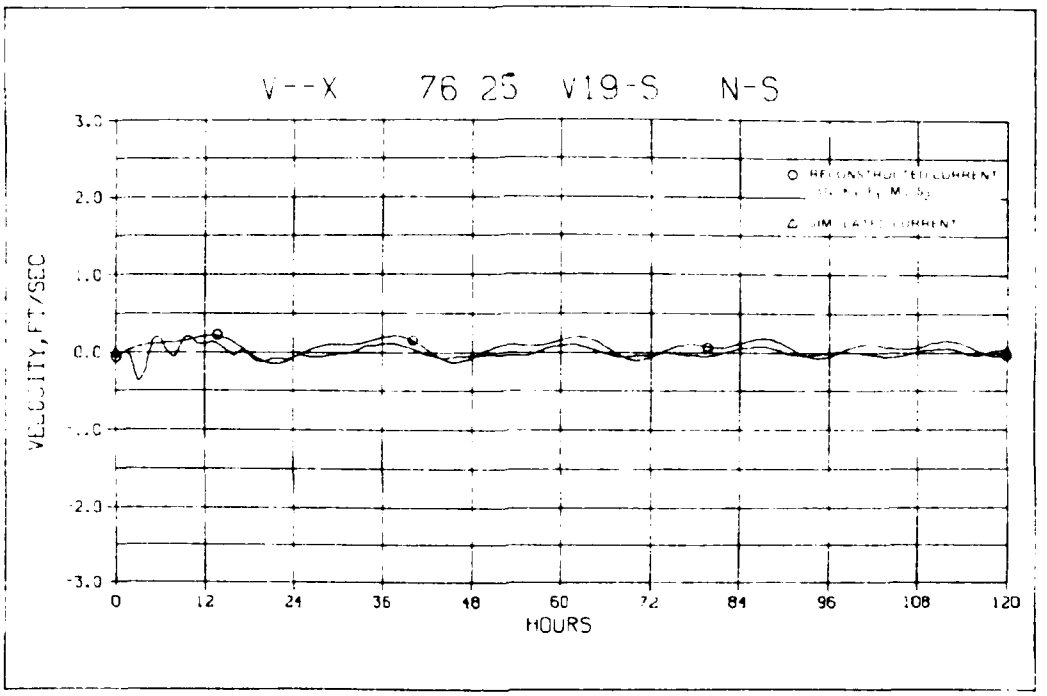

a. North-south

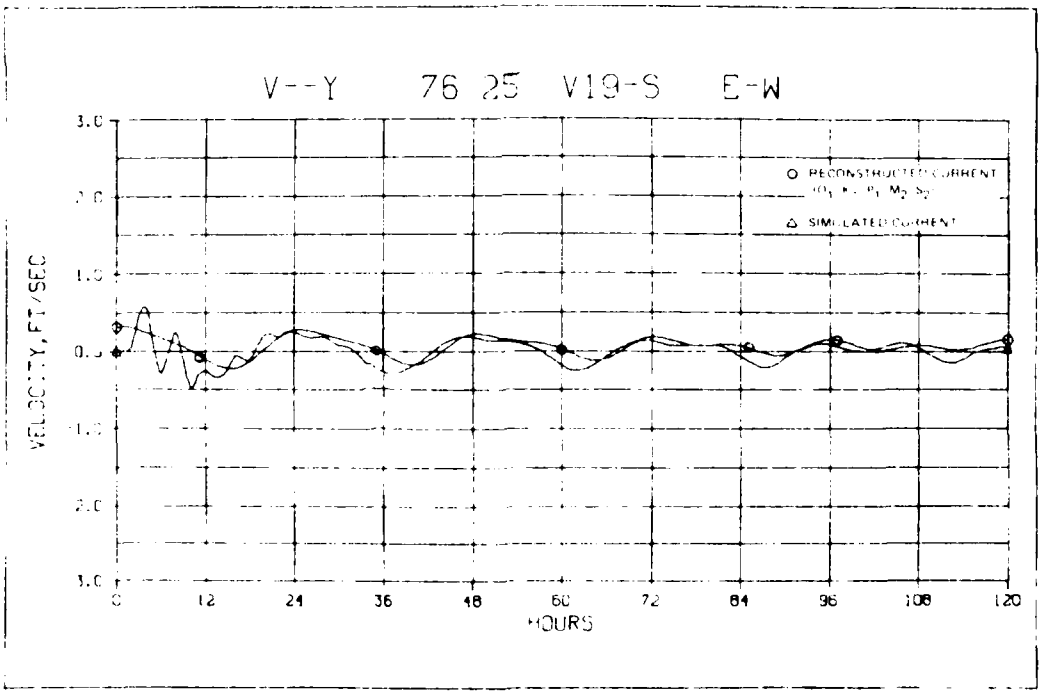

b. East-west

Figure X-17. Velocity components, simulated and predicted, at station V19-S, 20-24 September 1980

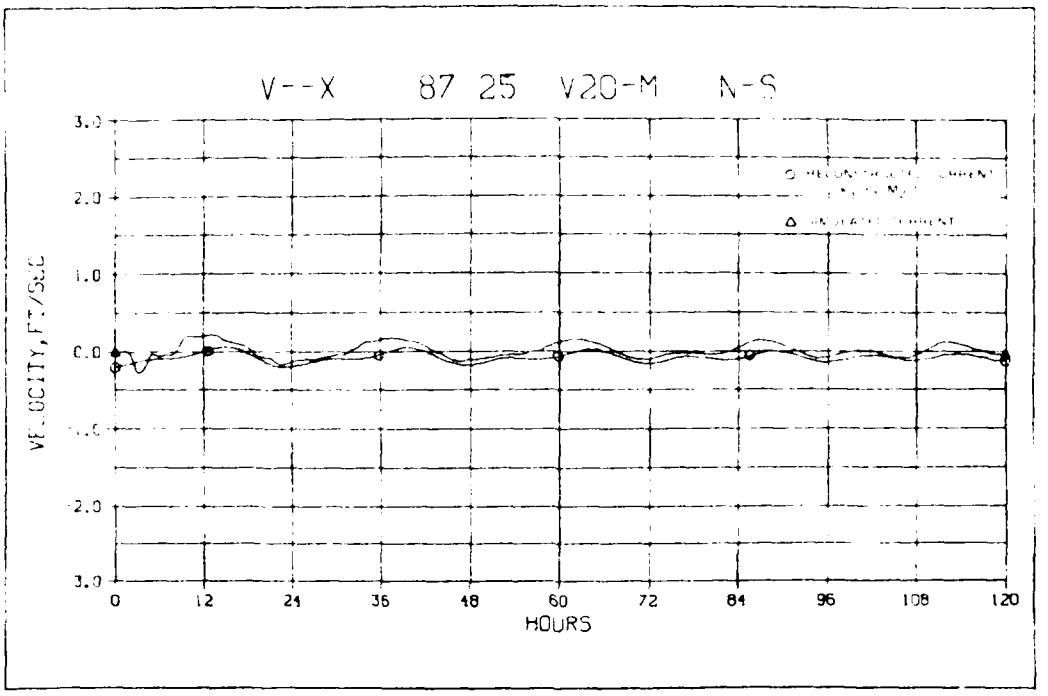

a. North-south

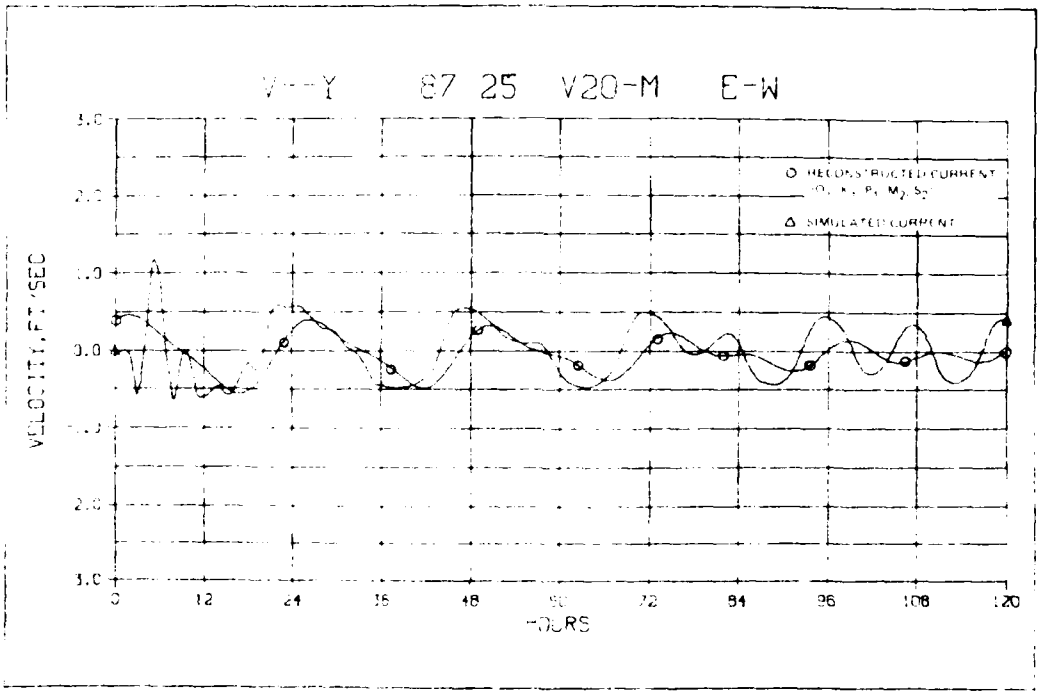

b. East-west

Figure X-18. Velocity components, simulated and predicted, at station V20-M, 20-24 September 1980

flood pattern, as the predicted (reconstructed) middepth velocity stations. Since the K_1 and P_1 tidal current components could not be separated and the calibration period is outside the period for which K_1 and P_1 was determined for all stations (refer to Table III-5), the middepth velocity station predicted (reconstructed) data should be interpreted only in terms of general structure.

127. In order to verify the adjustments to the GTM constituent amplitudes and the calibrated depth versus Manning's n relation, a second period 12-14 Jun 1980 was considered. During this time, the structure of the tide was determined by the three major diurnal constituents. Since the character of the tide remained relatively constant, only 3 days were simulated. Initially all water surface elevations and current components were set to zero. After the first day, simulated levels corresponded quite favorably to predicted levels. Plots of simulated versus predicted (reconstructed) water surface elevations are shown in Figures X-19 through X-29 for the 72-hr period starting 12 June hour 0000 CST. The simulated depth averaged currents are compared with predicted (reconstructed) middepth values in Figures X-30 through X-36. Simulated water surface elevations correspond more closely to predicted (reconstructed) values east of Gulfport, as in the case of the calibration period.

Summary of calibration and verification

128. The calibration and verification periods comprise two different tidal regimes. During the calibration period, the character of the tide is changing from daily to semidaily and the range is less than 1.2 ft (neap tide). During this period the semidiurnal tidal components dominate. During the verification period, the character of the tide is relatively constant and is daily with a range greater than 1.9 ft (spring tide). During this period the diurnal tidal components dominate.

129. Since the simulated tidal levels correspond well to the predicted (reconstructed) results, the model may be confidently used to predict tidal elevations and currents over the complete tidal (lunar) cycle.

Hypothetical Sand Island Regional Dredge Material Disposal Site

130. Consider a hypothetical regional dredge material disposal site in the vicinity of Sand Island. The water depths with respect to local mean sea

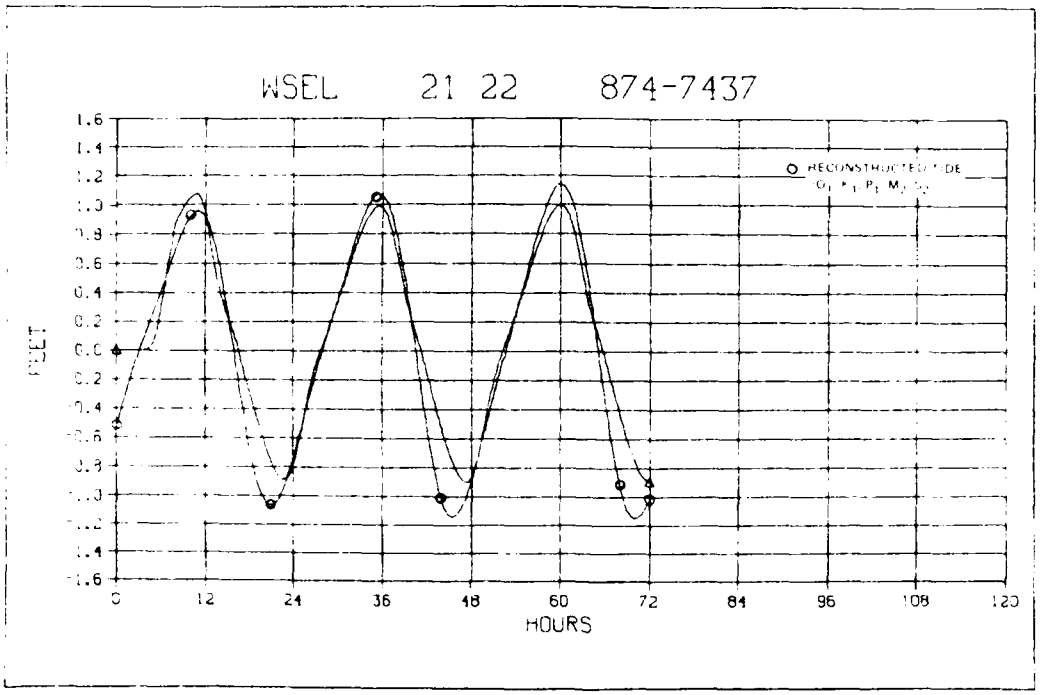

Figure X-19. Water surface elevations, simulated and predicted, at station 874-7437, 12-14 June 1980

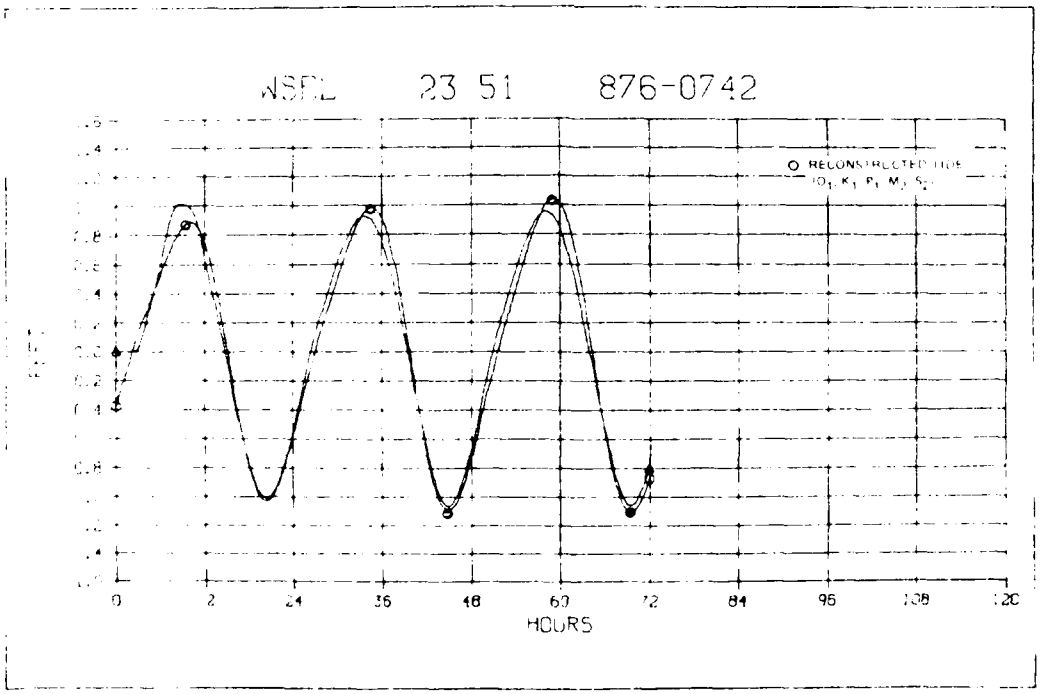

Figure X-20. Water surface elevations, simulated and predicted, at station 876-0742, 12-14 June 1980

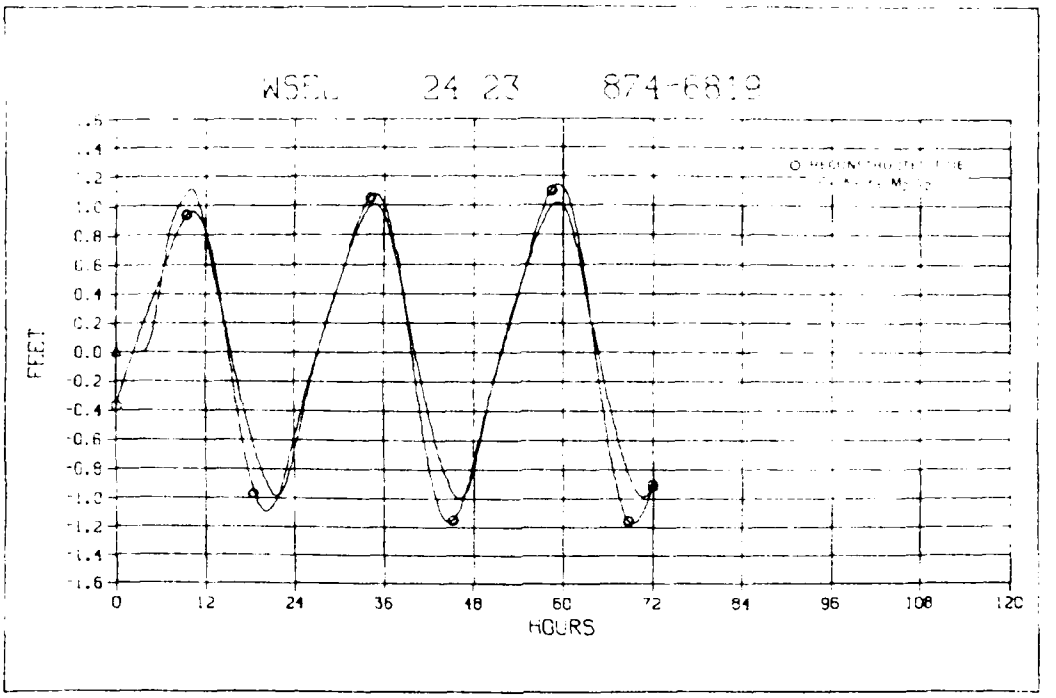

Figure X-21. Water surface elevations, simulated and predicted, at station 874-6819, 12-14 June 1980

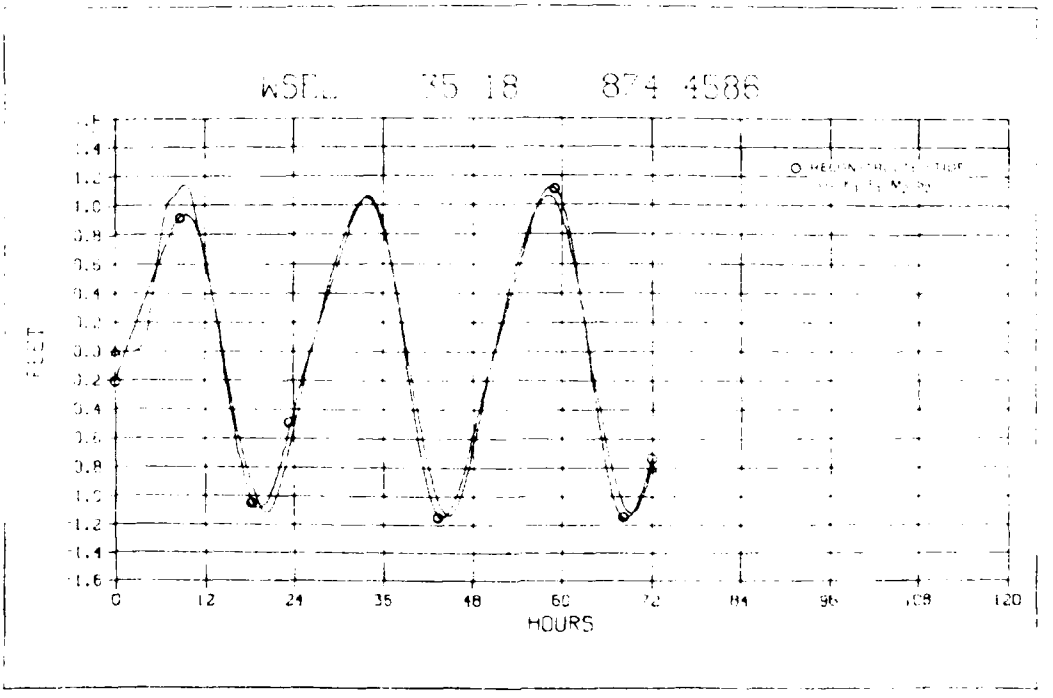

Figure X-22. Water surface elevations, simulated and predicted, at station 874-4586, 12-14 June 1980

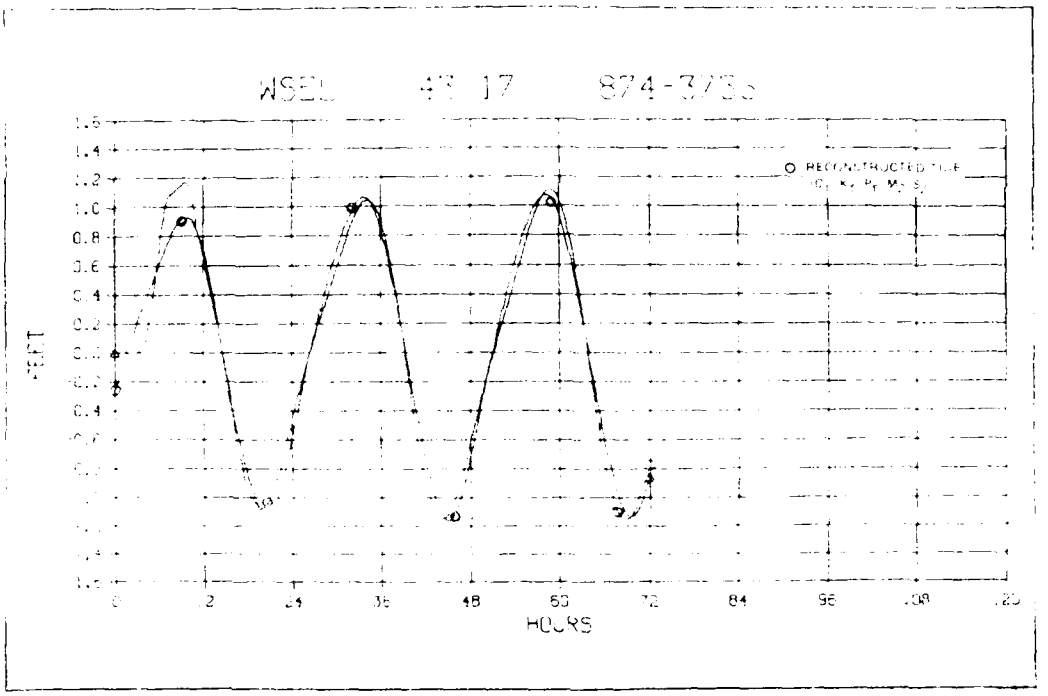

Figure X-23. Water surface elevations, simulated and predicted, at station 874-3735, 12-14 June 1980

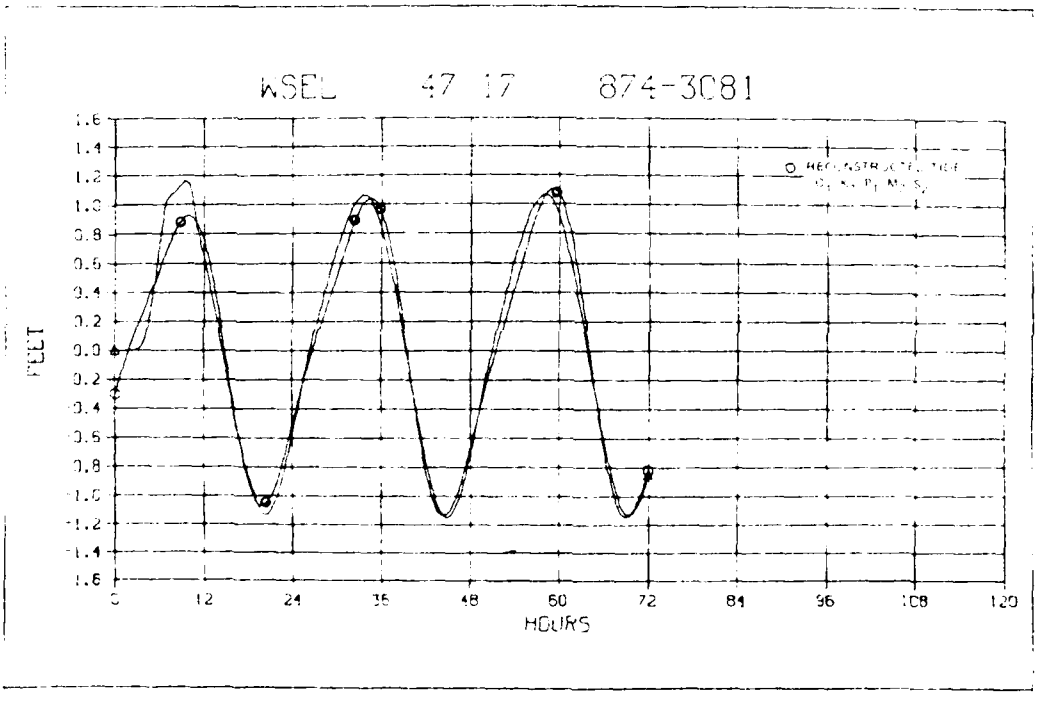

Figure X-24. Water surface elevations, simulated and predicted, at station 874-3081, 12-14 June 1980

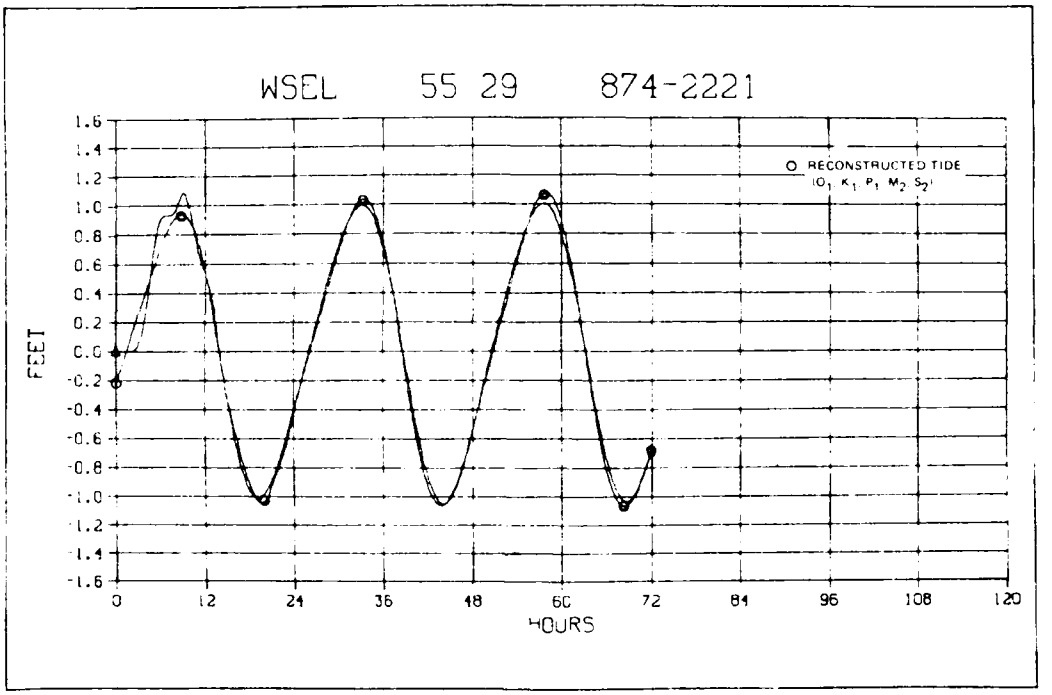

Figure X-25. Water surface elevations, simulated and predicted, at station 874-2221, 12-14 June 1980

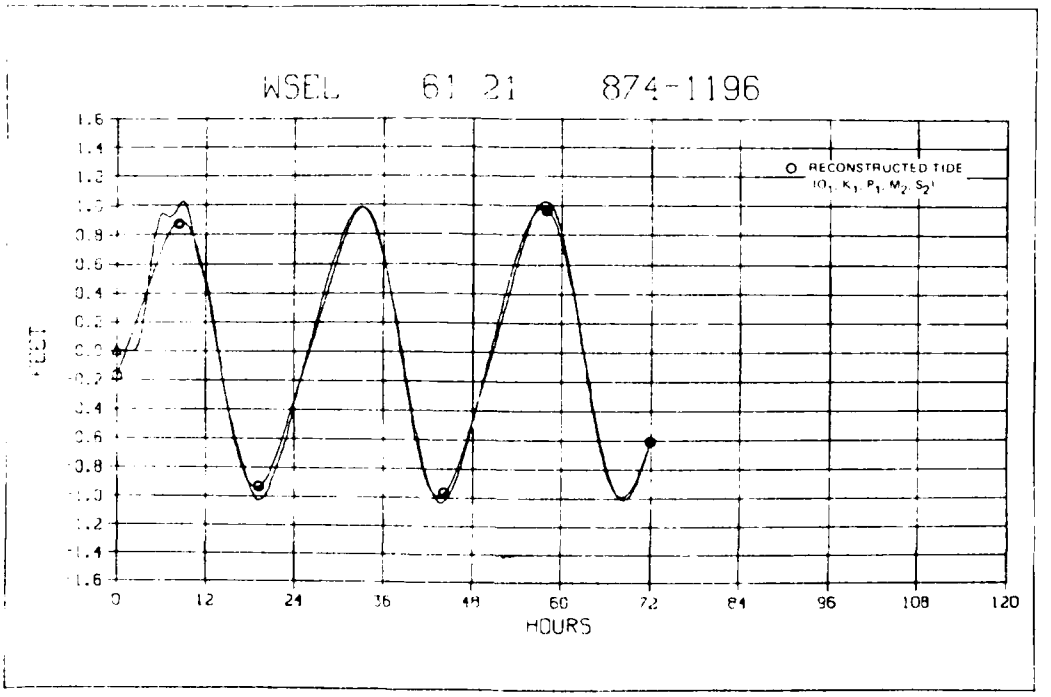

Figure X-26. Water surface elevations, simulated and predicted, at station 874-1196, 12-14 June 1980

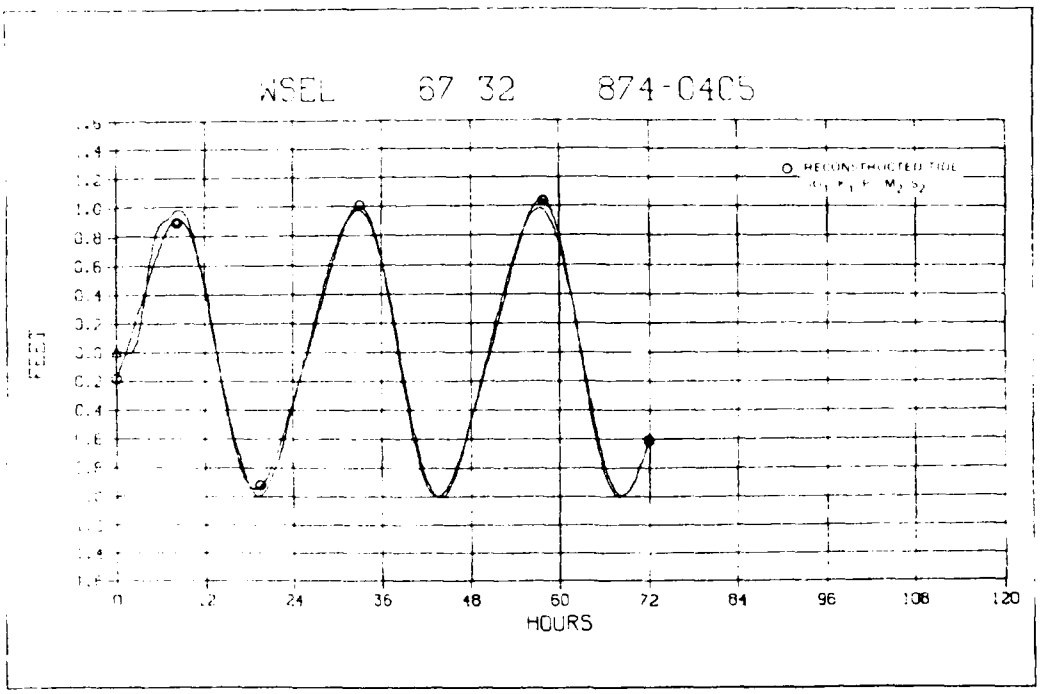

Figure X-27. Water surface elevations, simulated and predicted, at station 874-0405, 12-14 June 1980

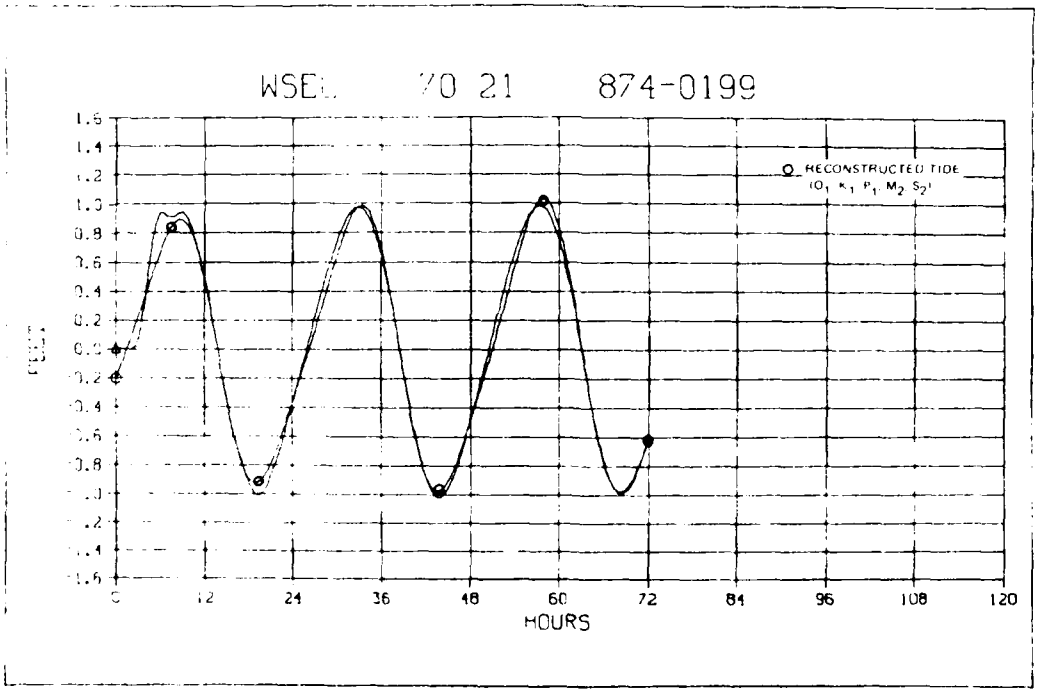

Figure X-28. Water surface elevations, simulated and predicted, at station 874-0199, 12-14 June 1980

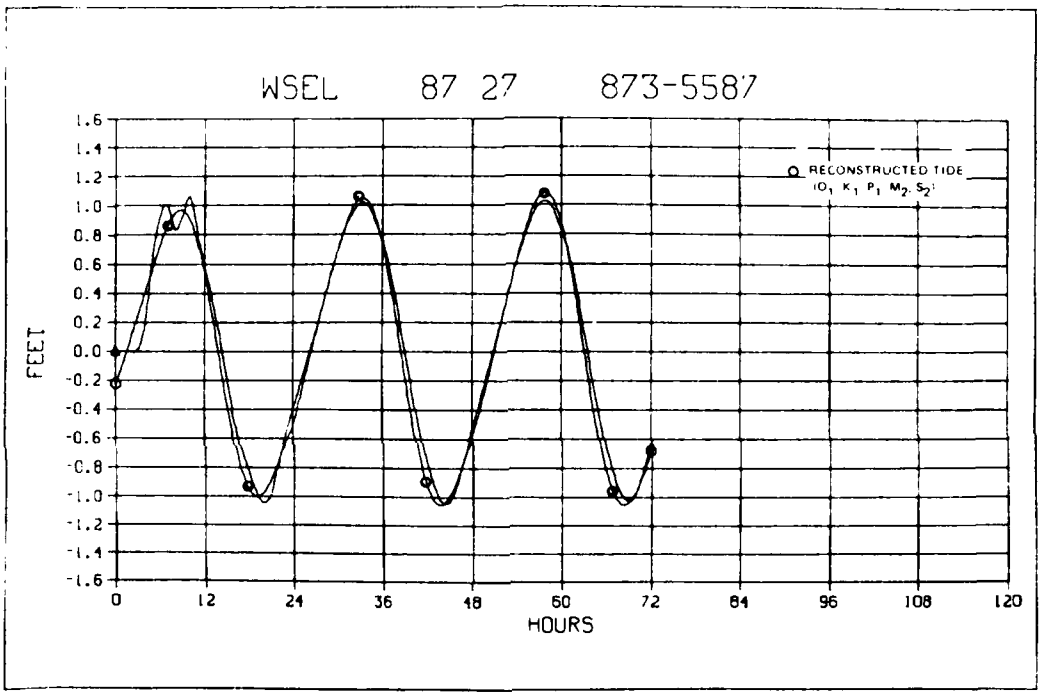

Figure X-29. Water surface elevations, simulated and predicted, at station 873-5587, 12-14 June 1980

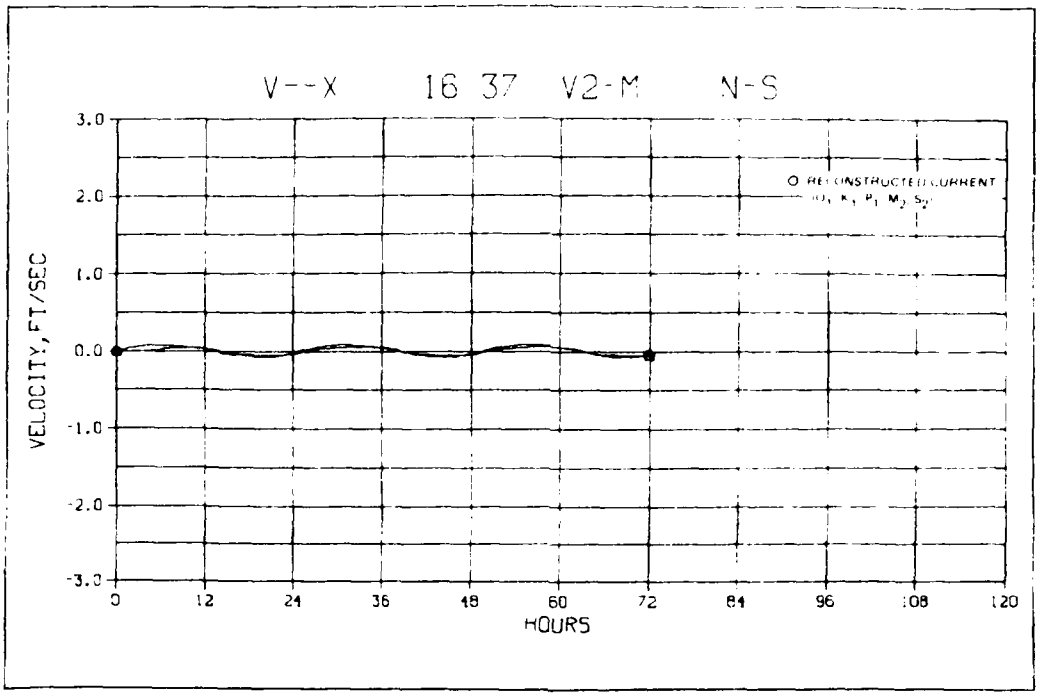

a. North-south

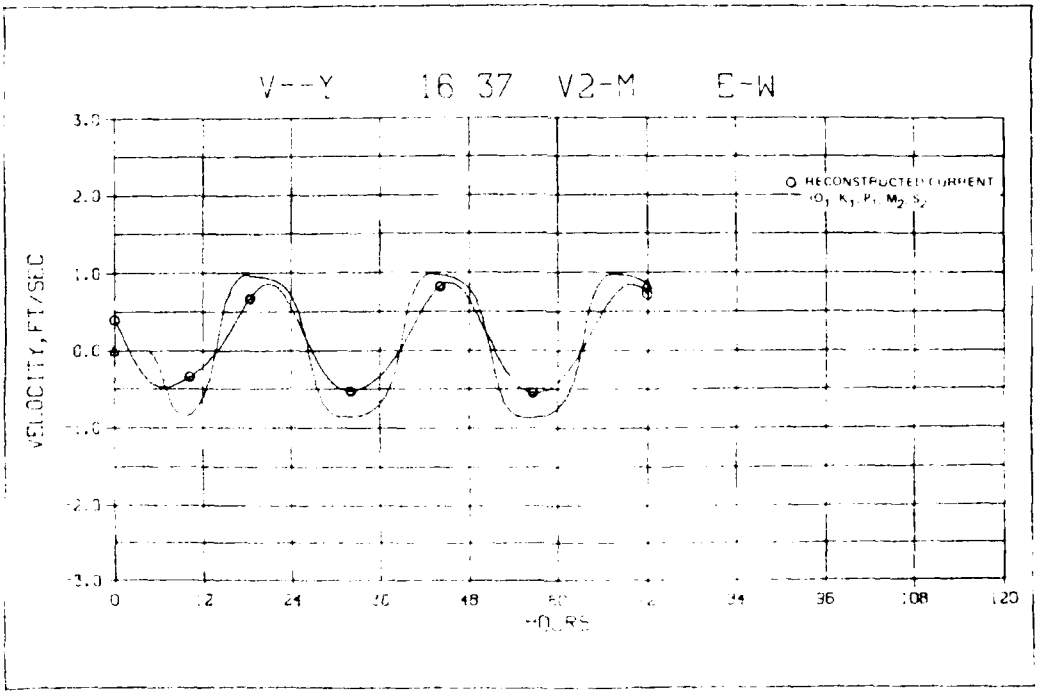

b. East-west

Figure X-30. Velocity components, simulated and predicted, at station V2-M, 20-24 September 1980

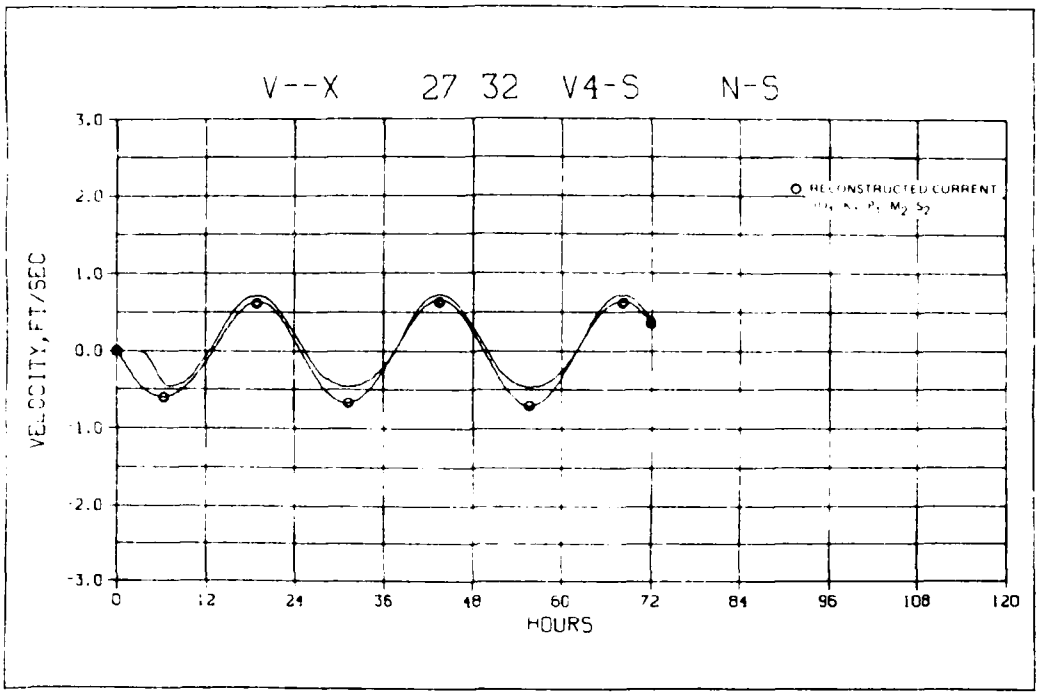

a. North-south

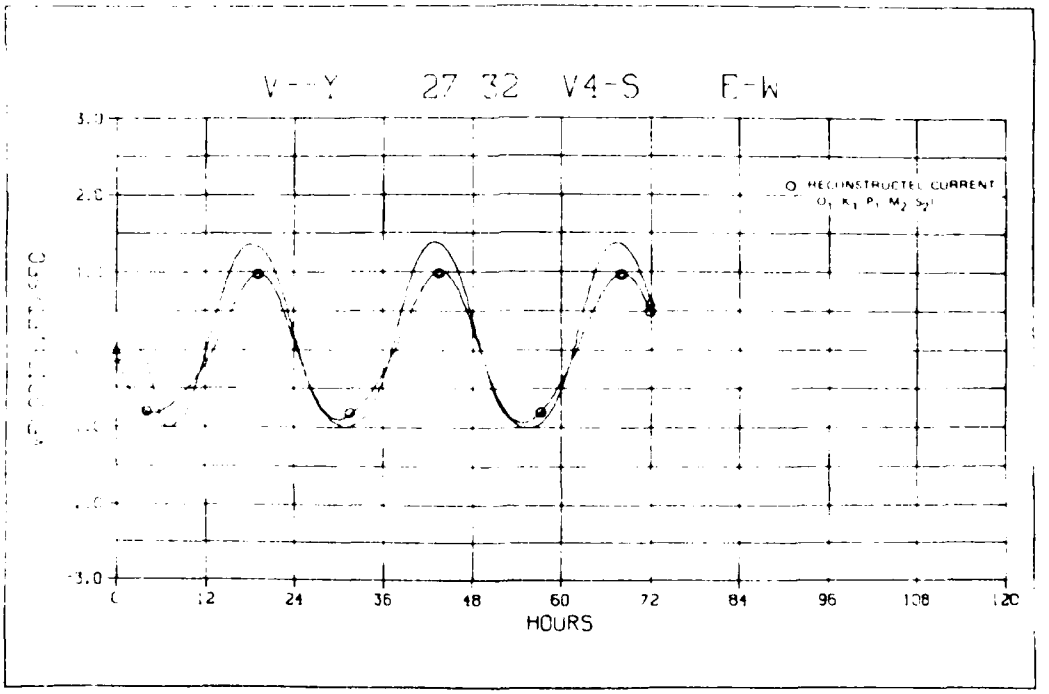

b. East-west

Figure X-31. Velocity components, simulated and predicted, at station V4-S, 20-24 September 1980

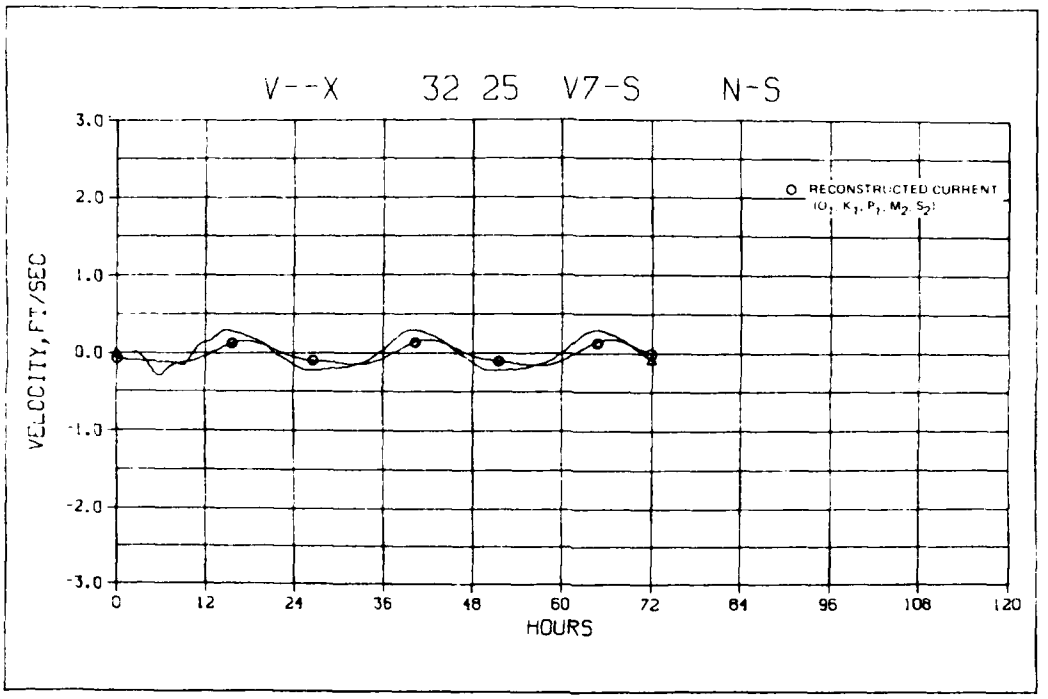

a. North-south

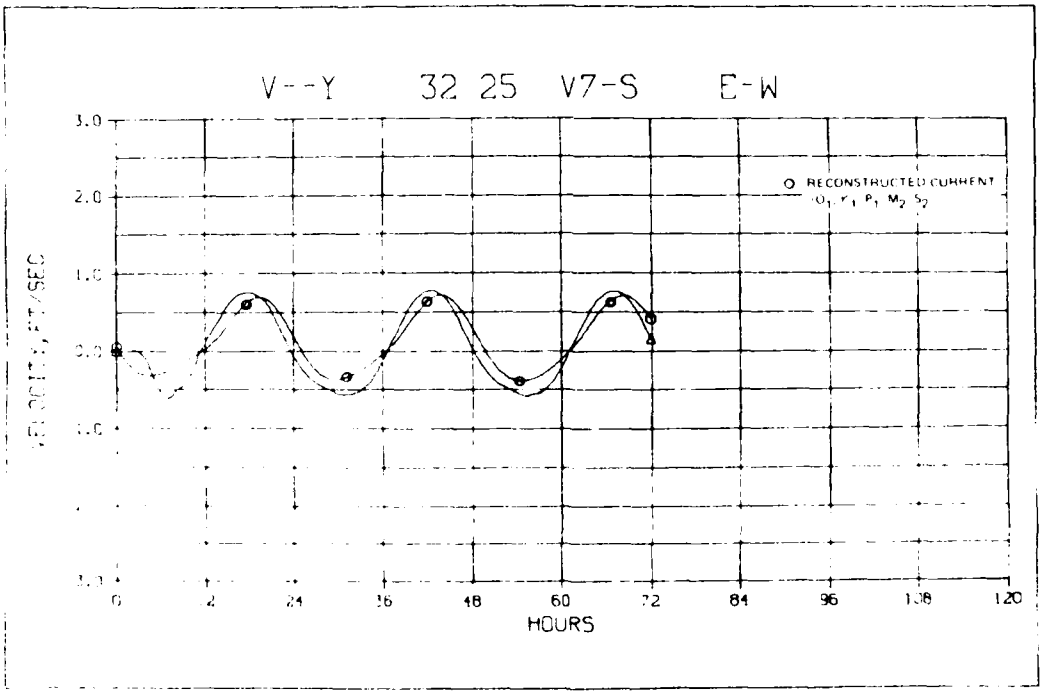

b. East-west

Figure X-32. Velocity components, simulated and predicted, at station V7-S, 20-24 September 1980

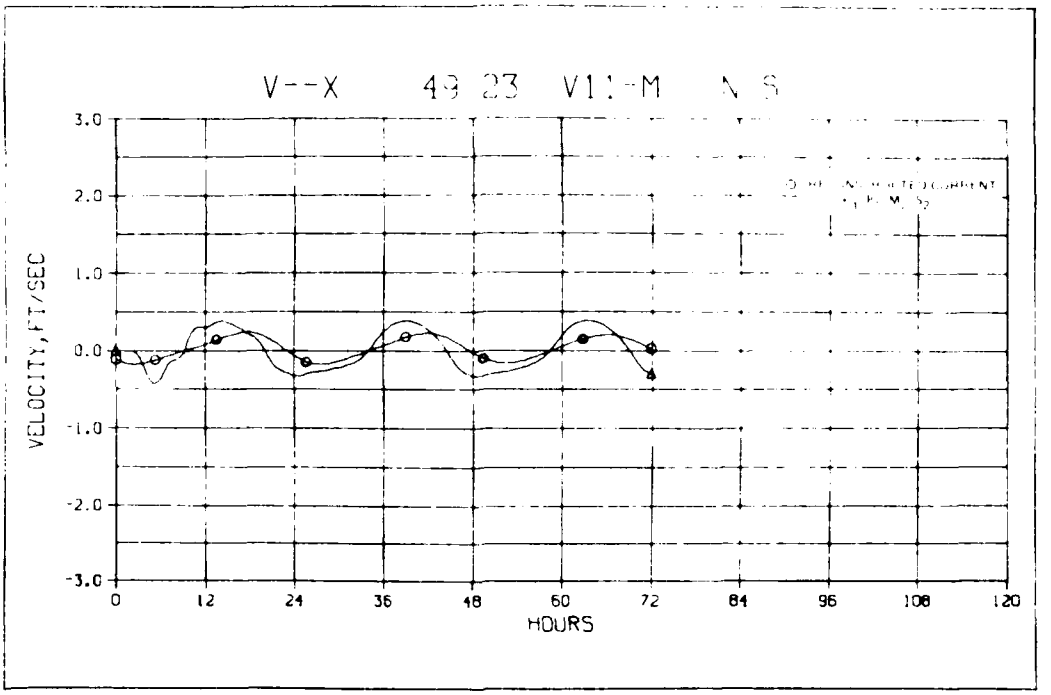

a. North-south

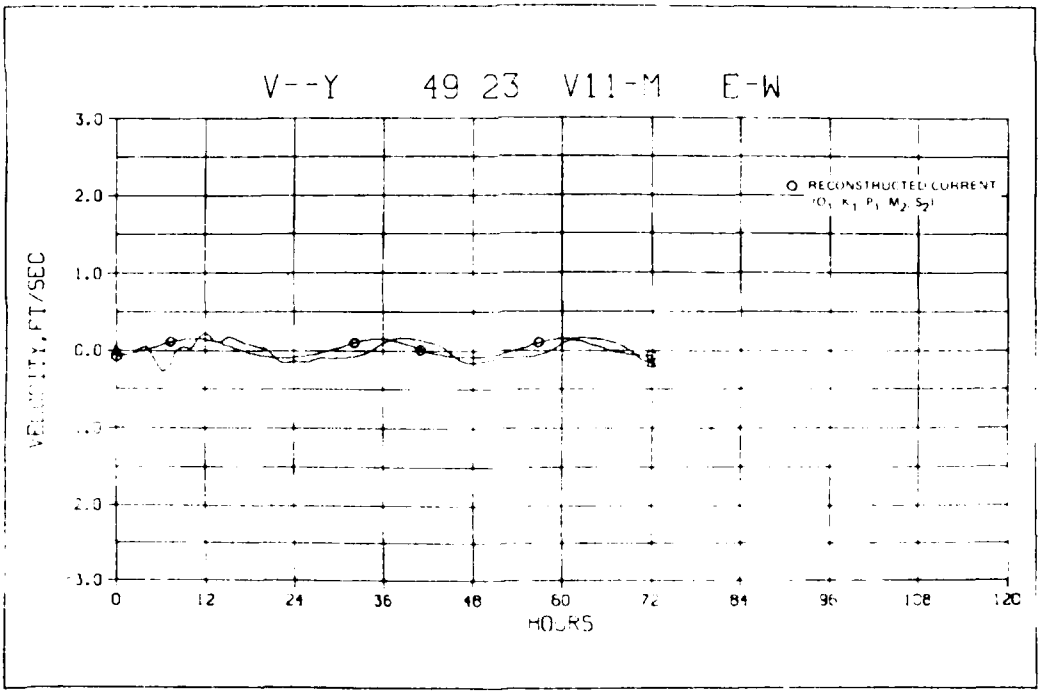

b. East-west

Figure X-33. Velocity components, simulated and predicted, at station V11-M, 20-24 September 1980

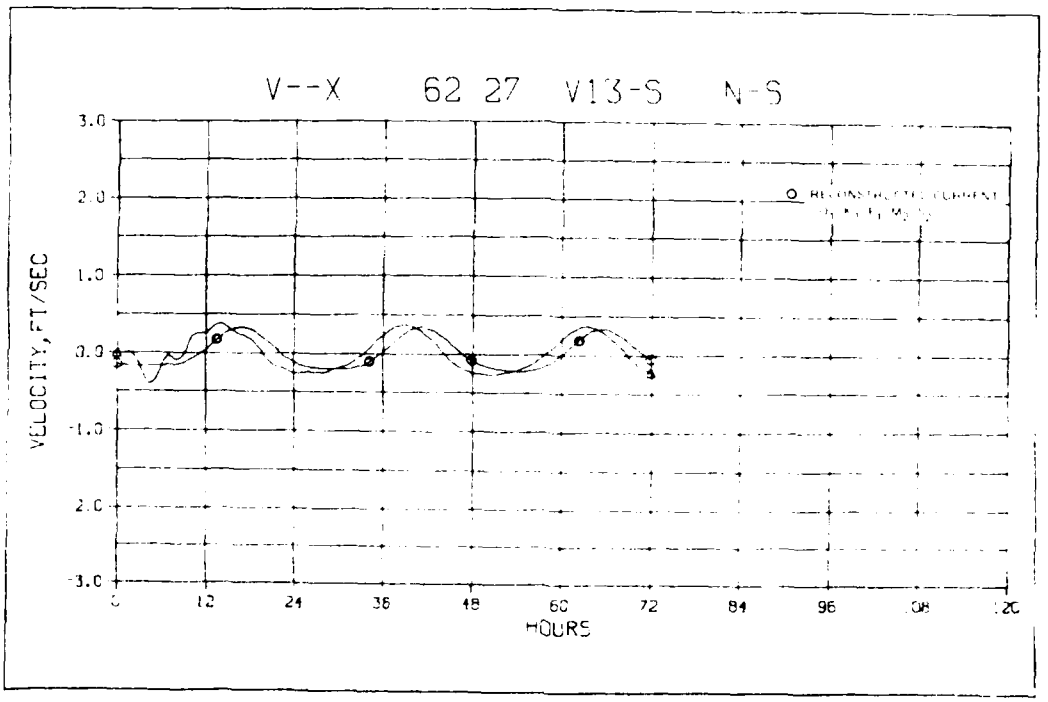

a. North-south

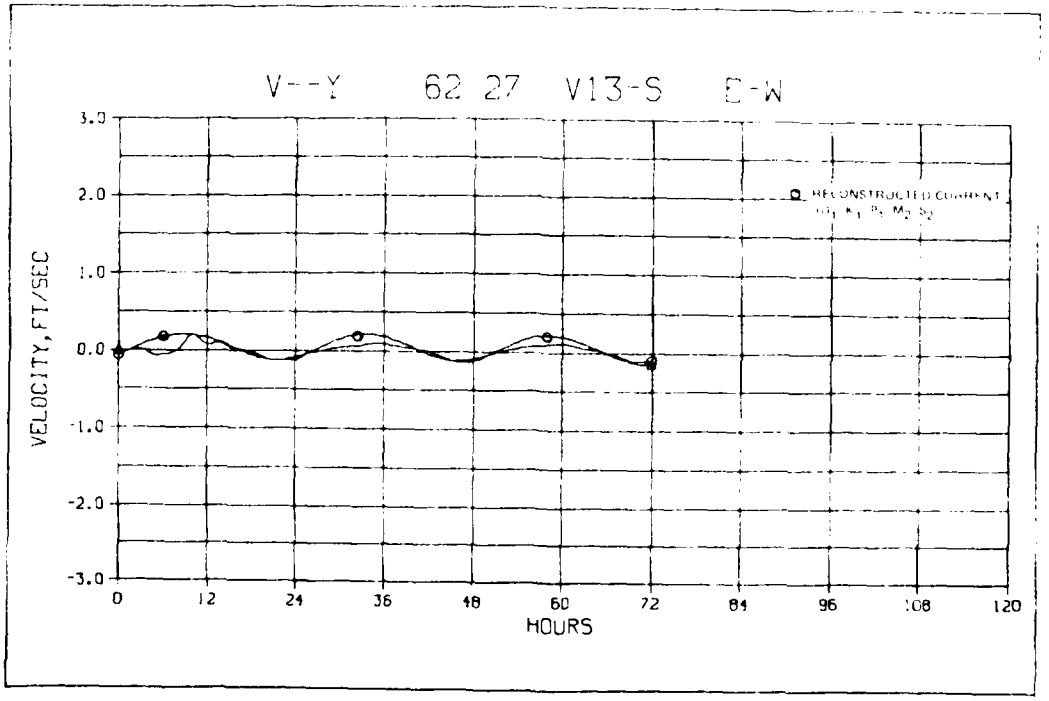

b. East-west

Figure X-34. Velocity components, simulated and predicted, at station V13-S, 20-24 September 1980

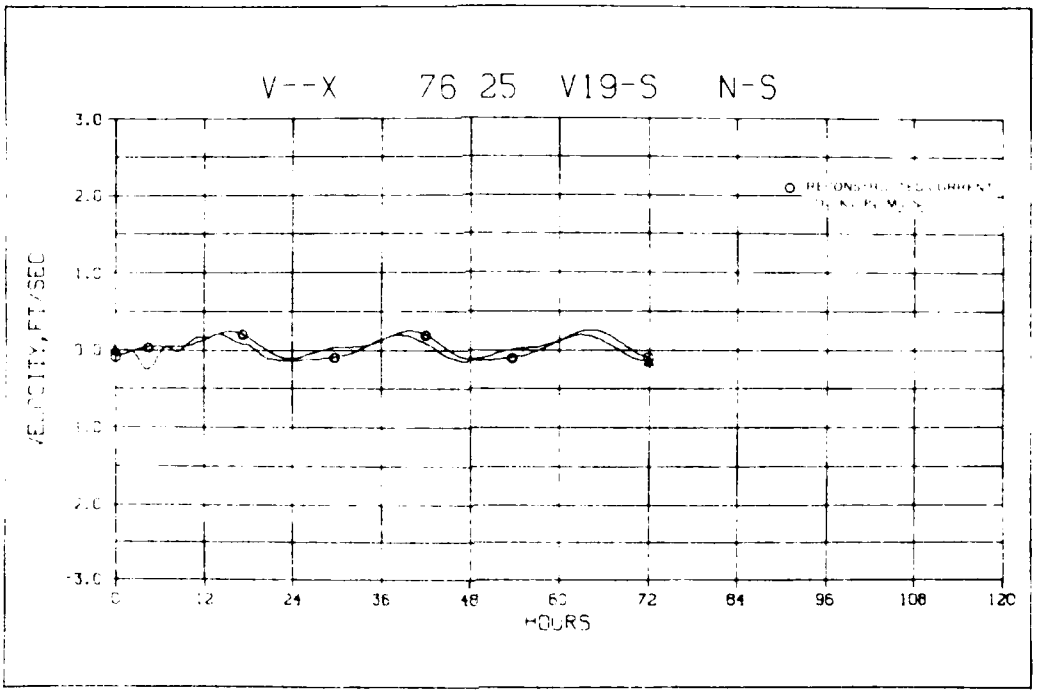

a. North-south

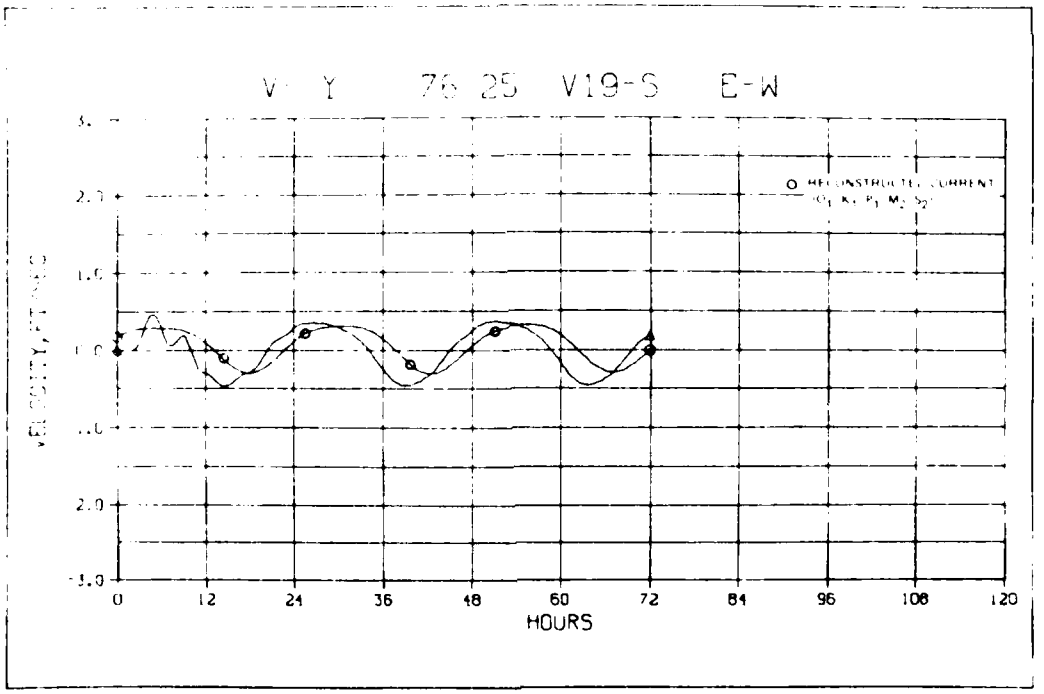

b. East-west

Figure X-35. Velocity components, simulated and predicted, at station V19-S, 20-24 September 1980

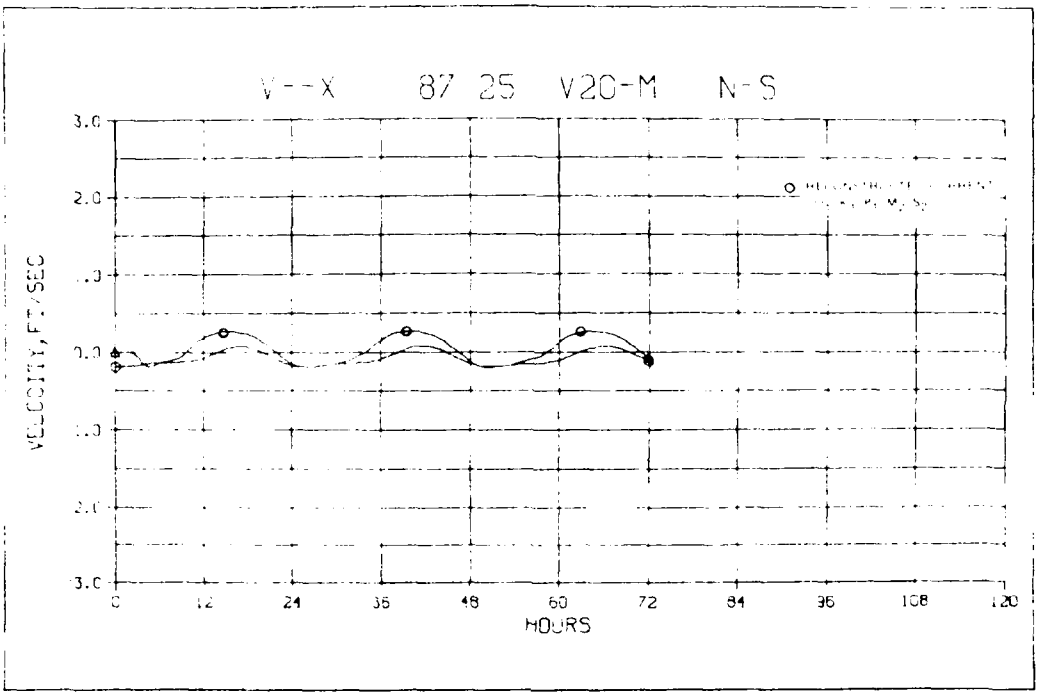

a. North-south

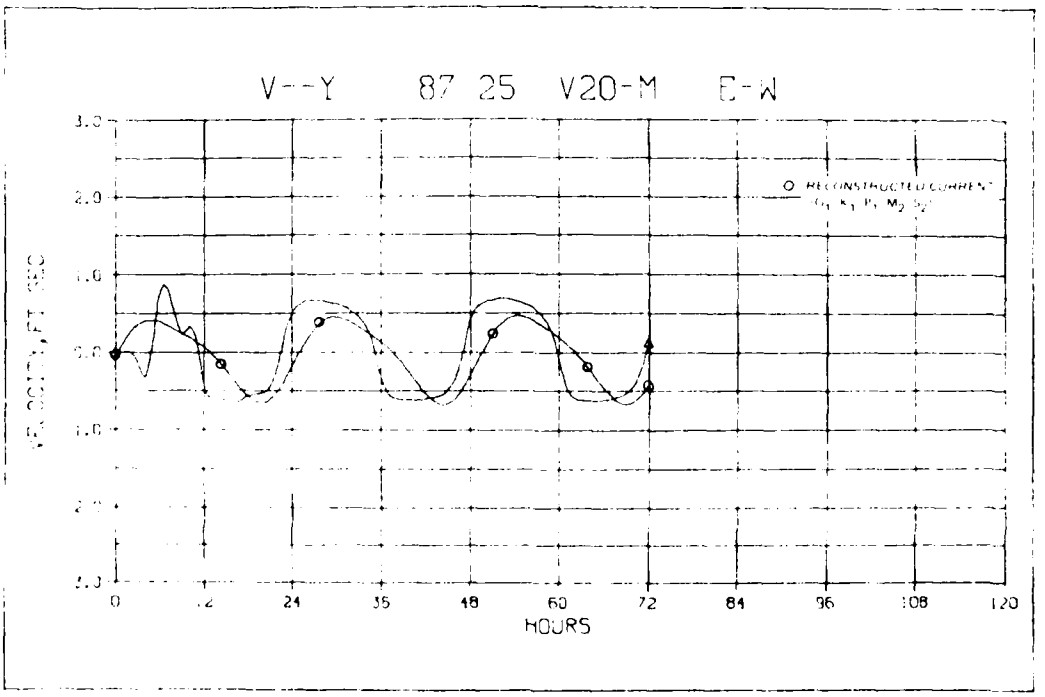

b. East-west

Figure X-36. Velocity components, simulated and predicted, at station V20-M, 20-24 September 1980

level are modified as shown in Table X-4 in the vicinity of Sand Island to reflect accumulated dumping of dredged materials. The regional site encompasses an area of approximately 4.35 square miles. The modified depths over this area reflect a disposal of approximately 1.27 billion cubic feet (47.03 million cubic yards) of dredged material. To place this figure in perspective, over the 8-year period (1970-1979) an average of 13.7 million cubic yards per year were removed from Mississippi Sound (USACE, Mobile District 1979).

131. The 20-24 September 1980 period as employed in the hydrodynamic calibration was simulated assuming the hypothetical Sand Island regional disposal site was in place. Simulated water levels under this alternative at 11 stations were compared with the calibration simulation levels previously determined. Water levels within the Sound are unaltered by this hypothetical offshore disposal site even at grid cell (87, 27).

132. The detailed flow patterns in the vicinity of Sand Island are shown in Tables X-5 and X-6 for the present conditions at hr 72 and 120, respectively. The flow patterns in the vicinity of the hypothetical site are shown in Tables X-7 and X-8 at hr 72 and 120, respectively. Comparing Tables X-5 and X-6 and Tables X-7 and X-8, one notes that the detailed flow structure is changed only in the immediate vicinity of the hypothetical dredge material disposal site. Changes in flow structure induced by system modifications in Mississippi Sound and adjacent waters similar to the hypothetical Sand Island site will be felt only in the immediate vicinity and will not propagate to the boundary. Therefore, these modifications may be effectively studied using the global grid developed in this study.

Table X-4

Global Grid Alternative

(Sand Island Complex)

Grid Cell	Original Depth ft*	Alternative Depth, ft*
(88, 31)	13.0	5
(88, 32)	30.0	5
(89, 31)	11.0	5
(89, 32)	19.0	5
(90, 31)	12.0	5
(90, 32)	8.0	5

* With respect to local mean sea level.

SUPPLEMENTAL NOTES FOR TABLES X-5 THROUGH X-8

IN ORDER TO INTERPRET TABLES X-5 THROUGH X-8 CONSIDER THE GRID NOTATION IN THE FOLLOWING FIGURE

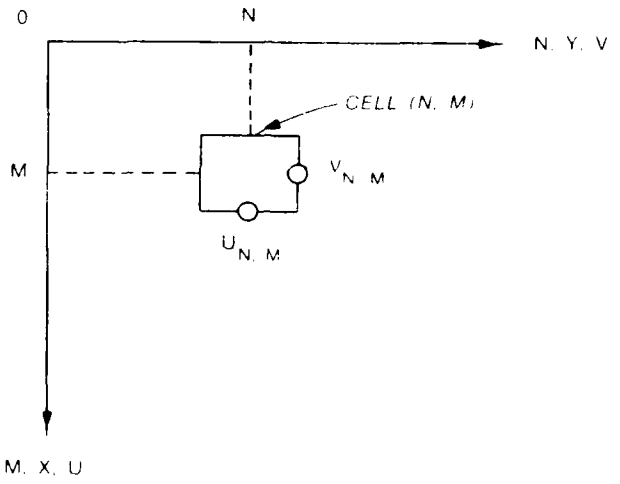

THEREFORE IN TABLE X-5 FOR COMPUTATIONAL CELL (95, 5) THE Y VELOCITY COMPONENT IS -0.1 FPS WHILE THE X VELOCITY COMPONENT IS + 5 FPS

OBSERVE IN TABLES X-7 AND X-8 THE HYPOTHETICAL DREDGE DISPOSAL SITE IS SKETCHED AS A SOLID LINE IN THE LOWER LEFT HAND CORNER

NOTE IN THE COMPUTATIONS ALL VELOCITIES NORMAL TO THIS LINE ARE ZERO

Table X-5

Simulated Global Grid Velocity Components (fps × 10) for the Original Sand Island Configuration at Hour 72

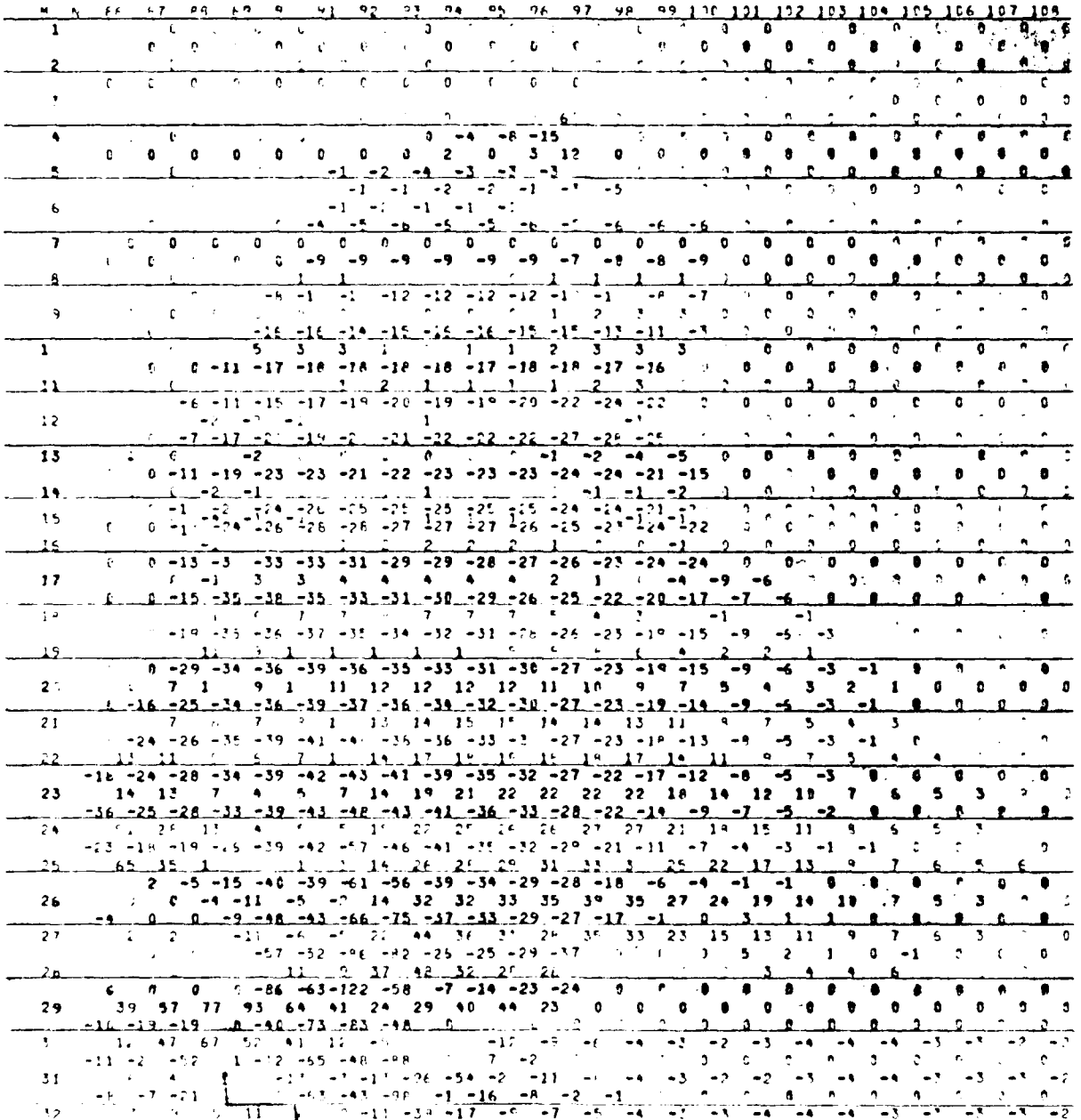

Table X-6

Simulated Global Grid Velocity Components (fps × 10) for the Original Sand Island Configuration at Hour 120

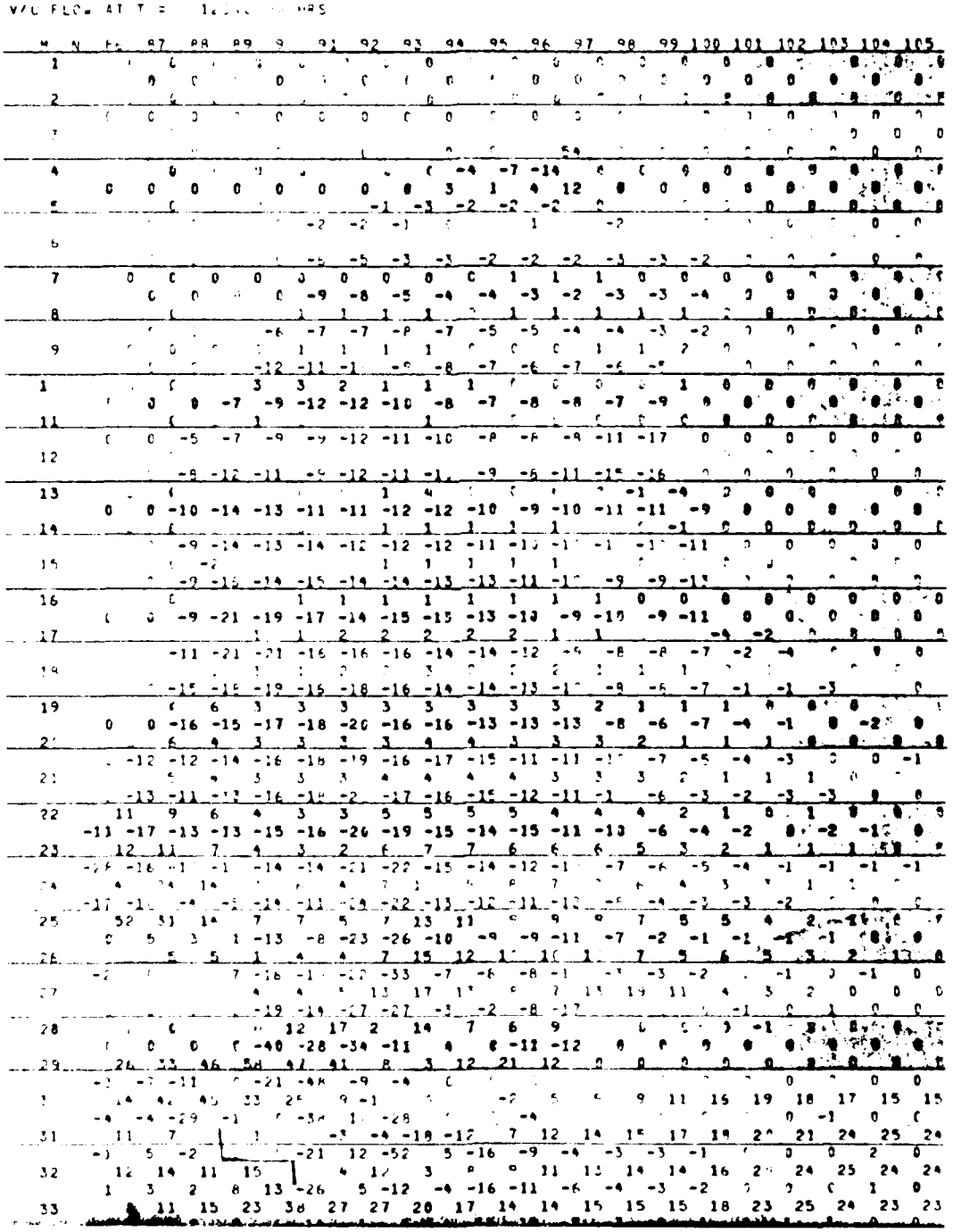

Table X-7

Simulated Global Grid Velocity Components (fps × 10) for the Sand Island Alternative at Hour 72

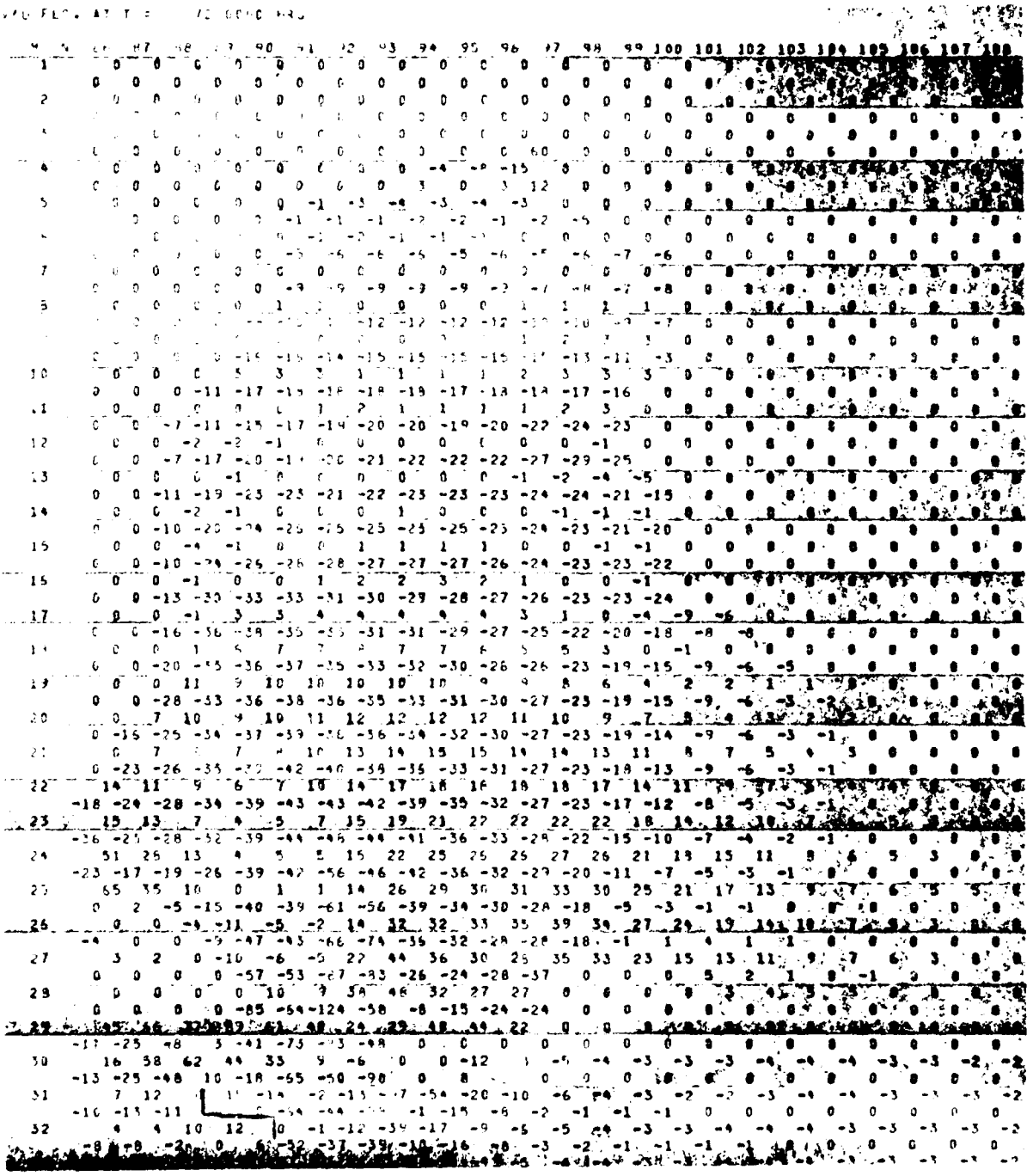

Table X-8

Simulated Global Grid Velocity Components (fps × 10) for the Sand Island Alternative at Hour 120

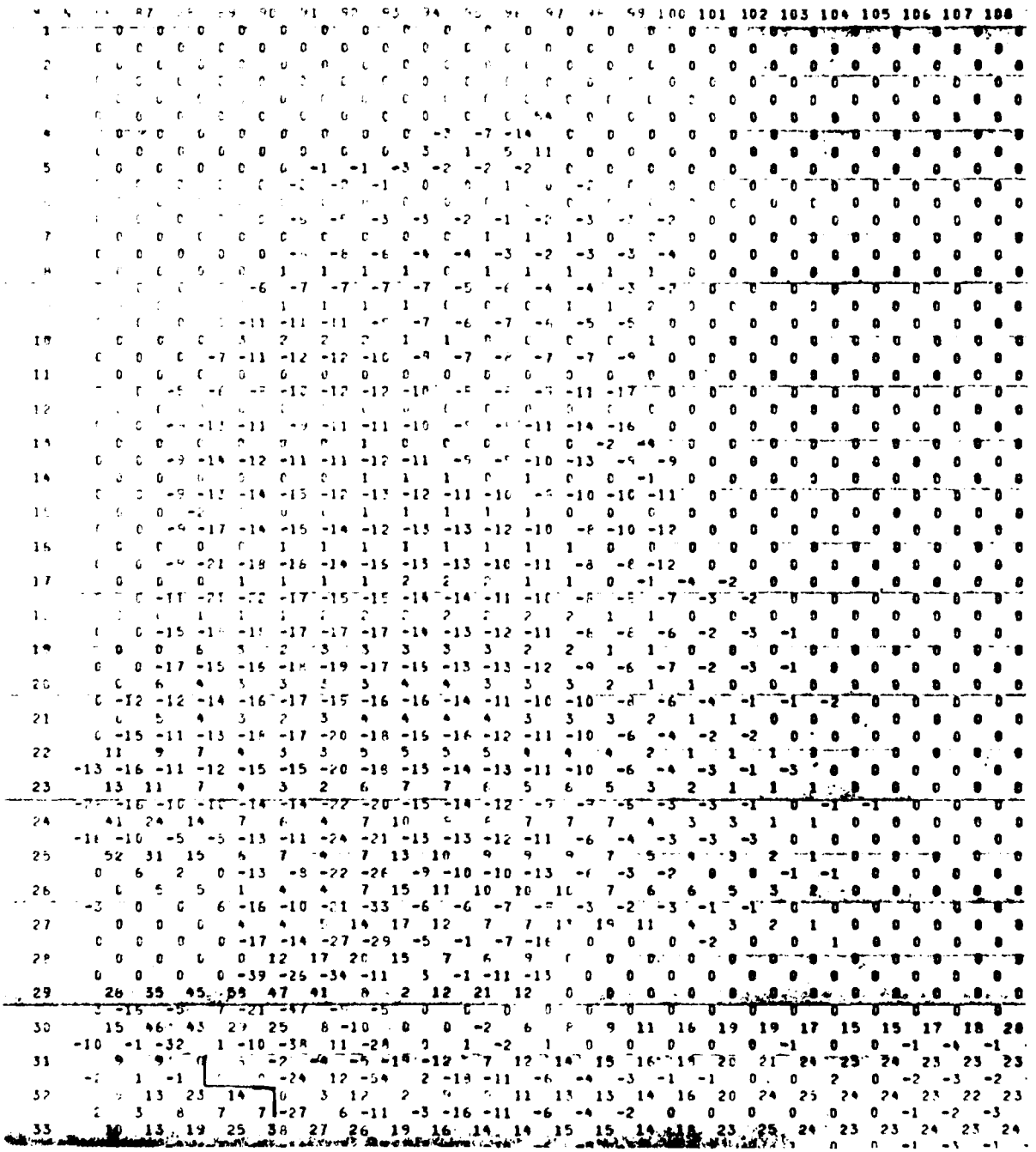

PART XI: REFINED GRID METHODOLOGY AND APPLICATION

133. The global grid previously developed is to be used to provide boundary information for a set of refined grids. Each refined grid is to be located around a potential channel alteration project. Detailed circulation in the vicinity of the proposed channel modifications is to be studied within the refined grid. The assumption underlying this approach is that alternative channel alignments and/or deepening effects will be localized and will affect circulation only within the area covered on the refined grid.

134. The width of the principal navigation channels within Mississippi Sound is from 220 to 350 ft. It is desired to use space steps on the same order in the refined grid. Since the maximum depth even under proposed deepening alternatives is approximately 40 ft, the gravity wave speed in the refined grid area is less than 38 fps. Therefore, the explicit time step limit is less than 9 sec. We attempt to employ an implicit time step of 60 sec.

135. Consider a refined grid system such that when a given time period is simulated, the computational cost incurred will not exceed the amount required to simulate the same time period on the global grid. Observe on the 6785-cell global grid a time step of 360 sec was utilized. Thus to advance the simulation one time step on the global grid, six time steps will need to be performed on the refined grid.

136. The cost involved in inverting a matrix by the Thomas algorithm as employed in WIFM is approximately proportional to its rank cubed. Estimate the rank of the matrix to be inverted for a given grid setup as the square root of the number of cells in the grid, N, and obtain the following relationship assuming a unit proportionality factor:

$$W = (N)^{3/2} \tag{XI.1}$$

where

W = cost involved in inverting the matrix for a given grid system

N = number of cells in the grid system

The total simulation cost, C, is then given by the following relation

$$C = MW \tag{XI.2}$$

where

C = total simulation cost

M = number of time steps in the simulation

W = cost involved in inverting the grid system matrix

Let us equalize simulation cost in considering a given time period on each grid. In so doing, an upper bound on the number of grid cells to employ in the refined grid is obtained as follows

$$M^g W^g = M^r W^r = (6M^g)\left(\frac{N_r}{N_g}\right)^{3/2} W^g \qquad \text{(XI.3)}$$

Therefore if approximately 5000 cells in the global grid are involved in the computations: $6\left(\frac{N_r}{5000}\right)^{3/2} = 1$ and $N \approx 1500$. Thus a refined grid involving approximately 1500 cells in the computations must be constructed.

137. Let us now consider the general orientation of the principal navigation channels to the axes in the global grid as shown in Figure XI-1. As may be observed, the navigation channels do not run parallel, throughout their extent, to the global grid axis. If the refined grid orientation corresponds to that of the global grid, stair-stepping is normally employed to resolve the channel sections nonparallel to the grid systems. This approach, however, would necessitate the reduction of the space step by more than 100 percent.

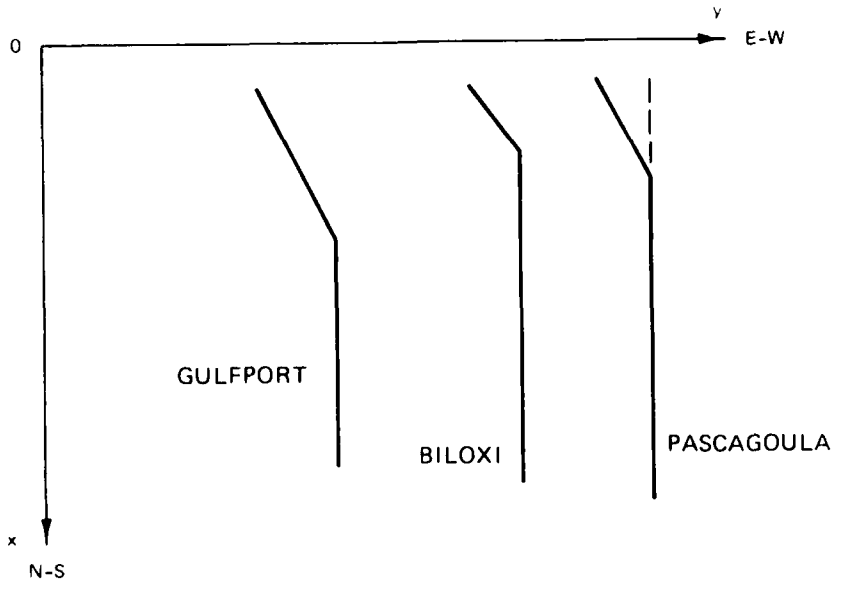

Figure XI-1. General orientation of major navigation channels in Mississippi Sound

As a result less than 750 cells could be used in the refined grid system to maintain a simulation cost for a given time equal to that of the global grid. This number of cells would probably be insufficient to resolve the channel properly in the refined grid. Therefore, it is necessary to idealize the channel systems somewhat within the refined grid. In order to demonstrate the refined grid approach on a typical navigation channel, the Pascagoula Channel was selected for further study. A refined grid was constructed in the idealized manner shown in Figure XI-2. By utilizing this channel idealization it was possible to employ the same orientation in the refined grid as in the global grid and use two dense vertical bands in the vicinity of the vertical channel sections and a single dense band of cells in the vicinity of the horizontal channel section. The details of the development of this refined grid system in the vicinity of the Pascagoula Channel are now presented.

Pascagoula Channel refined grid

138. Nautical Chart 11374 at a scale of 1:40000 was used in mapping the refined grid.

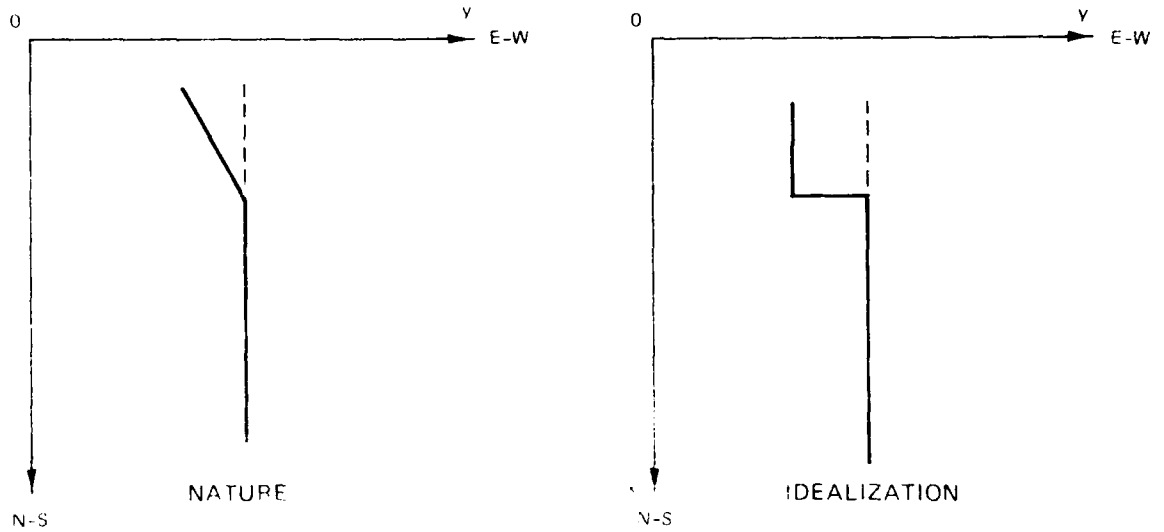

Figure XI-2. Pascagoula Channel configuration

139. The mapping for the horizontal (east-west) orientation is presented below in Table XI-1.

Table XI-1

East-West Orientation

MAPPING COMPLETE: 10 REGIONS

REG	LPR	REAL SPACE	ALPHA SPACE	GIVEN X PRIME	CALC X PRIME	A	B	C
1	2	1.0000	1	1.50000	1.50000	-.500000E+00	.150000E+01	.100000E+01
2	7	4.0000	3	1.50000	1.50000	-.645048E+01	.651158E+01	.430602E+00
3	2	11.1000	10	.75000	.75573	.159673E+02	-.173763E+03	-.155267E+01
4	2	12.3000	12	.50000	.47451	.129994E+02	-.427871E+09	-.814193E+01
5	2	12.8000	14	.10000	.11594	.141302E+02	-.332974E+02	-.122019E+01
6	2	13.0000	16	.10000	.08619	.129164E+02	.113476E-20	.164994E+02
7	2	13.5000	18	.50000	.53493	.121236E+02	.227525E-08	.699585E+01
8	5	15.0000	20	1.00000	1.00613	-.101645E+04	.972895E+03	.195090E-01
9	4	19.5000	25	.80000	.80841	.155682E+02	.256345E-06	.514025E+01
10	0	24.0000	29	1.50000	1.49453	0.	0.	0.

The mapping for the vertical (north-south) orientation is given in Table XI-2.

Table XI-2

North-South Orientation

MAPPING COMPLETE: 15 REGIONS

REG	LPR	REAL SPACE	ALPHA SPACE	GIVEN X PRIME	CALC X PRIME	A	B	C
1	4	1.0000	1	2.10000	2.10000	-.157166E+01	.257166E+01	.816592E+00
2	2	8.0000	5	1.56000	1.56323	.337351E+02	-.419579E+02	-.303715E+00
3	2	10.5000	7	1.00000	1.00812	.768585E+02	-.816147E+02	-.106344E+00
4	3	12.2500	9	.75000	.76342	.270150E+02	-.410470E+02	-.465341E+00
5	2	14.1000	12	.50000	.50082	.796248E+01	.538587E+00	.979202E+00
6	2	15.1000	14	.50000	.49922	.157612E+02	-.862203E+12	-.105706E+02
7	2	15.6000	16	.10000	.10648	.454064E+02	-.349252E+02	-.571608E-01
8	3	15.8000	18	.10000	.09402	.156492E+02	.122077E-14	.112259E+02
9	5	16.5000	21	.45000	.45479	.100641E+02	.702285E-01	.148394E+01
10	3	18.9000	26	.50000	.50431	.214908E+02	-.375466E+08	-.506097E+01
11	3	20.0000	29	.25000	.26017	.208723E+02	-.388994E+13	-.864969E+01
12	9	20.5000	32	.10000	.10063	.171161E+02	.125073E+00	.951571E+00
13	3	21.4000	41	.10000	.09943	.212172E+02	.199564E-36	.222980E+02
14	6	22.1000	44	.40000	.44739	.201316E+02	.721794E-16	.100007E+02
15	0	27.2000	50	1.40000	1.41377	0.	0.	0.

The grid obtained contains 49 × 28 = 1372 cells and is presented in Figure XI-3. In the above tables, the real space values are in map inches.

140. Program TGRID was employed to plot the refined grid at a scale of 1:40000 so that it would be overlaid on Chart 11374. The average depth over the cell was assigned as the cell depth in most cases. The hydrographic survey information was also used to modify channel depths and chart depths in the vicinity of the passes. The assigned depths are presented in Table XI-3, which was directly output from the model. All water depths are in feet preceded by a minus sign and are with respect to local mean sea level. All land is represented as +10 ft.

Barrier Island configuration

141. All barrier islands were located on cell faces and assigned on

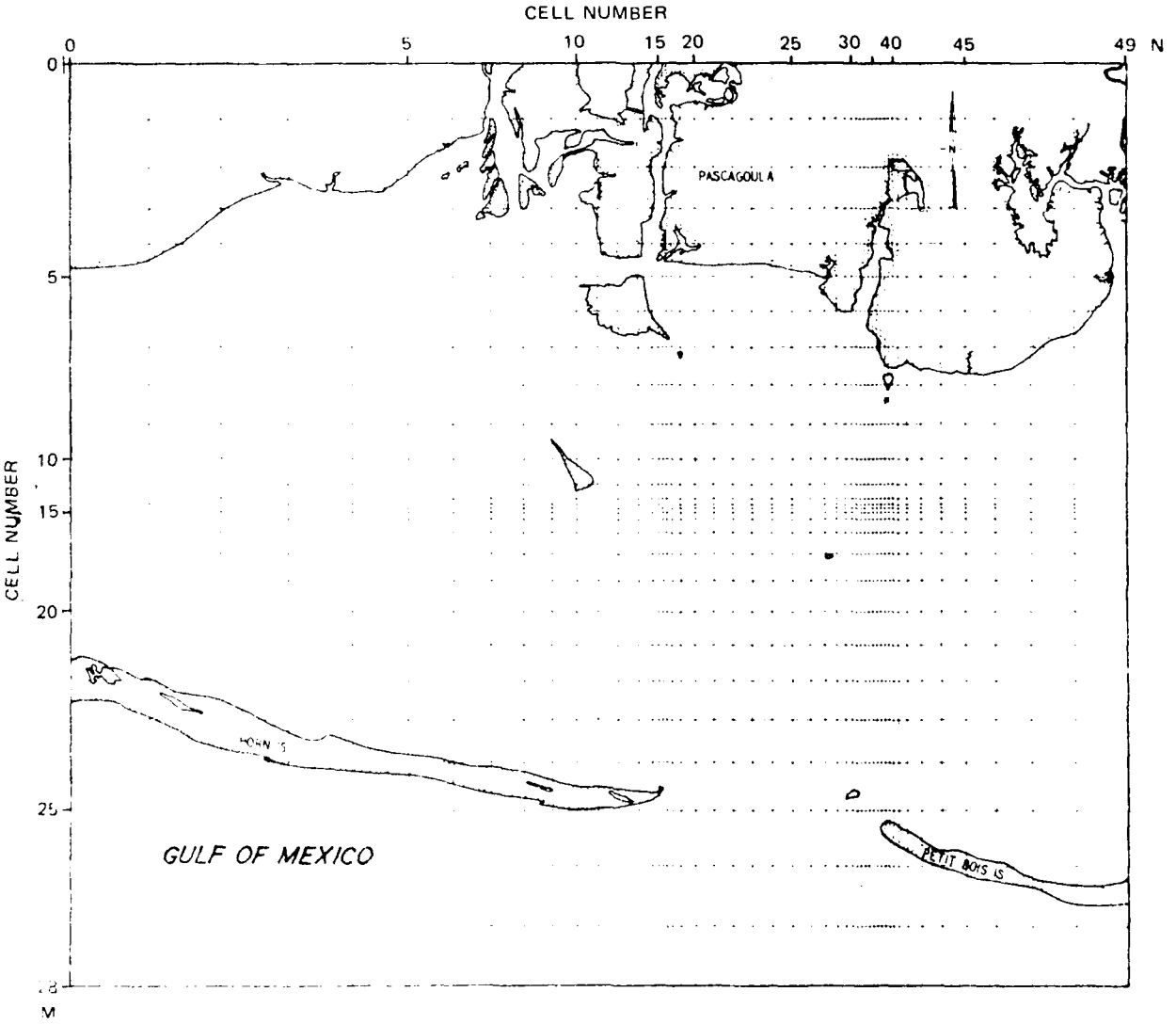

Figure XI-3 Pascagoula Channel refined grid

Table XI-3

Refined Grid Depth Field

M \ N	1	2	3	4	5	6	7	8	9	10	11	12	13	14	15	16	17	18	19	20
1	1[illegible]	1[illegible]	1[illegible]	1[illegible]	[illegible]	1[illegible]	1[illegible]	-19.	1[illegible]	1[illegible]	1[illegible]	1[illegible]	10.	1[illegible]	1[illegible]	-39.	10.	1[illegible]	10.	10.
2	1[illegible]	1[illegible]	1[illegible]	1[illegible]	1[illegible]	1[illegible]	-16.	-16.	1[illegible]	-3.	-3.	1[illegible]	10.	1[illegible]	-17.	-39.	-16.	1[illegible]	10.	1[illegible]
3	1[illegible]	1[illegible]	1[illegible]	1[illegible]	[illegible]	-4	-2	-11.	-2.	-3.	-3.	1[illegible]	1[illegible]	1[illegible]	-17.	-39.	-16.	1[illegible]	1[illegible]	1[illegible]
4	1[illegible]	1	-4.	-4.	-3.	-3.	-2	-7.	-2.	-3.	-3.	1	1[illegible]	1[illegible]	-31.	-39.	-16.	1[illegible]	1[illegible]	1[illegible]
5	1[illegible]	-4.	-5.	-3.	-5.	-5.	-7	-3.	-3.	-4.	-4.	-4.	-4.	-4.	-20.	-39.	-7.	10.	10.	10.
6	-4.	-7.	-8.	-7.	-6.	-5.	-3	-3.	-4.	-4.	-4.	-4.	10.	-4.	-9.	-39.	-7.	-7.	-8.	-5.
7	-5.	-8.	-5.	-4.	-7.	-6.	-6.	-6.	-7.	-7.	-6.	1[illegible]	10.	-4.	-9.	-39.	-7.	-7.	-7.	-6.
8	-8.	-9	-8.	-1	-8.	-7.	-8.	-8.	-8.	-8.	-8.	-9.	-8.	-8.	-8.	-39.	-7.	-7.	-7.	-7.
9	-9	-11	-10.	-1[illegible]	-11.	-[illegible]	-[illegible]	-5.	-7.	-8.	-10.	-1[illegible]	-9.	-9	-8.	-39.	-8.	-7.	-7.	-7.
1[illegible]	-1[illegible]	-1[illegible]	-[illegible]	-1[illegible]	-1[illegible]	-11.	-[illegible]	-7.	-4.	-4	-6.	-9.	-9.	-9	-8.	-39.	-9.	-9.	-7.	-7.
11	-11.	-14.	-14.	-14.	-14.	-13.	-12	-1[illegible]	-9.	-4.	1[illegible]	-5.	-6.	-7.	-1[illegible]	-39.	-13.	-9.	-7.	-7.
12	-15.	-15.	-15.	-14.	-14.	-13.	-12	-1[illegible]	-9.	-4.	-2.	-3.	-6.	-9.	-11.	-39.	-13.	-9.	-7.	-7.
13	-16.	-16.	-15.	-14.	-14.	-14.	-12.	-10.	-9.	-8.	-3.	-6.	-8.	-10.	-13.	-39.	-13.	-11.	-10.	-10.
14	-17.	-16.	-14.	-14.	-14.	-14.	-13.	-1[illegible]	-9.	-9.	-3.	-6.	-8.	-1[illegible]	-11.	-39.	-39.	-39.	-39.	-39.
15	-17.	-1[illegible]	-14.	-14.	-14.	-14.	-13.	-1[illegible]	-9.	-9.	-3.	-6.	-8.	-1[illegible]	-11.	-11.	-11.	-11.	-11.	-11.
16	-1[illegible]	-16.	-15.	-14.	-14.	-14.	-13	-11.	-9.	-6.	-3.	-9.	-9.	-1[illegible]	-11.	-11.	-11.	-11.	-11.	-12.
17	-1[illegible]	-1[illegible]	-15.	-14.	-14.	-14.	-12.	-1[illegible]	-9.	-7.	-3.	-8.	-10.	-1[illegible]	-11.	-11	-11.	-11.	-11.	-11.
18	-16.	-16.	-15.	-14.	-14.	-14.	-12.	-1[illegible]	-8.	-7.	-5.	-8.	-10.	-1[illegible]	-11.	-11.	-11.	-11.	-11.	-11.
19	-15.	-16.	-15.	-14.	-11.	-13.	-11.	-1[illegible]	-8.	-6.	-8.	-9.	-10.	-11.	-11.	-11.	-11.	-11.	-11.	-12.
20	-15.	-13.	-15.	-15.	-11.	-12.	-12	-9.	-9.	-9.	-11.	-12.	-13.	-13.	-13.	-13.	-13.	-13.	-14.	-15.
21	-11.	-11	-14.	-14.	-12.	-1	-1[illegible]	-1[illegible]	-11.	-12.	-12.	-12.	-13.	-14.	-14.	-14.	-14.	-14.	-14.	-16.
22	-3.	-7.	-13.	-[illegible]	-1[illegible]	-11.	-14.	-15.	-14.	-14.	-14.	-15.	-15.	-16.	-17.	-17.	-17.	-17.	-17.	-19.
23	1[illegible]	1[illegible]	-11.	-7.	-14.	-1	-13.	-14.	-14.	-15.	-16.	-17.	-17.	-17	-17.	-17.	-17.	-17.	-17.	-17.
24	-21.	-23.	1[illegible]	-11.	-11.	-11.	-13.	-15.	-15.	-17.	-18.	-18.	-17.	-16.	-15.	-15.	-15.	-15.	-14.	-14.
25	-28.	-3[illegible]	-26.	-25.	-23.	-25.	1[illegible]	1[illegible]	-4.	-4.	-6.	-1[illegible]	-6.	-11.	-9.	-7.	-7.	-7.	-9.	-9.
26	-36.	-35.	-33.	-33.	-33.	-33.	-29.	-29.	-28.	-29	-16.	-21.	-21.	-22.	-21.	-21.	-21.	-21.	-21.	-23.
27	-37.	-37	-[illegible]	-[illegible]	-[illegible]	-39.	-37	-39.	-[illegible]	-37.	-39.	-39.	-36.	-3[illegible]	-34.	-3[illegible]	-33.	-33.	-33.	-33.
28	-41.	-4[illegible]	-41.	-41.	-41.	-41.	-41.	-41.	-41.	-41.	-41.	-43.	-42.	-4[illegible]	-41.	-41.	-41.	-41.	-41.	-41.

(Continued)

(Sheet 1 of 3)

Table XI-3 (Continued)

M	N	21	22	23	24	25	26	27	28	29	30	31	32	33	34	35	36	37	38	39	40
1		1	1	1	1	1	1	1	1	1	1	10	1	10	1	1	1	10	11	1	1
2		1	1	1	1	1	1	1	1	1	1	1	1	1	1	1	1	1	1	1	1
3		1	1	1	1	1	1	1	1	1	1	1	1	1	1	1	1	1	1	1	1
4		1	1	1	1	1	1	1	1	1	1	1	1	1	1	-1	-3	1	1	1	1
5		1	1	1	1	1	1	1	1	1	1	1	1	1	1	-1	-3	1	1	1	1
6		-7	-7	-7	-7	-6	-6	-6	1	1	1	1	1	1	-1	-1	-4	-27	1	1	1
7		-6	-7	-7	-7	-7	-7	-7	-7	-7	-7	-7	-7	-7	-7	-7	-39	-7	-4	-3	10
8		-7	-7	-7	-7	-7	-7	-7	-7	-7	-7	-8	-8	-8	-8	-8	-39	-7	-5	-3	1
9		-7	-7	-7	-7	-7	-7	-7	-7	-7	-7	-8	-8	-8	-8	-8	-39	-7	-7	-7	-7
10		-7	-7	-7	-7	-7	-7	-7	-7	-7	-7	-8	-8	-8	-8	-8	-39	-8	-8	-8	-9
1		-7	-7	-7	-7	-7	-7	-7	-7	-7	-8	-8	-10	-10	-10	-10	-39	-10	-10	-10	-1
12		-7	-7	-7	-7	-8	-8	-8	-8	-8	-8	-1	-11	-11	-11	-11	-39	-11	-11	-11	-11
13		-11	-11	-11	-11	-11	-11	-11	-11	-12	-12	-13	-13	-13	-13	-13	-39	-14	-14	-14	-14
14		-39	-39	-39	-39	-39	-39	-39	-39	-39	-39	-39	-39	-39	-39	-39	-39	-14	-14	-14	-14
15		-11	-11	-11	-11	-12	-11	-12	-13	-13	-13	-13	-13	-13	-13	-13	-39	-15	-15	-15	-15
16		-13	-13	-14	-14	-15	-15	-15	-15	-14	-14	-15	-15	-15	-15	-15	-39	-16	-16	-16	-16
17		-13	-13	-14	-14	-16	-17	-17	-13	-13	-14	-14	-14	-14	-14	-14	-39	-16	-16	-16	-16
18		-13	-13	-14	-14	-17	-16	-16	-16	-16	-16	-16	-16	-16	-17	-17	-39	-17	-17	-17	-17
19		-13	-13	-15	-15	-17	-17	-17	-16	-17	-17	-17	-17	-17	-17	-17	-39	-17	-17	-17	-17
20		-14	-15	-15	-16	-16	-17	-17	-17	-17	-16	-15	-16	-17	-18	-19	-39	-18	-18	-18	-18
21		-16	-17	-16	-16	-17	-17	-17	-17	-18	-14	-15	-15	-17	-18	-19	-39	-19	-19	-19	-19
22		-17	-16	-15	-15	-16	-15	-17	-16	-16	-17	-17	-14	-16	-18	-19	-39	-19	-19	-19	-21
23		-17	-16	-15	-14	-15	-15	-16	-16	-15	-15	-15	-15	-14	-16	-17	-39	-19	-18	-18	-18
24		-15	-14	-13	-14	-16	-18	-17	-17	-16	-15	-14	-14	-11	-16	-16	-39	-17	-15	-15	-15
25		-6	-7	-1	-15	-11	-11	-12	-11	-16	-16	-16	-16	-19	-17	-13	-39	-22	-21	-20	-21
26		-23	-2	-2	-15	-16	-14	-11	-13	-15	-21	-23	-26	-41	-35	-5	-39	-16	10	10	1
27		-34	-34	-32	-31	-28	-31	-29	-19	-19	-21	-21	-26	-36	-26	-26	-39	-21	-21	-21	-21
28		-36	-35	-34	-31	-34	-38	-36	-34	-36	-37	-37	-37	-37	-37	-37	-39	-37	-37	-37	-37

(Continued)

Table XI-3 (Concluded)

M	N	41	42	43	44	45	46	47	48	49
1		10.	10.	1 .	1 .	1 .	1 .	1 .	1 .	10.
2		10.	10.	10.	1 .	10.	10.	10	10.	10.
3		1 .	1 .	1 .	1 .	1 .	1 .	1 .	1 .	1 .
4		1 .	1 .	1 .	1 .	1 .	1 .	1 .	1 .	1 .
5		1	1	1 .	1 .	1 .	1 .	1 .	1 .	1 .
6		1 .	1 .	1 .	1 .	1 .	1 .	1	1 .	1 .
7		10	10.	10.	1 .	10.	10.	10.	10.	-7.
8		1 .	1 .	1 .	1 .	1 .	1 .	1 .	-7.	-9.
9		-7.	-6.	-5.	-4.	-4.	-4.	-7.	-9.	-6.
1		-5.	-5.	-4.	-4.	-1 .	-1 .	-11.	-1 .	-6.
11		-1 .	-1 .	-1 .	-1 .	-13.	-12.	-12.	-1 .	-9.
12		-11.	-12	-14.	-13.	-13.	-14.	-1 .	-11.	-9.
13		-14.	-14.	-15.	-14.	-15.	-14.	-13.	-12.	-9.
14		-14.	-14.	-15.	-15.	-15.	-14.	-13.	-12.	-9.
15		-15.	-15.	-15.	-15.	-15.	-14.	-13.	-12.	-9.
16		-16	-16	-16.	-1 .	-15.	-16.	-14.	-13.	-9.
17		-16	-16.	-16.	-16.	-17.	-16.	-15.	-13.	-9.
18		-17.	-17.	-17.	-17	-17.	-17.	-16	-14.	-1 .
19		-18.	-18.	-18.	-18.	-18.	-17.	-16.	-15.	-13.
2		-18.	-19.	-19.	-18.	-18.	-18.	-17.	-16.	-15.
21		-19.	-19.	-19.	-18.	-19.	-19.	-17.	-17.	-15.
22		-2 .	-2 .	-2 .	-2 .	-2 .	-19.	-19.	-18.	-17.
23		-18.	-17	-19.	-17.	-19.	-2 .	-19.	-2 .	-19.
24		-16.	-16	-19.	-19.	-19.	-17.	-19.	-17.	-2 .
25		-21.	-18.	-18.	-12.	-13.	-15.	-11.	-15.	-15.
26		10.	10.	-9.	-9.	-9.	-7.	-11.	-11.	-16.
27		-21.	-21.	-24.	-16.	-16.	-13.	-12.	-13.	-11.
28		-37.	-36	-3 .	-3 .	-39.	-36.	-36	-35.	-31.

elevation of 10 ft above local mean sea level. The barriers were typed as exposed since no overtopping occurred. The barrier island configuration is shown in Table XI-4 below. The orientation numbered 1 corresponds to a barrier on the u-cell face, while orientation 2 represents a v-face barrier.

Table XI-4

Barrier Configuration

No.	Orientation	Location N	Location M
1	2	7	2
2	2	7	3
3	2	8	3
4	2	13	8
5	2	9	19
6	1	10	10
7	1	4	24
8	1	5	24
9	1	6	24
10	1	9	25
11	1	10	25
12	1	11	25
13	1	12	25
14	1	13	25
15	1	14	25
16	1	15	25
17	1	16	25
18	1	30	25
19	1	31	25
20	1	43	26
21	1	44	26
22	1	45	26
23	1	26	26
24	1	47	26
25	1	48	26

Flow inputs and calibration stations

142. Two flow inputs for the Pascagoula River System are considered. The Pascagoula River is assigned as input to cell (8,1) and the East Pascagoula River is assigned as input to cell (16,1). Average daily USGS flows corrected by drainage area ratios were used to specify input flows in cfs.

143. The location of tidal stations, velocity stations, and salinity transect stations on the refined grid system are shown in Table XI-5.

Table XI-5

Calibration Station Locations on the Refined Grid

Tide Station	WIFM Grid Coordinates
T4	(4,24)
T5	(25,6)
T6	(49,27)
T7	(49,8)
Velocity Station	**WIFM Grid Coordinates**
V12	(3,20)
V13	(35,20)
V14	(24,25)
V15	(30,27),(33,26)
V16	(49,22),(49,23)
Salinity Transect Station	**WIFM Grid Coordinates**
T54	(8,22)
T64	(17,6)
T62	(24,9)
T66	(31,7)
T60	(33,16)
T68	(49,19)
T56	(33,26)

Global grid boundary interface

144. A subgrid of the global grid encompassing the Pascagoula Channel system was plotted at a scale of 1:40000. The global grid subgrid was overlaid the refined grid and boundary cells in the global grid surrounding the area were assigned to the nearest corresponding cell center of the refined grid. The assignments are shown in Table XI-6. During execution of the global grid simulation water surface elevations are written to logical unit number 25 and salinities to logical unit number 35. During execution of the refined grid simulation these two files are accessed, and linear in time and area-centered linear in distance interpolations are performed to determine the refined grid water surface elevation and salinities at the boundary.

AD-A156 616 NUMERICAL MODEL INVESTIGATION OF MISSISSIPPI SOUND AND ADJACENT AREAS(U) COASTAL ENGINEERING RESEARCH CENTER VICKSBURG MS R A SCHMALZ FEB 85 CERC-MP-85-2 3/3

UNCLASSIFIED F/G 8/8 NL

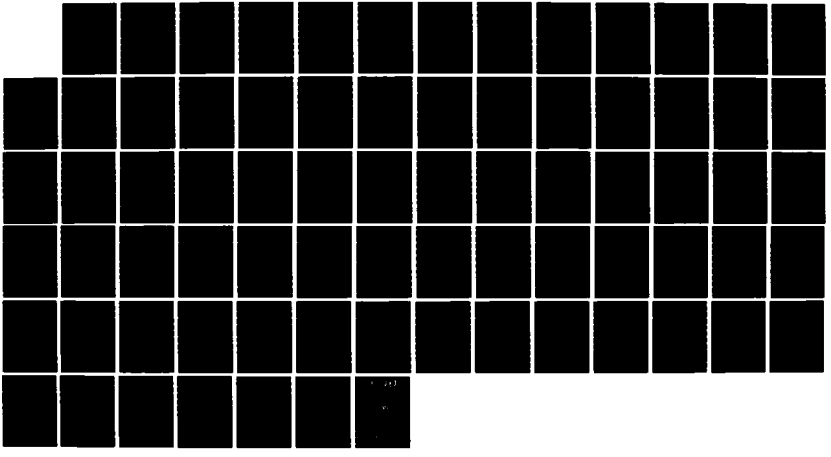

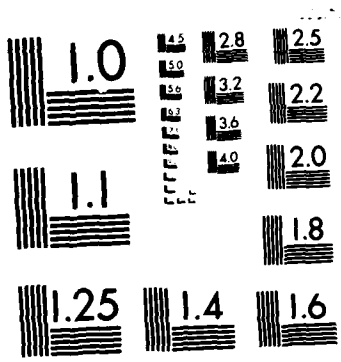

MICROCOPY RESOLUTION TEST CHART
NATIONAL BUREAU OF STANDARDS-1963-A

Table XI-6

Global Grid Cell-Refined Grid Cell Boundary Assignment

Tidal Signal No.	Global Grid Cell	Refined Grid Cell	Tidal Signal No.	Global Grid Cell	Refined Grid Cell
1	53, 21	1, 6	21	67, 29	49, 24
2	53, 22	1, 8	22	67, 30	49, 25
3	53, 23	1, 9	23	67, 31	49, 26
4	53, 24	1, 10	24	67, 32	49, 27
5	53, 25	1, 14	25	67, 33	49, 28
6	53, 26	1, 18	26	53, 33	1, 28
7	53, 27	1, 20	27	54, 33	2, 28
8	53, 28	1, 22	28	55, 33	4, 28
9	53, 29	1, 24	29	56, 33	5, 28
10	53, 30	1, 25	30	57, 33	8, 28
11	53, 31	1, 26	31	58, 33	11, 28
12	53, 32	1, 27	32	59, 33	17, 28
13	53, 33	1, 28	33	60, 33	23, 28
14	67, 22	49, 8	34	61, 33	26, 28
15	67, 23	49, 9	35	62, 33	31, 28
16	67, 24	49, 10	36	63, 33	42, 28
17	67, 25	49, 14	37	64, 33	45, 28
18	67, 26	49, 18	38	65, 33	47, 28
19	67, 27	49, 20	39	66, 33	48, 28
20	67, 28	49, 22	40	67, 33	49, 28

PART XII: REFINED GRID HYDRODYNAMIC CALIBRATION AND CHANNEL MODIFICATION

145. In this part, two hydrodynamic simulations over the Pascagoula Channel refined grid developed in Part XI are considered. Water surface elevations computed on the global grid for the 20-24 September 1980 calibration period were accessed to define the boundary conditions along the refined grid. The convective acceleration and eddy dispersion (advective terms) in the motion equation were not considered along the open and closed boundaries and around barriers (Appendix B) as well as in the two dense vertical bands used to describe the Pascagoula Channel and in the one dense horizontal band used to represent a section of the Pascagoula Channel. The sudden discontinuity in the depth profile outside the navigation channel was thought to perhaps cause problems in the advective calculations. For this reason, advection was not considered in the vicinity of the navigation channels.

146. In simulation one, the same Manning's n versus water depth relations considered in the global grid hydrodynamic calibration are used. The computed (Δ) versus predicted (reconstructed) water surface elevations are presented in Figures XII-1 through XII-4 for the 120-hr period starting 20 September hour 0000 CST. Simulated currents are shown in Figures XII-5 through XII-11. No predicted (reconstructed) currents are shown, since for this period, due to the K_1-P_1 separation problem, they cannot be determined. The simulated water surface elevations match very closely the predicted (reconstructed) levels. From this we may infer that the global grid boundary elevations are accurate and that the L-shaped representation of the Pascagoula Channel is sufficient to describe water surface elevations within the overall channel system.

Channel modification

147. In simulation two, the Pascagoula Channel was considered to be increased in width from 330 to 660 ft. The depth of the widened channel was maintained at 39 ft with respect to local mean sea level (model datum). The changes in depth required to update the original channel width are shown in Table XII-1. Hydrodynamics was considered over the same 5-day period used in simulation one. No wind effects were considered and salinity patterns were not simulated.

148. Simulated water levels for the channel modification are presented

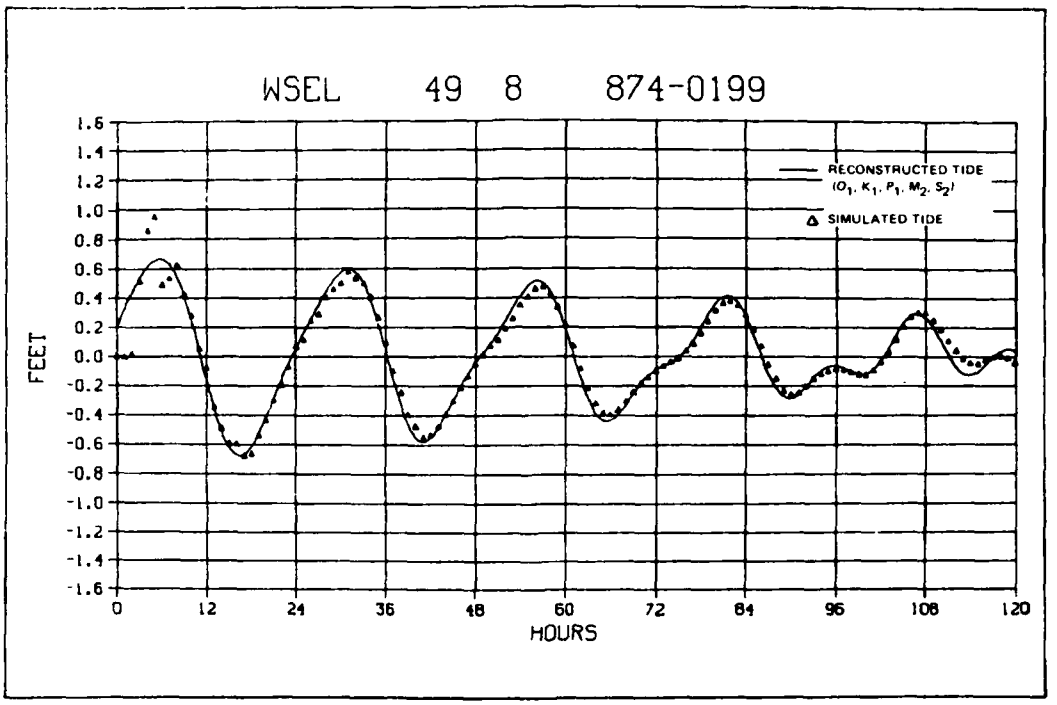

Figure XII-1. Simulated versus reconstructed water surface elevations at station 874-0199, 20-24 September 1980 (330-ft channel)

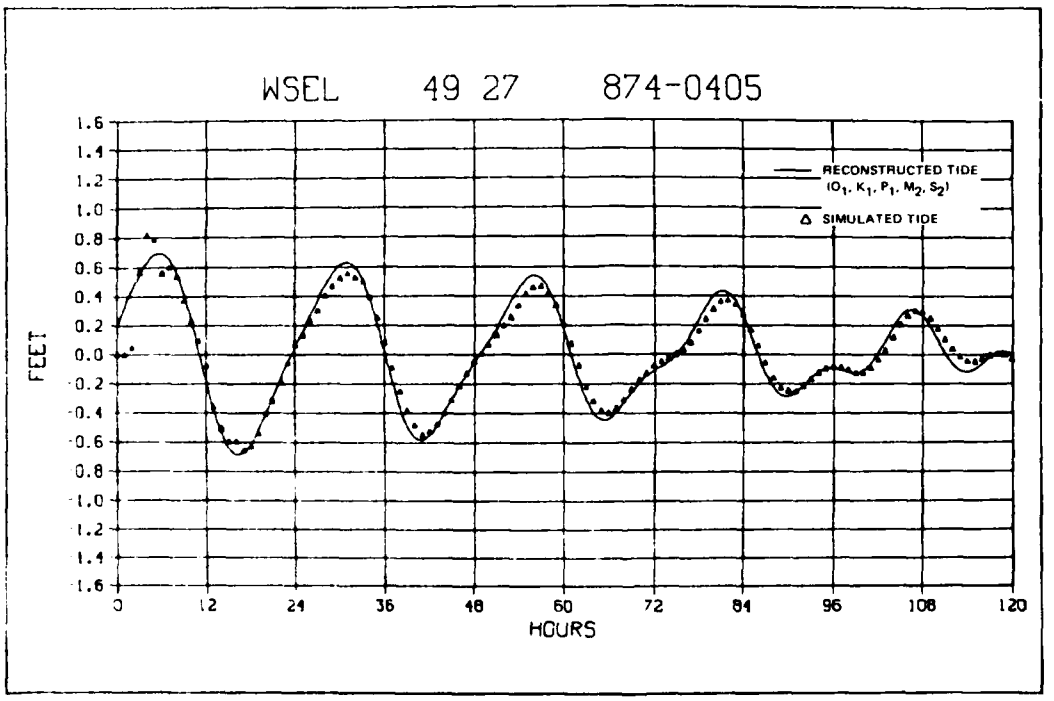

Figure XII-2. Simulated versus reconstructed water surface elevations at station 874-0405, 20-24 September 1980 (330-ft channel)

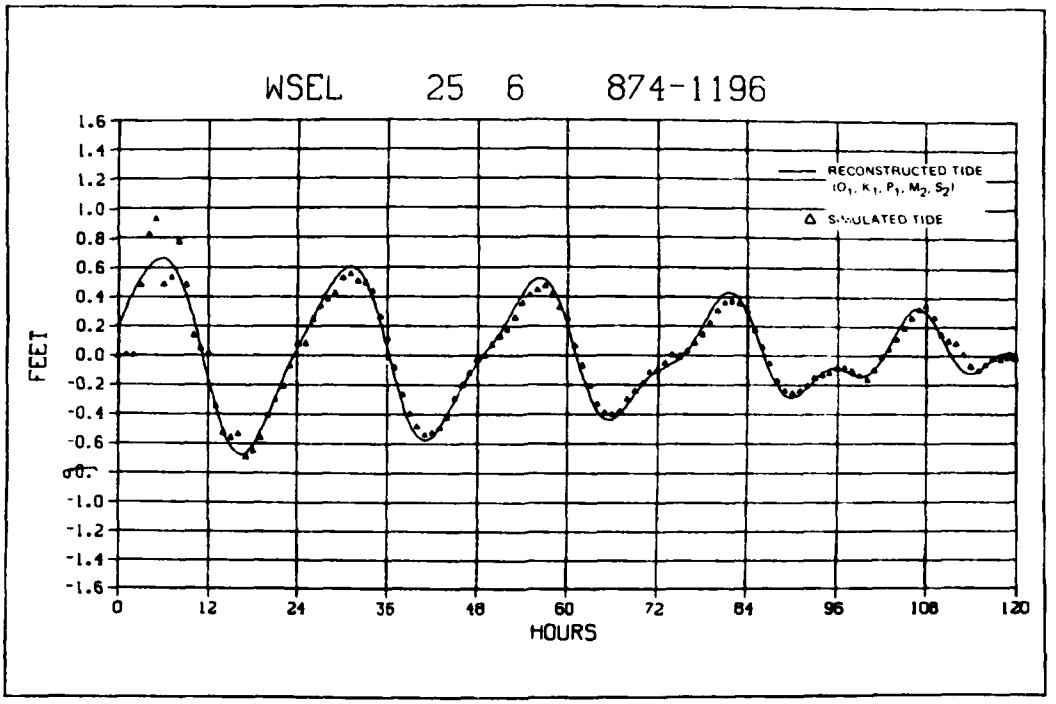

Figure XII-3. Simulated versus reconstructed water surface elevations at station 874-1196, 20-24 September 1980 (330-ft channel)

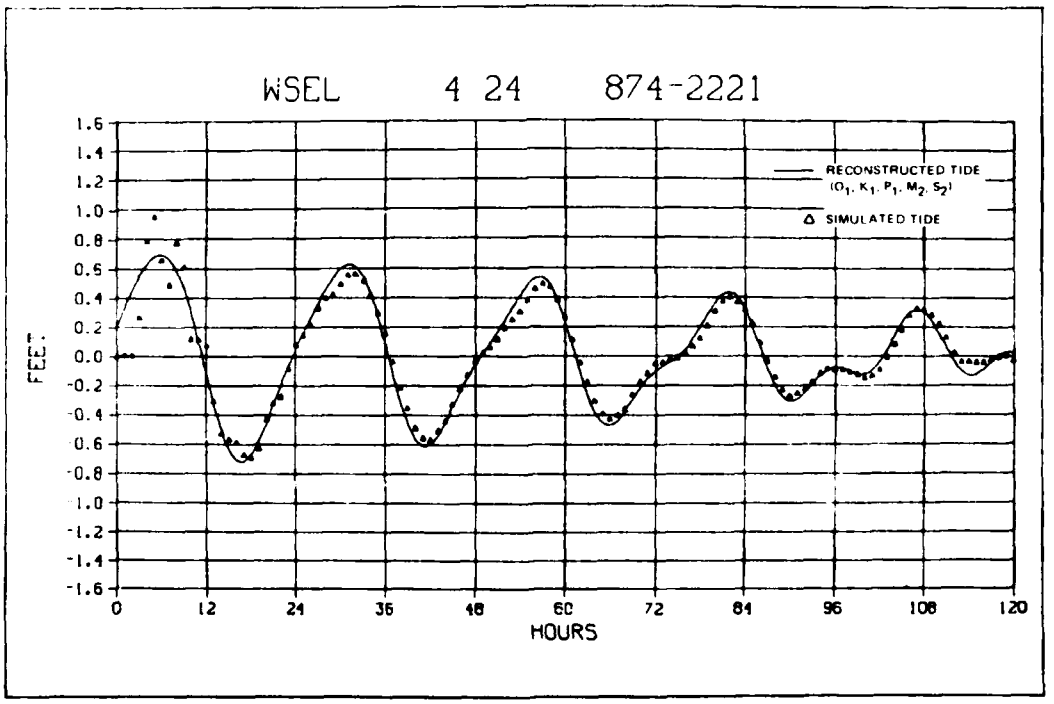

Figure XII-4. Simulated versus reconstructed water surface elevations at station 874-2221, 20-24 September 1980 (330-ft channel)

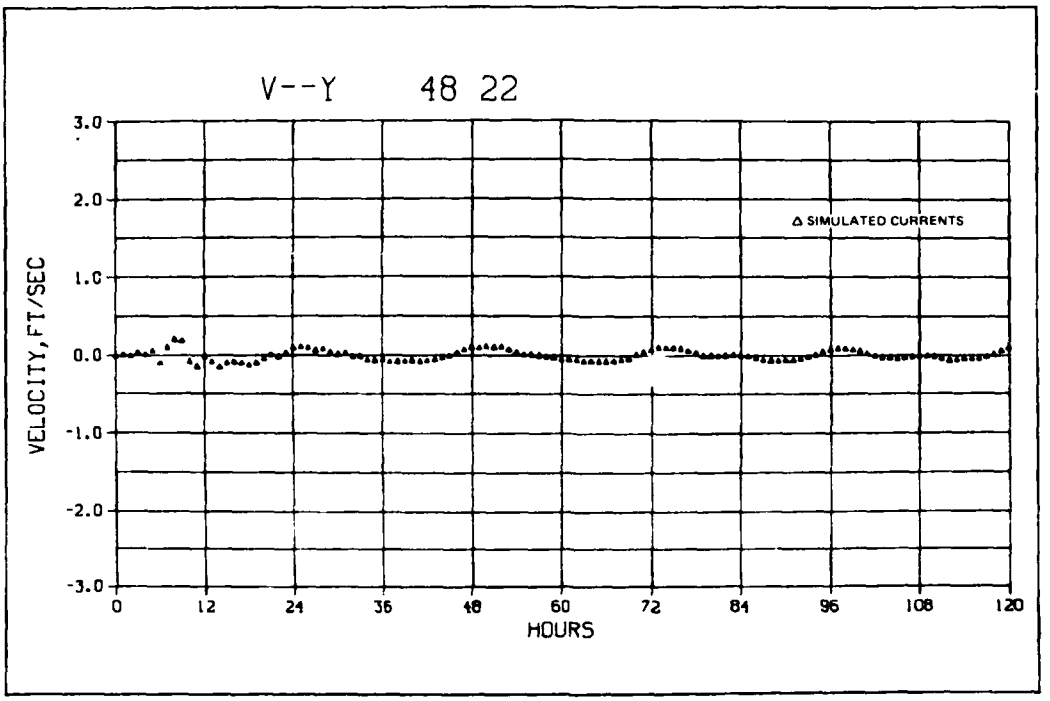

a. V-Y

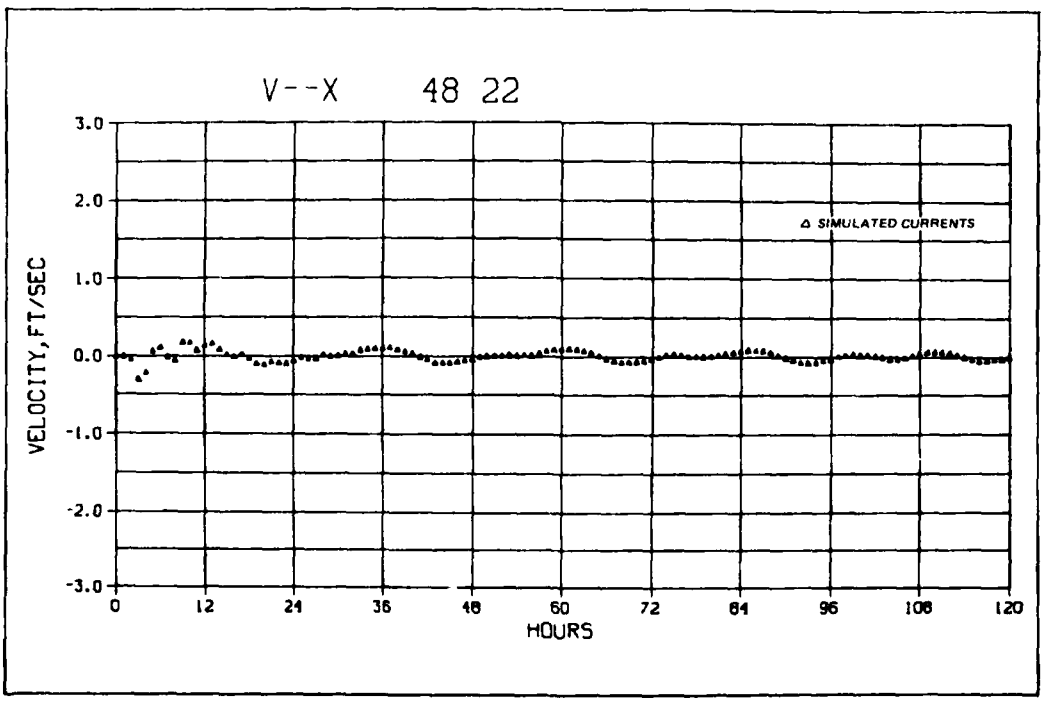

b. V-X

Figure XII-5. Simulated current velocities at station 48 22, 20-24 September 1980 (330-ft channel)

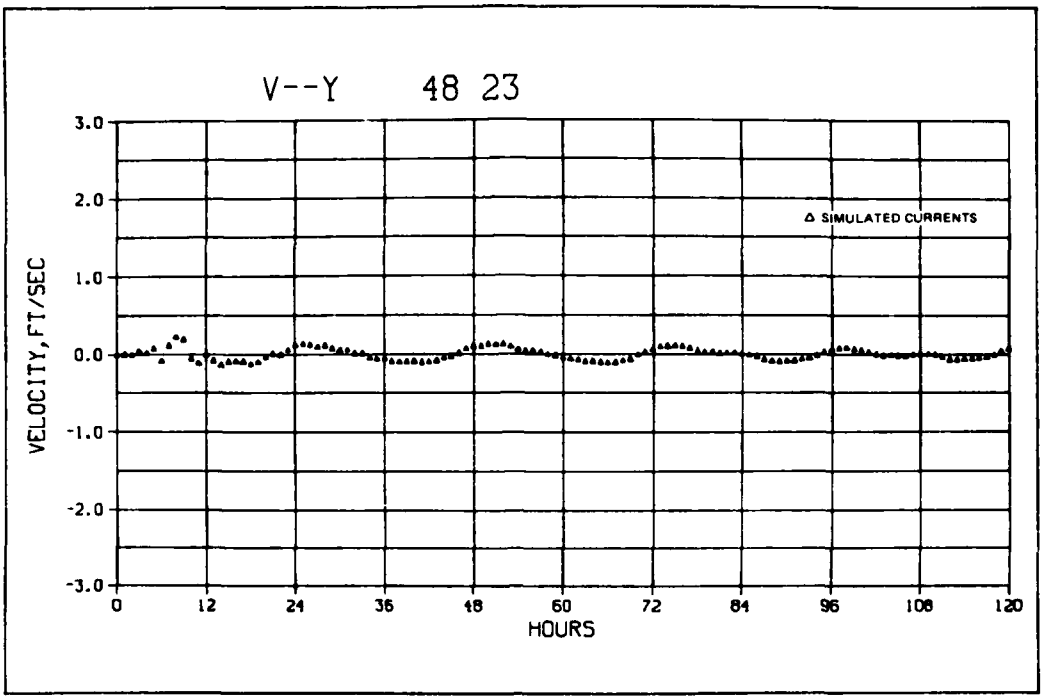

a. V-Y

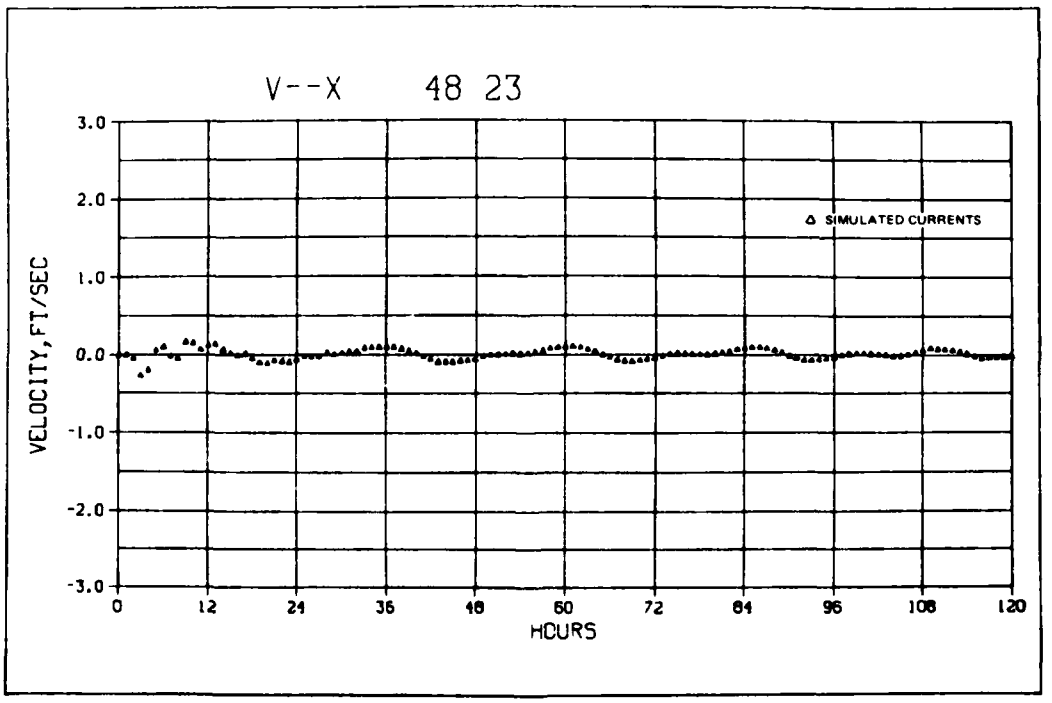

b. V-X

Figure XII-6. Simulated current velocities at station 48 23, 20-24 September 1980 (330-ft channel)

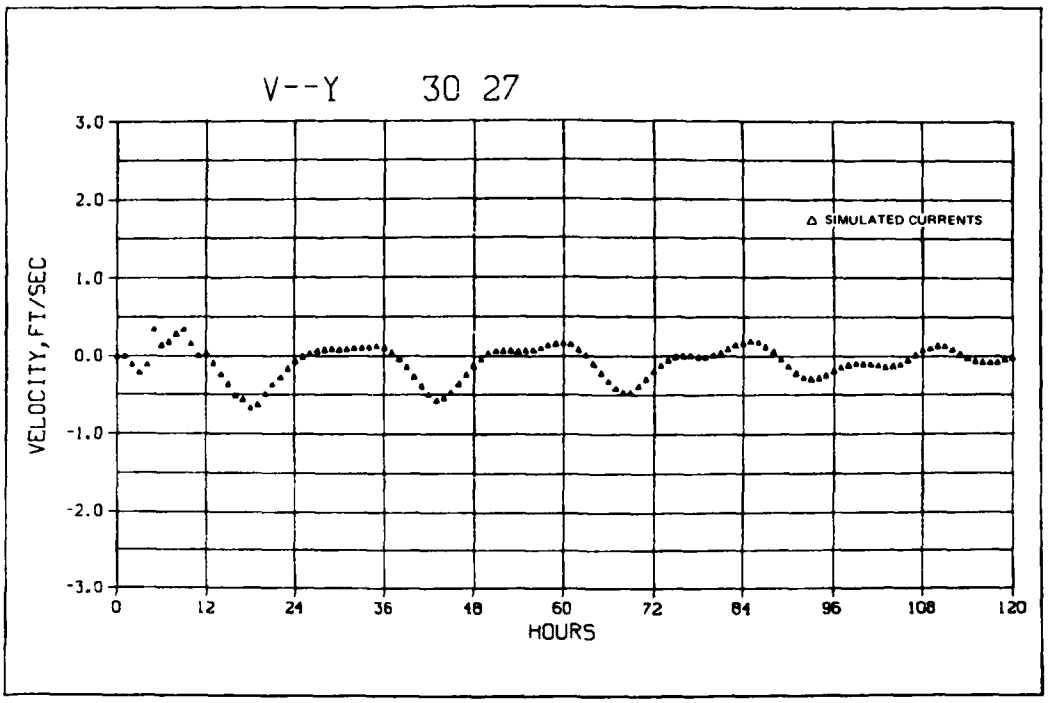

a. V-Y

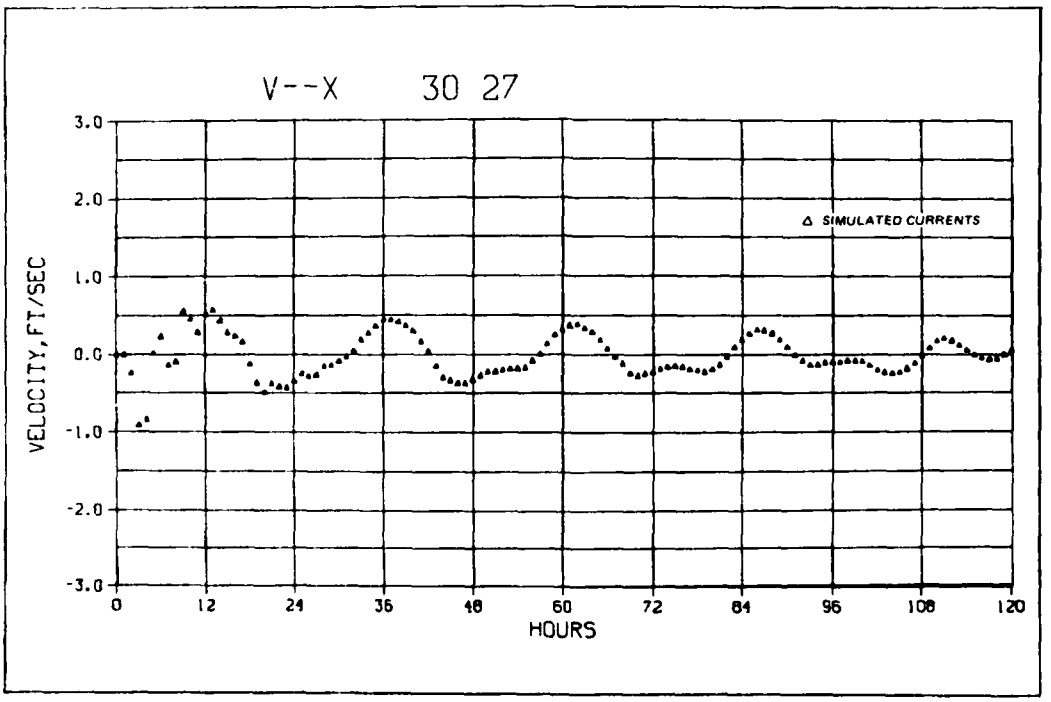

b. V-X

Figure XII-7. Simulated current velocities at station 30 27, 20-24 September 1980 (330-ft channel)

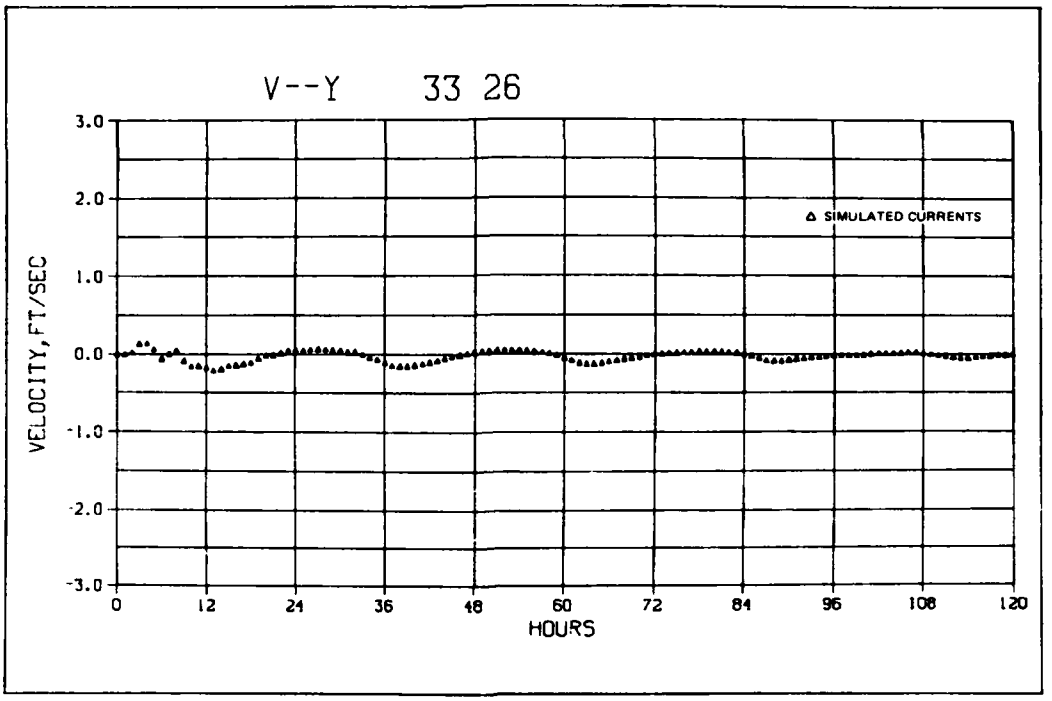

a. V-Y

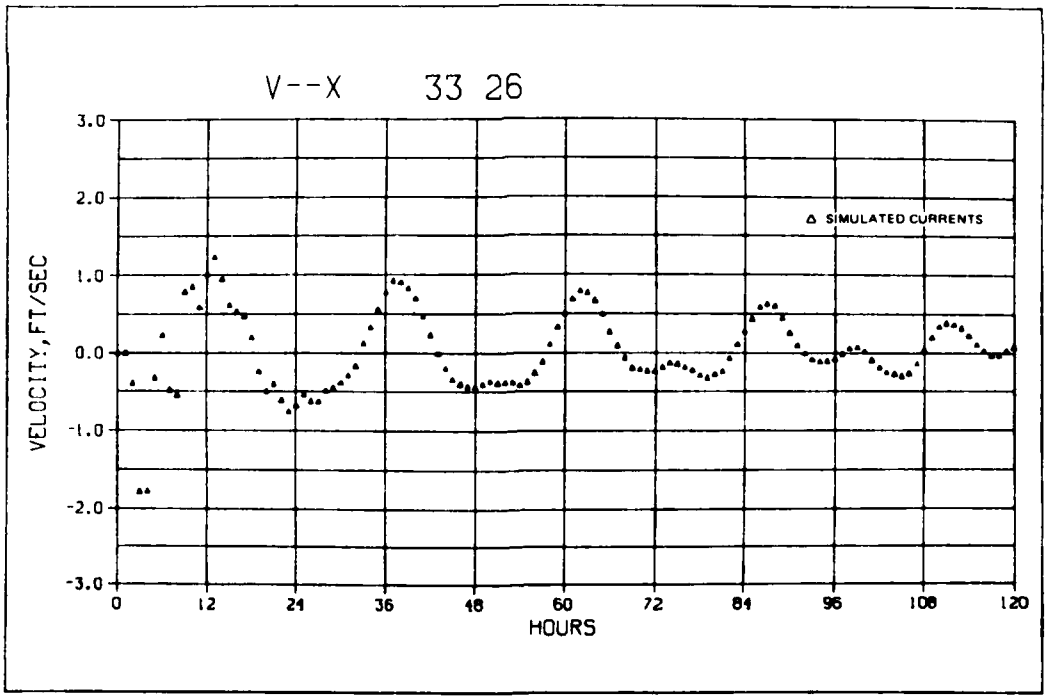

b. V-X

Figure XII-8. Simulated current velocities at station 33 26, 20-24 September 1980 (330-ft channel)

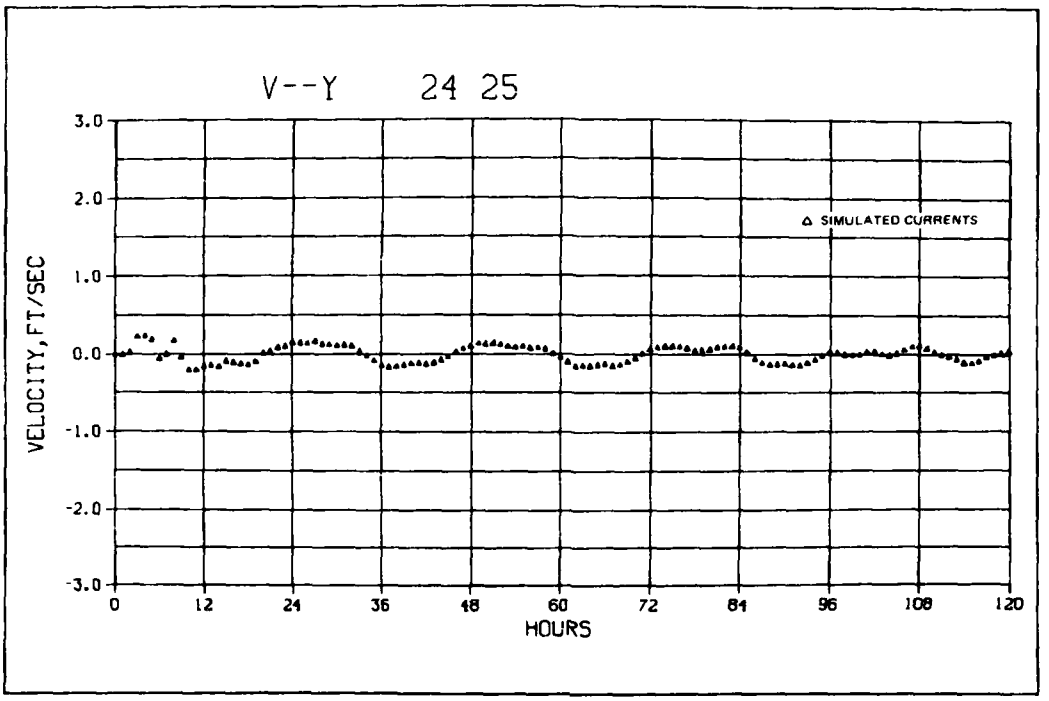

a. V-Y

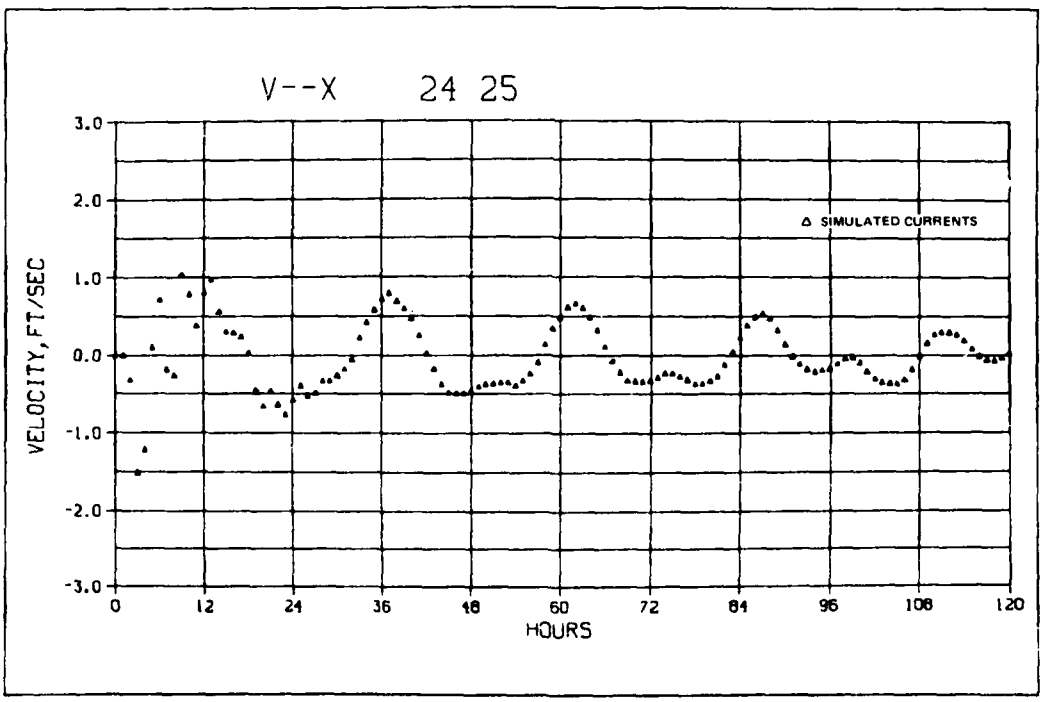

b. V-X

Figure XII-9. Simulated current velocities at station 24 25, 20-24 September 1980 (330-ft channel)

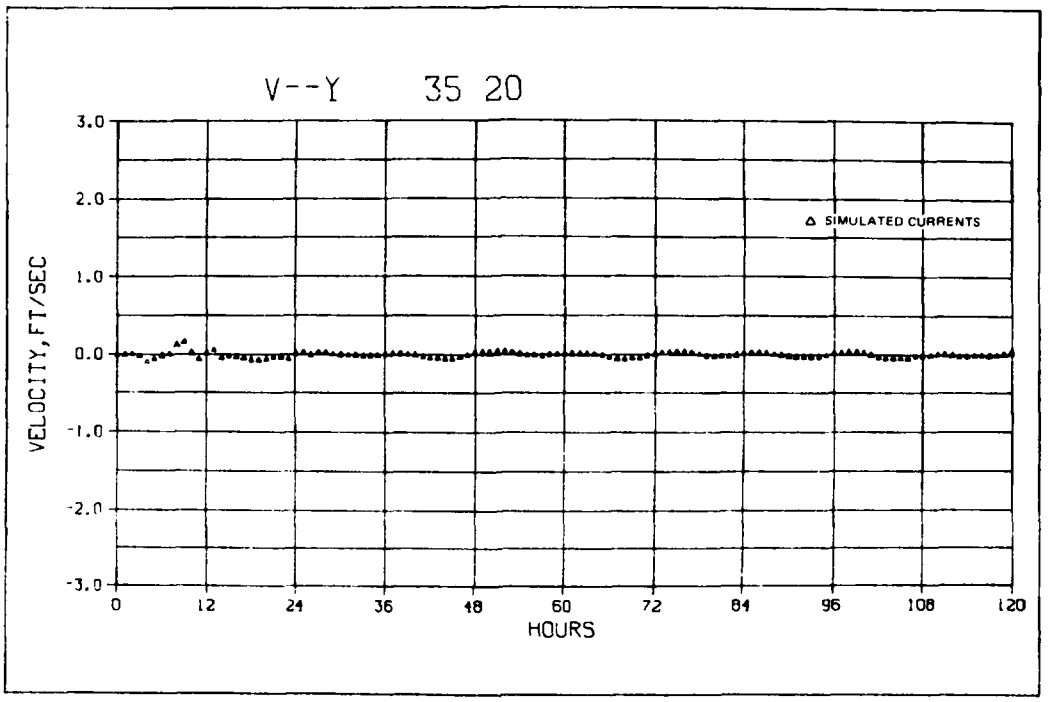

a. V-Y

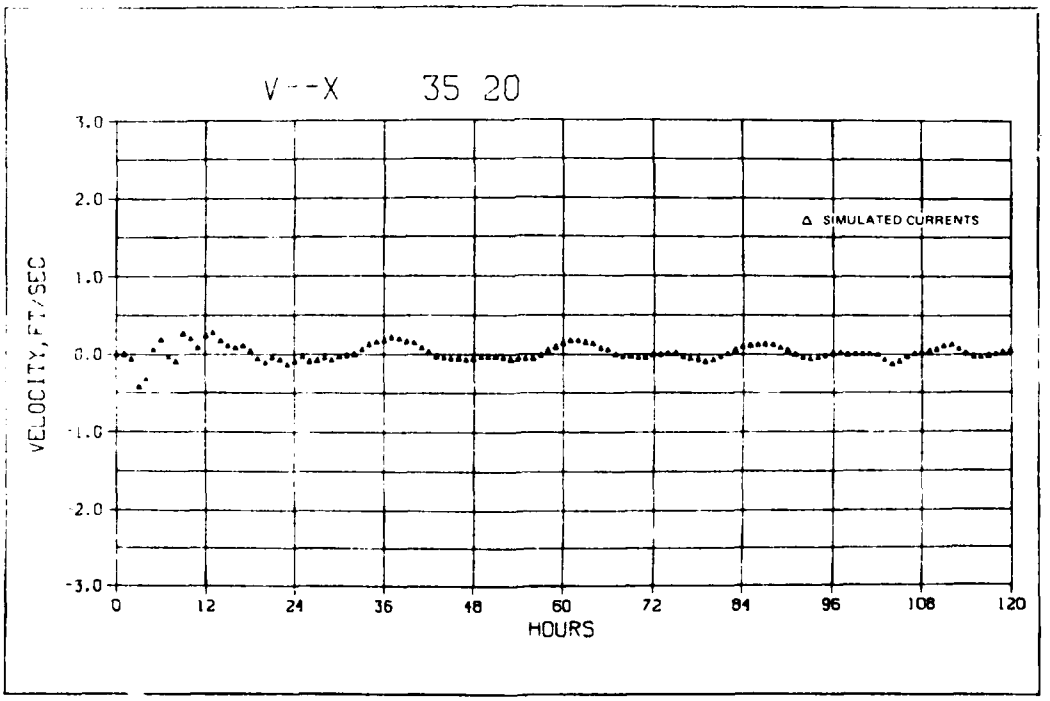

b. V-X

Figure XII-10. Simulated current velocities at station 35 20, 20-24 September 1980 (330-ft channel)

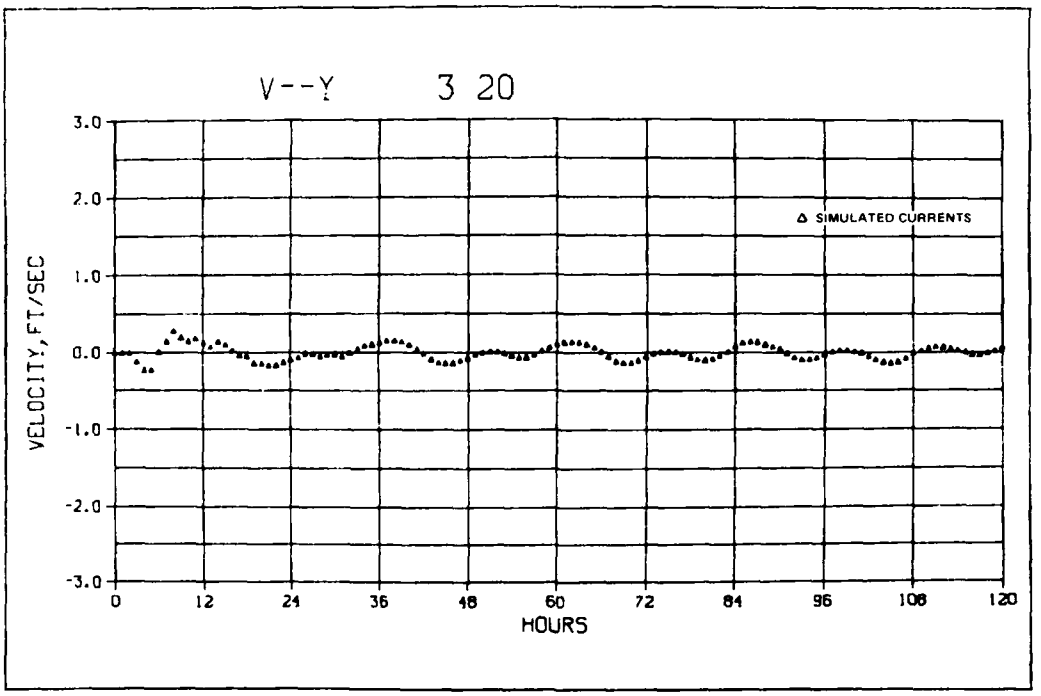

a. V-X

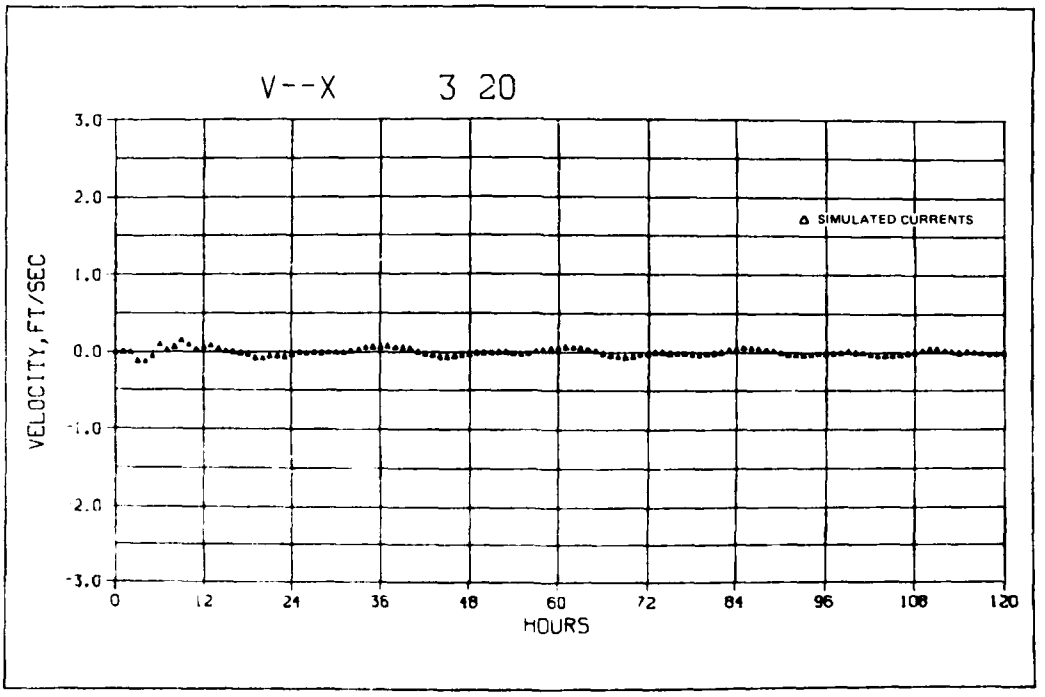

b. V-X

Figure XII-11. Simulated current velocities at station 3 20, 20-24 September 1980 (330-ft channel)

Table XII-1

Pascagoula Channel Widening

Grid Cell Range	Channel Depth, ft
(16, 1-15)	38.0
(17, 2-15)	38.0
(18-34, 14)	38.0
(18-34, 15)	38.0
(35, 15-28)	38.0

versus predicted (reconstructed) levels for the unmodified system in Figures XII-12 through XII-15. Water surface elevations with the widened channel corresponded to the predicted (reconstructed) levels for the unmodified system and hence to the simulation one results.

149. The simulated current structure at hr 72 of the 5-day simulation period is presented in Table XII-2 for the 330-ft channel (simulation one) and in Table XII-3 for the 660-ft channel (simulation two). In considering Tables XII-2 and XII-3, the reader should consult the note on page 174. Observe the outline of the channel is indicated as a set of solid lines in both tables. The impact of widening the channel is felt locally in the vicinity of the channel (2-3 cells in width), and generally the changes are extremely small.

150. Based upon these results, the nested (refined grid) approach is appropriate for studying or identifying the extent of channel alterations on the local circulation pattern. To study circulation patterns within the channel area, a three-dimensional or two-dimensional laterally averaged model is needed.

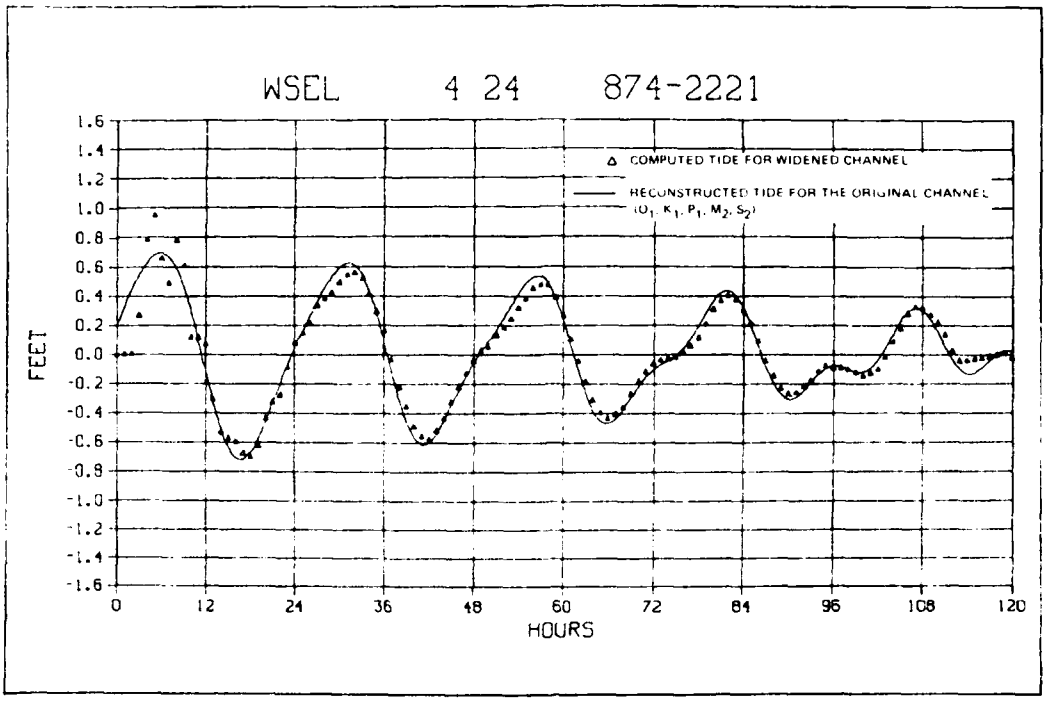

Figure XII-12. Computed and reconstructed water surface elevations at station 874-2221, 20-24 September 1980 (660-ft channel)

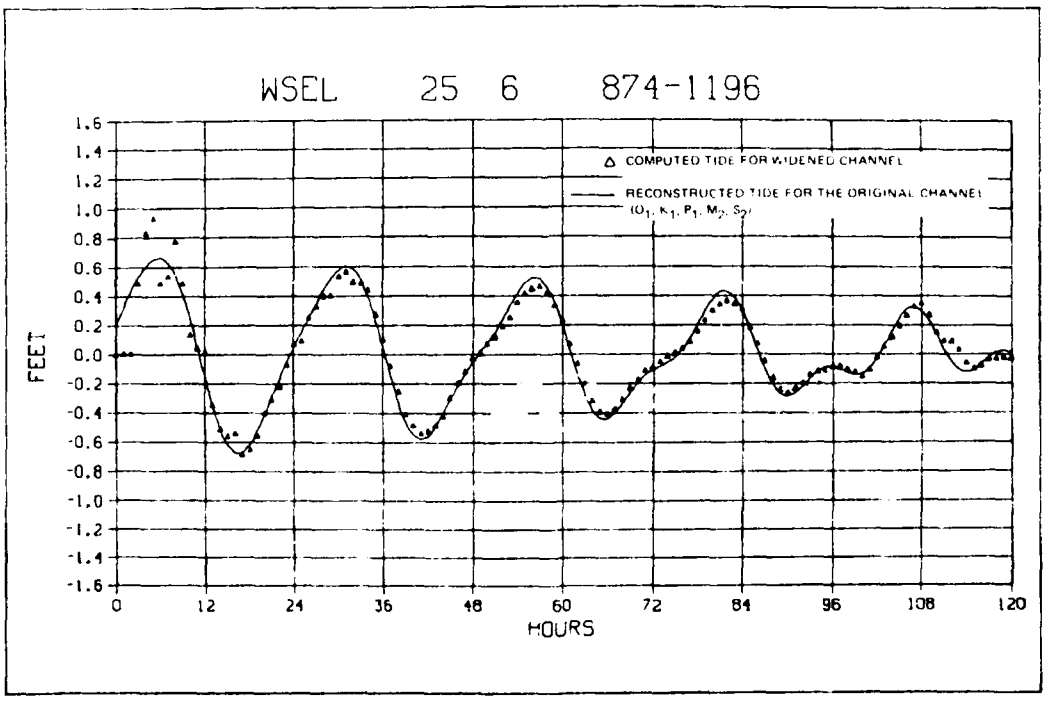

Figure XII-13. Computed and reconstructed water surface elevations at station 874-1196, 20-24 September 1980 (660-ft channel)

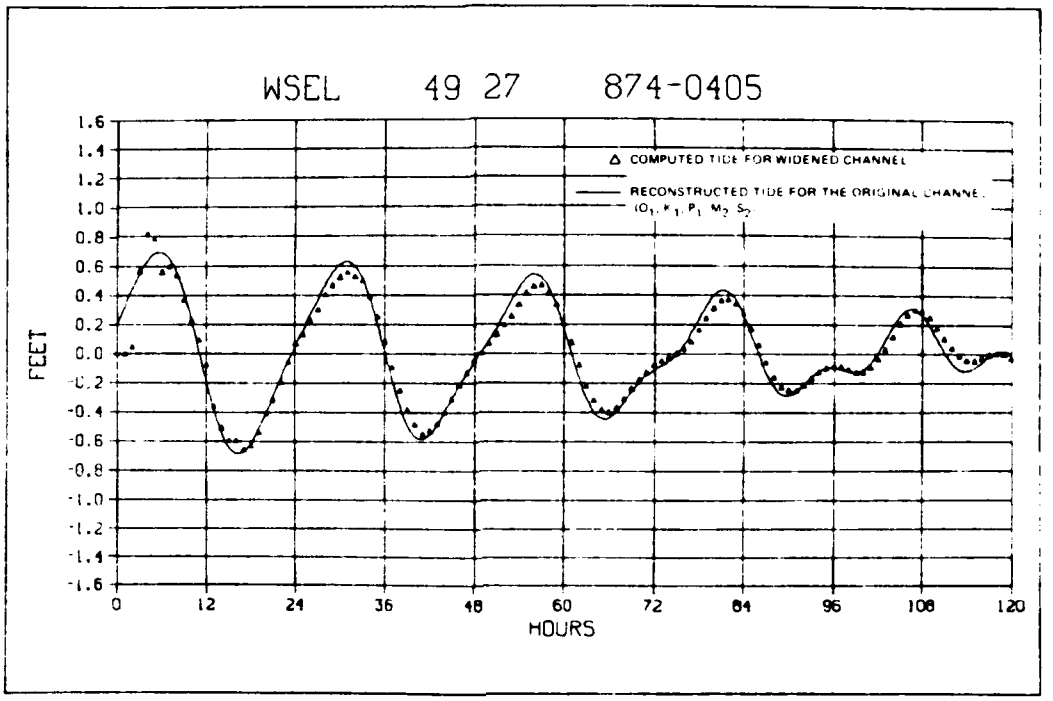

Figure XII-14. Computed and reconstructed water surface elevations at station 874-0405, 20-24 September 1980 (660-ft channel)

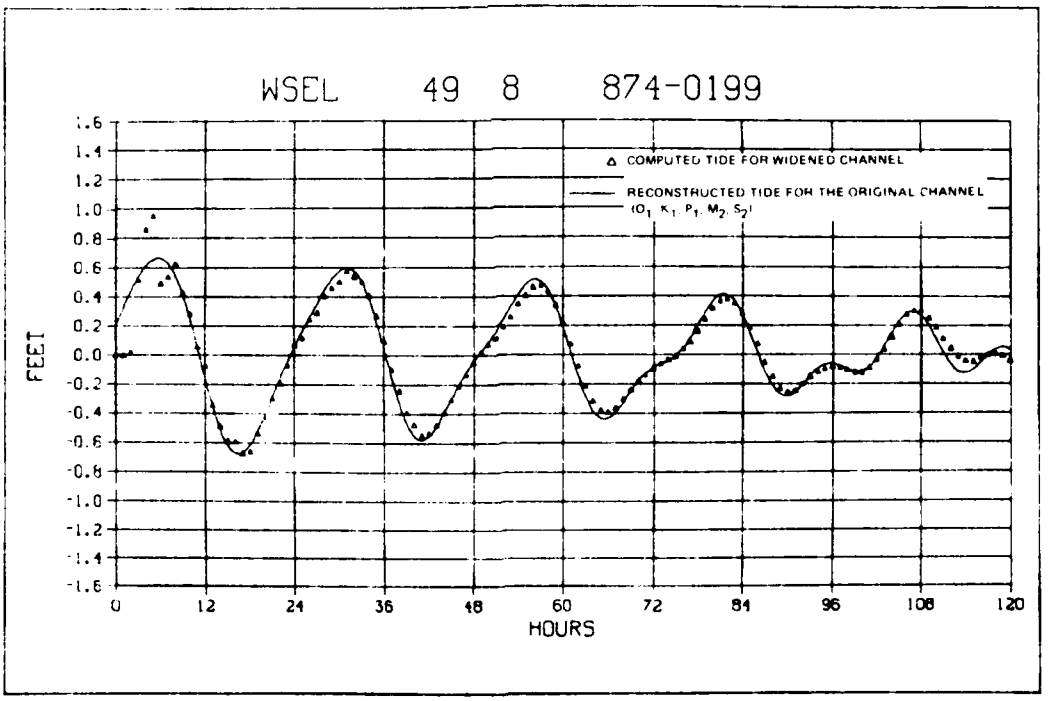

Figure XII-15. Computed and reconstructed water surface elevations at station 874-0199, 20-24 September 1980 (660-ft channel)

Table XII-2

Simulated Velocity Components (fps × 10) for the 330-ft Channel Width at Hour 72

V/U FLOW AT T = 72.0000 HRS

M N	14	15	16	17	18	19	20	21	22	23	24	25	26	27	28	29	30	31	32	33	34	35	36	37	38	39	40	41	42	43
1	0	0	0	0	0	0	0	0	0	0	0	0	0	0	0	0	0	0	0	0	0	0	0	0	0	0	0	0	0	0
	0	0	11	0	0	0	0	0	0	0	0	0	0	0	0	0	0	0	0	0	0	0	0	0	0	0	0	0	0	0
2	0	0	0	0	0	0	0	0	0	0	0	0	0	0	0	0	0	0	0	0	0	0	0	0	0	0	0	0	0	0
	0	3	7	3	0	0	0	0	0	0	0	0	0	0	0	0	0	0	0	0	0	0	0	0	0	0	0	0	0	0
3	0	0	0	0	0	0	0	0	0	0	0	0	0	0	0	0	0	0	0	0	0	0	0	0	0	0	0	0	0	0
	0	4	6	2	0	0	0	0	0	0	0	0	0	0	0	0	0	0	0	0	0	0	0	0	0	0	0	0	0	0
4	0	0	0	0	0	0	0	0	0	0	0	0	0	0	0	0	0	0	0	0	0	0	0	0	0	0	0	0	0	0
	0	4	6	0	0	0	0	0	0	0	0	0	0	0	0	0	0	0	0	0	0	0	0	0	0	0	0	0	0	0
5	0	0	0	0	0	0	0	0	0	0	0	0	0	0	0	0	0	0	0	0	0	0	0	0	0	0	0	0	0	0
	5	0	10	1	0	0	0	0	0	0	0	0	0	0	0	0	0	0	0	0	0	0	0	0	0	0	0	0	0	0
6	0	0	0	-1	-1	-2	-3	-2	0	0	1	1	1	0	0	0	0	0	0	0	0	0	0	0	0	0	0	0	0	0
	4	2	12	2	1	1	0	0	0	0	0	-1	0	0	0	0	0	0	0	0	0	1	0	0	0	0	0	0	0	0
7	-1	0	0	-2	-2	-2	-3	-2	-1	0	0	0	0	0	0	0	0	0	0	0	0	0	0	0	0	0	0	0	0	0
	1	2	11	2	0	0	0	-1	-1	-1	-2	-2	-2	-2	-2	-2	-2	-2	-1	-1	-1	-1	-1	-2	-2	0	0	0	0	0
8	-1	0	0	-3	-3	-3	-3	-2	-1	0	1	1	1	0	0	0	0	0	0	0	0	0	0	0	0	0	0	0	0	0
	2	2	12	2	0	-1	-1	-4	-4	-4	-4	-4	-4	-4	-5	-4	-4	-4	-4	-5	-5	-4	-1	-4	-4	-3	0	0	0	0
9	-7	-2	-1	-4	-3	-3	-2	-1	0	1	1	2	1	0	0	0	0	0	0	0	0	0	0	0	-3	-2	-2	-2	-1	0	1
	-6	-3	7	-3	-5	-5	-5	-7	-6	-6	-6	-6	-6	-6	-5	-5	-5	-5	-5	-4	-4	-3	1	-4	-4	-4	-3	-3	-3	-1	
10	-3	-1	0	-2	-2	-1	-1	0	1	2	3	3	2	1	1	0	0	0	0	0	0	0	0	0	-1	0	0	0	0	0	0
	-8	-6	6	-6	-7	-6	-6	-7	-5	-7	-6	-6	-6	-6	-5	-5	-5	-5	-5	-4	-4	-3	4	-3	-5	-4	-4	-4	-3	-1	
11	0	0	0	0	0	0	0	1	1	2	3	3	3	2	2	1	1	1	1	1	0	0	0	0	0	0	0	0	0	0	0
	-9	-7	5	-6	-8	-7	-6	-7	-5	-6	-5	-5	-5	-5	-4	-5	-4	-4	-3	-3	-3	-2	7	-2	-4	-3	-3	-3	-2	-1	
12	0	0	0	0	0	0	0	1	1	1	2	2	1	1	1	0	0	0	0	0	0	0	0	0	0	0	0	0	0	0	0
	-7	-5	4	-4	-7	-4	-7	-6	-5	-4	-4	-4	-4	-3	-3	-3	-2	-2	-2	-2	-1	7	-1	-2	-2	-2	-2	-1	0		
13	-3	-1	0	-2	-4	-5	-4	-3	-2	-2	-1	-1	-1	-1	0	0	0	0	0	0	0	0	0	0	0	0	0	0	0	0	0
	-5	-5	1	-1	-1	-2	-2	-2	-1	-1	-1	-1	-1	-1	-1	-1	-1	-1	-1	-1	-1	0	7	-1	-2	-2	-1	-1	-1	0	
14	-6	-1	2	4	4	3	1	0	-2	-3	-4	-4	-4	-3	-2	-1	-1	0	0	0	0	0	0	0	0	0	0	0	0	0	0
	-4	-7	-2	0	-2	-2	-2	-1	-1	-1	-1	-1	-1	-1	-1	-1	-1	-1	-1	-1	-1	0	7	0	-2	-2	-1	-1	-1	0	
15	-3	-7	-5	-3	-4	-4	-5	-5	-5	-4	-3	-2	-1	-1	0	0	0	0	0	0	0	0	0	0	0	0	0	0	0	0	0
	-4	-5	-7	-3	-4	-4	-4	-3	-3	-3	-3	-3	-3	-3	-3	-3	-3	-3	-3	-2	-2	0	7	0	-1	-1	-1	-1	-1	0	
16	-3	-5	-5	-4	-4	-4	-5	-5	-4	-4	-3	-2	-1	0	0	0	0	0	0	0	0	0	0	0	0	0	0	0	0	0	0
	-4	-3	-6	-4	-4	-4	-4	-3	-3	-3	-2	-3	-3	-4	-3	-3	-3	-2	-2	-2	-2	0	7	0	-1	-1	-1	-1	-1	0	
17	-4	-4	-4	-4	-4	-5	-5	-5	-5	-4	-3	-2	-1	0	0	0	0	0	0	0	0	0	0	0	0	0	0	0	0	0	0
	-4	-4	-5	-4	-4	-4	-4	-3	-3	-3	-3	-3	-3	-4	-3	-3	-2	-2	-2	-2	-1	0	7	0	-1	-1	-1	-1	0	0	
18	-4	-4	-4	-4	-4	-4	-5	-4	-4	-5	-2	-1	0	0	0	0	0	0	0	0	0	0	0	0	0	0	0	0	0	0	1
	-3	-3	-4	-4	-4	-4	-4	-3	-4	-3	-4	-4	-4	-3	-4	-3	-2	-1	-1	-1	-1	0	7	0	-1	-1	0	0	0	-1	
19	-5	-5	-5	-5	-5	-5	-5	-4	-3	-2	-1	-1	0	0	0	0	0	0	0	0	0	0	0	0	0	1	1	1	1	1	
	-3	-3	-3	-3	-3	-3	-3	-4	-4	-5	-5	-5	-5	-5	-4	-3	-2	-2	-1	-1	-1	0	7	0	-1	-1	-1	0	0	-3	
20	-7	-7	-7	-7	-7	-6	-6	-5	-4	-3	-1	0	0	0	1	1	1	1	1	1	1	1	1	1	1	1	1	1	1	1	2
	-2	-3	-3	-3	-3	-3	-3	-7	-6	-7	-7	-7	-7	-6	-3	-3	-3	-3	-2	-1	0	7	-1	-1	-1	-1	-1	-1	-1	-4	
21	-6	-6	-5	-4	-4	-6	-6	-6	-4	-3	-1	0	1	2	2	2	3	3	3	3	2	1	1	2	2	2	2	2	2	3	
	-2	-2	-2	-2	-2	-2	-2	-10	-8	-10	-11	-11	-11	-10	-10	-5	-4	-4	-4	-4	-2	-1	7	-2	-2	-2	-1	-1	-1	-6	
22	-10	-9	-9	-10	-10	-8	-8	-7	-5	-3	-1	0	2	3	4	4	4	4	5	5	5	3	2	4	4	4	4	4	4	4	
	-1	-1	-2	-2	-2	-2	-2	-16	-14	-15	-16	-16	-16	-14	-13	-9	-8	-7	-6	-6	-5	-4	9	-4	-4	-4	-2	-2	-1	-8	
23	-12	-12	-12	-12	-12	-11	-9	-7	-5	-2	0	1	4	5	7	7	8	8	8	8	8	5	4	7	7	7	7	8	8	8	
	-1	-2	-3	-4	-5	-7	-7	-22	-20	-22	-23	-20	-19	-18	-18	-12	-11	-11	-11	-12	-10	-8	10	-7	-8	-7	-6	-5	-4	-10	
24	-16	-16	-15	-14	-13	-10	-3	-1	0	2	6	7	9	10	12	13	13	12	14	15	13	8	8	15	16	15	15	14	15	13	
	-6	-11	-14	-21	-25	-30	-32	-35	-33	-32	-32	-29	-27	-25	-24	-13	-7	-8	-16	-20	-19	-22	6	-12	-7	-6	-5	-4	-5	-7	
25	-16	-23	-28	-23	-15	-7	2	0	2	4	7	10	10	10	10	13	12	11	13	14	21	13	13	22	22	21	21	21	22	22	
	0	0	0	-48	-44	-42	-39	-22	-26	-27	-32	-31	-32	-31	-33	-38	0	0	-39	-25	-33	-23	-12	-43	0	0	0	0	0	6	
26	5	6	6	5	3	0	-5	-14	-12	-12	-9	-8	-6	-5	-4	-5	-1	0	0	0	0	0	0	0	0	0	0	0	0	0	1
	-4	-2	-4	-6	-7	-6	-6	6	-19	-16	-26	-21	-23	-19	-21	-23	-23	-25	-22	-24	-20	-22	-24	0	0	0	0	0	0	0	
27	-4	-5	-6	-7	-8	-10	-13	-13	-14	-20	-23	-22	-20	-21	-23	-20	-18	-15	-14	-14	-14	-11	-12	-17	-15	-13	-11	-9	-4	1	
	5	9	5	5	6	7	7	3	0	-8	-16	-15	-19	-24	-27	-23	-21	-24	-22	-23	-23	-22	-22	-22	-22	-22	-22	-22	-20	-20	-18
28	0	0	0	0	0	0	0	0	0	0	0	0	0	0	0	0	0	0	0	0	0	0	0	0	0	0	0	0	0	0	
	0	0	0	0	0	0	0	0	0	0	0	0	0	0	0	0	0	0	0	0	0	0	0	0	0	0	0	0	0	0	

Table XII-3

Simulated Velocity Components (fps × 10) for the 660-ft Channel Width at Hour 72

V/U FLOS AT T = [illegible]

M \ N	14	15	16	17	18	19	20	21	22	23	24	25	26	27	28	29	30	31	32	33	34	35	36	37	38	39	40	41	42	43
1	0	0	0	0	0	0	0	0	0	0	0	0	0	0	0	0	0	0	0	0	0	0	0	0	0	0	0	0	0	0
	0	0	11	0	0	0	0	0	0	0	0	0	0	0	0	0	0	0	0	0	0	0	0	0	0	0	0	0	0	0
2	0	0	0	0	0	0	0	0	0	0	0	0	0	0	0	0	0	0	0	0	0	0	0	0	0	0	0	0	0	0
	0	3	5	5	0	0	0	0	0	0	0	0	0	0	0	0	0	0	0	0	0	0	0	0	0	0	0	0	0	0
3	0	0	0	0	0	0	0	0	0	0	0	0	0	0	0	0	0	0	0	0	0	0	0	0	0	0	0	0	0	0
	0	3	5	4	0	0	0	0	0	0	0	0	0	0	0	0	0	0	0	0	0	0	0	0	0	0	0	0	0	0
4	0	0	0	0	0	0	0	0	0	0	0	0	0	0	0	0	0	0	0	0	0	0	0	0	0	0	0	0	0	0
	0	4	5	4	0	0	0	0	0	0	0	0	0	0	0	0	0	0	0	0	0	1	1	0	0	0	0	0	0	0
5	0	0	0	0	0	0	0	0	0	0	0	0	0	0	0	0	0	0	0	0	0	0	0	0	0	0	0	0	0	0
	5	0	7	5	0	0	0	0	0	0	0	0	0	0	0	0	0	0	0	0	0	1	1	0	0	0	0	0	0	0
6	0	0	0	0	0	0	0	-1	-1	-2	-2	-2	-1	0	0	0	0	0	0	0	0	0	0	0	0	0	0	0	0	0
	1	0	7	6	0	-1	-2	-2	-2	-2	-2	-2	-1	0	0	0	0	0	0	0	2	2	1	0	0	0	0	0	0	0
7	0	0	0	0	-1	-1	-2	-2	-1	-1	-1	-1	-1	0	0	-1	-1	-1	-1	-1	-1	0	0	0	0	0	0	0	0	0
	0	1	7	7	0	-1	-2	-3	-3	-3	-3	-3	-2	-2	-2	-2	-1	-1	-1	-1	0	0	0	-1	-1	0	0	0	0	0
8	0	0	0	0	-3	-3	-3	-2	-1	0	0	0	0	0	0	0	0	0	0	0	0	0	0	0	0	0	0	0	0	0
	2	3	3	2	0	-1	-4	-4	-4	-4	-4	-4	-4	-4	-4	-3	-3	-3	-3	-3	-4	-5	0	-3	-3	-1	0	0	0	0
9	-7	-2	0	-1	-2	-2	-1	0	0	0	0	1	1	0	0	0	0	0	0	0	0	0	0	-2	-2	-1	-1	0	0	2
	-5	-2	4	5	-2	-3	-4	-5	-5	-5	-5	-5	-5	-5	-5	-4	-4	-4	-4	-4	-3	-2	2	-3	-4	-3	-3	-3	-2	-1
10	-3	-1	0	0	0	0	0	0	1	1	1	2	1	1	1	1	1	1	1	1	1	0	0	0	0	0	0	0	0	1
	-8	-7	2	3	-6	-7	-7	-8	-7	-7	-7	-7	-6	-6	-5	-5	-5	-4	-4	-4	-4	-2	5	-3	-5	-4	-4	-4	-3	-1
11	0	0	0	0	0	1	1	1	2	2	2	2	2	2	2	2	2	1	1	1	1	0	0	0	0	0	0	0	0	0
	-5	-5	1	2	-6	-7	-9	-9	-9	-8	-7	-6	-5	-5	-4	-5	-4	-4	-3	-3	-3	-2	8	-2	-4	-4	-4	-3	-2	-1
12	0	0	0	0	0	0	1	1	1	1	1	1	1	2	2	1	1	0	0	0	0	0	0	0	0	0	0	0	0	0
	-6	-5	1	2	-5	-10	-8	-7	-6	-6	-5	-4	-4	-3	-3	-2	-2	-2	-2	-2	-2	0	9	-1	-3	-3	-3	-3	-2	-1
13	-3	-1	0	0	-5	-5	-3	-3	-2	-2	-1	0	0	0	0	0	0	0	0	0	0	-1	-2	-1	-2	-1	-1	-1	0	0
	-6	-5	0	1	0	-3	-3	-2	-2	-2	-2	-1	-1	-1	-1	-1	-1	-1	0	0	0	2	8	-2	-4	-3	-3	-3	-2	-1
14	-7	-2	0	1	2	2	1	0	0	0	-1	-1	-1	-1	0	0	0	0	0	0	0	0	0	0	0	0	0	0	0	0
	-5	-6	-1	0	0	-2	-2	-1	-1	-1	-1	-1	-1	0	0	0	0	0	0	0	0	2	7	-2	-4	-3	-3	-2	-2	-1
15	-6	-2	0	1	2	1	0	0	-1	-1	-1	-1	-1	0	0	0	1	1	1	1	1	0	0	1	0	0	0	0	0	0
	-4	-6	-4	-3	-1	-2	-2	-2	-2	-1	-1	-1	-1	-1	-1	-1	-1	-1	-1	-1	0	3	7	-1	-3	-3	-2	-2	-2	-1
16	-2	-5	-6	-5	-4	-5	-5	-5	-4	-3	-3	-3	-2	-1	0	0	0	0	0	0	0	1	1	0	0	0	0	0	0	0
	-4	-4	-8	-7	-4	-5	-5	-4	-4	-3	-3	-3	-3	-3	-3	-3	-3	-2	-2	-2	-2	0	4	7	-1	-3	-2	-2	-2	-1
17	-3	-3	-4	-5	-4	-4	-5	-5	-5	-4	-3	-2	0	0	0	0	0	0	0	0	0	0	0	0	0	0	0	0	0	0
	-4	-4	-6	-6	-5	-5	-5	-4	-4	-3	-3	-3	-3	-3	-3	-3	-2	-2	-2	-2	0	5	7	-1	-2	-2	-2	-2	-2	-1
18	-4	-4	-4	-4	-4	-5	-5	-4	-3	-2	-1	0	0	0	0	1	0	0	0	0	0	0	0	0	0	0	0	0	0	1
	-3	-3	-4	-4	-4	-4	-4	-4	-4	-4	-4	-3	-4	-3	-4	-3	-2	-1	-1	-1	0	6	7	-1	-2	-2	-2	-2	-1	-3
19	-5	-5	-5	-5	-5	-6	-6	-5	-3	-2	-1	0	0	0	1	1	1	1	1	1	0	0	0	1	1	1	1	1	0	1
	-2	-3	-3	-3	-3	-3	-3	-4	-4	-4	-5	-5	-4	-4	-4	-3	-2	-2	-2	-1	-1	7	6	-1	-2	-2	-2	-2	-1	-4
20	-7	-7	-8	-8	-7	-7	-7	-5	-4	-3	-1	0	0	1	1	1	1	2	1	1	1	0	1	1	1	1	1	1	1	2
	-2	-2	-2	-3	-3	-2	-2	-6	-5	-6	-7	-7	-7	-6	-6	-3	-3	-3	-3	-2	-1	7	6	-2	-2	-2	-2	-2	-2	-5
21	-9	-9	-9	-9	-9	-9	-9	-6	-5	-3	-1	0	1	2	3	3	3	3	3	3	3	1	1	1	2	2	2	2	2	3
	-2	-2	-2	-2	-2	-2	-1	-10	-8	-10	-10	-10	-10	-9	-9	-4	-3	-4	-3	-3	-2	7	6	-3	-3	-3	-2	-2	-2	-7
22	-10	-10	-10	-10	-10	-10	-10	-7	-5	-3	-1	1	2	3	4	4	5	5	5	5	3	2	2	4	4	4	3	4	3	4
	-1	-1	-1	-2	-2	-2	-2	-15	-15	-15	-16	-16	-16	-14	-13	-8	-7	-6	-6	-5	-5	8	7	-4	-5	-5	-3	-3	-2	-9
23	-13	-13	-13	-12	-12	-11	-10	-7	-5	-2	0	2	4	5	7	8	8	8	8	8	5	3	4	7	7	7	7	8	8	8
	-1	-2	-3	-4	-5	-6	-7	-22	-20	-22	-23	-20	-19	-18	-18	-12	-11	-10	-10	-11	-9	8	7	-8	-9	-8	-7	-6	-5	-11
24	-17	-16	-15	-14	-13	-10	-3	-1	0	2	6	9	9	11	13	13	14	13	15	16	8	6	8	16	16	15	15	15	15	13
	-8	-11	-15	-21	-25	-30	-32	-35	-33	-33	-33	-30	-27	-25	-25	-13	-7	-8	-16	-20	-20	5	5	-13	-9	-7	-6	-6	-6	-8
25	-17	-24	-30	-24	-16	-9	1	0	2	4	8	10	10	10	9	12	11	10	12	14	11	9	14	22	23	22	21	22	23	23
	0	0	0	-49	-45	-43	-39	-23	-27	-28	-33	-31	-32	-31	-34	-39	0	0	-40	-25	-33	-11	-12	-42	0	0	0	0	0	5
26	5	5	6	4	2	-1	-6	-15	-12	-12	-9	-8	-6	-5	-4	-5	-1	0	0	0	0	0	0	0	0	0	0	0	0	1
	-3	-2	-3	-6	-6	-6	-6	5	-20	-17	-26	-21	-23	-20	-22	-24	-23	-23	-25	-22	-22	-17	-19	-24	0	0	0	0	0	0
27	-4	-6	-7	-8	-9	-11	-14	-13	-19	-21	-23	-23	-21	-22	-24	-21	-19	-17	-15	-15	-12	-9	-12	-17	-15	-13	-11	-8	-4	1
	6	10	6	3	6	7	8	3	0	-9	-15	-15	-18	-24	-27	-23	-22	-24	-21	-23	-22	-22	-22	-22	-22	-22	-22	-20	-20	-18
28	0	0	0	0	0	0	0	0	0	0	0	0	0	0	0	0	0	0	0	0	0	0	0	0	0	0	0	0	0	0
	0	0	0	0	0	0	0	0	0	0	0	0	0	0	0	0	0	0	0	0	0	0	0	0	0	0	0	0	0	0

PART XIII: SALINITY CALIBRATION ON THE GLOBAL AND REFINED GRID SYSTEMS

151. The simulation of salinity requires the consideration of meteorological as well as astronomical effects. Atmospheric pressure anomalies were not considered in this study. Predominate meteorological effects in most cases are due to wind. Therefore, the wind pattern must be studied for the period of consideration. The wind pattern is applied to develop a surface shear stress, which affects the hydrodynamic computations. Wind effects were not considered in the GTM simulations used to specify elevations along the boundary of the global grid. In performing combined global and refined grid simulations, the same wind pattern applied over the global grid is applied over the refined grid to develop the water surface shear stress effects over this grid. During the global grid simulation, water surface elevations and salinities are saved at various points within the global grid, which encompass the refined grid area. During the simulation on the refined grid, the previously saved water surface elevations and salinities are accessed to develop the appropriate boundary conditions.

Wind stress relations

152. The following form of wind stress is employed

$$\tau_w = C_D \rho_a V_w^2 \qquad \text{(XIII.1)}$$

where

τ_w = wind stress on the water surface
C_D = dimensionless drag coefficient
V_w = wind speed at the anemometer level
ρ_a = air density

153. Several relationships are available for the determination of C_D. Wilson (1962) employs $C_D = 0.0015$ for light wind conditions. Van Dorn (1953) employs $C_D = 0.000923$ for winds less than or equal to 14 knots.

154. Garret (1977) suggests the following power law relation

$$C_D \times 10^3 = 0.51 V_w^{0.46} \qquad \text{(XIII.2)}$$

where V_w is measured at the anemometer level in knots. (Note: 1 knot = 1.6884 fps = 0.5146 mps.) Evaluating XIII-2 at 14 knots, one obtains C_D = 0.00126 .

155. We observe the units of stress in Equation XIII-1 above are force per unit area (M/LT^2). In the motion equations in the x and y directions, the units are in terms of acceleration (L/T^2). Thus, in applying Equation XIII-1 to a motion equation, one divides the stress by the product of water density and depth; e.g., $(L/T^2) = (M/LT^2)/(M/L^2)$. Formally,

$$a_w = \frac{C_D \rho_a V_w^2}{\rho D} = \frac{K}{D} V_w^2 \qquad \text{(XIII.3)}$$

where

a_w = acceleration induced by wind stress
D = water depth
ρ_a = air density
ρ = water density
V_w = wind speed at the anemometer level
K = dimensionless coefficient

If we use $C_D = 0.001$, we obtain $K = 1.191 \times 10^{-6}$. If we employ British units (slug, ft, sec), and V_w is given in mph , we multiply K by $(1.4667)^2$ to obtain 2.562×10^{-6} . This is the coefficient employed in the computer code.

Dispersion coefficients

156. The effective dispersion coefficients are assumed to have the form given in Equation V.64. The dispersion offsets due to wind are assumed equal to zero.

Global Grid Salinity Simulations

12-16 June 1980

157. This period was originally considered as a verification of the salinity computations. Initial conditions in Mississippi Sound were developed on the global grid based on salinity transect data. In order to verify the effective dispersion coefficients, model results were to be compared with continuous salinity data at the end of the 5-day period. Upon further study of the continuous salinity data and comparison with the salinity transect data

at common time and spatial location, it appeared that the continuous data were always lower than the transect data. Raytheon Ocean Systems acknowledged a biological fouling problem with the conductivity-temperature probe. Continuous salinity values always increased drastically after the meters were serviced. As a result of these data uncertainties, it was decided not to consider this period in the salinity study.

20-24 September 1980

158. This period was selected for calibration of the dispersion coefficients in the salinity algorithm. Salinity transect values were available on 20 and 21 September. These values were located on the global grid and two rectangular areas were set up in which salinity values were visually interpolated from the located transect values. National Marine Fisheries (1981) data were obtained for cruises #106 (April 1980) and #112 (November 1980) of the OREGON II. These data provided a general understanding of salinity patterns in the vicinity of the Mississippi Delta. A deep sea vertically averaged value of 36 parts per thousand was employed.

159. Initial conditions were assigned in a three-step process as shown in Table XIII-1. In step one, values were assigned based on cell water depth. In step two, salinity values were specified within Mississippi Sound based on salinity transect data. In step three, initial salinity values within Lake Borgne were specified in a zone format. In this process each succeeding step overrides the previous step.

160. Salinity boundary conditions which remained constant over time are shown in Table XIII-2. A cell-centered spatial interpolation analogous to that employed for water surface elevations was used to determine salinity values along the seaward boundary.

161. Meteorological effects were treated in the following manner. The surge setup due to tropical storm Hermine was approximately in the range 0.1-0.5 ft. The effect causes an increase or shift in the nodal datum corresponding to local mean sea level equal to the setup, which is less than 0.5 ft. Since soundings are not known to this accuracy in most areas of the Sound, the surge setup effect is negligible and was not considered. However, if one attempts to compare simulated water levels with the unfiltered (raw) elevation data, then the datum of simulated levels must be adjusted by this surge setup. Wind data over the period are presented in Table XIII-3. Based upon a study of the spatial and temporal wind variations shown in Table XIII-3,

Table XIII-1

Initial Salinity Conditions on the Global Grid

Water Depth ft	Initial Salinity Value, ppt
0 - 10	22.0
10 - 20	23.0
20 - 30	25.0
30 - 50	30.0
50 - 75	34.0
75 - 100	34.3
100 - 120	34.5
120 - 200	35.0
200 - 300	35.5
300 - 5000	36.0

Salinity Grid Cell by Grid Cell Interpolated Limits

Patch	Global Grid Cell Range N	M
1	15 - 27	19 - 39
2	28 - 87	15 - 32

Salinity Zone Specified Initial Conditions

Zone	Global Cell Range N	M	Salinity ppt
1	1 - 15	33 - 50	15.0

Table XIII-2

Global Grid Boundary Salinity Conditions

Tidal Signal	Global Grid Cell	Salinity Value, ppt
1	(115, 58)	36.0
2	(115, 56)	36.0
3	(115, 50)	36.0
4	(115, 37)	36.0
5	(115, 22)	34.0
6	(31, 59)	30.0
7	(42, 59)	36.0
8	(57, 59)	36.0
9	(73, 59)	36.0
10	(87, 59)	36.0
11	(103, 59)	36.0
12	(110, 59)	36.0
13	(112, 59)	36.0
14	(115, 59)	36.0

Fresh-water Inflow	Global Grid Cell*	Salinity Value, ppt
1	(97, 3)	0.0
2	(59, 19)	24.0
3	(59, 17)	24.0
4	(13, 33)	15.0
5	(19, 20)	17.0
6	(33, 15)	23.0

* Refer to Table VI-9.

Table XIII-3

Wind Data for 20-24 September 1980

Julian Day	GMT Hour	MET 1		MET 3		MET 4		MET 5		Average Speed/ Direction
		Speed	Direction	Speed	Direction	Speed	Direction	Speed	Direction	
	24	4.9	123	12.5	110	9.1	114	12.0	103	9.6/112
264	6	4.3	156	4.6	154	7.4	162	12.8	156	7.3/157
	12	4.1	154	3.4	46	3.1	122	10.3	100	5.2/105
	18	5.1	135	8.3	152	7.4	142	9.7	134	7.6/141
	24	4.7	145	6.8	156	4.5	157	7.3	152	5.8/152
265	6	4.7	141	9.3	148	7.8	142	13.3	163	8.7/148
	12	6.1	192	3.7	195	3.2	160	6.6	138	4.9/171
	18	4.8	130	8.1	158	6.5	135	6.6	144	6.5/142
	24	5.8	153	9.0	153	6.3	160	7.9	168	7.2/158
266	6	11.1	167	8.1	160	5.0	163	8.1	153	8.0/161
	12	7.1	176	4.0	184	3.7	162	7.3	148	5.5/167
	18	4.6	153	7.0	170	6.0	102	6.2	143	5.9/142
	24	6.9	154	8.9	165	6.6	167	8.0	177	7.6/166
267	6	7.0	172	4.9	181	3.0	164	3.8	171	4.6/172
	12	3.4	35	6.2	357	2.8	15	1.4	31	3.4/27
	18	4.7	123	8.7	147	9.1	87	3.9	77	6.6/108
	24	5.6	159	7.5	163	5.7	162	8.2	157	6.7/160
268	6	8.2	180	6.8	176	5.1	166	9.6	158	7.4/170
	12	2.9	147	4.1	73	3.7	161	6.2	166	4.2/137
	18	3.6	188	8.3	184	4.5	238	4.3	193	5.1/201
	24	5.2	154	7.5	156	5.4	145	8.9	156	6.7/153*

Note: MET 2 was nonfunctioning this period.
MET 3 and MET 1 are "land" stations.
MET 4 and MET 5 are "island" stations.
Speed (mph).
Direction (magnetic).
GMT = CST + 6 hr.
* For Julian Day 269, GMT hr 6; average speed/direction = 9.4/158.

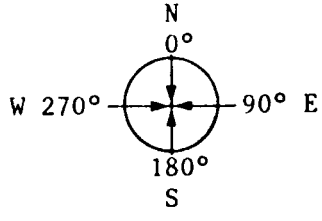

wind speed and direction were spatially averaged at 6-hr intervals.

162. A time step of 360 sec was employed 1200 times in order to simulate a 120-hr period starting at hour 0000 CST, 20 September. In order to remove the effects of transients in the hydrodynamics from the salinity computations, salinity computations were initiated after 240 time steps (1 day prototype time). Thus salinity computations were performed over the period 21-24 September. The initial conditions specified over the western portion of the Sound corresponded to the transect data taken on 20 September. Since salinity time variations in salinity were extremely small during this period, it was assumed that conditions on 21 September were effectively equal to conditions on 20 September. Simulation results at the end of the simulation (hour 2400 CST 24 September) were compared with transect data obtained over the western half of the Sound during the day of 24 September and over the eastern half of the Sound during the day of 25 September. Since time variations in salinity were extremely small, this was felt to be a valid procedure. Wind information input at 6-hr intervals was interpolated in time at each time step. Both salinity schemes were considered using the effective dispersion coefficient parameters shown in Table XIII-4. Note that C_x and C_y are in the interval of experimentally determined values (5.93, 20.2) as developed in Part V. The reduction factor, $F = 0.0388$, employed equals the ratio of the lateral to longitudinal dispersion coefficient as determined by Elder (1959) as reported in Part V. Therefore, the values of the calibrated dispersion coefficients are within the range of or are equal to experimentally determined values. The scheme 1 FCT results and the scheme 2 three-time level results are compared with measured data as shown in Table XIII-5. In most regions of the Sound, the scheme 1 and scheme 2 results are nearly identical and are in agreement with measured salinity values. However, in the vicinity of the Upper Mobile Bay freshwater inflow the results diverge as shown in Table XIII-6. The scheme 1 results are nonnegative and exhibit no oscillations. The scheme 2 results exhibit oscillations behind the freshwater front. Thus in order to study sharp front problems, scheme 1 is recommended.

Refined Grid Salinity Simulation

163. The 20-24 September period was simulated on the Pascagoula Channel refined grid using the Scheme 1 FCT approach. Boundary salinity and elevations

Table XIII-4

Calibrated Dispersion Coefficient Parameters

$C_x = C_y = 10$
$D_x = D_y = 0$
Reduction factor (F) = 0.0388

Table XIII-

Transect Station	Global Grid Cell	20-21 Sep 1980 Measured	Initial Condition	24 Sep 1980 Measured	Computed 1	Computed 2
T26	(15,39)	16.0	16.0	14.2	19.9	20.5
T30	(16,35)	17.0	17.0	17.2	17.4	18.4
T28	(16,38)	17.3	17.0	15.1	17.9	18.0
T32	(18,33)	17.5	17.0	17.6	17.9	17.9
T24	(18,38)	19.2	19.0	19.3	20.2	20.2
T34	(20,31)	19.2	19.0	19.5	19.4	19.4
T22	(21,35)	23.7	24.0	21.8	23.7	24.1
T36	(23,29)	21.8	22.0	21.1	21.5	20.8
T20	(24,33)	24.9	25.0	24.1	25.3	25.5
T38	(26,29)	22.0	22.0	23.1	22.2	26.0
T40	(27,24)	22.4	22.0	21.0	22.3	22.4
T18	(27,33)	26.8	27.0	25.7	24.3	23.2
T42	(29,26)	23.7	24.0	23.0	23.2	23.1
T6	(29,20)	24.0	24.0	23.8	24.1	24.1
T8	(31,23)	24.8	25.0	23.9	25.0	25.2
T10	(32,26)	25.6	26.0	25.0	25.0	25.0
T12	(33,29)	27.3	27.0	25.5	25.8	25.7
T4	(34,23)	25.2	25.0	23.9	24.5	24.3
T14	(34,31)	28.3	28.0	27.1	25.6	24.6
T16	(34,32)	28.3	28.0	26.8	26.1	26.1
T2	(40.27)	26.1	26.0	25.6	26.1	26.4
T44	(49,21)	23.6	24.0	23.4	25.2	25.3
T46	(49,24)	26.9	27.0	26.2	25.9	25.5
T48	(49,27)	28.2	28.0	27.8	27.4	28.1
T50	(49,29)	28.3	28.0	28.7	27.5	27.2
T52	(53,25)	26.3	26.0	26.7	26.1	26.0
T54	(57,28)	27.3	27.0	27.6	28.8	28.8
T64	(59,21)	27.7	28.0	27.5	27.8	28.7
T62	(60,23)	28.5	28.0	26.8	27.8	28.3
T66	(62,22)	27.3	27.0	27.7	27.0	26.9
T60	(62,24)	28.1	28.0	29.1	27.5	27.4
T58	(62,28)	29.1	29.0	29.6	28.4	28.2
T56	(62,32)	29.7	30.0	30.3	30.0	29.4
T68	(67,26)	27.9	28.0	27.5*	28.1	28.2
T70	(71,28)	28.4	28.0	29.9*	28.1	28.1
T74	(75,26)	28.1	28.0	--	28.4	28.3
T72	(75,30)	28.7	29.0	28.5*	26.3	26.9
T76	(76,25)	26.6	27.0	--	28.1	28.0
T78	(81,25)	22.5	22.0	--	22.5	22.7
T80	(86,25)	22.9	23.0	--	22.6	23.1

* 28 Sep 1980.

Table XIII-6

Upper Mobile Bay Salinity (ppt x 100) Results on the Global Grid After 120 Hours

Scheme 1 (Flux Corrected Transport)

M \ N	[illegible]	[illegible]	[illegible]	[illegible]	[illegible]	[illegible]	[illegible]	[illegible]	[illegible]	[illegible]	91	92	93	94	95	96	97	98	99	100
1	[illegible]	[illegible]	[illegible]	[illegible]	[illegible]	[illegible]	[illegible]	[illegible]	[illegible]	[illegible]	0.	0.	0.	0.	0.	0.	0.	0.	0.	0.
2	[illegible]	[illegible]	[illegible]	[illegible]	[illegible]	[illegible]	[illegible]	[illegible]	0.	0.	0.	0.	0.	0.	0.	0.	0.	0.	0.	0.
3	[illegible]	[illegible]	[illegible]	[illegible]	[illegible]	[illegible]	[illegible]	[illegible]	0.	0.	0.	0.	0.	0.	0.	0.	0.	0.	0.	0.
4	[illegible]	[illegible]	[illegible]	[illegible]	[illegible]	[illegible]	[illegible]	[illegible]	[illegible]	[illegible]	0.	0.	0.	57.	-0.	0.	0.	0.	0.	0.
5	[illegible]	[illegible]	[illegible]	[illegible]	[illegible]	[illegible]	[illegible]	[illegible]	[illegible]	[illegible]	[illegible]	2215.	1857.	244.	0.	39.	268.	2301.	0.	0.
6	[illegible]	[illegible]	[illegible]	[illegible]	[illegible]	[illegible]	[illegible]	[illegible]	0.	[illegible]	2199.	2206.	2149.	1673.	947.	37.	1352.	2301.	2218.	2222.
7	[illegible]	[illegible]	[illegible]	[illegible]	[illegible]	[illegible]	[illegible]	[illegible]	[illegible]	[illegible]	[illegible]	2200.	2194.	2173.	1973.	1051.	1568.	2200.	2274.	2245.
8	[illegible]	[illegible]	[illegible]	[illegible]	[illegible]	[illegible]	[illegible]	[illegible]	0.	2201.	2200.	2199.	2201.	2178.	2171.	2005.	1970.	2204.	2287.	2291.
9	[illegible]	[illegible]	[illegible]	[illegible]	[illegible]	[illegible]	[illegible]	[illegible]	0.	2200.	2200.	2203.	2200.	2229.	2261.	2241.	2174.	2276.	2293.	2294.
10	[illegible]	[illegible]	[illegible]	[illegible]	[illegible]	[illegible]	[illegible]	0.	2201.	2194.	2207.	2226.	2235.	2292.	2250.	2240.	2278.	2289.	2271.	2250.
11	[illegible]	[illegible]	[illegible]	[illegible]	[illegible]	[illegible]	[illegible]	[illegible]	[illegible]	[illegible]	[illegible]	2234.	2279.	2310.	2298.	2300.	2299.	2284.	2216.	0.
12	[illegible]	[illegible]	[illegible]	[illegible]	[illegible]	[illegible]	[illegible]	[illegible]	[illegible]	2214.	[illegible]	2231.	2291.	2310.	2283.	2283.	2257.	2239.	2215.	0.
13	[illegible]	[illegible]	[illegible]	[illegible]	[illegible]	[illegible]	[illegible]	[illegible]	[illegible]	[illegible]	2262.	2243.	2275.	2312.	2298.	2294.	2252.	2211.	2211.	2209.
14	[illegible]	[illegible]	[illegible]	[illegible]	[illegible]	[illegible]	[illegible]	2202.	2206.	2263.	2276.	2281.	2285.	2303.	2299.	2299.	2284.	2259.	2256.	2215.
15	[illegible]	[illegible]	[illegible]	[illegible]	[illegible]	[illegible]	[illegible]	[illegible]	[illegible]	[illegible]	2277.	2295.	2295.	2301.	2299.	2301.	2295.	2285.	2232.	2203.

Scheme 2 (Explicit Three Time Level)

M \ N	[illegible]	[illegible]	[illegible]	[illegible]	[illegible]	[illegible]	[illegible]	[illegible]	[illegible]	[illegible]	91	92	93	94	95	96	97	98	99	100
1	[illegible]	[illegible]	[illegible]	[illegible]	[illegible]	[illegible]	[illegible]	[illegible]	0.	0.	0.	0.	0.	0.	0.	0.	0.	0.	0.	0.
2	[illegible]	[illegible]	[illegible]	[illegible]	[illegible]	[illegible]	[illegible]	[illegible]	0.	0.	0.	0.	0.	0.	0.	0.	0.	0.	0.	0.
3	[illegible]	[illegible]	[illegible]	[illegible]	[illegible]	[illegible]	[illegible]	[illegible]	0.	0.	0.	0.	0.	0.	0.	0.	0.	0.	0.	0.
4	[illegible]	[illegible]	[illegible]	[illegible]	[illegible]	[illegible]	[illegible]	[illegible]	0.	0.	0.	0.	0.	-747.	-667.	1013.	-2135.	0.	0.	0.
5	[illegible]	[illegible]	[illegible]	[illegible]	[illegible]	[illegible]	[illegible]	[illegible]	0.	0.	2146.	2256.	1975.	141.	-505.	283.	551.	2973.	0.	0.
6	[illegible]	[illegible]	[illegible]	[illegible]	[illegible]	[illegible]	[illegible]	[illegible]	0.	0.	2200.	2203.	2162.	1686.	1160.	[illegible]	1522.	2297.	2130.	2223.
7	[illegible]	[illegible]	[illegible]	[illegible]	[illegible]	[illegible]	[illegible]	[illegible]	0.	0.	2200.	2200.	2194.	2134.	1991.	1259.	1552.	2217.	2274.	2250.
8	[illegible]	[illegible]	[illegible]	[illegible]	[illegible]	[illegible]	[illegible]	[illegible]	0.	2200.	2200.	2200.	2204.	2157.	2169.	2030.	2016.	2205.	2310.	2301.
9	[illegible]	[illegible]	[illegible]	[illegible]	[illegible]	[illegible]	[illegible]	[illegible]	0.	2202.	2200.	2202.	2141.	2237.	2266.	2250.	2193.	2277.	2294.	2325.
10	[illegible]	[illegible]	[illegible]	[illegible]	[illegible]	[illegible]	[illegible]	[illegible]	2201.	2207.	2205.	2227.	2239.	2294.	2287.	2280.	2272.	2298.	2289.	2200.
11	[illegible]	[illegible]	[illegible]	[illegible]	[illegible]	[illegible]	[illegible]	2176.	2213.	2143.	2154.	2233.	2263.	2325.	2304.	2329.	2335.	2288.	2171.	0.
12	[illegible]	[illegible]	[illegible]	[illegible]	[illegible]	[illegible]	[illegible]	2155.	2156.	2255.	2295.	2176.	2294.	2340.	2277.	2267.	2224.	2249.	2207.	0.
13	[illegible]	[illegible]	[illegible]	[illegible]	[illegible]	[illegible]	[illegible]	2202.	2219.	2231.	2317.	2256.	2284.	2317.	2291.	2284.	2250.	2151.	2212.	2200.
14	[illegible]	[illegible]	[illegible]	[illegible]	[illegible]	[illegible]	[illegible]	2200.	2204.	2247.	2242.	2301.	2292.	2303.	2298.	2293.	2290.	2278.	2314.	2221.
15	[illegible]	[illegible]	[illegible]	[illegible]	[illegible]	[illegible]	[illegible]	[illegible]	2226.	2270.	2256.	2310.	2297.	2301.	2300.	2300.	2299.	2290.	2204.	2197.

were accessed from the scheme 1 FCT global grid simulation for this period at the locations shown in Table XI-6. Temporal and spatial interpolation were employed to develop the boundary information at intermediate cells along the refined grid boundary. Initial conditions over the refined grid were determined from transect data collected on 20 and 21 September and were specified on a cell by cell basis. Since salinity variations in time were extremely small, it was assumed that the initial conditions were representative of conditions at hour 2400 CST on 20 September. In order to study the behavior of a purely freshwater inflow, zero values of salinity were specified for cells (8,1) and (16,1) representing the West Pascagoula and Pascagoula River inflows. Flows during the period were taken from Table VII-1 and were approximately 1600 and 1000 cfs for the West Pascagoula and Pascagoula. The surge setup generated by tropical storm Hermine was not considered.

164. A 60-sec time step was employed 7200 times in order to simulate the 120-hr period beginning hour 0000 CST 20 September. In order to allow hydrodynamic transients associated with initial conditions to dissipate, the salinity computations were initiated at time step 1440 (hour 2400 CST 20 September). Wind information employed for the global grid simulation at 6-hr intervals was interpolated in time at each time step. The calibrated effective dispersion coefficient parameters in Table XIII-4 were used to determine dispersion.

165. The growth of the freshwater influence is represented by computing the 24-ppt contour after 48, 72, 96, and 120 hr shown in Figures XIII-1 through XIII-4. Initial salinity values were larger than 24 ppt. Therefore, freshwater must dilute the water in any given cell to obtain a cell concentration less than or equal to 24 ppt. Salinity values in the shaded areas in Figures XIII-1 through XIII-4 are less than 24 ppt. Tidal conditions at 48, 72, 96, and 120 hr correspond to a mean level between high and low tides as shown in Figure XIII-5, which represents the water surface elevation at Pascagoula obtained during the global grid simulation. At 72, 96, and 120 hr, the tide is a lower high tide in a semidiurnal (neap) period.

166. Figures XIII-1 through XIII-5 indicate that the growth of the freshwater influence is a complicated function of wind loading (wind magnitude and direction history), freshwater flow rate, and tidal condition. It appears that salinity conditions are beginning to stabilize at the end of this 5-day period. However, the tidal range is relatively low corresponding to a neap

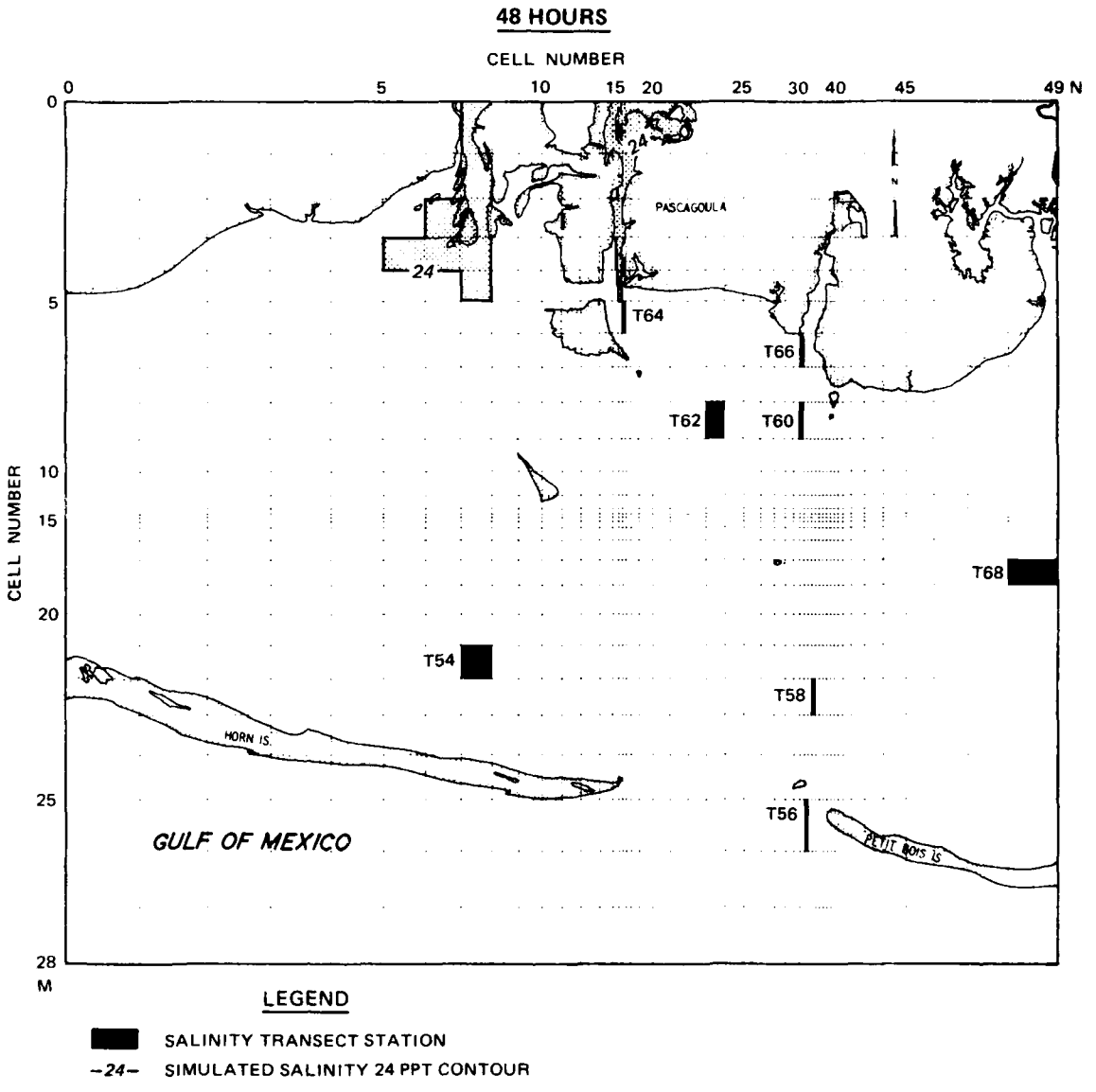

Figure XIII-1. Refined grid, 24-ppt salinity contour, 48 hr

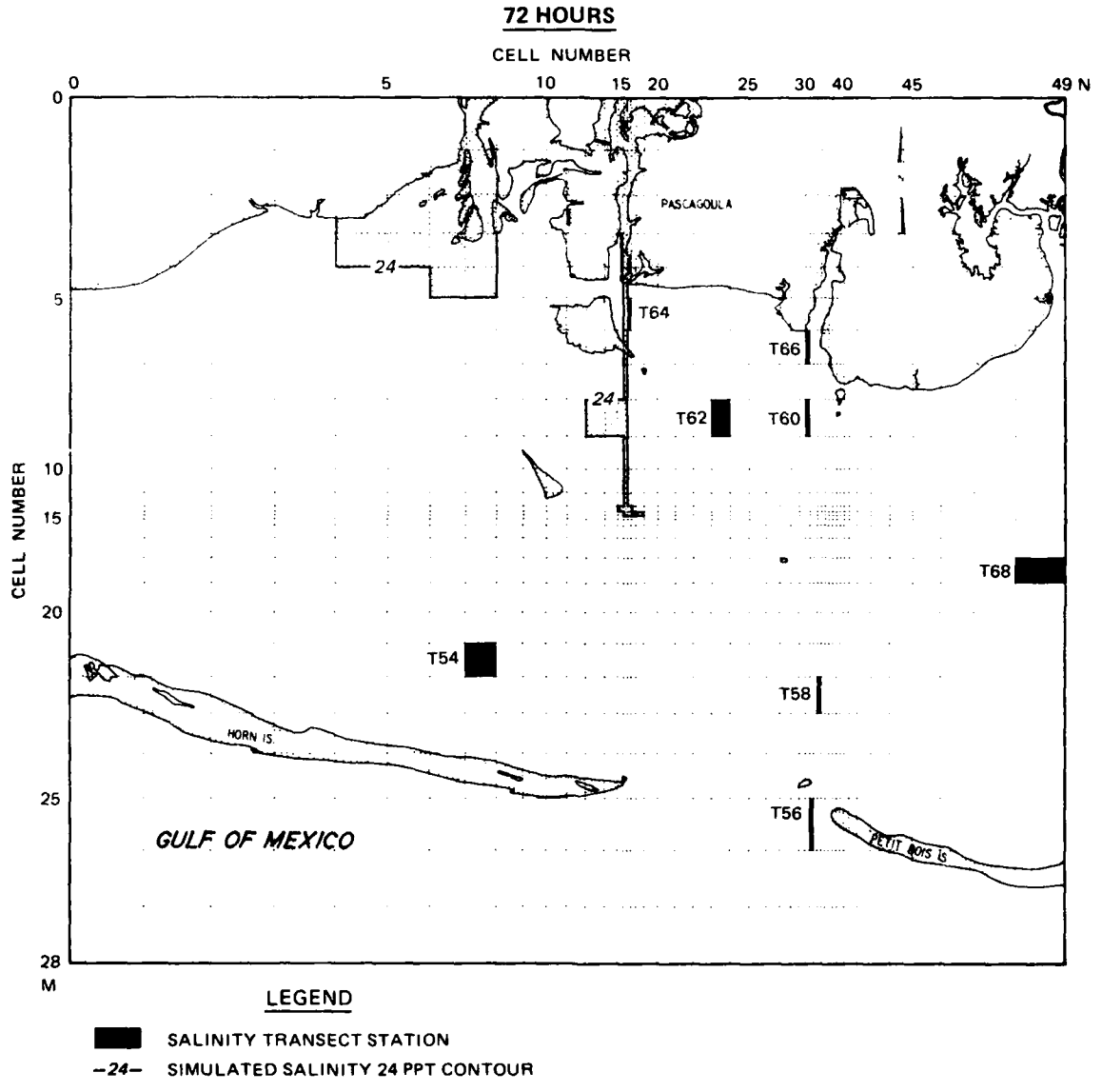

Figure XIII-2. Refined grid, 24-ppt salinity contour, 72 hr

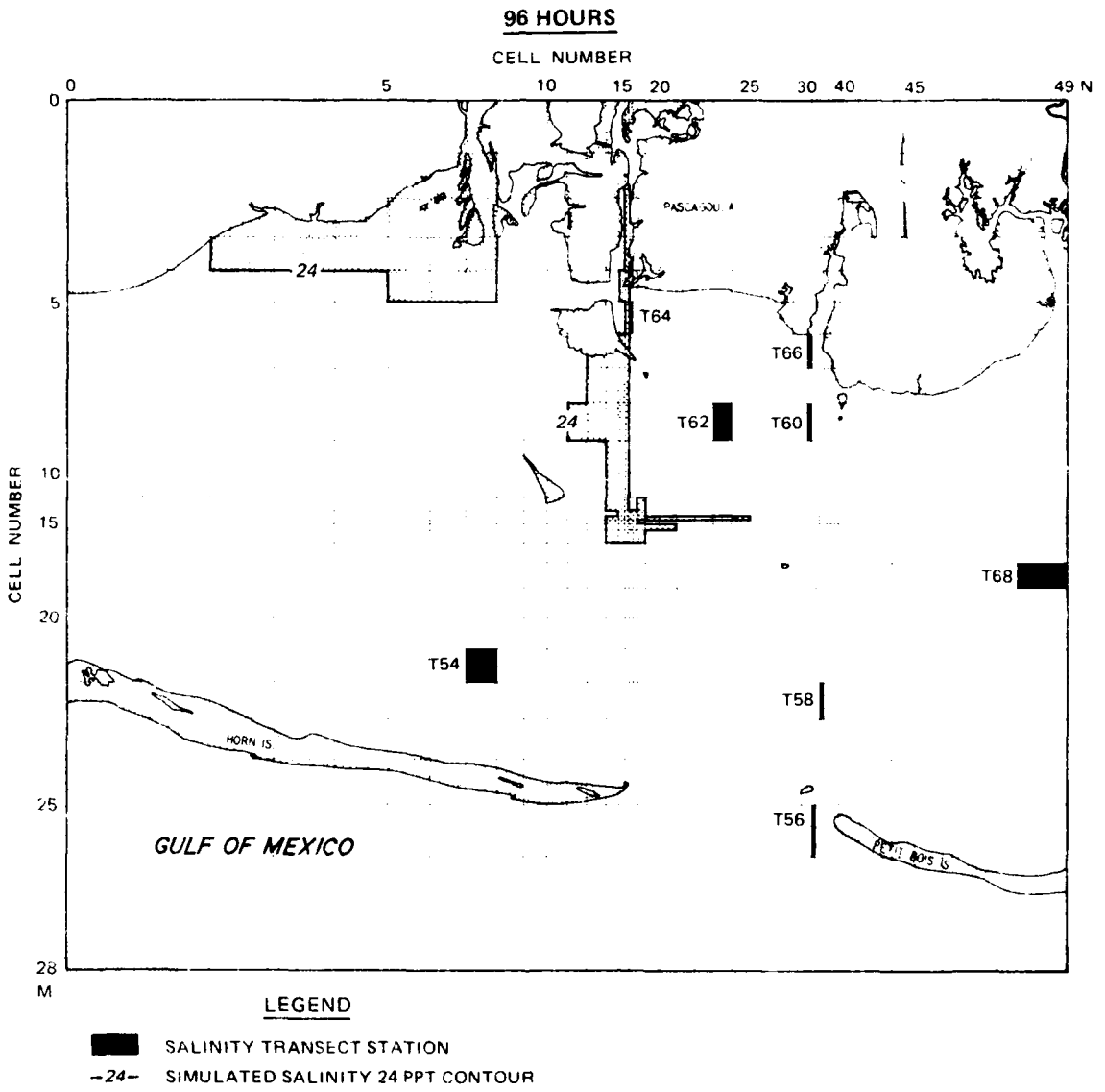

Figure XIII-3. Refined grid, 24-ppt salinity contour, 96 hr

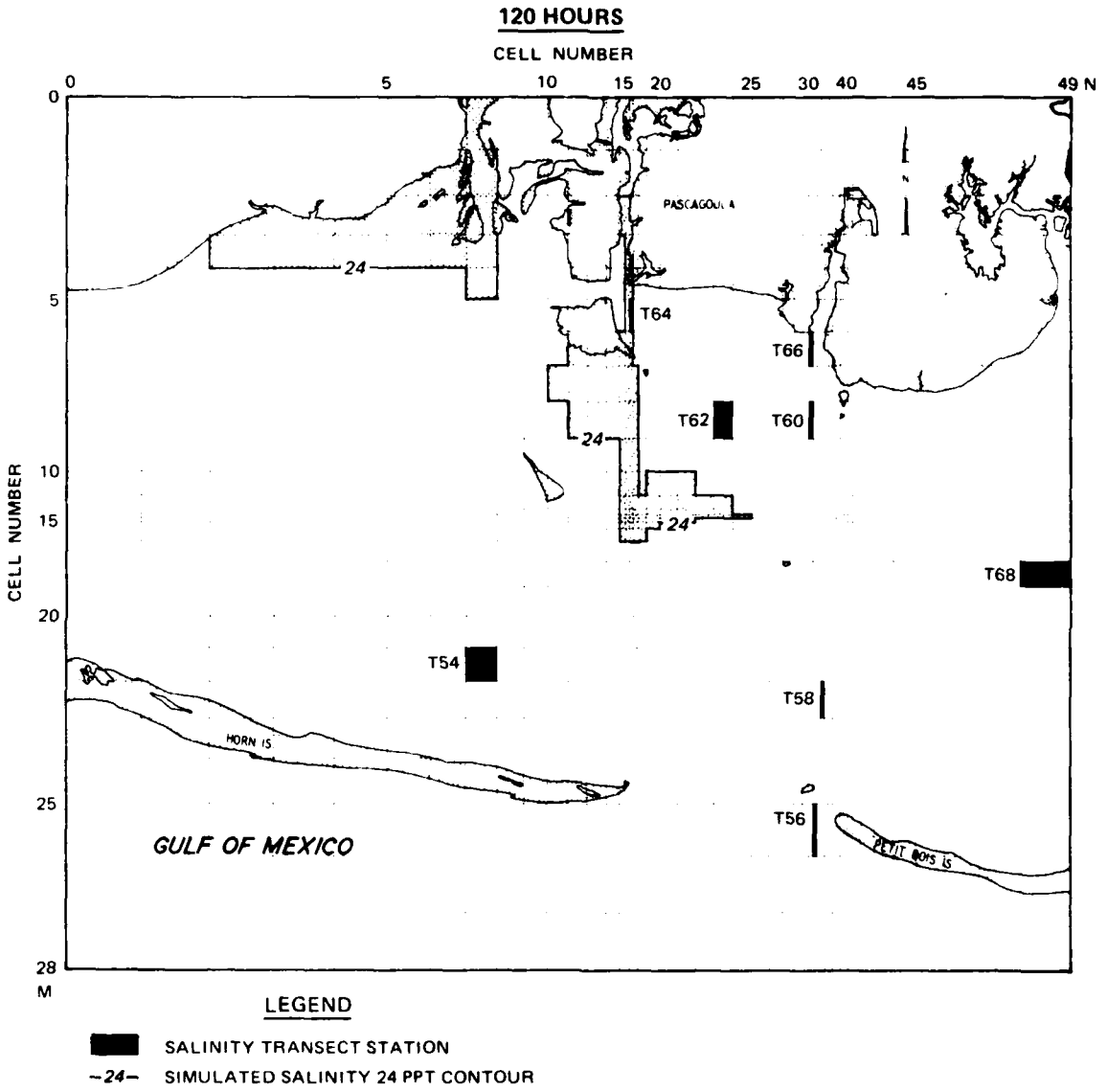

Figure XIII-4. Refined grid, 24-ppt salinity contour, 120 hr

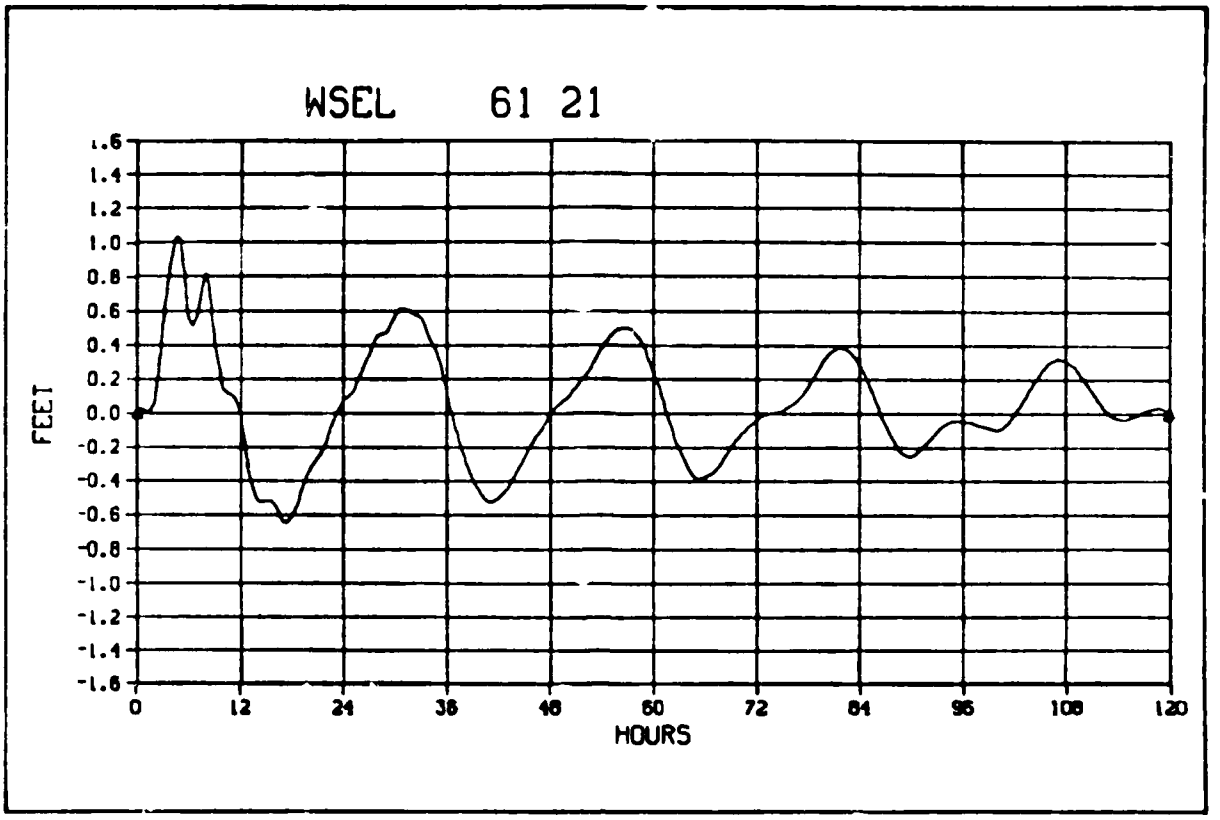

Figure XIII-5. Simulated global grid water surface elevation at Pascagoula including wind effect

tide and the Pascagoula River system inflows correspond to a late summer low flow condition. For higher tidal ranges and inflows it may require a significantly longer period in order to stabilize the salinity distribution.

167. Simulated velocity levels at 120 hr (24 September hour 24 CST) are compared with transect values measured on 24 and 25 September in Table XIII-7 at locations indicated in the darkened cells in Figures XIII-1 through XIII-4. As may be noted from these figures, the freshwater influence does not reach any of the transect stations. Therefore, the specification of inflow salinity values does not influence the simulation results at these locations. Simulated salinity levels at the transect station location correspond closely to observed values and further verify the dispersion coefficient parameters employed.

168. In order to study the behavior of refined grid simulation results in the neighborhood of the Pascagoula Channel inflow on a cell by cell basis, the initial salinity levels are compared with simulated levels at 120 hours (24 September hour 24 CST) in Table XIII-8. The simulated results appear to

Table XIII-7

Salinity Conditions on the Refined Grid

Transect Station	Refined Grid Cell	20-21 Sep 1980		24 Sep 1980	
		Measured	Initial Condition	Measured	Computed Scheme 1
T54	(8,22)	27.3	27.0	27.6	28.8
T64	(17,6)	27.7	28.0	27.5	28.2
T62	(24,9)	28.5	29.0	26.8	27.7
T66	(31,7)	27.3	27.0	27.7	27.9
T60	(33,7)	28.1	27.0	29.1	27.9
T58	(36,23)	29.1	29.0	29.6	27.7
T56	(34,26)	29.7	30.0	30.3	27.9
T68	(49,19)	27.9	28.0	27.5*	28.1

* 28 Sep 1980.

Table XIII-8

Behavior of Refined Grid Salinity Simulation in the Vicinity of the Pascagoula River Inflow

Initial Conditions, 24 hr, Salinity (ppt)

M N	10	11	12	13	14	15	16	17	18	19	20
1	0.	0.	0.	0.	0.	0.	24.	0.	0.	0.	0.
2	24.	24.	0.	0.	0.	25.	25.	25.	0.	0.	0.
3	24.	24.	0.	0.	0.	25.	25.	25.	0.	0.	0.
4	24.	24.	0.	0.	0.	26.	26.	25.	0.	0.	0.
5	24.	24.	25.	25.	26.	26.	27.	26.	0.	0.	0.
6	25.	25.	0.	0	27.	29.	29.	28.	28.	28.	28.
7	27.	27.	0.	0.	27.	27.	28.	28.	28.	28.	28.
8	27.	27.	27.	28.	28.	28.	28.	28.	28.	28.	28.
9	27.	27.	27.	28.	28.	28.	28.	28.	28.	28.	28.
10	28.	28.	28.	28.	28.	28.	28.	28.	28.	28.	28.
11	28.	0	28.	28	28.	28.	28.	28.	28.	28.	28.
12	28.	28.	28.	28.	28.	28.	28.	28.	28.	28.	28.
13	28.	28.	28.	28.	28.	28.	28.	28.	28.	28.	28.
14	28.	28.	28.	28.	28.	28.	28.	28.	28.	28.	28.
15	28.	28.	28.	28.	28.	28.	28.	28.	28.	28.	28.
16	28.	28.	28.	28	28.	28.	28.	28.	28.	28.	28.
17	28.	28.	28.	28.	28.	28.	28.	28.	28.	28.	28.
18	28.	28.	28.	28.	28.	28.	28.	28.	28.	28.	28.
19	28.	28.	28.	28.	28.	28.	28.	28.	28.	28.	28.
20	27.	27.	27.	28.	28.	28.	28.	28.	28.	28.	28.
21	27.	27.	27.	28.	28.	28.	28.	28.	28.	28.	28.
22	27.	27.	27.	28.	28.	28.	28.	28.	28.	28.	28.
23	27.	27.	27.	28.	28.	28.	28.	28.	28.	28.	28.
24	27.	27.	27.	28	28.	28	28.	28.	28.	28.	28.
25	27.	27.	27.	28.	28.	28.	28.	28.	28.	28.	28.
26	28.	28.	28.	28.	28.	28.	28.	28.	28.	28.	28.
27	28.	28.	28.	28.	28.	28.	28.	28.	28.	28.	28.
28	30.	30.	30.	30.	30.	30.	30.	30.	30.	30.	30.

Simulated Conditions, 120 hr, Salinity (× 100 ppt)

M N	10	11	12	13	14	15	16	17	18	19	20
1	0.	0.	0.	0.	0.	0.	0.	0.	0.	0.	0.
2	2413.	2432.	0.	0.	0.	1915.	865.	2597.	0.	0.	0.
3	2475.	2487.	0.	0.	0.	2118.	975.	1444.	0.	0.	0.
4	2474.	2531.	0.	0.	0.	2436.	738.	2158.	0.	0.	0.
5	2611.	2581.	2657.	2644.	2559.	2557.	745.	1925.	0.	0.	0.
6	2716.	2581.	0.	0.	2141.	2415.	2717.	2920.	2759.	2903.	2737.
7	2651.	2532.	0.	0.	2146.	2536.	2582.	2615.	2628.	2739.	2755.
8	2474.	2554.	2598.	2648.	2150.	1922.	2072.	2291.	2558.	2607.	2632.
9	2715.	2615.	2632.	2232.	2171.	1575.	1778.	2253.	2346.	2407.	2554.
10	2716.	2772.	2811.	2831.	2411.	2113.	1904.	2234.	2367.	2515.	2431.
11	2716.	0.	2811.	2636.	2411.	2238.	1935.	2246.	2365.	2437.	2501.
12	2715.	2725.	2741.	2554.	2471.	2353.	2052.	2207.	2275.	2305.	2501.
13	2716.	2741.	2741.	2704.	2541.	2385.	2149.	2149.	2225.	2273.	2279.
14	2717.	2806.	2712.	2722.	2503.	2279.	2117.	2186.	2137.	2232.	2252.
15	2716.	2811.	2754.	2701.	2573.	2221.	2117.	2130.	2175.	2330.	2334.
16	2653.	2816.	2756.	2744.	2511.	2281.	2250.	2229.	2311.	2336.	2275.
17	2717.	2814.	2770.	2716.	2603.	2275.	2336.	2325.	2326.	2354.	2331.
18	2816.	2829.	2819.	2851.	2642.	2648.	2610.	2701.	2652.	2762.	2812.
19	2817.	2836.	2903.	2873.	2875.	2853.	2857.	2856.	2860.	2848.	2830.
20	2841.	2837.	2861.	2877.	2867.	2850.	2872.	2871.	2865.	2855.	2844.
21	2819.	2812.	2817.	2851.	2817.	2853.	2875.	2853.	2855.	2857.	2855.
22	2811.	2813.	2814.	2851.	2805.	2845.	2817.	2877.	2852.	2850.	2846.
23	2817.	2812.	2847.	2842.	2854.	2817.	2826.	2817.	2815.	2810.	2836.
24	2946.	2943.	2955.	2945.	2949.	2948.	2943.	2945.	2935.	2942.	2933.
25	2947.	2951.	2952.	2959.	2952.	2948.	2947.	2950.	2947.	2945.	2945.
26	2955.	2975.	2974.	2972.	2970.	2956.	2956.	2957.	2953.	2954.	2953.
27	2951.	2955.	2956.	2955.	2951.	2948.	2953.	2955.	2953.	2959.	2939.
28	2947.	2946.	2944.	2945.	2943.	2943.	2942.	2942.	2952.	2942.	

exhibit spurious fluctuations in cells (15-17, 2-6). This area of cells is located within the Pascagoula River itself as shown in Figure XIII-4. Although simulated salinity values are nonnegative, the behavior of the simulation indicates that the refined grid cannot be used effectively to predict salinity levels within the Pascagoula River itself. The numerical difficulties are due to the averaging process employed in coupling a two time level salinity finite difference scheme with a three time level hydrodynamic scheme. In practice, these difficulties would be resolved by employing an even more refined grid in the vicinity of the Pascagoula Channel inflow.

PART XIV: STUDY RESULTS, CONCLUSIONS, AND RECOMMENDATIONS

169. Salient study results are presented and the following conclusions are drawn.

a. Twenty-two tide gages, three deep sea pressure gages, and twenty-one oceanographic moorings arrayed with current meters at various depths were deployed over Mississippi Sound and adjacent waters over the period April-November 1980. Outlaw (1983) performed a harmonic analysis on filtered elevations and currents and determined tidal characteristics for nine constituents (O_1, K_1, P_1, M_1, J_1, Q_1, M_2, S_2, and N_2). Since the GTM used to drive the global grid produced tidal characteristics for the five major tidal constituents (O_1, K_1, P_1, M_2, and S_2), tidal elevations at 11 stations and currents at 7 stations throughout the study area were reconstructed using Outlaw's (1983) results using these five major constituents for the calibration period 24-25 September and verification period 12-14 June 1980. Simulated water levels over the global grid matched reconstructed levels to within 0.2 ft at stations west of Pascagoula and to within 0.1 ft at Pascagoula and the stations to the east for both periods. Simulated current components exhibited the same general trend (flow reversal times) as the reconstructed currents at meters nearest middepth.

Based upon these results, the prototype data collection program and subsequent harmonic analysis provided sufficient water surface elevation and current data to calibrate and verify the bottom friction mechanics in the global grid hydrodynamics.

b. The simulated water surface elevations on the global grid for the calibration period 20-25 September were used to provide boundary elevations for a refined grid simulation for the same period. Simulated water surface elevations agreed with the reconstructed levels to within 0.1 ft at four data stations

within the refined grid. An L-shaped idealization was employed to represent the branching of the Pascagoula Channel.

Based upon these results, the idealization of the channel represented the actual system in sufficient detail to effectively simulate reconstructed levels on the refined grid.

c. In the hydrodynamic simulation outlined in a and b, astronomic tide conditions were considered. Meteorological effects, namely, pressure anomaly, and long-wave setup must be considered if one attempts to compare simulated hydrodynamic water levels and currents with the observed (unfiltered) data. For the calibration period, the long wave setup due to tropical storm Bonnie is estimated to be approximately 0.3 ft.

d. It was necessary to increase the amplitude of the diurnal (O_1 , K_1 , P_1) and decrease the amplitudes of the semidiurnal (M_2 , S_2) tidal constituents from the values produced by the GTM in order to achieve hydrodynamic calibration and verification on the global grid and hydrodynamic calibration on the refined grid.

e. Since M_2 and S_2 were dominant during the calibration period and O_1 , K_1 , and P_1 were dominant during the verification period, effectively all five constituents were considered during the calibration and verification process. Therefore, the hydrodynamics for any period may be effectively simulated on the global grid and refined grid.

f. A hypothetical regional dredge disposal site in the vicinity of Sand Island studied on the global grid appeared to alter the tidal pattern only in lower Mobile Bay. Since the tidal pattern was not changed near the boundary, the boundary conditions supplied by the GTM remain valid and regional disposal alterations of this nature may be effectively studied on the global grid.

g. The hydrodynamic effects of doubling the present channel width of the Pascagoula Channel as studied on the refined grid are localized to a narrow band of cells outlining the channel and

do not propagate to the boundary. As a result, adjustments to the navigation channels (minor adjustments in alignment, deepening, and widening) will induce changes in the flow pattern only in a narrow band of cells surrounding the area in which the adjustments are made. Flow changes will not propagate to the boundary, and the integrity of the global grid supplied boundary conditions will be maintained. This finding indicates that proposed changes in navigation channels may be studied on a case by case basis by developing individual refined grids around the appropriate channels. Boundary conditions for each of these refined grids may be developed using the global grid developed in this study.

i. Salinity data were collected at 40 stations encompassing Mississippi Sound over a 2-day period at regular intervals over the period April-November 1980. Conductivity-temperature readings were recorded and converted to salinity on a continuous basis at six locations over the entire Sound during the same period. Due to biological fouling of the conductivity-temperature probes, continuous salinity data could not be considered reliable and were not used to calibrate the salinity component of the model.

As a result, no observed time-varying salinity data were available. Transect data on 20-21 September and 24-25 September were used to establish initial conditions and provide conditions to compare with simulated salinities. Both the FCT scheme 1 and full three-time local explicit scheme 2 were considered on the global grid. Meteorological effect due to wind only was considered. Within Mississippi Sound simulation results for both schemes were nearly identical and corresponded to observed levels to within 1 ppt. In upper Mobile Bay, within the freshwater influence, scheme 2 results oscillated behind the freshwater front. The scheme 1 FCT results were nonnegative and nonoscillatory. Although due to the nonavailability of time varying salinity data, the global grid salinity calibration is not as rigorous as the hydrodynamic, the

calibrated dispersion coefficient parameters are within experimentally determined ranges.

j. The simulated water surface elevations and salinity levels on the global grid for the calibration period 20-24 September were used to provide boundary conditions for a refined grid simulation for the same period. Temporal and spatial distributions of freshwater fronts associated with the Pascagoula River system were studied using the FCT scheme 1 approach. Meteorological effect due to wind only was considered. During the 21-24 September period, the freshwater front associated with the Pascagoula River inflow (1000 cfs) extended along the channel and into the middle of the Sound. In contrast, the freshwater front associated with the West Pascagoula River inflow (1600 cfs) was confined to an area near the shoreline. This front appeared to be driven to the west by the prevailing winds which were from the south-southeast. Simulated salinity levels corresponded to within 2.3 ppt of measured transect values at all eight stations, which all were located outside the region of freshwater influence.

As a result of the closeness of the comparison, the calibrated values of effective dispersion coefficient parameters were substantiated further.

k. The growth of the freshwater fronts associated with the Pascagoula and West Pascagoula Rivers was influenced by the wind magnitude and direction, the magnitude of the freshwater inflows, and the astronomic tide.

As a result, in considering alternatives to the Pascagoula Channel, care must be taken in developing representative conditions for these phenomena.

170. The following recommendations are made based upon study results.

a. In the development of additional refined grids for study of alternate channel systems, an implicit time step in the neighborhood of 60 sec can be economically employed with a minimum

space step on the order of the channel width and a grid with 1000-1500 computational cells.

b. In studying the effects on salinity of dredge practices on either the global or refined grid, the FCT scheme 1 is preferred over scheme 2 for sharp front problems. However, scheme 1 is on the order of three times slower than scheme 2. Thus, if fronts are not sharp; i.e., if one specifies the same value of salinity for the flow input as is found in the neighboring cells of the inflow, scheme 2 may be effectively employed.

c. Additional research is warranted to flux correct the three time level explicit scheme (scheme 2). This research would produce a reasonably fast (approximately 50 percent faster than the present scheme 1) but accurate transport scheme and eliminate the averaging of the hydrodynamic variables used in scheme 1 FCT.

d. Due to the dependence of the salinity distribution associated with freshwater fronts on wind, flow rate, and astronomical tide, it is recommended that additional simulations be performed in order to develop the sensitivity of the salinity distribution with respect to each of these influences. The results of this sensitivity analysis would provide useful information in developing design scenarios for each channel alteration project.

REFERENCES

Bettandorff, J. M. 1972. "Selected Characteristics of Mississippi Streams; Part 3: Coastal River Basins," Bulletin 72-2, US Geological Survey.

Butler, H. L. 1980. "Evolution of a Numerical Model for Simulating Long-Period Wave Behavior in Ocean-Estuarine Systems," in Estuarine and Wetland Processes, Hamilton, P., and Macdonald, K. (eds.), Plenum Press, New York.

Cry, George W., et al. 1980. Tropical Cyclones of the North Atlantic Ocean, 1871-1977, National Climatic Center, Asheville, N. C., June 1978 (1980 Supplement to Appendix B).

Elder, J. W. 1959. "The Dispersion of Marked Fluid in Turbulent Shear Flow," Journal of Fluid Mechanics, Vol 5, p 544.

Garratt, J. R. 1977. "Review of Drag Coefficients Over Oceans and Continents," Monthly Weather Review, Vol 105, pp 915-929.

Harvey, Edward J., et al. 1965. Water Resources of the Pascagoula Area Mississippi, Geological Survey Water-Supply Paper 1763, US Government Printing Office, Washington, DC.

Leendertse, J. J. 1970. A Water-Quality Simulation Model for Well-Mixed Estuaries and Coastal Seas, Vol 1, Principles of Computation, Report RM-6230-RC, the Rand Corporation.

_____. 1971. A Water-Quality Simulation Model for Well-Mixed Estuaries and Coastal Seas, Vol 2, Computation Procedures, R-708-NYC, the Rand Corporation.

National Marine Fisheries Service. 1981. Temperature and Salinity Data FRS OREGON II Cruises #106 and #112, Southeast Fisheries Center, Mississippi Laboratories, Pascagoula Facility, P. O. Drawer 1207, Pascagoula, Miss.

Outlaw, D. G. 1983. "Prototype Tidal Data Analysis for Mississippi Sound and Adjacent Areas," Miscellaneous Paper CERC-83-1, US Army Engineer Waterways Experiment Station, Vicksburg, Miss.

Parker, Gary. Letter: February 16, 1981 to Mr. Douglas Outlaw, US Army Engineer Waterways Experiment Station, Vicksburg, Miss.

Raytheon Ocean Systems. 1981. Final Report, Mississippi Sound Data Collection Program (Draft), submitted to US Army Engineer District, Mobile, Mobile, Ala.

Reid, R. O., and Whitaker, R. E. 1981 (Sep). "Numerical Model for Astronomical Tides in the Gulf of Mexico," prepared for US Army Engineer Waterways Experiment Station under Contract No. DACW 39-79-C-0074.

Schmalz, R. A. 1983a (Sep). "The Development of a Numerical Solution to the Transport Equation; Report 1: Methodology," Miscellaneous Paper CERC-83-2, US Army Engineer Waterways Experiment Station, Vicksburg, Miss.

_____. 1983b (Sep). "The Development of a Numerical Solution to the Transport Equation; Report 2: Computational Procedures," Miscellaneous Paper CERC-83-2, US Army Engineer Waterways Experiment Station, Vicksburg, Miss.

_____. 1983c (Sep). "The Development of a Numerical Solution to the Transport Equation; Report 3: Test Results," Miscellaneous Paper CERC-83-2, US Army Engineer Waterways Experiment Station, Vicksburg, Miss.

Schmalz, R. A. 1984. "User Guide for WIFM-SAL: A Two Dimensional Vertically Integrated, Time Varying Estuarine Water Quality Model," Instruction Report EL-84- , US Army Engineer Waterways Experiment Station, Vicksburg, Miss.

Schroeder, W. W. 1979 (Aug). "Dispersion and Impact of Mobile River System Waters in Mobile Bay, Alabama," OWRT Project A-058-ALA, WRRI.

Schureman, P. 1940. Manual of Harmonic Analysis and Prediction of Tides, NOAA, Special Publication 98.

Taylor, G. I. 1954. "Dispersion of Matter in Turbulent Flow Through a Pipe," Proceedings of the Royal Society of London (A), Vol 223.

US Army Corps of Engineers, Mobile District. 1979 (Mar). Mississippi Sound and Adjacent Areas Dredged Material Disposal Study (Stage 1) Reconnaissance Report, Appendix C.

Van Dorn, W. G. 1953. "Wind Stress on an Artificial Pond," Journal of Marine Research, Vol 12, No. 3, pp 249-276.

Wilson, B. W. 1962. "Note on Surface Wind Stress Over Water at Low and High Speeds," Journal of Geophysical Research, Vol 65, pp 3377-3382.

APPENDIX A: GUIDE TO WIFM MODEL INPUT REQUIREMENTS

1. The preparation of the necessary input data required by WIFM is considered in light of the need to develop additional refined grids in the vicinity of navigation channels (Gulfport and Biloxi). This appendix is not intended to be a complete user guide but to outline in detail the requirements necessary in developing an input data deck for a refined grid system. The basic requirements are presented in Table A1. Each item in this table is discussed in terms of WIFM-SAL input requirements using the Pascagoula Channel refined grid system developed in this study. A complete description of model input variables and required data formats is reported by Schmalz (1984).

Table A1

WIFM Input Requirements for a Refined Grid

I.	Plot global subgrid encompassing the refined grid region
II.	Map the refined grid system
III.	Specify the depth field
IV.	Specify the barrier characteristics
V.	Specify flow input locations and discharges
VI.	Specify tidal signal input
VII.	Specify initial salinity conditions
VIII.	Specify wind information
IX.	Specify simulation control variables

Mapping the Global Subgrid of Pascagoula Region

2. Initial development of the refined grid required reproducing the complete global grid of Mississippi Sound.

3. Program MAPIT was executed using the table of input variables previously prepared in generating the global grid. Once this file was stored a subgrid of the region selected (in this case, Pascagoula Channel) was plotted at the same scale (1:40000) as that chosen for the refined grid. The global subgrid was overlaid on the project map (chart 11374) for the refined grid in order to facilitate commonality of feature specification.

Mapping of Pascagoula Channel

4. The first effort to map a grid of approximately one thousand (1000) cells having three (3) bands of high resolution was unacceptable.

5. The aspect ratio (cell width versus length) exceeded desirable limits. Aspect ratios should be less than 20.

6. To reduce the aspect ratio and total number of cells required, the second effort eliminated two of the high resolution bands. This grid, while only 1034 cells (47 × 22), once plotted and overlaid chart 11374 was clearly inadequate (with only one high resolution band) to model the branching channel into Pascagoula.

7. The third effort attempted increasing the number of cells, decreasing the region to be mapped and adding a fourth band of high resolution. This produced a grid of 2058 cells (49 × 42). While the grid would allow better idealization of the channels and rivers it was considered too large for economical computation.

8. Using this third grid as a guide, the following decisions were made with regard to producing the final grid:

a. Left boundary of refined grid coincided with global grid, N = 53 .

b. Bottom or seaward boundary of the refined grid coincided with global grid M = 33 .

c. Three high resolution bands whose cells, 0.1 map inches in width (300 ft in nature), were positioned to achieve an idealized channel. Two dense bands were mapped in the y direction, at the main channel and at the west river, and one band was mapped in the x direction at the channel junction.

d. The right boundary of the refined grid extended to approximately global grid N = 67 .

e. The upper (land) boundary extended to approximately global grid M = 18 .

9. The final grid covered an area from near Bellafontaine Point to near Point Aux Chenes Bay. Tables A2 and A3 show the Y , Y' , and α and X , X' , and α for the Y direction and the X direction, respectively. These input variables for Program MAPIT produced a grid of 1372 points (49 × 28). The scale is 1:40000 and the file is ordered as follows: Y direction

Table A2

Y Direction Mapping*

Y Map in.	Y' Map in.	α
1.0	2.10	1
8.0	1.56	4
10.5	1.00	2
12.25	0.75	2
14.1	0.50	2
15.1	0.50	2
15.6	0.10	2
15.8	0.10	2
16.5	0.45	3
18.9	0.50	5
20.0	0.25	3
20.5	0.10	3
21.4	0.10	9
22.1	0.40	3
27.2	1.40	6

* The Y direction was mapped from west to east (left to right), thus the WIFM numbering convention was followed.

Table A3

X Direction Mapping*

X Map in.	X' Map in.	α
1.0	1.5	1
4.0	1.5	2
11.1	0.75	7
12.3	0.5	2
12.8	0.1	2
13.0	0.1	2
13.5	0.5	2
15.0	1.0	2
19.5	0.8	5
24.0	1.5	4

* The X direction was mapped south to north (bottom to top). The WIFM numbering convention was not observed, thus the file is ordered in the opposite direction, i.e. refined grid cell M = 2 is global cell number M = 27 .

followed by X direction. The refined grid was then plotted on paper and mylar by using the DOGRID procedure.

10. The stretching coefficients were also punched using the DOGRID procedure for subsequent input to WIFM-SAL.

Depth Field Specification

11. The depth field was digitized from nautical chart 11374 (Ed 16) dated November [illegible]. Areas designated as the idealized channel were set to depth -38 ft [illegible] cells representing land were set to depth +10 ft. The datum was [illegible] Coast Datum.

12. The bathymetry [illegible] Southern Ocean Systems Co. June/July 1980) for Horn Island Pass [illegible] was reviewed to ensure that depths assigned to the band of high [illegible] cells in the pass would reflect the survey. The depth field comprises [illegible] group 13.

Barrier Specification

13. Barriers were specified for the refined grid based upon the island configuration and shallow depth areas. For barrier specification all the barriers were assumed to be exposed throughout simulation and barrier elevations were set to +10 ft.

14. Barriers are located on either the u or v face of each cell. Figure A-1 shows this orientation.

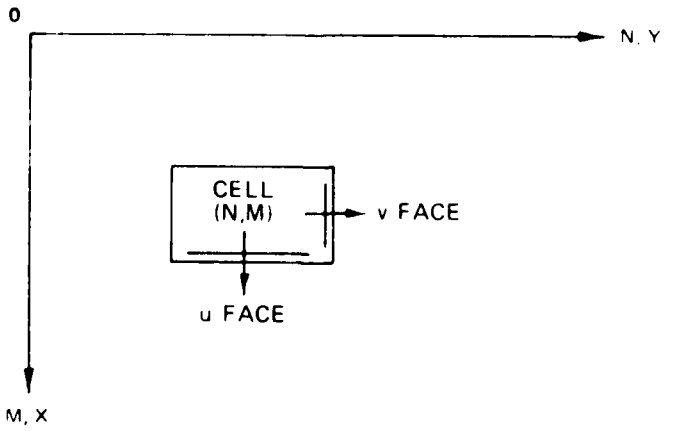

Figure A1. Barrier cell face orientation

15. To code the barrier location, IDIR is set to 1 for a u face barrier and set to 2 for a v face barrier. IDIR indicates flow direction.

16. Further to locate the barrier it has to be specified by its refined grid indices and their range. The following examples illustrate:

A barrier on the u cell faces of cells (4, 24) (5, 24) and (6, 24) is coded thus:

ITYP	INDX	IDIR	I1	I2	I3
			M	N_a	N_b
1	1	1	24	4	6

I1 is the M row of the u face barrier location. I2 and I3 correspond to the range of columns (N's) that the barrier extends along row M (I1).

17. Alternately, a barrier on the v cell faces of cell (7, 2) and (7, 3) is coded:

ITYP	INDX	IDIR	I1	I2	I3
			N	M_a	M_b
1	1	2	7	2	3

I1 is the N column of the u face barrier and I2 and I3 correspond to the range of rows that the barrier extends along column N (I1). Barrier location codes are the first set of input variables in Card Group 17.

Flow Specification

18. Freshwater inflow locations were noted for the Pascagoula and West Pascagoula Rivers in terms of the refined grid coordinate system.

19. Location information is specified in the boundary input Card Group 17. For the West Pascagoula the input is specified as follows.

			Refined Grid Indices		
ITYP	INDX	IDIR	M	N_1	N_2
9	1	1	1	8	8

ITYP = 9 for a flow input. IDIR = 1 for a vertical oriented x axis oriented inflow. INDX specifies the discharge array. Since this inflow is the first inflow specified, INDX = 1 .

20. Note in simulating salinity, salinity values associated with the given inflow must also be specified in Card Group 21.

Tidal Signal Input Specification

21. To specify the locations for the tidal signal inputs, where the global and refined grid interface, the cell centers of the global grid cells on the refined grid boundaries must be referenced in their respective refined grid indices. To accomplish this, all cells in the global grid where tidal inputs would be made to the refined grid were identified and numbered. Forty (40) global grid cells lie along refined grid (water) boundaries. To identify their centers in optimum refined grid indices, the refined grid was overlaid the global grid. Table A4 lists the tidal signal inputs and their N, M indices in both the global and refined grid. The refined grid M indices are the IGX array; the N indices are the IGY array (Card Group 3a).

22. The forty cells in the table are assigned boundary values based upon the results obtained at their corresponding locations in the global grid. For intermediate refined grid points interpolation is required. To specify interpolation along the x-axis for cells (1, 6) through (1, 8) in the refined grid the following data are required.

			I1	I2	I3	I4	I5	I6
			Refined Grid			Boundary Sweep	Tide Inputs	
ITYP	INDX	IDIR	N	M_1	M_2	Orientation	$Signal_A$	$Signal_B$
8	1	2	1	6	8	0	1	2

Note I4 = 0 for a lower sweep boundary and IDIR = 2 for x interpolation ITYP = 8 for a tidal elevation boundary. Observe in Table A4 that signals 1 and 2 correspond to cells (1, 6) and (1, 8) in the refined grid. Thus values at refined cell (1, 7) will be interpolated from the values of tidal signal inputs 1 and 2 (based upon x distance).

23. To specify interpolation along the y-axis for cells (5,28) through (8,28) in the refined grid the following data are required.

			I1	I2	I3	I4	I5	I6
			Refined Grid			Boundary Sweep	Tide Inputs	
ITYP	INDX	IDIR	M	N_1	N_2	Orientation	$Signal_A$	$Signal_B$
8	1	1	28	5	8	1	29	30

Table A4

Global Grid Cell-Refined Grid Cell Boundary Assignment

Tidal Signal No.	N,M Indices Global Grid	Refined Grid	Tidal Signal No.	N,M Indices Global Grid	Refined Grid
1	53, 21	1, 6	21	67, 29	49, 24
2	53, 22	1, 8	22	67, 30	49, 25
3	53, 23	1, 9	23	67, 31	49, 26
4	53, 24	1, 10	24	67, 32	49, 27
5	53, 25	1, 14	25	67, 33	49, 28
6	53, 26	1, 18	26	53, 33	1, 28
7	53, 27	1, 20	27	54, 33	2, 28
8	53, 28	1, 22	28	55, 33	4, 28
9	53, 29	1, 24	29	56, 33	5, 28
10	53, 30	1, 25	30	57, 33	8, 28
11	53, 31	1, 26	31	58, 33	11, 28
12	53, 32	1, 27	32	59, 33	17, 28
13	53, 33	1, 28	33	60, 33	23, 28
14	67, 22	49, 8	34	61, 33	26, 28
15	67, 23	49, 9	35	62, 33	31, 28
16	67, 24	49, 10	36	63, 33	42, 28
17	67, 25	49, 14	37	64, 33	45, 28
18	67, 26	49, 18	38	65, 33	47, 28
19	67, 27	49, 20	39	66, 33	48, 28
20	67, 28	49, 22	40	67, 33	49, 28

Freshwater Flow Inputs			
1	West Pascagoula	57, 19	8, 1
2	Pascagoula	59, 19	16, 1

Reference to Card Group 3a - Tidal signal input locations

1. Each M index of the refined grid indices is an element of the IGX array
2. Each N index of the refined grid indices is an element of the IGY array

Reference to Card Group 17.

1. The tidal signal numbers are I5 and I6.
2. The N, M indices locate where the tidal signals or flows are input on the refined grid.

Note I4 = 1 for an upper sweep boundary and IDIR = 1 for y interpolation. ITYP = 8 for a tidal boundary. Observe in Table A4 that signals 29 and 30 correspond to cells (5, 28) and (8, 28) in the refined grid. Thus values at refined cells (6, 28) and (7, 28) will be interpolated from the values of tidal signals 1 and 2 (based upon y distance).

Salinity Initial Condition Specification

24. The calibration period (20-24 September 1980) was selected for simulating salinity on the refined grid.

25. Initial conditions for each cell were specified by transferring the calibration period initial salinity values from the global subgrid to the refined grid. To facilitate this task, the global subgrid (scale 1:80000) was reproduced and the initial salinity values were recorded thereon. Then the refined grid was reproduced at scale 1:80000 and overlaid on the subgrid.

26. Initial salinity conditions for the global subgrid had been specified based upon salinity transect surveys taken during 20-21 September 1980.

27. See Table A5 for transect station location summary.

28. Salinity initialization is specified in Card Group 13b.

Specification of Wind Information

29. The user has the option of considering wind effects on the hydrodynamics and the salinity. Wind speeds are input in miles per hour and wind directions are in the meteorological or "from" convention as opposed to the oceanographic or "to" convention (0° from the N , 90° from the E , etc). Wind speeds and directions may be entered in tabular form in Card Group 11.

Development of Simulation Control Variables

30. Simulation control variables determined by the grid and depth characteristics are DX , DY , and TAU , which are specified in Card group 4.

31. DX is the vertical spatial stepsize, while DY is the horizontal spatial stepsize. These variables are determined from the scale at which the grid was mapped. In this case the mapping was at the 1:40000 scale, where 1 in. equals 40,000 in.

DX is the real space prototype distance (ft) represented by one [illegible] in the vertical or M direction. Thus

$$DX = \frac{4000 \text{ in.}}{12 \text{ in./ft}} \quad \text{or} \quad 3333.33 \text{ ft}$$

33. DY is the corresponding value associated with the Y or N direction of the grid. In the refined grid the same scale was used for mapping both directions. DX equals DY .

34. TAU is the time-step length and was determined in the following manner.

$$\Delta t = \frac{\Delta S \text{ min (ft)}}{\sqrt{g(\text{ft/sec}^2) * d_{max}(\text{ft})}}$$

where ΔS is the minimum of DX times the smallest X expansion coefficient (Mu) and DY times the smallest Y expansion coefficient (Nu).
[Mu is the smallest X expansion coefficient; i.e., the smallest X prime chosen for the mapping = 0.10].
[Nu is the smallest y expansion coefficient; i.e., the smallest y prime chosen for the mapping = 0.10].

g is the acceleration of gravity = 32.2 ft/sec.

d_{max} is the maximum depth of water assigned to a cell in the depth field = 50 ft.

Δt is the explicit time step limit.

Thus

$$\Delta t = \frac{3333.33 \text{ ft} * 0.1}{\sqrt{32.2 \text{ ft/sec}^2 * 50 \text{ ft}}} = 8.3 \text{ sec}$$

This is the maximum time step that can be used for explicit modeling. Since WIFM-SAL is an implicit model, TAU can be up to 10 times larger than Δt . TAU for the refined grid was set to 60 sec.

35. Surface elevation, velocity, and salinity stations within the region represented by the refined grid were plotted onto nautical chart 11374 (Ed 16). This put all the prototype data station location and the depth information for the model in one place. Station locations were then plotted onto the refined

grid and global subgrid. Table A5 summarizes the locations and their N, M indices in both grids.

36. This table forms the basis for assignments to the control variables in Card Groups 25, 26, and 27 which are the plotting controls.

NNPOT - number of surface elevation stations

NVELPN - number of velocity stations

INPOT - N indices of surface elevation stations

IMPOT - M indices of surfaces elevation stations

NVCORD - N indices of velocity stations

MVCORD - M indices of velocity stations

37. The value of NFREQ (input Card Group 5) can be determined here. NFREQ = $\frac{3600 \text{ sec/hr}}{\text{Tau sec}}$ or $\frac{3600}{60 \text{ sec}}$ = 60/hr. Thus hydrodynamic data will be printed every 60 time steps or once per hour at each of the data stations.

38. The N, M indices of the hydrodynamic gages form the two arrays NPOT and MPOT which are WIFM-SAL input Card Group 8. The total number of hydrodynamic prototype gages is the value of NGAGE (input Card Group 5).

Table A5

Data Station Location Summary

Station	Location		N, M Indices Global Grid	Refined Grid
Velocity				
V12	30°16.14'	88°40.82'	54,27	3,20
V13	30°15.96'	88°30.61'	62,27	35,20
V14	30°13.32'	88°32.40'	60,30	24,25
$V15_A$	30°12.45'	88°30.75'	62,31	33,26
$V15_B$	30°12.00'	88°31.00'	62,32	30,27
$V16_A$	30°14.83'	88°27.07'	67,28	49,23
$V16_B$	30°14.95'	88°26.10'	68,28	49,22 [1]
Surface Elevation				
T4 Horn Island	30°14.1'	88°39.2'	55,29	4,24
T5 Pascagoula	30°20.4'	88°32.0'	61,21	25,6
T6 Petit Bois	30°12.2'	88°26.5'	67,32	49,27
T7 Grand Batture	30°20.5'	88°24.4'	70,21	49,5 [2]
Salinity Transect				
T54	30°15.3'	88°36.25'		8,22
T56	30°12.4'	88°30.7'		33,26/34,26 [3]
T58	30°14.8'	88°30.45'		36,23
T60	30°17.05'	88°30.65'		32,16/33,16 [4]
T62	30°18.8'	88°32.3'		24,9
T64	30°20.4'	88°33.8'		17,6
T66	30°19.85'	88°30.8'		31,7
T68	30°16.4'	88°26.65'		49,19

1. Station $V16_B$ located beyond right of cell 49,22 outside the refined grid.
2. Station T7 located beyond right of cell 49.5 outside the refined grid.
3. Station T56 located at cell boundary between 33,26 and 34,26.
4. Station T60 located at cell boundary between 32,16 and 33,16.

APPENDIX B: PROGRAM TIDE

1. Program TIDE is a general purpose program to predict the tidal characteristics (elevation or current component) given the harmonic constants and prediction period. The program also will access water surface elevation and current component tapes containing the results of the standard harmonic analysis (filtered and unfiltered values). Based upon the harmonic constants for the analyzed stations, the program predicts the station tidal characteristics and outputs the value next to the unfiltered and filtered values at each hour. This serves as a check on the harmonic analysis. The program also will write to a WIFM compatible plot file the predicted tidal characteristic at user specified locations. During the WIFM simulation, this plot file is accessed to enable overplotting of predicted tidal characteristics on computed results at common locations, thereby aiding the hydrodynamic calibration process.

2. The input variables are defined followed by a listing of the program.

Program TIDE:

IYEAR - Year of the prediction (e.g. 1980)
IMONTH - Month of the prediction (e.g. 9)
IDAY - Day of the prediction (e.g. 20)
IHR - Hour of the prediction (e.g. 00)

} Start Time of the Prediction Period

ICONST - 37 element array, specify 1 in the appropriate array element if the constituent in NCONST array is to be considered in developing node factors and equilibrium arguments.

NTIDE - Number of tide stations

NCOMP - Number of tidal components (1 - elevation; 2 - currents)

NT - Tape logical unit number

NCON - Number of tidal constituents to include in the predictions

ICONST(J), J = 1, NCON - Number of the array element in NCONST corresponding to each tidal constituent considered.

IEL - Data Tape Access Switch [1 Access harmonic analysis data tape; 0 Don't access harmonic analysis data tape]

NUL - Lower hour of prediction period to write to WIFM plot file

NUH - Upper hour of prediction period to write to WIFM plot file

IWR - Number of stations to write to WIFM plot file

NWR (I), I = 1, IWR - Number of the station to write to WIFM plot file based on the input sequence of all stations

NTT - Logical unit number of WIFM plot file

Subroutine TAPE: Harmonic Analysis Data Tape Format

TITL(J, I1, I), J = 1, 8 - Title on the harmonic analysis data tape of the current station information file

Note: (I1 = 1, NST), where NST is the number of stations

(I = 1, NR), where NR = 2* NCOMP (filtered and unfiltered files)

JDAY - Start Julian Day

IHR - Start Hour

IMIN - Start Minute

DELT - Data Interval (Minutes)

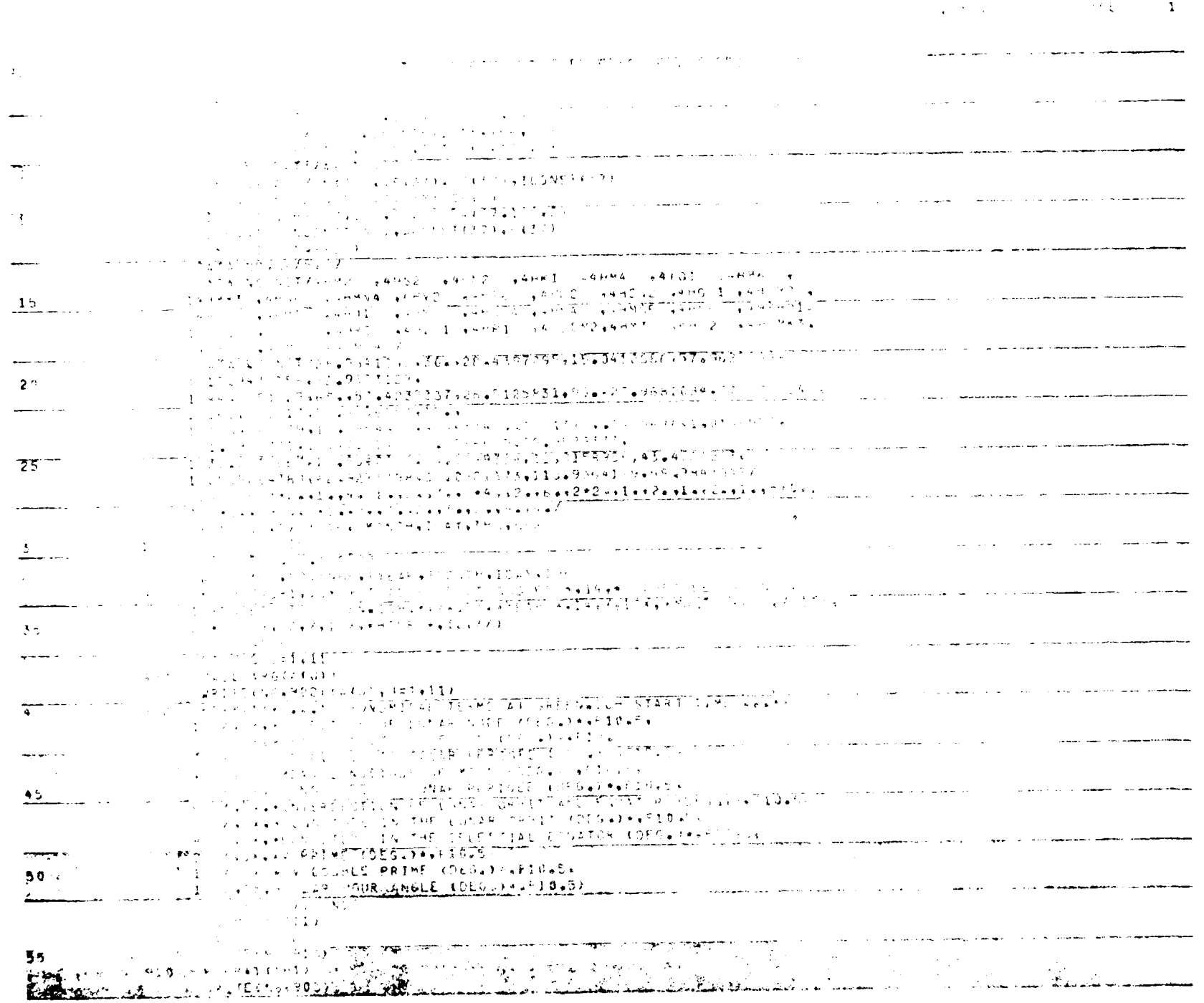
DOUBLE PRIME (DEG.)
HOUR ANGLE (DEG.)

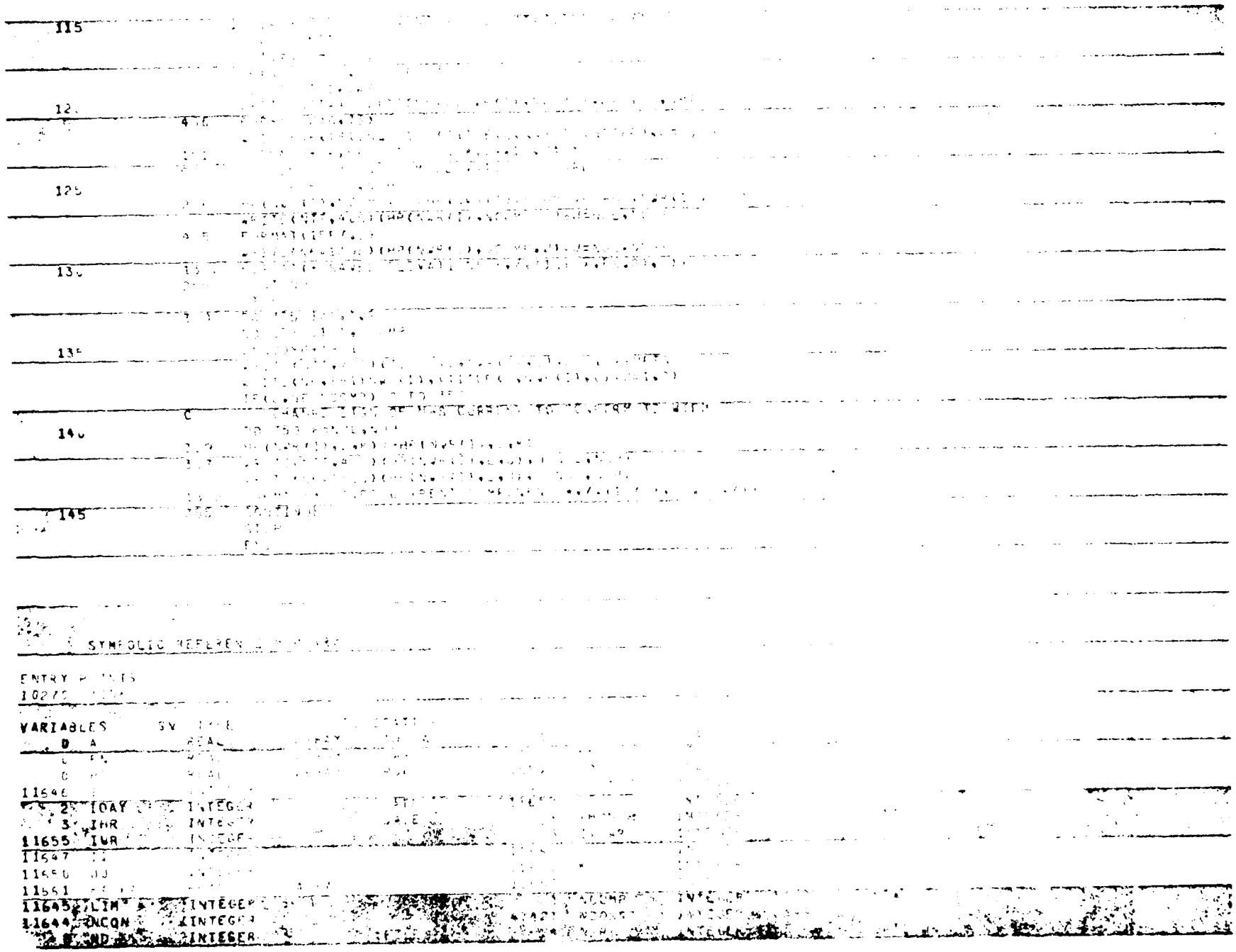

```
115
12.
125
130
135
140
145
```

SYMBOLIC REFEREN

ENTRY POINTS
10272

VARIABLES SV TYPE

D	A	REAL				
11646						
2	IDAY	INTEGER				
3	IHR	INTEGER				
11655	IWR	INTEGER				
11647						
11650						
11651						
11645	LIM	INTEGER			NCOMP	INTEGER
11644	NCON	INTEGER				INTEGER
	ND	INTEGER				INTEGER

```
      C     ... INTERSECTION OF LUNAR ORBIT AND EQUATOR, AS
      C     ... VERTEX IN THE CELESTIAL EQUATOR, V
      C     ... UNIT ... IN ...
      F1=ATAN(1.03883*TAN(DR*AN/2.))/DR
      F2=ATAN(.96412*TAN(DR*AN/2.))/DR
      EPAN=F1-F2
      ...
      C     ... TIME (YR) ... TIME (YRS)
      ... ...*...)/(...**...*COS(DR*V)+...
      VP=ATAN(VP)/DR
      ...SIN(2.*AI)*SIN(2.*AI)*SIN(2.*VP*V)/(SIN(DR*...*SIN(DR*...
     ...SIN(2.*VP*V)+...727)
      ...
      RETURN
      END
```

ENTRY POINTS
   1 ASTRO

VARIABLES		SN	TYPE						
	AI		REAL				AN	REAL	
							C	REAL	
15	DR		REAL						
360	FOC		REAL				361	F1	REAL
362	F2		REAL					H	REAL
354	I		INTEGER					IANC	INTEGER
	IDAY		INTEGER					IMN	INTEGER
	IJDAY		INTEGER					IJDAYS	INTEGER
351	IL		INTEGER						
352	ILIM		INTEGER				356	ILIMI	INTEGER
363	IMON		INTEGER	ARRAY			1	IMONTH	INTEGER
350	IREF		INTEGER				0	IYEAR	INTEGER
353	J		INTEGER					JDAY	INTEGER
	JDAY		INTEGER					JD	INTEGER
	NOW		INTEGER					JY	INTEGER
1	N6		INTEGER				4	P	REAL
2	P1		REAL				3	Q	REAL
12	T		REAL				3	THRE	REAL
1	TEC		REAL					V	REAL
10	VP		REAL				11	VPP	REAL

EXTERNALS	TYPE	ARGS				
ACOS	REAL	1	LIBRARY	ATAN	REAL	1 LIBRARY
COS	REAL	1	LIBRARY	SIN	REAL	1 LIBRARY
TAN	REAL	1	LIBRARY			

INLINE FUNCTIONS							
FLOAT	REAL	1	INTRIN	MAX0	INTEGER	2	INTRIN
MOD	A=INTEGER	2	INTRIN				

```
1                SUBROUTINE EVAL(
                 COMMON/AB/TH,DR,PI,S,AI,T,V,VF,VFF,I,DR
                 COMMON/FUNC/FN(37),VE(37),UE(37),ICONST(37)
                 I=1
5                IF(I-1)1,2,1
                 DO 2 J=1,37
1                FN(J)=((COS(DR*AI/2.))**4)/.9154
                 VE(J)=2.*(F-S*H)
                 UE(J)=2.*(E-V)
                 I=I+1
2                DO 3 J=1,37
                 FN(J)=1.
                 VE(J)=T
                 UE(J)=0.
                 GO TO 1
15       3       FN(J)=(COS(DR*AI/2.))**4/.9154
                 VE(J)=T*(-S*SIN(DR*AI)+H)
                 UE(J)=2.*(E-V)
                 GO TO 1
4                FN(J)=(.7*(.2523*SIN(2.*DR*AI)+SIN(2.*DR*AI)+.1689*SIN(2.*DR*AI)
20              1 *COS(DR*V)+.0285)/.5305
                 VE(J)=T*H-99.
                 UE(J)=-VF
                 GO TO 1
5                IF(ICONST(1).LE.0)GO TO 100
25               FN(J)=FN(J)*FN(1)
                 VE(J)=2.*VE(1)
                 UE(J)=2.*UE(1)
                 I=I+1
6                FN(J)=(.5*(SIN(DR*AI)*COS(DR*AI/2.)+COS(DR*AI/2.))/.38
                 VE(J)=T*H-S*S*99.
                 UE(J)=2.*E-V
                 GO TO 1 0
                 IF(ICONST(1).LE.0)GO TO 100
                 FN(J)=FN(1)**3
                 VE(J)=3.*VE(1)
                 UE(J)=3.*UE(1)
                 GO TO 1 4
8                IF(ICONST(1).LE.0)GO TO 100
                 IF(ICONST(4).LE.0)GO TO 100
40               FN(J)=FN(1)*FN(4)
                 VE(J)=VE(1)+VE(4)
                 UE(J)=UE(1)+UE(4)
                 GO TO 1 4
9                IF(ICONST(2).LE.0)GO TO 100
45               FN(J)=1.
                 VE(J)=4.*T
                 UE(J)=0.
                 GO TO 1
10               IF(ICONST(1).LE.0)GO TO 100
50               IF(ICONST(3).LE.0)GO TO 100
                 FN(J)=FN(1)*FN(3)
                 VE(J)=VE(1)+VE(3)
                 UE(J)=UE(1)+UE(3)
                 GO TO 1 0
55       300     IJ=J-10
                 IF(IJ-10)400,400,500
         400     GO TO (11,12,13,14,15,16,17,18,19,20),IJ
```

```
      GO TO 100
   22 FN(J)=1.
      VE(J)=H
```

```
      UE(J)=0.
      GO TO 1
   23 IF(ICONST(2).LE.0)GO TO 100
      FN(J)=FN(2)
      VE(J)=[illegible]*(P-E)
      UE(J)=[illegible]
      GO TO 1[illegible]
   24 FN(J)=SIN(DR*AI)*SIN(DR*AI)/.1578
      VE(J)=[illegible]
      UE(J)=[illegible]
      GO TO 1
   25 IF(ICONST(6).LE.0)GO TO 100
      FN(J)=FN(6)
      VE(J)=T+3.*(H-S)-P+90.
      UE(J)=UE(6)
      GO TO 1
   26 IF(ICONST(6).LE.0)GO TO 100
      FN(J)=FN(6)
      VE(J)=T+H-3.*S+P+90.
      UE(J)=UE(6)
      GO TO 1[illegible]
   27 FN(J)=[illegible]
      VE(J)=[illegible]-H+[illegible]*T
      UE(J)=[illegible]
      GO TO 1[illegible]
   28 FN(J)=1.
      VE(J)=H-[illegible]+180.+2.*T
      UE(J)=[illegible]
      GO TO 1
   29 IF(ICONST(6).LE.0)GO TO 100
      FN(J)=FN(6)
      VE(J)=T-4.*S+H+2.*P+90.
      UE(J)=UE(6)
      GO TO 1
   30 FN(J)=1.
      VE(J)=T-[illegible]
      UE(J)=0.
      GO TO 1[illegible]
   70 IJ=J-3[illegible]
      GO TO ([illegible],[illegible],[illegible],[illegible],[illegible],[illegible],[illegible]),IJ
   31 IF(ICONST(1).LE.0)GO TO 100
      FN(J)=FN(1)
      VE(J)=2.*(T+S-H)
      UE(J)=2.*(V-E)
      GO TO 1[illegible]
   32 FN(J)=[illegible](DR*AI/2.)**6/.8758
      VE(J)=3.*(T-S+H)
      UE(J)=3.*(E-V)
      GO TO 1[illegible]
   33 IF(ICONST(1).LE.0)GO TO 100
      FN(J)=FN(1)*SQRT(1.-12.*TAN(DR*AI/2.)*TAN(DR*AI/2.)*
     1 COS(2.*DR*(P-E))+36.*TAN(DR*AI/2.)**4)
      VE(J)=2.*(S+H)-S-P+180.
      R=1./TAN(DR*AI/2.)
      P= ATAN(SIN(2.*DR*(P-E))/(R*R/6.-COS(2.*DR*(P-E))))
      UE(J)=2.*(E-V)-R/DR
      GO TO 1[illegible]
```

```
      SUBROUTINE ARG(THP)
      ITHETA=THP/360.
      THP=THP-FLOAT(ITHETA)*360.
      ITHETA=THP
      FRAC=THP-FLOAT(ITHETA)
      IT=MOD(ITHETA,360)
      THP=FLOAT(IT)+FRAC
      IF(THP.LT.0.)THP=THP+360.
      RETURN
      END
```

```
      SYMBOLIC REFERENCE MAP (R=1)

ENTRY POINTS
    3  ARG

VARIABLES      SN  TYPE            RELOCATION
   25  FRAC        REAL                          26  IT          INTEGER
   24  ITHETA      INTEGER                           THP         REAL                F.P.

INLINE FUNCTIONS    TYPE    ARGS
       FLOAT        REAL      1  INTRIN                MOD         INTEGER    2  INTRIN

STATISTICS
  PROGRAM LENGTH                  27        23
        52000B CM USED
```

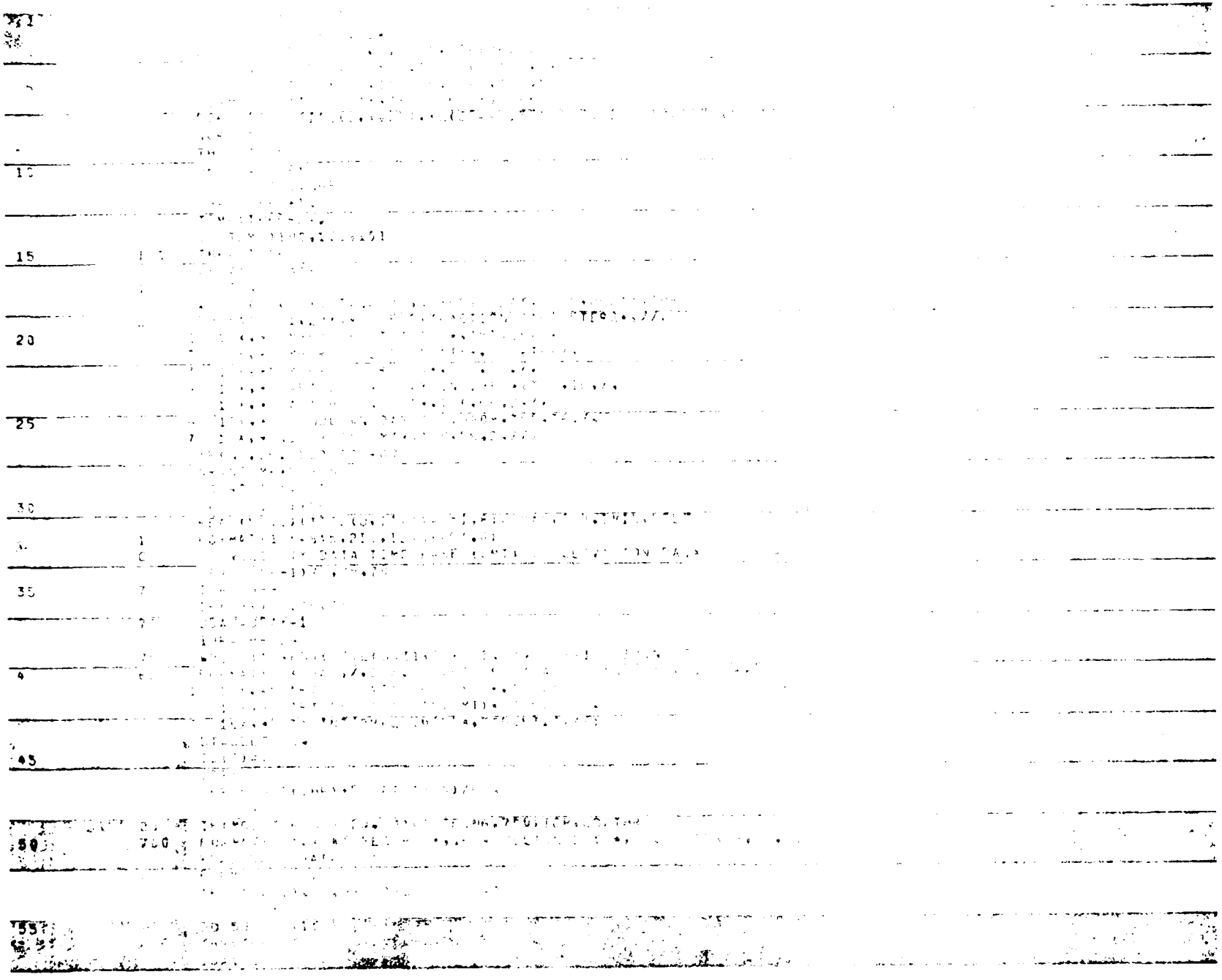

```
                      FORMAT(1H1,2X,'MOVD DATUM ',F6.2)
                      WRITE(6,*)(NC(I),I=1,2),M(I,II)
                      FORMAT(//,1X,A5)
                      IF(LIM.EQ.1) GO TO 450
                      WRITE(6,*)(HC(I,II),I=1,2),M(I,II)
                      FORMAT(1H0,2X,'MOVD DATUM ',F6.2)
                      LIM=1
                      GO TO 451
                      FORMAT(1H1,2X,'MOVD DATUM ',F6.2)
                      WRITE(6,*)(NC(I),I=1,2),M(I,II)
                      FORMAT(//,1X,A5)
                      LIM=1
                      WRITE(6,*)(HC(I,II),I=1,2),M(I,II)
                      FORMAT(1H0,2X,'MOVD DATUM ',F6.2)
                      LIM=1
                      WRITE(6,*)(HC(I,II),I=1,2),M(I,II)
                      FORMAT(1H0,2X,'MOVD DATUM ',F6.2)
                      LIM=1
                      WRITE(6,*)(NC(I),I=1,2),M(I,II)
                      FORMAT(//,1X,A5
```

```
  115                 LIMU=MIN0(LIMU+10,NHR+1)
                      GO TO 155
                 350  CONTINUE
                      RETURN
                      END
```

SYMBOLIC REFERENCE MAP (R=1)

ENTRY POINTS
1 TAPE

VARIABLES		TYPE		DECLARATION					
37610	DATA	REAL	ARRAY		[illegible]	FELT	REAL		
716	DT	REAL			[illegible]	FRAC	REAL		
0	HP	REAL	ARRAY	PDAT	16514	HT	REAL		[illegible]
675	I	INTEGER			37622	IC	INTEGER	[illegible]	
707	ICP	INTEGER			2	IDAY	INTEGER		[illegible]
[illegible]	[illegible]	[illegible]			[illegible]	IMIN	INTEGER		
1	IMONTH	INTEGER		DATE	[illegible]	IRR	INTEGER		[illegible]
	[illegible]	INTEGER		DATE	[illegible]	I1	INTEGER		
701	J	INTEGER			711	JD	INTEGER		
702	JDAY	INTEGER			2	JFDAY	INTEGER		JDATE
0	JJDAY	INTEGER		JDATE	713	LIM	INTEGER		
716	LIMU	INTEGER			71[illegible]	LIMU	INTEGER		
37766	NC	INTEGER	ARRAY		1	NCOMP	INTEGER		STA
[illegible]	[illegible]	INTEGER		FILES	674	NGRPS	INTEGER		
4	NHR	INTEGER		DATE	677	NR	INTEGER		
0	NST	INTEGER		STA	8	N5	INTEGER		FILES
1	NR	INTEGER		FILES	676	TEMP	REAL		
71[illegible]	[illegible]	REAL			[illegible]	THRF	REAL		JDATE
[illegible]	[illegible]	REAL		JDATE	72[illegible]	TITL	REAL	[illegible]	
[illegible]	[illegible]	REAL	ARRAY	STA	276	XL	REAL	[illegible]	
714	X1	REAL			715	X2	REAL		

INLINE FUNCTIONS	TYPE	ARGS					
[illegible]	REAL	1	INTRIN	FLOAT	REAL	[illegible]	[illegible]
MIN	INTEGER	0	INTRIN	MOD	INTEGER	[illegible]	[illegible]

STATEMENT LABELS

451	1	FMT		531	2	FMT		114	4		
0	5		INACTIVE	0	8		INACTIVE	[illegible]	[illegible]		
213	1			575	11	FMT		[illegible]	[illegible]		
14[illegible]	4[illegible]			143	50			[illegible]	51		INACTIVE
122	5[illegible]			[illegible]	53		INACTIVE	[illegible]	54		
136	55			[illegible]	56		INACTIVE	403	69	FMT	
540	62	FMT		465	65	FMT		0	70		INACTIVE
0	73		INACTIVE	45	75			17	100		
	101		INACTIVE	321	155			610	[illegible]	FMT	
632	205	FMT		276	250			[illegible]	300		
361	350			[illegible]	400			691	450	FMT	
652	452	FMT		662	453	FMT		554	500	FMT	
563	550	FMT		615	555	FMT		515	700	FMT	

APPENDIX C: CUBIC POLYNOMIAL FEATHERING

1. In employing tidal constituent signals along the grid boundary, there is no guarantee that at simulation start time these signals will be zero. In fact, in general this will not be the case. Since water surface elevations and currents are set to zero at the start of the simulation, there is a discontinuity or impulse at the boundary; e.g., the boundary level is not consistent with the initial condition. This phenomenon may lead to oscillations in the numerical solution, which may persist over several computational cycles.

2. In order to avoid this problem, the true tidal signal, $g(t)$, is replaced by a more well-behaved signal, $f(t)$, at model start and for a number of initial time steps of length Δt. The well-behaved signal is zero at simulation start time and at some time T_1, > 0, the well-behaved signal and one or more derivatives equal the true signal and its corresponding derivatives. Consider the following cubic polynomial, $f(T) = aT^3 + bT^2 + cT + d$,

$$f(o) = o \rightarrow d = o$$

$$f(T_1) = aT_1^3 + bT_1^2 + cT_1 \tag{C.1}$$

$$f'(T_1) = 3aT_1^2 + 2bT_1 + c \tag{C.2}$$

$$f''(T_1) = 6aT_1 + 2b \tag{C.3}$$

From Equations C.1 through C.3, we obtain a, b, and c:

$$a = \left[f(T_1) - T_1 f(T_1) + \frac{T_1^2}{2} f''(T_1)/T_1^3 \right] \tag{C.4}$$

$$b = (f''(T_1) - 6aT_1)/2 \tag{C.5}$$

$$c = f'(T_1) - 3aT_1^2 - 2bT_1 \tag{C.6}$$

Thus, we have determined a cubic polynomial with value zero at $t = 0$, and whose functional plus first two derivative values equal those of the true

boundary signal. Required information for determining a , b , and c are $f(T_1)$, $f'(t_1)$, and $f''(T_1)$.

3. Consider the true boundary signal to be a periodic signal as shown in Figure C1 below.

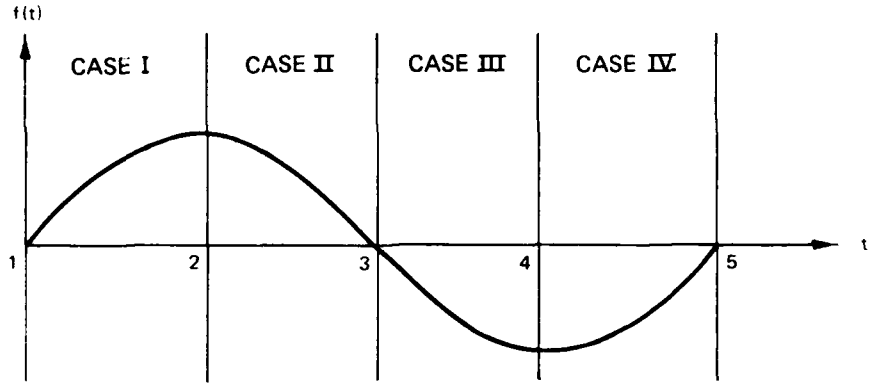

Figure C1. Periodic boundary signal

4. Since the start time may be arbitrary, the vertical axis may fall anywhere between 1 and 5 and four cases must be considered as shown in Figure C-2. A level $x > 0$ is specified (XLEVEL), this enables $f(T_1)$ to be determined in each case. The following approximations are employed for $f'(T_1)$ and $f''(T_1)$.

$$f'(T_1) \equiv \frac{g(T_1 + \Delta t) - g(T_1 - \Delta t)}{2\Delta t} \tag{C.7}$$

$$f''(T_1) \equiv \frac{g(T_1 + \Delta t) + g(T_1 - \Delta t) - 2g(T_1)}{(\Delta t)^2} \tag{C.8}$$

Note $f(T_1) = g(T_1)$.

5. The flow inputs were also feathered in the following fashion. The user specifies the number of time steps (NTID) over which the feathering is to take place. The feathered signal equals zero at the start of the simulation. At each intermediate time step less than NTID, the feathered signal is obtained by linearly interpolating between its zero value at time zero and the true boundary value at time step NTID.

6. The feathering procedures are contained in Subroutine POLY, which is listed in Table B1. This subroutine is called if the user specifies IFETR = 1 on input.

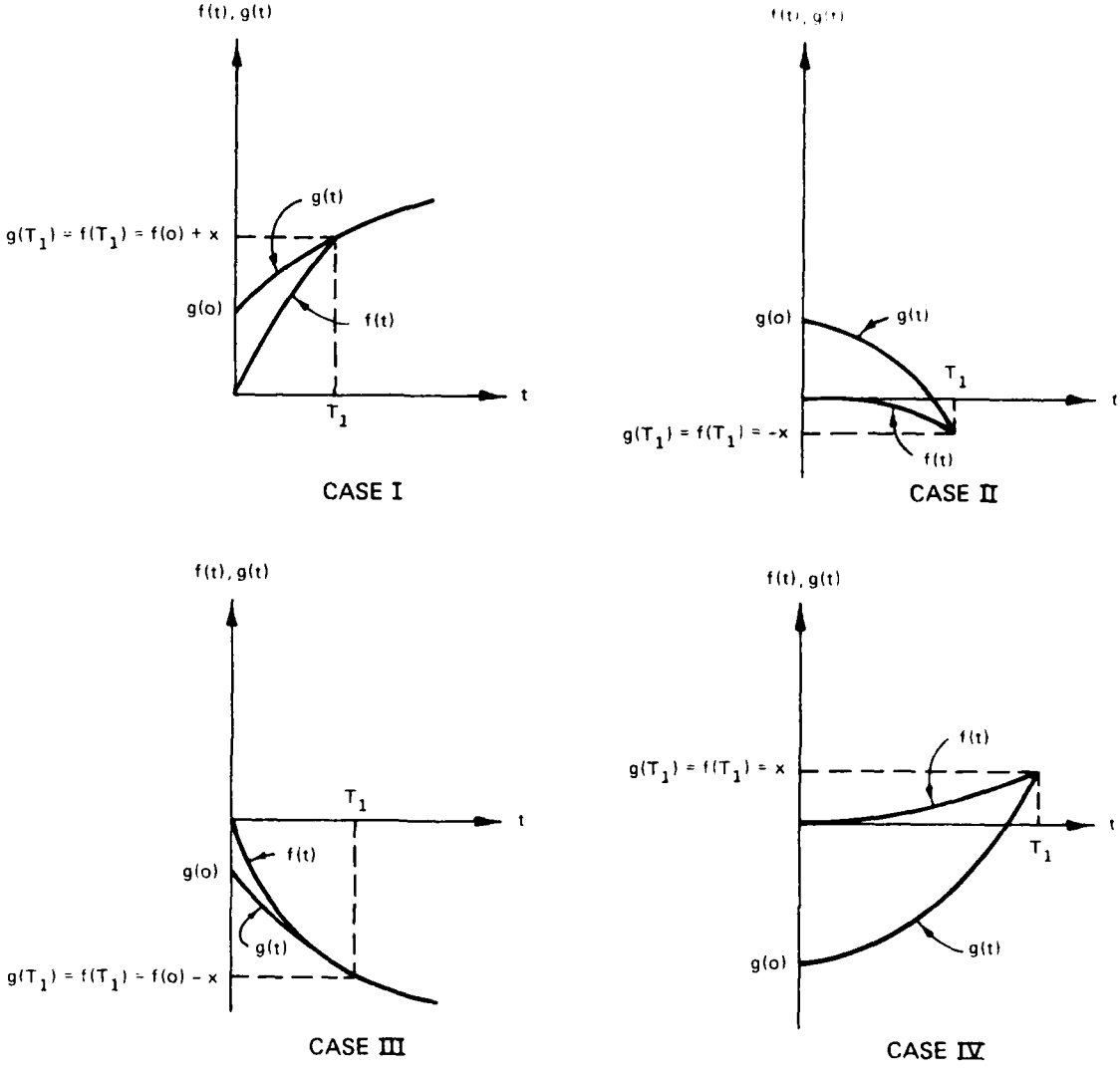

Figure C2. Cubic polynomial feathering conditions

Table C-1

Subroutine POLY

```
      SUBROUTINE POLY                                                    POLY      2
      PARAMETER (NUMPT=6785,NDIM=115,MDIM=59,NPTS=100)                   PARMS     3
      PARAMETER(IERR=305,IOXS=20,IPUT=1500,ITDS=14,JPUT=1500,JFLS=6)     PARMS     4
      LOGICAL ITAPE,IPT,IDUMP                                            SCALAR    2
      COMMON /V1/ NMAX,MMAX,NTID,JFLG,ITID,JPID,NPIT,NP1,NFC,NFB,NPR,    SCALAR    3
     1 MFW,MAXTIM,INIT,IDELAY,IFLOT,NGAGE,N1,M1,NX1,MX1,NFP,MFP,         SCALAR    4
     2 IFIME,IF1,IFF,NFSEG,IFBCHK,IX,MX,NMK,MFORE,NXX,NYY,NZB,NDIAG,     SCALAR    5
     3  JFB,NREST,KS1,KS2,KS3,KS4,KS5,KSUB,NNEXT,MSKE,MDLY,ITAPE,IPT,    SCALAR    6
     4 IDUMP,INC,NFT,NFI,NFF,ITYE,NFCK,IDIAG,IFLAG,NFRAME,NPG,MFG,KSB    SCALAR    7
     5 ,IFAIL,NCONT,IDYN,ILEVL,KW,IOPT,NCIFF,ITW,NWAT,NAE,MLIM           SCALAR    8
     6 ,NS2,NS,NEL,NC,NF,NFAT,IVEL,IFLT,IOUT,IGRC,NTABLE,               SCALAR    9
     7 IFOR,NCHA,KMG,IMX,IGLF,NCHG,NDAM                                 SCALAR   10
     8  ,NGCS                                                           SCALAR   11
      COMMON /V2/ TAU,DT,DX,DY,D2,DX2,G,G2,ALAT,XI,WA,THETA,EPSD,        SCALAR   12
     1 EPSC,CPSI,EPSM4,EPSF,DCON1,ROTA,ST1M,PI,PI2,TOX,TSY,             SCALAR   13
     2 AIV,VIS,GMEX,GMAXG,FINIT,APSE,TPRC,TMF,                          SCALAR   14
     3 XLAST,XMODE,XMAX,TC1,TC2,TAUX,TAUY,EX,DXE,DYE,,NS,ZN2            SCALAR   15
     4 ,X0,Y0,XU1,YU1,DCON2,WATER,OLIMIT                                SCALAR   16
     5 ,GTSX,GTSY,FG1,FG2,FF2,TDX,GDY,GDT,,T,ZP                         SCALAR   17
     6  ,EXS,EY,PATMS,ISAL,ISALC,CMAX,AMS,LAPLCT,IFETR                  SCALAR   18
      COMMON /AA7/ FRIC(IERR,IOXS),SURFE(IPUT,ITDS),DCHRGE(JPUT,JFLS)    ARRAY     2
     2  ,CONC(IPUT,ITDS),COND(JPUT,JFLS)                                ARRAY     3
      READ(5,102)XLEVEL,NTD                                              POLY      6
  100 FORMAT(F8.0,I5)                                                    POLY      7
      PRINT 900,XLEVEL,NTD                                               POLY      8
  900 FORMAT(* XLEVEL NTD *,F9.2,I6)                                     POLY      9
      DO 1 I=1,NTID                                                      POLY     10
      SIGN=-1.                                                           POLY     11
      IF(SURFE(1,I).LT.SURFE(2,I))SIGN=1.                                POLY     12
      XL=SIGN*XLEVEL                                                     POLY     13
      IF(SIGN*SURFE(1,I))250,1,205                                       POLY     14
  205 XL=SURFE(1,I)+XL                                                   POLY     15
  250 KCOUNT=1                                                           POLY     16
      DO 110 J=1,NSTP                                                    POLY     17
      IF(SIGN*(SURFE(J,I)-XL))4,5,5                                      POLY     18
    4 KCOUNT=KCOUNT+1                                                    POLY     19
  110 CONTINUE                                                           POLY     20
    5 FT=SURFE(KCOUNT,I)                                                 POLY     21
      TT=FLOAT(KCOUNT)*TAU                                               POLY     22
      MCOUNT=MAX0(KCOUNT-1,1)                                            POLY     23
      DTP=1./TAU                                                         POLY     24
      FP=(SURFE(KCOUNT,I)-SURFE(MCOUNT,I))*DTP                           POLY     25
      FPP=(SURFE(KCOUNT+1,I)+SURFE(MCOUNT,I)-2.*SURFE(KCOUNT,I))         POLY     26
     1  *DTP*DTP                                                         POLY     27
      A=(FT-TT*FP+.5*TT*TT*FPP)/(TT*TT*TT)                               POLY     28
      B=.5*FPP-3.*A*TT                                                   POLY     29
      C=FP-3.*A*TT*TT-2.*B*TT                                            POLY     30
      TT=0                                                               POLY     31
      PRINT 500,I,(SURFE(J,I),J=1,KCOUNT+1)                              POLY     32
  500 FORMAT(* TIDAL SIGNAL *,I4,* ORIGINAL VALUES *,/,                  POLY     33
     1  (1X,10(F8.2,2X),/))                                             POLY     34
      PRINT 501,KCOUNT,T,FT,FP,FPP,A,B,C                                 POLY     35
  501 FORMAT(* KCOUNT,T,FT,FP,FPP,A,B,C *,/,I6,/(5X,6(2X,E12.5)))        POLY     36
      DO 6 J=1,KCOUNT                                                    POLY     37
      SURFE(J,I)=TT*(A*TT*TT+B*TT+C)+FT                                  POLY     38
    6 TT=TT+TAU                                                          POLY     39
      PRINT 505,I,(SURFE(J,I),J=1,KCOUNT+1)                              POLY     40
  505 FORMAT(* TIDAL SIGNAL *,I4,* FEATHERED VALUES *,/,                 POLY     41
     1  (1X,10(F8.2,2X),/))                                             POLY     42
    1 CONTINUE                                                           POLY     43
      DO 10 I=1,NFLO                                                     POLY     44
      PRINT 910,I,(DCHRGE(J,I),J=1,NTD+1)                                POLY     45
  910 FORMAT(* FLOW INPUT *,I4,* ORIGINAL VALUES *,/,                    POLY     46
     1  (1X,10(F8.1,2X),/))                                             POLY     47
      TT=0.                                                              POLY     48
      DTP=1./(FLOAT(NTD)*TAU)                                            POLY     49
      DO 12 J=1,NTD                                                      POLY     50
      DCHRGE(J,I)=TT*DTP*DCHRGE(J,I)                                     POLY     51
   12 TT=TT+TAU                                                          POLY     52
      PRINT 912,I,(DCHRGE(J,I),J=1,NTD+1)                                POLY     53
  912 FORMAT(* FLOW INPUT *,I4,* FEATHERED VALUES *,/,                   POLY     54
     1  (1X,10(F8.1,2X),/))                                             POLY     55
   10 CONTINUE                                                           POLY     56
      RETURN                                                             POLY     57
      END                                                                POLY
```

APPENDIX D: SUBROUTINE ADVBAR

1. WIFM-SAL employs a cell face flag convention to control the hydrodynamic computations in each sweep of the computational grid. The cell flag codes are stored in two arrays: ICU for the x sweep u-face control and ICV for the y-sweep v-face control. The ICU array consists of a two-digit pair, U_1U_2 , while the ICV array contains the two-digit V_1V_2 pair for each cell in the grid. For an open-cell face the first digit U_1 or V_1 is a six. The second digit U_2 or V_2 controls the advection approximation employed in evaluating the convective acceleration and eddy-dispersion terms in the motion equations as tabulated below:

0 - no advection

1 - x-direction only

2 - y-direction only

3 - both x- and y-directions

4 - normal in y-direction, approximation in x-direction

5 - normal in x-direction, approximation in y-direction

6 - approximation in x-direction only

7 - approximation in y-direction only

8 - approximation in both x- and y-directions

At the grid boundaries, solid boundaries, and cell-face barriers, no advection has been performed in the computations for both the global and refined grids. Therefore no approximations to these terms have been made (linearized motion equation has been considered) and codes 4-8 have not been used in this study. Subroutine ADVBAR, as shown in Table D-1, determines the appropriate codes for U_2 and $V_2 \equiv (0 , 1 , 2 , 3)$ for linearizing the appropriate motion equations around cell-face barriers. Prior to the development of this routine, the model user was required to specify these codes through input for cells surrounding cell-face barriers. In the Mississippi Sound global grid 111 bariers (Table VI-8) are employed, while on the refined grid 25 barriers are employed. The work required in developing the codes by the user would have been indeed substantial in this application and has been eliminated through the use of Subroutine ADVBAR.

Table D-1

Subroutine ADVBAR

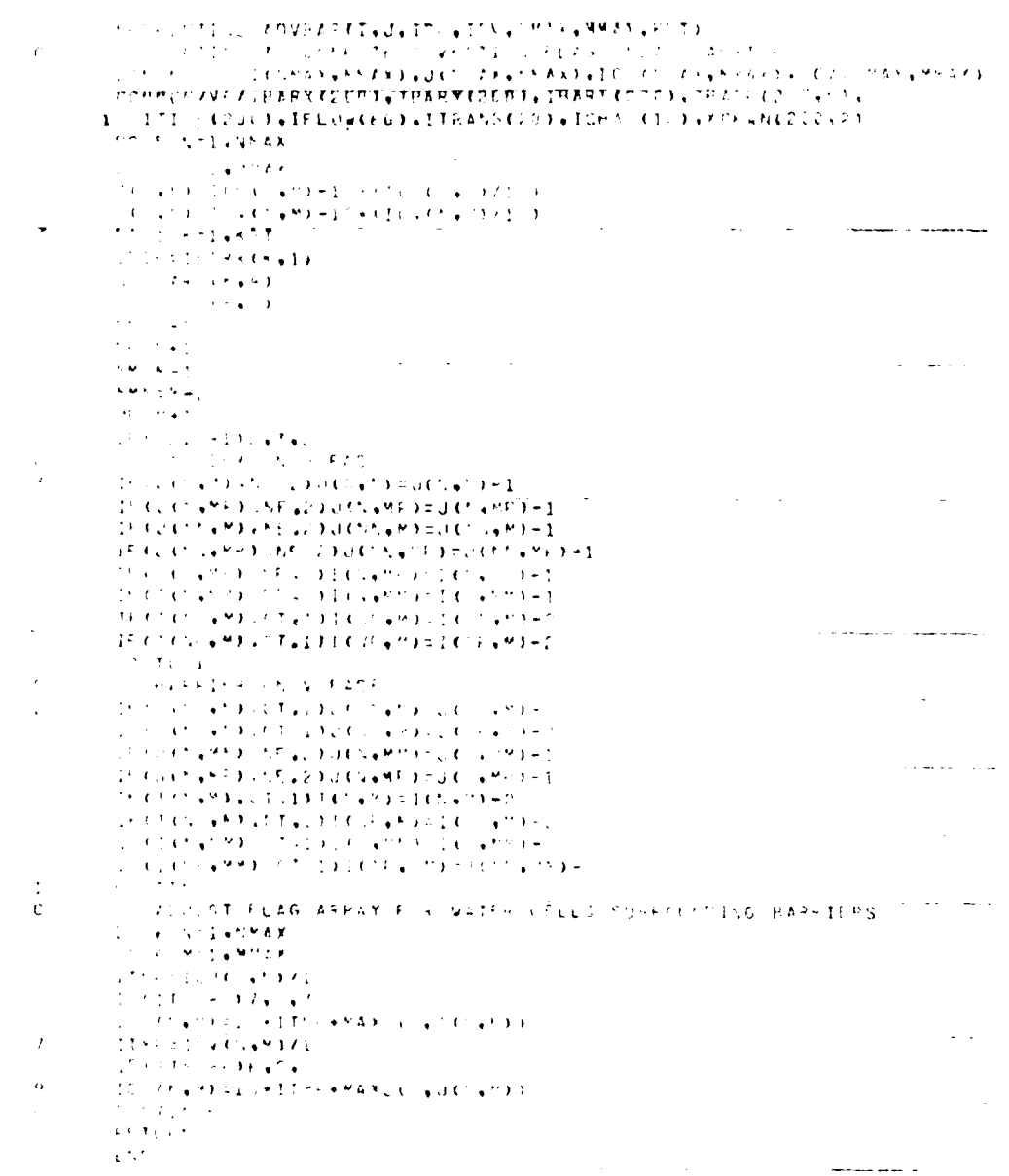

END

FILMED

8-85

DTIC